Advanced diagnostics and novel therapeutics for platelet function disorders

Minka Zivkovic

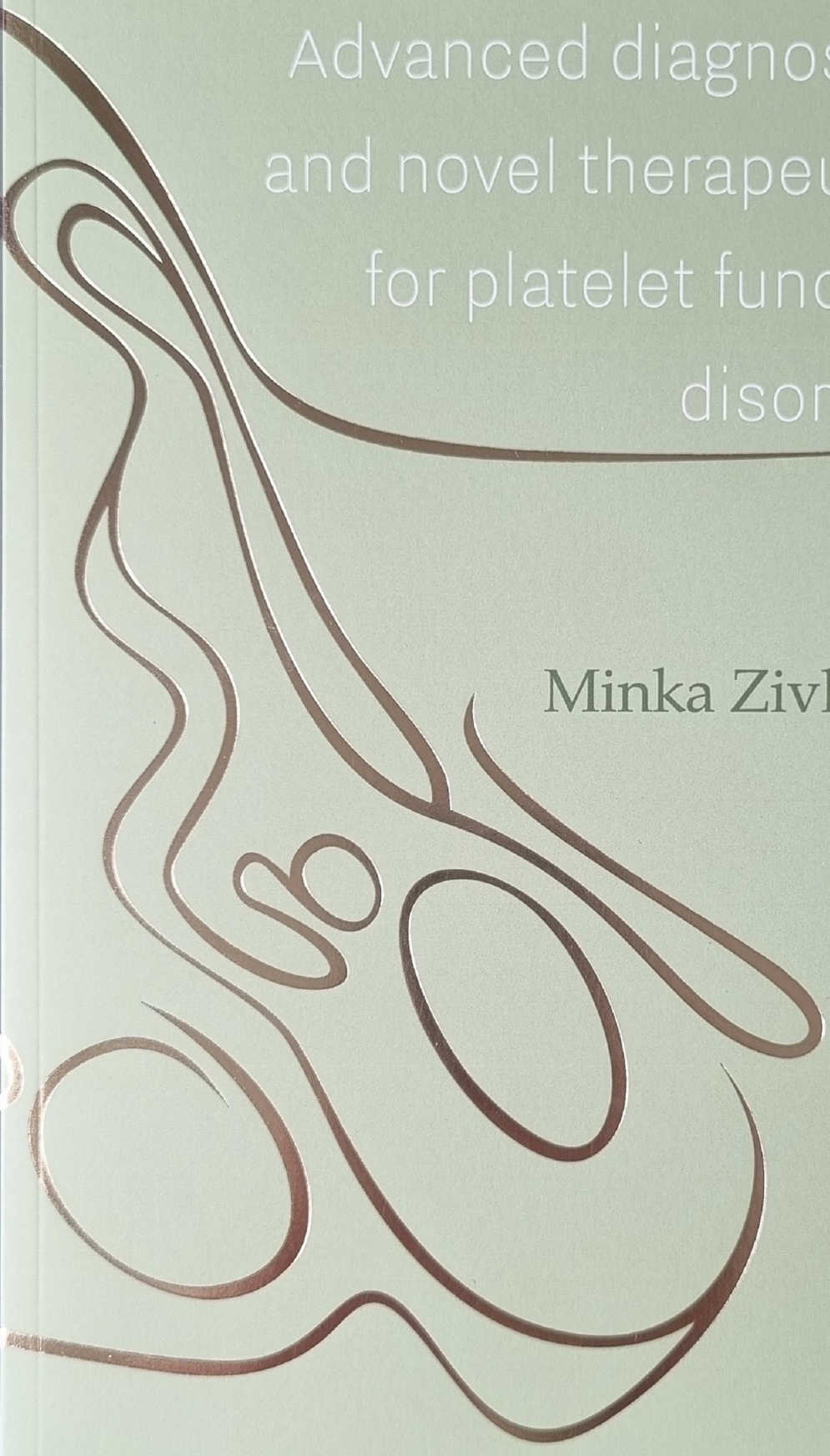

Advanced Diagnostics and Novel Therapeutics for Platelet Function Disorders

ISBN:	978-90-393-7856-4
DOI:	https://doi.org/10.33540/2845
Cover design:	Minka Zivkovic
Lay-out & cover:	Karin Jansen, persoonlijkproefschrift.nl
Printing:	Ridderprint, ridderprint.nl

Financial support for printing this thesis was kindly provided by CSL Behring, Hemab Therapeutics and Stichting Zeldzame Bloedziekten.

Advanced Diagnostics and Novel Therapeutics for Platelet Function Disorders

Geavanceerde diagnostiek en nieuwe therapeutische benaderingen voor bloedplaatjesfunctiestoornissen

(met een samenvatting in het Nederlands)

Proefschrift

ter verkrijging van de graad van doctor aan de
Universiteit Utrecht
op gezag van de
rector magnificus, prof. dr. ir. W. Hazeleger,
ingevolge het besluit van het College voor Promoties
in het openbaar te verdedigen op

donderdag 22 mei 2025 des middags te 2.15 uur

door

Minka Živković

geboren op 11 maart 1997
te Ede

Promotor:

Prof. dr. R.E.G. Schutgens

Copromotor:

Dr. R.T. Urbanus

Beoordelingscommissie:

Prof. dr. ir. Y. Henskens
Prof. dr. J.H.W. Leusen (voorzitter)
Prof. dr. J.A. Lisman
Prof. dr. M.C. Minnema
Prof. dr. J.P.G. Sluijter

Dit proefschrift werd (mede) mogelijk gemaakt met financiële steun van het SYMPHONY consortium (NWO-NWA projectnummer 1160.18.038).

TABLE OF CONTENTS

Chapter 1	**General introduction** Outline of this thesis	6
Part I Advanced diagnostics		
Chapter 2	Functional characterization of a nanobody-based glycoprotein VI-specific platelet agonist	22
Chapter 3	A rapid whole-blood adenosine triphosphate secretion test can be used to exclude platelet-dense granule deficiency	52
Chapter 4	Proteomic analysis indicates lower abundance of platelet alpha-granule proteins in Glanzmann thrombasthenia	74
Part II Novel therapeutics		
Chapter 5	A bispecific antibody approach for the potential prophylactic treatment of inherited bleeding disorders	106
Chapter 6	**Summary and General discussion**	178
Appendices		
	Dutch summary (Nederlandse samenvatting)	196
	List of publications	198
	Acknowledgements (dankwoord)	202
	About the author	209

Chapter 1

General introduction

GENERAL INTRODUCTION

Platelet function in hemostasis

Platelets are small, anucleate cell fragments derived from megakaryocytes in the bone marrow. With a lifespan of approximately 7 to 10 days, platelets play a pivotal role in maintaining hemostasis, the process by which the body stops bleeding and repairs vascular injury[1]. These cellular components are crucial in the initial response to vascular damage, facilitating the formation of a hemostatic plug to prevent excessive blood loss. Their function is regulated through a complex interplay of vascular, cellular, and molecular mechanisms (**Fig. 1**)[2].

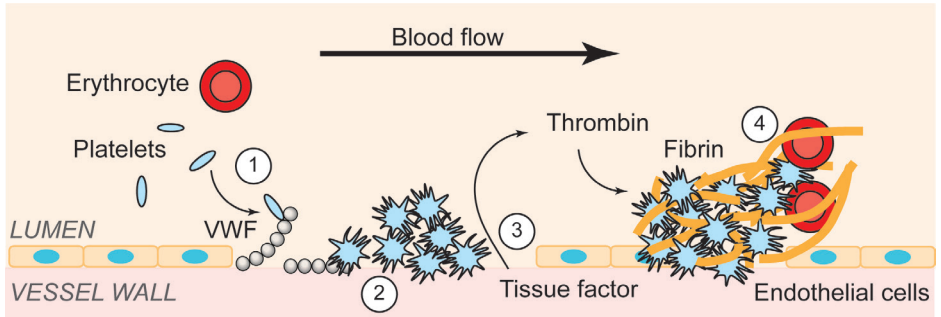

Fig. 1: Platelets play a pivotal role in maintaining hemostasis.

Hemostasis is a highly regulated and dynamic process that can be divided into primary and secondary hemostasis. In primary hemostasis, platelets adhere to the exposed subendothelial matrix at sites of vascular injury. This adhesion is mediated by interactions between platelet surface receptors and matrix proteins such as collagen and von Willebrand Factor (VWF)[3]. Upon activation, platelets release their granule content, including adenosine diphosphate (ADP), thromboxane A2 (TxA2), and serotonin, which further promote platelet activation, aggregation and vasoconstriction[4,5]. Aggregating platelets form a temporary platelet plug, that quickly seals small vascular injuries[6]. Secondary hemostasis involves the activation of the coagulation cascade through the extrinsic and intrinsic pathway, which stabilizes the initial platelet plug with a fibrin mesh[7]. Platelets provide a phospholipid surface that is essential for the assembly of various coagulation factors, facilitating the conversion of prothrombin to thrombin[8,9]. Thrombin then converts fibrinogen to fibrin, which polymerizes to form a stable clot[10]. Failure to form a platelet plug results in immediate

bleeding, while failure to form sufficient amounts of fibrin is associated with temporary cessation of bleeding, followed by re-bleeding when the platelet plug disintegrates.

Platelet activation and aggregation

Platelet activation is a multi-step process involving shape change, granule release, and surface receptor expression[11]. In the bloodstream, platelets are pushed towards the vessel wall by the presence of red blood cells that are in the center of the flowing blood[12]. In this way, platelets can bind to subendothelial collagen that is exposed at sites of vascular injury. Under high shear stress, platelets are captured from the circulation through glycoprotein Ib (GPIb) by VWF bound to collagen[13]. As a result, platelets tether to the surface and roll over VWF until they can adhere to the extracellular matrix (ECM). Platelets can then adhere firmly to the ECM through interactions between integrins and ECM proteins, like α2β1 to collagen, αIIbβ3 to VWF and αvβ3 to laminin[14–16]. Activation of platelets is triggered by collagen through GPVI and thrombin through Protease-Activated Receptor (PAR)-1 and PAR-4, leading to secretion of granule content[4,17]. Platelets contain several organelles, including lysosomes and platelet-specific storage organelles: alpha (α)-granules and dense (δ)-granules. α-granules contain mainly proteins such as platelet factor-4, β-thromboglobulin, fibrinogen and VWF, whereas δ-granules contain serotonin, ADP and calcium[4]. Upon platelet activation, myosin associates with actin filaments, leading to centralization of the granules and eventually their secretion[18]. Secretion of ADP and synthesis of TxA2 from released arachidonic acid (AA) results in further platelet activation by binding to their respective receptors on the platelet surface. This also activates platelets more remote from the ECM. The binding of these agonists initiates elevation of cytosolic calcium ions and intracellular signaling pathways, leading to the activation of integrin receptors such as the fibrinogen receptor αIIbβ3[19,20]. When platelets are activated, fibrinogen can bind to αIIbβ3, resulting in platelet-platelet interaction and aggregation to form a hemostatic plug[21,22] (**Fig. 2**).

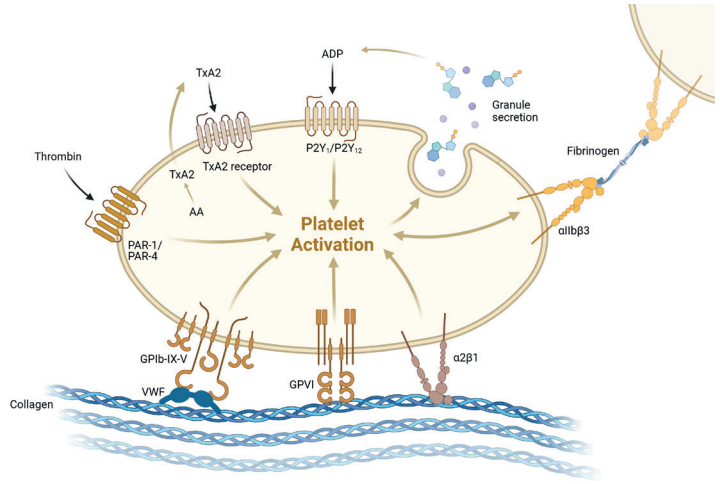

Fig. 2: Platelet adhesion, activation and aggregation. Platelets are captured from the circulation through VWF bound to collagen via the GPIb-IX-V complex and can stably adhere to collagen through GPVI and integrin α2β1. Additionally, platelets are activated with thrombin through PAR-1 and PAR-4. Platelet activation leads to α- and δ-granule secretion, containing ADP. ADP further activates platelets through P2Y1/P2Y12. Thromboxane A2 (TxA2) synthesized from arachidonic acid (AA) also activates platelets through the TxA2 receptor. Activation of platelets triggers intrinsic signaling pathways, leading to activation of integrin αIIbβ3. This results in platelet-platelet interaction through fibrinogen and platelet aggregation. *Created in https://BioRender.com.*

Clinical implications of platelet defects

The regulation of platelet activity and hemostasis is crucial to maintain the balance between bleeds and thrombosis. Defects in platelet function or inadequate numbers of circulating platelets (thrombocytopenia) can lead to significant clinical consequences. A normal platelet count ranges from 150 to 450 x 10^9 platelets per liter blood. Severe thrombocytopenia can result in excessive bleeding after trauma (<30 x 10^9 / L) or spontaneous bleeds (<10 x 10^9 / L)[23]. On the other hand, thrombocythemia, an abnormally high platelet count, can increase the risk of thrombotic events[24,25]. However, when high platelet counts are associated with impaired platelet function, like in essential thrombocythemia, bleeding complications can occur[26].

Dysfunctional platelets can lead to severe bleeds. Platelet disorders can be divided into several categories, like deficient surface integrins or storage granules (**Table 1**). Understanding the role of platelets in hemostasis is essential for diagnosing and treating these conditions. In this thesis, we focus on the current gaps in both diagnosing and treatment of inherited platelet disorders.

Table 1: Inherited platelet disorders.

Category	Disorder	Biology	Bleeding severity
Deficient adhesion / aggregation surface receptors	Glanzmann thrombasthenia[27]	Defects of fibrinogen receptor αIIbβ3: Type 1: <5% Type 2: 5-20% Type 3: >20% but non-functional No binding of fibrinogen → no platelet aggregation.	Severe
	Bernard-Soulier syndrome[28]	Defects of GPIb: deficient or non-functional. No binding to VWF → no platelet adhesion.	Severe
Deficient activation surface receptors	GPVI deficiency[29]	Defects of collagen receptor GPVI. No platelet response to collagen or CRP-XL.	Mild
	$P2Y_{12}$ deficiency[30]	Defects of ADP receptor $P2Y_{12}$. No platelet response to ADP and decreased secondary platelet activation.	Mild to moderate
Defects in secondary platelet activation	TxA2 pathway[31]	Defects of TxA2 or TxA2 receptor → decreased platelet activation and aggregation.	Mild to moderate
	Delta storage pool disease - Hermansky-Pudlak[32] - Chédiak-Higashi[33]	Decreased number or content of δ-granules, causing decreased secondary platelet activation.	Mild
α-granule defects	Gray platelet syndrome[34]	Large platelets with decreased number or content of α-granules, causing short platelet survival.	Mild
Signal transduction defects	Impaired pleckstrin phosphorylation[35]	Impaired αIIbβ3 activation, leading to decreased platelet aggregation.	Mild
	$G\alpha_q$ deficiency[36]	Impaired agonist induced platelet aggregation and secretion.	Mild
(Macro) thrombocytopenia	MYH9-related platelet disorders[37]	Large platelets and low platelet count. No platelets in small vessels.	Varies from no symptoms to mild bleeds
	Thrombocytopenia[38]	Low platelet count resulting in decreased platelet adhesion and aggregation.	Varies from no symptoms to severe bleeds

Diagnostic challenges of platelet disorders

Current diagnostics for platelet function disorders include a range of laboratory techniques for evaluating platelet count, function, and reactivity. The initial assessment typically involves a complete blood count to measure platelet number and mean platelet volume (MPV)[39]. For functional analysis, light transmission aggregometry (LTA) remains the gold standard, where platelets are exposed to various agonists, like ADP, collagen and epinephrin to assess aggregation response[40]. Flow cytometry is increasingly used to analyze surface marker expression and granule release, providing insights into specific platelet activation pathways[41]. Additionally, genetic testing and sequencing can also be used to identify hereditary platelet disorders by detecting mutations in genes encoding for platelet glycoproteins, granule constituents, and signaling molecules. Although these diagnostic tools provide a comprehensive evaluation of platelet function, most of the currently used tests for platelet function disorder are associated with several disadvantages.

LTA for example has an inadequate sensitivity for detecting mild platelet function disorders, like storage pool disease (SPD). Moreover, there is no consensus regarding the diagnostic criteria for SPD. This has a major impact on adequate diagnosis of SPD. Furthermore, the agonists used in diagnostic assays are poorly standardized. A multicenter study of the Scientific and Standardization Committee of the International Society on Thrombosis and Haemostasis aimed for standardization of several platelet agonists in LTA[42]. Although the first steps are made for introduction of some changes to current research and clinical practices, additional research is needed to establish standardized diagnostics, like extending the concentration range of agonists that are used at different sites.

Although genetic testing and sequencing seems promising according to some studies[43], application of genetic testing for patients without a confirmed platelet function disorder seems to be minimally effective[44]. Moreover, this approach is particularly effective for thrombocytopenia but less so for mild platelet function disorders. This is primarily due to limited understanding of the exact molecular processes in platelets: the list of genes implicated in platelet disorders comprises only 70 genes, whereas around 7000 genes, of which ca. 30% non-coding, are involved in platelet function[45].

Low prevalent platelet function disorders, like Glanzmann thrombasthenia and Bernard-Soulier syndrome are relatively easy to diagnose[46]. These rare conditions often show distinct clinical features and specific laboratory findings in platelet morphology or function. In contrast, the more prevalent platelet disorders, such as secretion defects, pose a substantial diagnostic challenge[46]. These defects may present with subtle or non-specific clinical symptoms and often require advanced diagnostic techniques. **Figure 3** displays the relative prevalence, severity and diagnostic difficulty for platelet function disorders and other inherited bleeding disorders. The diagnostic difficulty for high-prevalence platelet disorders underscores the critical need for improved diagnostic methodologies.

Other challenges in diagnostics for platelet function disorders include that some tests require large amounts of blood, which can especially be challenging for pediatric patients or those with difficult venous access. Additionally, the samples often need processing before testing, making it time-consuming and labor-intensive. Due to the complexity of some tests, they often show long turn-around times, which is disadvantageous for rapid patient management and clinical decision-making. Another critical disadvantage is the necessity for specialized laboratories. Diagnosing platelet function disorders often requires advanced techniques, equipment and expertise, that are not commonly available in general laboratories. As a result, samples or patients need to be sent to specialized centers, which adds logistical challenges and further delays. Moreover, patients can even remain underdiagnosed, due to lack of standardized diagnostic tools and external quality assurance for platelet assays.

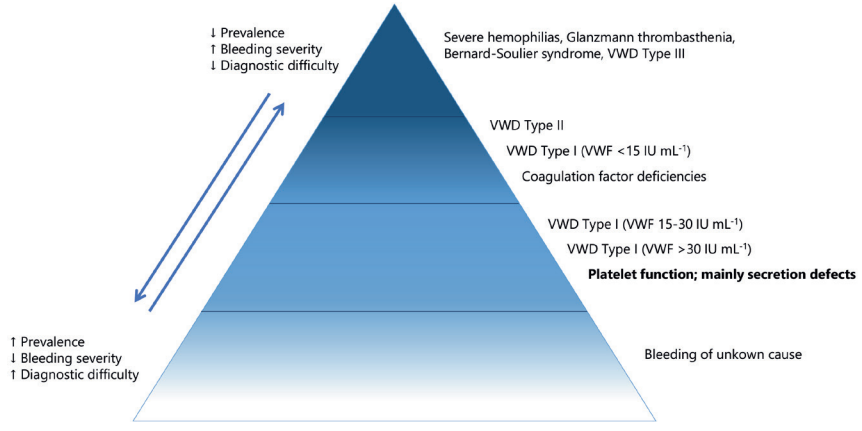

Fig. 3: Relative prevalence, bleeding severity and diagnostic difficulty of inherited bleeding disorders. The higher in the triangle, the lower the prevalence of the disorder, higher the severity and less difficult to diagnose. Lower in the triangle are disorders that are high in prevalence, lower in severity and more difficult to diagnose. VWD, von Willebrand Disease; VWF, von Willebrand Factor. *According to Mezzano and Quiroga*[46].

No prophylactic treatment for platelet function disorders

Current treatment for platelet function disorders is specific for the type and severity of the disorder, and aims to prevent bleeding complications with minimal adverse effects. For inherited platelet function disorders such as Glanzmann thrombasthenia and Bernard-Soulier syndrome, prophylactic treatment is not available and therapeutic approaches always include on-demand treatment, such as the use of antifibrinolytic agents (e.g. tranexamic acid and aminocaproic acid) to prevent bleeds during minor surgical procedures[47]. Another effective method in management of bleeding episodes in patients with platelet defects is administration of hemostatic agents like recombinant activated coagulation factor VII (rFVIIa) (NovoSeven®)[48,49]. Agents like this prove that enhancement of secondary hemostasis can address issues in primary hemostasis. However, its short half-life of 2-4 hours poses challenges for its use as prophylactic treatment. Lastly, platelet transfusions are highly efficient in managing severe bleeding episodes, although they carry risks such as alloimmunization and are not always accessible in emergency situations[50,51].

Emerging therapies, such as gene therapy and novel pharmacological agents are under investigation and hold promise for more effective and individualized treatment strategies. Besides its proven effectiveness for severe hemophilia A[52], gene therapy is also emerging for platelet disorders, such as Wiskott-Aldrich syndrome[53].

However, as of now, no prophylactic treatment is available for patients with inherited platelet function disorders. The development of such treatment would be life-changing for patients suffering from platelet defects.

OUTLINE OF THIS THESIS

In summary, platelet function disorders such as secretion defects have a high diagnostic difficulty. Their relatively high prevalence underscores the necessity for improved diagnostic assays. Additionally, currently no prophylactic treatment is available for inherited platelet function disorders. Therefore, the aims of this thesis are to improve diagnostic tools for platelet function disorders and to develop potential novel therapeutics for inherited bleeding disorders.

The first part of this thesis focuses on advanced diagnostics for inherited platelet function disorders (IPFD). In **Chapter 2**, we show a tetrameric nanobody-based glycoprotein VI (GPVI) platelet agonist. We studied the ability of this agonist to activate platelets in a similar way as current used agonists in material of patients with IPFDs. In **Chapter 3** we validate a novel rapid test for delta storage pool disease (δ-SPD). Here we show that this whole blood microarray is able to distinguish δ-SPD from non-SPD patients and that this test can be used for exclusion of δ-SPD in first-line platelet diagnostics. **Chapter 4** focuses on the proteomic landscape of platelets of patients with Glanzmann thrombasthenia. We have seen that, compared with platelets of healthy controls, Glanzmann platelets show a reduction in expression of several platelet α-granule proteins.

The second part of this thesis describes novel potential prophylactic treatment for patients with inherited bleeding disorders. **Chapter 5** reports a bispecific antibody, HMB-001, for the potential prophylactic treatment of inherited bleeding disorders. HMB-001 recognizes activated coagulation factor FVII (FVIIa) with one arm and activated platelet specific receptor TREM-Like Transcript-1 (TLT-1) with its other arm. As a result, HMB-001 targets endogenous FVIIa to the activated platelet surface, resulting in thrombin formation and subsequent fibrin formation. The findings of this thesis are summarized and discussed within a broader perspective in **Chapter 6**.

REFERENCES

1. Holinstat M. Normal platelet function. *Cancer Metastasis Rev*. 2017;36(2):195-198. doi:10.1007/s10555-017-9677-x
2. van der Meijden PEJ, Heemskerk JWM. Platelet biology and functions: new concepts and clinical perspectives. *Nat Rev Cardiol*. 2019;16(3):166-179. doi:10.1038/s41569-018-0110-0
3. Ruggeri ZM, Mendolicchio GL. Adhesion mechanisms in platelet function. *Circ Res*. 2007;100(12):1673-1685. doi:10.1161/01.RES.0000267878.97021.ab
4. Golebiewska EM, Poole AW. Platelet secretion: From haemostasis to wound healing and beyond. *Blood Rev*. 2015;29(3):153-162. doi:10.1016/j.blre.2014.10.003
5. Vanhoutte PM, Houston DS. Serotonin, platelets, and vascular function. In: Magro A, Osswald W, Reis D, Vanhoutte P, eds. *Central and Peripheral Mechanisms of Cardiovascular Regulation*. Springer US; 1986:135-161. doi:10.1007/978-1-4615-9471-0_6
6. LaPelusa A, Dave HD. Physiology, Hemostasis. In: *StatPearls*. StatPearls Publishing; 2024.
7. Stassen JM, Arnout J, Deckmyn H. The hemostatic system. *Curr Med Chem*. 2004;11(17):2245-2260. doi:10.2174/0929867043364603
8. Koseoglu S, Meyer AF, Kim D, et al. Analytical characterization of the role of phospholipids in platelet adhesion and secretion. *Anal Chem*. 2015;87(1):413-421. doi:10.1021/ac502293p
9. Krishnaswamy S. The transition of prothrombin to thrombin. *J Thromb Haemost*. 2013;11 Suppl 1(0 1):265-276. doi:10.1111/jth.12217
10. Stemberger A, Blümel G. Fibrinogen-fibrin conversion and inhibition of fibrinolysis. *Thorac Cardiovasc Surg*. 1982;30(4):209-214. doi:10.1055/s-2007-1022389
11. Blockmans D, Deckmyn H, Vermylen J. Platelet activation. *Blood Rev*. 1995;9(3):143-156. doi:10.1016/0268-960x(95)90020-9
12. Aarts PA, van den Broek SA, Prins GW, Kuiken GD, Sixma JJ, Heethaar RM. Blood platelets are concentrated near the wall and red blood cells, in the center in flowing blood. *Arteriosclerosis*. 1988;8(6):819-824. doi:10.1161/01.atv.8.6.819
13. Kroll MH, Harris TS, Moake JL, Handin RI, Schafer AI. von Willebrand factor binding to platelet GpIb initiates signals for platelet activation. *J Clin Invest*. 1991;88(5):1568-1573. doi:10.1172/JCI115468
14. Thomas MR, Storey RF. The role of platelets in inflammation. *Thromb Haemost*. 2015;114(3):449-458. doi:10.1160/TH14-12-1067
15. Jennings LK. Mechanisms of platelet activation: need for new strategies to protect against platelet-mediated atherothrombosis. *Thromb Haemost*. 2009;102(2):248-257. doi:10.1160/TH09-03-0192
16. Clemetson KJ. Platelets and primary haemostasis. *Thromb Res*. 2012;129(3):220-224. doi:10.1016/j.thromres.2011.11.036

17. Andersen H, Greenberg DL, Fujikawa K, Xu W, Chung DW, Davie EW. Protease-activated receptor 1 is the primary mediator of thrombin-stimulated platelet procoagulant activity. *Proc Natl Acad Sci USA*. 1999;96(20):11189-11193. doi:10.1073/pnas.96.20.11189
18. Fox JE, Phillips DR. Role of phosphorylation in mediating the association of myosin with the cytoskeletal structures of human platelets. *J Biol Chem*. 1982;257(8):4120-4126.
19. Ma YQ, Qin J, Plow EF. Platelet integrin alpha(IIb)beta(3): activation mechanisms. *J Thromb Haemost*. 2007;5(7):1345-1352. doi:10.1111/j.1538-7836.2007.02537.x
20. Varga-Szabo D, Braun A, Nieswandt B. Calcium signaling in platelets. *J Thromb Haemost*. 2009;7(7):1057-1066. doi:10.1111/j.1538-7836.2009.03455.x
21. Rumbaut RE, Thiagarajan P. Platelet Aggregation. 2010.
22. Aoki T, Tomiyama Y, Honda S, et al. Association of the antagonism of von Willebrand factor but not fibrinogen by platelet alphaIIbbeta3 antagonists with prolongation of bleeding time. *J Thromb Haemost*. 2005;3(10):2307-2314. doi:10.1111/j.1538-7836.2005.01534.x
23. Arnold DM. Bleeding complications in immune thrombocytopenia. *Hematology Am Soc Hematol Educ Program*. 2015;2015:237-242. doi:10.1182/asheducation-2015.1.237
24. Ma W, Karakas D, Chen ZY, Ni H. Aging, chronic inflammation, and platelet hyperactivity. *Ann Blood*. 2020;5:18-18. doi:10.21037/aob-20-32
25. Schafer AI. Thrombocytosis and thrombocythemia. *Blood Rev*. 2001;15(4):159-166. doi:10.1054/blre.2001.0162
26. Elliott MA, Tefferi A. Pathogenesis and management of bleeding in essential thrombocythemia and polycythemia vera. *Curr Hematol Rep*. 2004;3(5):344-351.
27. Krause KA, Graham BC. Glanzmann Thrombasthenia. In: *StatPearls*. StatPearls Publishing; 2024.
28. Almomani MH, Mangla A. Bernard-Soulier Syndrome. In: *StatPearls*. StatPearls Publishing; 2024.
29. Arthur JF, Dunkley S, Andrews RK. Platelet glycoprotein VI-related clinical defects. *Br J Haematol*. 2007;139(3):363-372. doi:10.1111/j.1365-2141.2007.06799.x
30. Cattaneo M. The platelet $P2Y_{12}$ receptor for adenosine diphosphate: congenital and drug-induced defects. *Blood*. 2011;117(7):2102-2112. doi:10.1182/blood-2010-08-263111
31. Mundell SJ, Mumford A. TBXA2R gene variants associated with bleeding. *Platelets*. 2018;29(7):739-742. doi:10.1080/09537104.2018.1499888
32. De Jesus Rojas W, Young LR. Hermansky-Pudlak Syndrome. *Semin Respir Crit Care Med*. 2020;41(2):238-246. doi:10.1055/s-0040-1708088
33. Talbert ML, Malicdan MCV, Introne WJ. Chediak-Higashi syndrome. *Curr Opin Hematol*. 2023;30(4):144-151. doi:10.1097/MOH.0000000000000766
34. Michelson AD. Gray platelet syndrome. *Blood*. 2013;121(2):250. doi:10.1182/blood-2012-09-455550

35. Gabbeta J, Yang X, Sun L, McLane MA, Niewiarowski S, Rao AK. Abnormal inside-out signal transduction-dependent activation of glycoprotein IIb-IIIa in a patient with impaired pleckstrin phosphorylation. *Blood*. 1996;87(4):1368-1376.

36. Gabbeta J, Yang X, Kowalska MA, Sun L, Dhanasekaran N, Rao AK. Platelet signal transduction defect with Galpha subunit dysfunction and diminished Galphaq in a patient with abnormal platelet responses. *Proc Natl Acad Sci USA*. 1997;94(16):8750-8755. doi:10.1073/pnas.94.16.8750

37. Althaus K, Greinacher A. MYH9-related platelet disorders. *Semin Thromb Hemost*. 2009;35(2):189-203. doi:10.1055/s-0029-1220327

38. Greenberg EML, Kaled ESS. Thrombocytopenia. *Crit Care Nurs Clin North Am*. 2013;25(4):427-434, v. doi:10.1016/j.ccell.2013.08.003

39. Kottke-Marchant K, Corcoran G. The laboratory diagnosis of platelet disorders. *Arch Pathol Lab Med*. 2002;126(2):133-146. doi:10.1043/0003-9985(2002)126<0133:TLDOPD>2.0.CO;2

40. Frontroth JP. Light transmission aggregometry. *Methods Mol Biol*. 2013;992:227-240. doi:10.1007/978-1-62703-339-8_17

41. Linden MD. Platelet flow cytometry. *Methods Mol Biol*. 2013;992:241-262. doi:10.1007/978-1-62703-339-8_18

42. Alessi M-C, Coxon C, Ibrahim-Kosta M, et al. Multicenter evaluation of light transmission platelet aggregation reagents: communication from the ISTH SSC Subcommittee on Platelet Physiology. *J Thromb Haemost*. 2023;21(9):2596-2610. doi:10.1016/j.jtha.2023.05.027

43. Downes K, Megy K, Duarte D, et al. Diagnostic high-throughput sequencing of 2396 patients with bleeding, thrombotic, and platelet disorders. *Blood*. 2019;134(23):2082-2091. doi:10.1182/blood.2018891192

44. Blaauwgeers MW, van Asten I, Kruip MJHA, et al. The limitation of genetic testing in diagnosing patients suspected for congenital platelet defects. *Am J Hematol*. 2020;95(1):E26-E28. doi:10.1002/ajh.25667

45. Xie G-Y, Liu C-J, Miao Y-R, Xia M, Zhang Q, Guo A-Y. A comprehensive platelet expression atlas (PEA) resource and platelet transcriptome landscape. *Am J Hematol*. 2022;97(1):E18-E21. doi:10.1002/ajh.26393

46. Mezzano D, Quiroga T. Diagnostic challenges of inherited mild bleeding disorders: a bait for poorly explored clinical and basic research. *J Thromb Haemost*. 2019;17(2):257-270. doi:10.1111/jth.14363

47. Estcourt LJ, Desborough M, Brunskill SJ, et al. Antifibrinolytics (lysine analogues) for the prevention of bleeding in people with haematological disorders. *Cochrane Database Syst Rev*. 2016;3(3):CD009733. doi:10.1002/14651858.CD009733.pub3

48. Hedner U. NovoSeven as a universal haemostatic agent. *Blood Coagul Fibrinolysis*. 2000;11 Suppl 1:S107-11. doi:10.1097/00001721-200004001-00020

49. Zotz RB, Poon M-C, Di Minno G, D'Oiron R, Glanzmann Thrombasthenia Registry Investigators. The international prospective glanzmann thrombasthenia registry: pediatric treatment and outcomes. *TH Open*. 2019;3(3):e286-e294. doi:10.1055/s-0039-1696657

50. Khan AI, Anwer F. Platelet Transfusion. In: *StatPearls*. StatPearls Publishing; 2023.

51. Grainger JD, Thachil J, Will AM. How we treat the platelet glycoprotein defects; Glanzmann thrombasthenia and Bernard Soulier syndrome in children and adults. *Br J Haematol*. 2018;182(5):621-632. doi:10.1111/bjh.15409

52. Valoctocogene roxaparvovec (Roctavian) - a gene therapy for severe hemophilia A. *Med Lett Drugs Ther*. 2023;65(1686):157-158. doi:10.58347/tml.2023.1686c

53. Labrosse R, Chu JI, Armant MA, et al. Outcomes of hematopoietic stem cell gene therapy for Wiskott-Aldrich syndrome. *Blood*. 2023;142(15):1281-1296. doi:10.1182/blood.2022019117

Part I

ADVANCED DIAGNOSTICS

Chapter 2

Functional characterization of a nanobody-based glycoprotein VI-specific platelet agonist

Minka Zivkovic[1,2], Elisabeth Pols - van Veen[1,2], Vossa van der Vegte[1,2], Silvie AE Sebastian[1,3], Annick S de Moor[1], Suzanne JA Korporaal[3], Roger EG Schutgens[1], Rolf T Urbanus[1,2]; for the TiN study group and SYMPHONY consortium

[1] Center for Benign Haematology, Thrombosis and Haemostasis, Van Creveldkliniek, University Medical Center Utrecht, Utrecht University, Utrecht, the Netherlands

[2] Circulatory Health Research Center, University Medical Center Utrecht, Utrecht, the Netherlands

[3] Central Diagnostic Laboratory, University Medical Center Utrecht, Utrecht, the Netherlands

Res Pract Thromb Haemost. 2024 Oct 3;8(7):102582.

SUMMARY

Background: Glycoprotein (GP)VI is a platelet-specific collagen receptor required for platelet activation during hemostasis. Platelet reactivity toward collagen is routinely assessed during diagnostic workup of platelet disorders. GPVI can be activated by inducing receptor clustering with suspensions of fibrillar collagen or synthetic cross-linked collagen-related peptide (CRP-XL). However, these suspensions are poorly standardized or difficult to produce. Nanobodies are small recombinant camelid-derived heavy-chain antibody variable regions. They are highly stable, specific, and ideal candidates for developing a stable GPVI agonist for diagnostic assays.

Objectives: Develop a stable nanobody-based GPVI agonist.

Methods: Nanobody D2 (NbD2) was produced as dimers and purified. Tetramers were generated via C-terminal fusion of dimers with click chemistry. Nanobody constructs were functionally characterized with light transmission aggregometry (LTA) in platelet-rich plasma and whole blood flow cytometry. Diagnostic performance was assessed in patients with inherited platelet function disorders with LTA and flow cytometry.

Results: NbD2 was specific for human platelet GPVI. Dimers did not result in platelet activation in LTA or flow cytometry settings and fully inhibited CRP-XL-induced P-selectin expression and fibrinogen binding in whole blood and attenuated collagen-induced platelet aggregation in platelet-rich plasma. However, NbD2 tetramers caused full platelet aggregation, as well as P-selectin expression and fibrinogen binding. NbD2 tetramers were able to discriminate between inherited platelet function disorder patients and healthy controls based on fibrinogen binding, similar to CRP-XL.

Conclusion: Nanobody tetramers to GPVI induce platelet activation and can be used to assess the GPVI pathway in diagnostic assays.

Keywords: Diagnostic Tests; Glycoprotein; Nanobodies; Platelet Activation; Platelet Function Tests

INTRODUCTION

Glycoprotein (GP)VI is a megakaryocyte and platelet surface-specific membrane glycoprotein that is identified as the major activating receptor for collagen and also a receptor for other ligands, including fibrin[1]. Upon vessel wall injury, extravascular collagen is exposed to platelets in the circulation. Interaction of platelets with collagen through GPVI results in platelet activation and contributes to thrombus formation[2,3]. GPVI is a type I transmembrane receptor protein and belongs to the immunoglobulin (Ig)-like receptor family. It consists of 2 extracellular Ig domains (D1 and D2), a mucin-like stalk domain, and a short cytoplasmic tail containing calmodulin- and Src kinase-binding sites[2,3]. On the platelet surface, the signaling of GPVI depends on its association with the Fc receptor γ-chain, which contains an immunoreceptor tyrosine-based activation motif. The binding of collagen to GPVI induces receptor cross-linking, leading to the recruitment and activation of downstream signaling molecules, including the receptor tyrosine kinase SYK[4].

Activation of platelets through GPVI signaling is often assessed in diagnostic assays for platelet disorders. Different inherited and acquired disease-causing variants of GPVI are known, which include mutations in the GP6 gene causing the bleeding disorder platelet-type 11, a mild to moderate bleeding disorder characterized by defective platelet activation and aggregation in response to collagen[5-7]. Also, platelets may be deficient in GPVI due to inherited or acquired loss of the protein, the latter through, eg, autoantibody-induced receptor shedding. For instance, the GPVI/Fc receptor γ-chain complex is absent on the platelet surface in anti–GPVI-associated immune thrombocytopenia[8]. Additionally, GPVI deficiency could be nonimmune and associated with Gray platelet syndrome[9]. Besides deficiency of GPVI, some patients have a normal surface expression of GPVI but present with a congenital or acquired GPVI-related signaling defect[10,11]. In these disorders, reduced collagen-induced platelet activation in diagnostic assays is a prominent feature. Secondary deficits in the response to collagen are observed in storage pool deficiencies (SPDs)[12], and since activation of the fibrinogen receptor after collagen stimulation depends on secondary activation through adenosine diphosphate (ADP) secretion or thromboxane A2 production, platelets can show a decreased response to collagen when thromboxane A2 or ADP secretion are decreased or absent[13].

Current agonists that are used in diagnostic assays for platelet function disorders, like aggregation assays and flow cytometry assays[14], include insoluble collagen fiber suspensions, the soluble agonist cross-linked collagen-related peptide (CRP-XL), and the snake venom tetramer protein convulxin. Only the latter 2 are specific to GPVI. Limitations of the GPVI-specific agonists are that they are poorly standardized and difficult to produce, leading to large batch-to-batch variability. Their application in a diagnostic setting would require extensive cross-calibration. As fibrillar collagen suspensions are unsuitable for flow cytometry assays, the critical need for the development of a novel, stable GPVI agonist is underscored most for flow cytometry.

Specific heavy-chain variable domain antibodies, or nanobodies, are small heavy-chain only antibodies derived from camelids such as llamas. Nanobodies retain the antigen specificity of the parental antibody, are highly stable, and can be efficiently produced on a large scale. This makes nanobodies ideal candidates for diagnostic purposes[15]. Within the SYMPHONY consortium[16], one of the aims is the improvement of laboratory diagnostics for patients with inherited bleeding disorders. In the current study, we developed a nanobody that specifically targets the extracellular domain of platelet GPVI. Based on the tetramer structure of convulxin, we produced a tetramer GPVI nanobody that induces platelet activation. We here describe the developmental and functional characterization and clinical validation of this nanobody-based GPVI-specific platelet agonist.

MATERIALS AND METHODS

Subjects

Healthy donors

Healthy controls were recruited among personnel and students at University Medical Center Utrecht by the MiniDonor biobank facility of the University Medical Center Utrecht (Biobank number 18-774) and were free of nonsteroid anti-inflammatory drugs. Approval was obtained from the local ethics review board, and all participants provided written informed consent.

Patients with suspected primary hemostasis disorder

People with a (suspected) platelet disorder in the Netherlands were included in the Thrombocytopathy in the Netherlands study (study number NL53207.041.15), a nationwide cross-sectional study on disease phenotyping, diagnostics, and genetics

at the University Medical Center Utrecht[17,18]. Exclusion criteria were von Willebrand disease and a coagulation factor deficiency. Patients came for a single hospital visit, and blood was collected for whole blood analysis, aggregation with 4 agonists, platelet surface receptor expression, nucleotide content, and genetic analysis. All measurements were done in the same sample, nonblinded. Medical ethical committee approval was obtained, and all patients provided written informed consent.

Blood samples

In all participants, blood was collected from the antecubital vein in 3.2% trisodium citrate vacutainer tubes (BD) through phlebotomy. Blood was processed within 1 to 4 hours after collection. Platelet-rich plasma (PRP) was obtained by centrifugation at 160 × g without brake at room temperature (RT) for 15 minutes. Platelet-poor plasma (PPP) was obtained by centrifugation of the remainder of the blood at 2000 × g for 10 minutes at RT. Washed platelets were isolated from PRP, as described previously[19]. PRP was acidified and centrifuged at 340 × g for 15 minutes. The platelet pellet was resuspended in 4-(2-hydroxyethyl)-1-piperazineethanesulfonic acid (HEPES)-Tyrode's buffer, pH 6.5, with 10 ng/mL prostacyclin. Platelets were centrifuged again at 340 × g for 15 minutes and resuspended in HEPES-Tyrode's buffer, pH 7.3 to a platelet count of 200 × 10^9/L. After isolation, washed platelets were allowed to rest for 30 minutes at RT.

Nanobody selection

The recombinant soluble extracellular domain of human GPVI (sGPVI; amino acids 21-267) was produced as monomer and purified by U-protein express (Utrecht, the Netherlands). Two llamas (*Lama glama*) received 4 rounds of subcutaneous immunizations with 50 µg sGPVI at day 0, 14, 28 and 56. Blood was drawn at 3 months after immunization for peripheral blood B-lymphocyte isolation. Phage display libraries containing the sequences of all V_HH regions of heavy-chain only antibodies were constructed by QVQ (Utrecht, the Netherlands), as described[20]. Nanobodies were selected as described[21], with a few modifications. In short, Nunc PolySorp microtiter plates were coated with NeutrAvidin® (Life Technologies, Carlsbad, CA; 5 µg/mL) in 50 mM Na_2CO_3, 50 mM $NaHCO_3$, 0.05% N_3, pH 9.6 at 4 °C overnight, washed and blocked with 1% bovine serum albumin (BSA) in 137 mM NaCl, 2.7 mM KCl, 9.2 mM Na_2HPO_4, 1.76 mM KH_2PO_4, pH 7.4 (PBS-BSA). All subsequent incubations took place at RT for 1 hour under gentle agitation on a plate shaker, unless otherwise indicated. GPVI was biotinylated with EZ-Link Sulfo-NHS-LC-Biotin according to manufacturer's

instructions (Life Technologies) and incubated in NeutrAvidin coated wells (1.5 µg/mL). Plates were washed and incubated with phages in PBS-BSA under gentle agitation for 2 hours. Plates were washed 15 times with PBS containing 0.1% Tween-20, followed by 3 times with PBS only. Bound phages were eluted with 0.1 M triethylamine, collected and transferred to neutralizing buffer (1 M Tris/HCl, pH 7.5, sterile). *Escherichia coli* (*E. coli*) (strain TG1) were incubated with phages, plated on Yeast Tryptone Broth agar plates containing 2% glucose and 100 µg/mL ampicillin and grown overnight at 37 °C. Single colonies were picked, grown for 5 hours at 37 °C, followed by induction of nanobody production with isopropyl β-D-1-thiogalactopyranoside (IPTG, 1 mM) overnight. Binding of nanobodies to GPVI was assessed on microtiter plates with NeutrAvidin captured GPVI-biotin. GPVI-specific nanobodies were sequenced. Unique clones were produced in large quantity and purified with immobilized metal affinity chromatography (IMAC) on TALON® Superflow™ Sepharose. Lead nanobody D2 (NbD2) had the highest apparent affinity and was used for the current study.

Nanobody production and purification

The DNA sequence of anti-GPVI clone D2 was designed as a monomer or as a dimer with a 5-residue glycine-serine linker (GGGGS) codon optimized for production in Escherichia coli and ordered as a GeneBlock (Integrated DNA Technologies) with 5′ BamHI and 3′ NotI restriction sites. NbD2 dimer was then cloned into the pTH4.click production vector, which encodes a C-terminal Myc-tag for detection, a flexible glycine-serine linker, the LPETG sortase recognition sequence, and a His-tag for purification[21]. Nanobodies were expressed in BL21 Star (DE3)pLysS One Shot Chemically Competent E. coli (Invitrogen) in a bioreactor with autoinduction medium (1% tryptone, 0.5% yeast extract, 25 mM $[NH_4]_2SO_4$, 50 mM KH_2PO_4, 50 mM Na_2HPO_4, 54 mM glycerol, 2.8 mM glucose, 5.6 mM lactose, 1 mM $MgSO_4$) with 100 µg/mL ampicillin and 34 µg/mL chloramphenicol at RT overnight. Bacteria were harvested from the bioreactor and centrifuged at 5000 × g for 15 minutes at 4 °C. Pelleted bacteria were resuspended in 25 mM HEPES, 500 mM NaCl, pH 7.8 with 1 µg/mL DNAse, and 10 µM $MgCl_2$. Bacteria were lysed with 3 subsequent freeze-thaw cycles in liquid nitrogen at 37 °C, followed by incubation with lysozyme from chicken egg white (Sigma-Aldrich) for 10 minutes at 37 °C. Lysed bacteria were centrifuged for 1 hour at 13,000 × g at 4 °C to pellet insoluble material, and nanobodies were purified from the supernatant with immobilized metal affinity chromatography on TALON Sepharose (Cytiva). All nanobodies were separated from remaining impurities with size-exclusion chromatography (SEC) on a HiLoad 26/600 75 pg gel column (Cytiva).

Tetramer generation with copper-free click chemistry

NbD2 dimers were labeled with a C-terminal azide using a sortagging procedure, as described[21]. In short, 100 µM purified NbD2 dimer was incubated with 1 µM sortase A (SrtA) and 1 mM H-$(Gly)_3$-Lys(N3)-OH*HCl (IRIS Biotech GmbH) for 2 hours at 25 °C to replace the C-terminal His-tag with a C-terminal azido group. Unlabeled dimers and SrtA were removed with immobilized metal affinity chromatography on TALON Sepharose. Next, azide-conjugated dimers were incubated for 18 hours at RT with the bivalent DBCO-PEG4-DBCO linker (BroadPharm) to generate tetramers. Tetramers were separated from unclicked dimers with SEC on a HiLoad 26/600 200 pg gel column. Purity was assessed with sodium dodecyl sulfate–polyacrylamide gel electrophoresis and Coomassie blue staining.

Determination of binding affinity to recombinant GPVI

The binding of NbD2 to soluble GPVI (sGPVI) was analyzed with surface plasmon resonance on a Biacore T100 system (Cytiva). A monoclonal anti–c-Myc antibody (clone 9E10; in-house produced; 50 µg/mL) was immobilized on reference and measurement flow channels of a CM5 sensor chip (Cytiva) with amine-coupling chemistry, according to the manufacturer's instructions. Binding experiments were performed in flow buffer (10 mM HEPES, 150 mM NaCl, pH 7.4 with 0.05% Tween 20). NbD2 dimers (12.5 µg/mL) were captured on the measurement flow channels at a flow rate of 30 µL/min, followed by injection of sGPVI (0, 5, 10, 25, 50, and 100 nM) into reference and measurement channels at a flow rate of 30 µL/min for 1 minute to allow analysis of 1:1 protein interactions without contributions of avidity. Dissociation was monitored for 10 minutes. All flow channels were regenerated with 100 mM glycine, pH 2.7, at a flow rate of 30 µL/min for 1 minute, followed by a 10-minute stabilization period. Sensorgrams were adjusted for signal in the reference channel, and binding kinetics were determined by fitting the data to a 1:1 Langmuir binding model with Biacore T100 Evaluation software, version 2.0.4 (Cytiva).

Light transmission aggregometry

The aggregation of platelets was assessed with light transmission aggregometry (LTA) in a Chrono-Log model 700 (Kordia). The platelet count in PRP was adjusted to 200 × 10^9/L with PPP. PPP was used as a blank in the aggregometer. To assess inhibition of aggregation by NbD2 monomers and NbD2 dimers, PRP was stimulated with either an excess (1 µM) NbD2 dimers alone or PRP was preincubated for 15 minutes at 37 °C at 900 rpm with 400 nM NbD2 monomers followed by 5 µg/mL Collagen

Reagens HORM suspension (Takeda production site in Linz) or 1 µM D2 dimers followed by either 4 µg/mL HORM collagen or 1 µg/mL CRP-XL (CambCol Laboratories). Washed platelets (200 × 10^9/L) were stimulated with 50 µg/mL fibrin directly or after preincubation with either 1 µM NbD2 dimers alone or in the presence of 300 µM Gly-Pro-Arg-Pro acetate (Sigma-Aldrich) to inhibit fibrin polymerization for 15 minutes at 37 °C at 900 rpm. Fibrin was prepared as described previously[22]. In short, 1 mg/mL fibrinogen in 0.06 M potassium phosphate buffer pH 6.8 was incubated with 2.5 U/mL human α thrombin for 1 hour at RT. The clot was washed in the same buffer, and 50 µM Phe-Pro-Arg-chloromethylketone (Prolytix) was added to inactivate thrombin. Fibrin polymers were dissolved in 0.02 M acetic acid. To investigate whether fibrin activates platelets through GPVI and initiates fibrinogen-dependent platelet aggregation through αIIbβ3 rather than fibrin-dependent and αIIbβ3-independent agglutination, 500 µM D-Arg-Gly-Asp-Trp (dRGDW; Bachem) was added to platelets to inhibit αIIbβ3, followed by stimulation with fibrin.

To study the ability of NbD2 tetramers to initiate platelet aggregation, PRP was stimulated with 18 nM NbD2 tetramers or 1 µg/mL CRP-XL. To assess whether NbD2 tetramers are useful in diagnostics, platelet responses toward 1, 2, and 18 nM NbD2 tetramers were obtained in inherited platelet function disorder (IPFD) patients and compared with responses toward 1 and 4 µg/mL HORM collagen. Reference ranges for these agonists were determined in healthy donors.

Flow cytometry assays

Platelet surface expression of GPVI and platelet reactivity toward GPVI agonists were assessed with flow cytometry as described[23]. In short, whole blood was incubated with fluorophore-conjugated nanobodies or antibodies, with or without platelet agonists, and incubated in the dark at 37 °C for 10 minutes. In some experiments, whole blood from healthy controls was incubated with 5 µM $P2Y_{12}$ platelet inhibitor cangrelor tetrasodium salt (Sigma-Aldrich) or 200 µM platelet cyclo-oxygenase 1 inhibitor indomethacin (Sigma-Aldrich) at RT for 30 minutes prior to use. Reactions were stopped by fixation with fixative buffer (137 mM NaCl, 2.7 mM KCl, 1.12 mM NaH_2PO_4, 1.15 mM KH_2PO_4, 10.2 mM Na_2HPO_4, 4 mM EDTA, 1.11% formaldehyde, pH 6.8) at RT for 20 minutes in the dark. After fixation, samples were diluted 1:1 (v/v) in HEPES-buffered saline (HBS: 10 mM HEPES, 150 mM NaCl, 1 mM $MgSO_4$, 5 mM KCl, pH 7.4) and analyzed on a BD FACSCanto II Flow Cytometer (BD Biosciences). Platelets were gated based on forward and sideward scatter, as well as CD42b (GPIbα)

expression. Platelet P-selectin expression and fibrinogen binding were assessed as described[23] to determine platelet reactivity. Platelet agonists were NbD2 dimers (0-30 nM), NbD2 tetramers (0-30 nM), ADP (50 µM), or CRP-XL (1 µg/mL) as indicated. For analysis of the inhibition of platelet reactivity toward CRP-XL with NbD2 dimers, whole blood was added to HBS with D2 dimers (0-30 nM), incubated at 37 °C for 10 minutes and stimulated with CRP-XL (1 µg/mL) at 37 °C for another 10 minutes. For detection of platelet GPVI with NbD2 dimers, whole blood was added to HBS with AlexaFluor 647-conjugated NbD2 (0-74.2 nM) and Rhodophyta-phycoerythrin (R-PE)-conjugated anti-GPIbα nanobody (clone 17; in-house produced; 15 µg/mL). In whole blood from IPFD patients, P-selectin expression and fibrinogen binding were assessed after stimulation with 18 nM NbD2 tetramer or 1 µg/mL CRP-XL. Data are expressed as median fluorescent intensity (MFI).

Inhibition assay

Competition between NbD2 monomers and CRP-XL on sGPVI was assessed using enzyme-linked immunosorbent assay. Soluble GPVI (2 µg/mL) in coating buffer (15 mM Na_2CO_3, 35 mM $NaHCO_3$, 3 mM NaN_3) was coated on a MaxiSorp 96-well plate (Nunc) for 30 minutes at RT under gentle agitation and then overnight at 4 °C. Wells were emptied and blocked for 1 hour with a blocking buffer (2% phosphate buffer saline–bovine serum albumin+ 0.05% Tween 20). All incubation steps were performed at RT and under gentle agitation. A non-saturating concentration of NbD2 monomers (2.5 nM) together with a concentration series of CRP-XL (20-0 µg/mL) in blocking buffer were added to the wells and incubated for 1 hour. After washing, NbD2 was detected with monoclonal mouse anti–c-Myc IgG1 (clone 9E10; in-house produced; 1 µg/mL) for 1 hour. After washing, wells were incubated with polyclonal horseradish peroxidase-conjugated rabbit anti-mouse IgG (DAKO; 1:1000) for 1 hour. Wells were washed and stained with 50 µL 3,3′,5,5′-tetramethylbenzidine. Substrate conversion was stopped by adding 25 µL 0.3 M sulfuric acid, and absorbance was measured at 450 nm in a SpectraMax iD3 (Molecular Devices).

Measurement of protein phosphorylation

Measurement of protein phosphorylation was performed as described in Martin *et al.*[24]. Washed platelets were diluted to 400 × 10^9/L and preincubated with 500 µM dRGDW to prevent platelet aggregation and with or without 10 µM Src inhibitor dasatinib (AbMole BioScience) or 1 µM SYK inhibitor PRT-060318 (Selleck Chemicals) for 30 minutes at RT. Platelets were stimulated with either 1 µg/mL CRP-XL, 18 nM

NbD2 dimer, or 18 nM NbD2 tetramer, remained unstimulated, or were treated with dimethyl sulfoxide. After, platelets were lysed in reducing 3× sample buffer (15.5% glycerol, 96.8 mM Tris-HCl, pH 6.8, 0.6% sodium dodecyl sulfate, 0.003% bromophenol blue, 25 mM dithiothreitol) and heated for 10 minutes at 95 °C. Samples were run on a precast Bolt 4% to 12% Bis-Tris Plus polyacrylamide gel (Invitrogen) in 3-morpholinopropane-1-sulphonic acid buffer at 100 V. Proteins were transferred to an Immobilon-FL 0.45 µm PVDF membrane (Millipore) at 125 V. Phosphorylation of signal transduction proteins was detected with monoclonal mouse anti-phosphotyrosine (clone PY20; Biosource; 1:500) and monoclonal rabbit anti-phosphoSYK Tyr 525/526 (clone F.724.5; Invitrogen; 1:500). Monoclonal mouse anti-SYK (clone 4D10; Santa Cruz; 1:200) and polyclonal rabbit anti-GAPDH (Abcam; 1:1000) were used as lane loading controls. Secondary antibodies were goat anti-mouse AlexaFluor 680 (Thermo Fisher Scientific) and goat anti-rabbit IRDye800 (LI-COR) (1:10,000). Western blots were scanned using the Odyssey M fluorescence imaging system (LI-COR).

RESULTS

Anti-GPVI NbD2 blocks CRP-XL-induced platelet aggregation

Nanobodies directed against GPVI were selected from phage display libraries obtained from 2 llamas immunized with the extracellular domain of human GPVI. NbD2 was identified as the best binder to immobilize GPVI and was used for further characterization. First, binding kinetics were analyzed with surface plasmon resonance analysis (**Fig. 1a**). NbD2 showed a mean (SD) association rate of 5.1 (0.5) × 10^5 $M^{-1}s^{-1}$, a mean (SD) dissociation rate of 1.3 (0.1) × 10^{-3} s^{-1}, and a mean (SD) dissociation constant of 2.5 (0.4) nM, confirming that NbD2 has a high affinity for recombinant human GPVI. Next, the ability of D2 dimers to bind to native platelet GPVI was assessed with flow cytometry in human whole blood (**Fig. 1b**). NbD2 dimers showed dose-dependent binding to platelet GPVI, confirming that NbD2 recognizes native human GPVI on platelets (dissociation constant 1.3 nM). Platelet activation via GPVI requires receptor clustering. To explore whether ligation of GPVI with NbD2 dimers induced platelet activation, human whole blood from healthy donors was incubated with NbD2 dimers, followed by analysis of P-selectin expression and fibrinogen binding with flow cytometry (**Fig. 1c**). No increase in P-selectin expression or fibrinogen binding was observed after stimulation with NbD2 dimers, whereas stimulation with CRP-XL under the same conditions resulted in substantial P-selectin expression and fibrinogen binding. Similar results were obtained with LTA (**Fig. 1d**). While stimulation with

collagen or CRP-XL resulted in full platelet aggregation, platelet aggregation did not occur when PRP was stimulated with a saturating concentration (1 µM) of NbD2 dimers. As this could indicate that NbD2 recognizes an epitope remote from the collagen-binding site on GPVI, competition between collagen or CRP-XL and NbD2 dimers was assessed (**Fig. 1d**). No aggregation occurred after stimulation with CRP-XL when platelets were preincubated with NbD2 dimers, and hardly any aggregation occurred after stimulated with collagen when platelets were preincubated with NbD2 monomers or NbD2 dimers, suggesting that NbD2 recognizes an epitope on GPVI overlapping with, or in close proximity to, the CRP-XL and collagen-binding site. To confirm that NbD2 binds to the collagen-binding site on GPVI, we performed a competitive enzyme-linked immunosorbent assay of NbD2 and CRP-XL on sGPVI. In line with our observations on the functional effects of NbD2, CRP-XL competed with NbD2 monomers for binding to sGPVI (**Fig. 1e**), suggesting the collagen and NbD2 binding sites overlap.

As fibrin has also been described to activate platelets in a GPVI-dependent manner[25], we assessed the ability of NbD2 dimers to inhibit fibrin-induced platelet activation (**Fig. 1f**). Stimulation of washed platelets with fibrin resulted in full aggregation, which was severely abrogated in the presence of fibrinogen receptor inhibitor dRGDW, confirming that stimulation of platelets with fibrin results in platelet activation and fibrinogen- and αIIbβ3-dependent aggregation, rather than fibrin-dependent, αIIbβ3-independent platelet agglutination[26]. Fibrin-dependent platelet aggregation required polymerized fibrin, as aggregation did not occur in the presence of fibrin polymerization inhibitor Gly-Pro-Arg-Pro acetate. In contrast with the effect of NbD2 dimers on collagen-induced platelet aggregation, preincubation with NbD2 dimers failed to inhibit fibrin-initiated platelet aggregation.

Having established that NbD2 specifically blocks the collagen-binding site, we further characterized the inhibitory effect of NbD2 dimers on GPVI-mediated platelet activation. Hereto, human whole blood was preincubated with NbD2 dimers and stimulated with CRP-XL, followed by analysis of P-selectin expression and fibrinogen binding with flow cytometry (**Fig. 1g, h**). The addition of NbD2 dimers resulted in a dose-dependent reduction in P-selectin expression and fibrinogen binding after stimulation with CRP-XL, with a mean (95% CI) half-maximal inhibitory concentration of 1.9 (0.1-2.8) nM for P-selectin expression and a mean (95% CI) half-maximal inhibitory concentration of 2.0 (1.1-2.7) nM for fibrinogen binding.

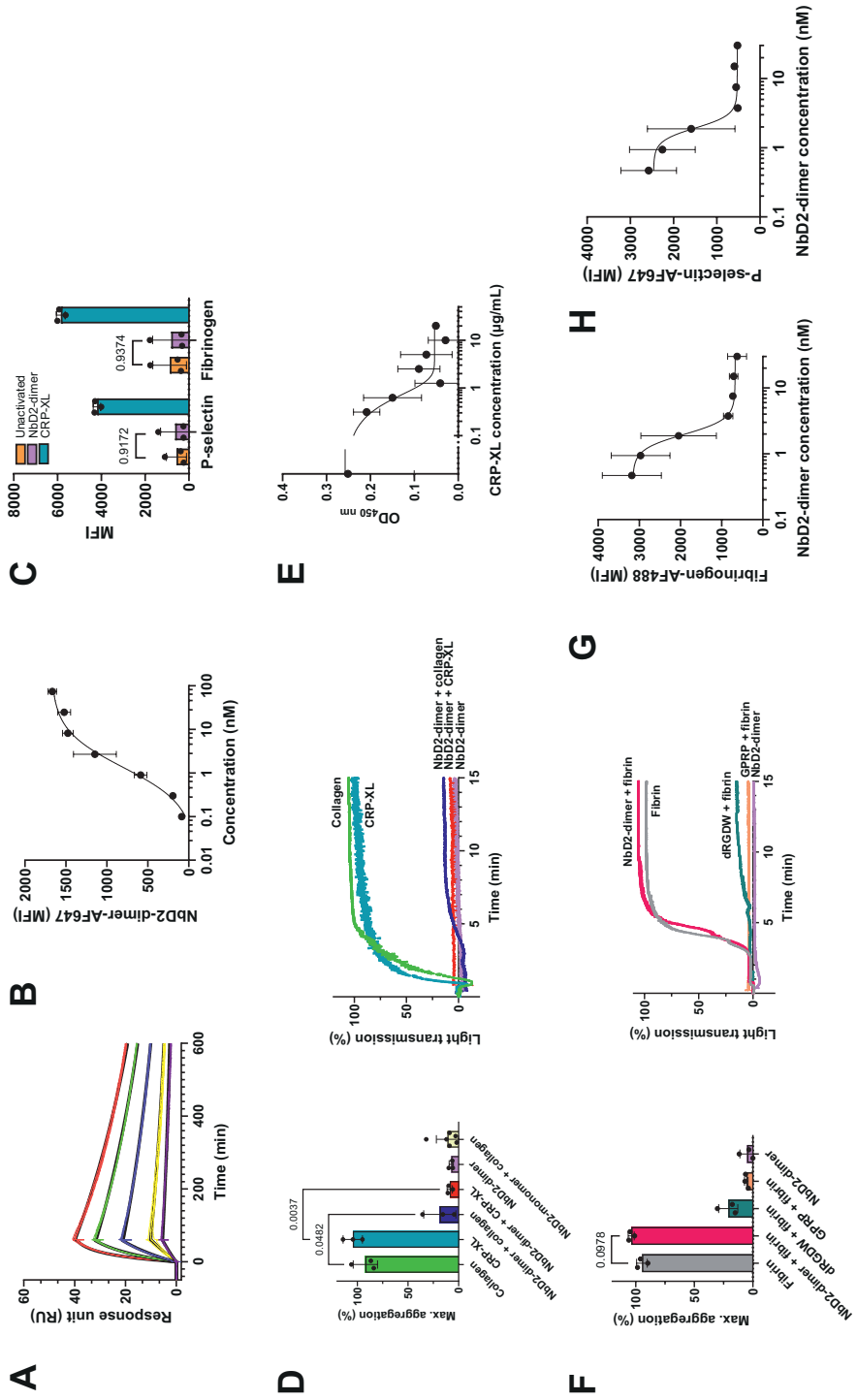

Fig. 1: Anti-glycoprotein (GP)VI nanobody D2 (NbD2) blocks cross-linked collagen-related peptide (CRP-XL)-induced platelet aggregation. a, Affinity of NbD2 dimers (5, 10, 25, 50, and 100 nM) to soluble GPVI was studied with surface plasmon resonance (n = 3). Colored lines indicate binding data. Solid black lines indicate fitted data. **b**, Binding of NbD2 dimers was assessed in a flow cytometer. Whole blood from healthy donors (n = 3) was incubated for 10 minutes with AlexaFluor (AF)647-conjugated NbD2 dimer. Data are expressed as median fluorescent intensity (MFI). **c**, Human whole blood from healthy donors was stimulated with either 1 µM NbD2 dimer, 1 µg/mL CRP-XL, or buffer for 10 minutes at 37 °C (n = 3). P-selectin expression and fibrinogen binding were assessed using flow cytometry. **d**, Platelet-rich plasma from healthy donors was preincubated with either 1 µM NbD2 dimer alone or 1 µM NbD2 dimer, followed by stimulation with 4 µg/mL collagen or 1 µg/mL CRP-XL (n = 3) or 400 nM NbD2 monomer followed by 5 µg/mL collagen (n = 6) in a light transmission aggregometer. Aggregation was monitored for 15 minutes at 37 °C at 900 rpm. Bar graphs represent the maximum amplitude of aggregation. Representative traces of a single donor are shown. **e**, sGPVI was incubated with 2.5 nM NbD2 in the presence of CRP-XL (0 to 20 µg/mL), and residual NbD2 binding was assessed (n = 3). Optical density (OD) was measured at 450 nm and plotted against CRP-XL concentration. **f**, Human-washed platelets (n = 3) were preincubated with either 1 µM NbD2 dimer, 500 µM D-Arg-Gly-Asp-Trp (dRGDW), or 300 µM Gly-Pro-Arg-Pro acetate (GPRP), followed by stimulation with 50 µg/mL fibrin in a light transmission aggregometer. Aggregation was monitored for 15 minutes at 37 °C at 900 rpm. Bar graphs represent the maximum amplitude of aggregation. Representative traces of a single donor are shown. **g**,**h**, Whole blood from healthy donors (n = 3) was preincubated with NbD2 dimers as indicated, followed by stimulation with 1 µg/mL CRP-XL. (**g**) Platelet P-selectin expression and (**h**) fibrinogen binding were assessed in a flow cytometer, and MFIs were plotted as a function of NbD2 dimer concentration. Statistical analyses were performed with a 1-way analysis of variance (anova) with Šidák correction. Error bars represent mean ± SD.

Tetramers of anti-GPVI NbD2 induce platelet activation

Dimerization of GPVI was insufficient to induce platelet activation. To investigate whether higher-order multimers would induce platelet activation, we engineered NbD2 tetramers. Hereto, NbD2 dimers were treated with SrtA to introduce a glycinilated azide tail. C-termini of 2 NbD2 dimers were linked with copper-free click chemistry to ensure optimal availability of the complementarity-determining regions in NbD2. (**Fig. 2a**). Purification of tetramers yielded a band of approximately 56 kDa, twice the size of dimers (27 kDa) on a Coomassie blue staining (**Fig. 2b**).

To assess whether NbD2 tetramers were capable of inducing platelet activation, NbD2 tetramers were compared with CRP-XL using LTA. NbD2 tetramers showed immediate and full platelet aggregation, similar to CRP-XL, with a maximum aggregation of 99.5 ± 7.1% in 3 healthy volunteers with NbD2 tetramers compared with 106.0 ± 10.6% with CRP-XL (**Fig. 2c**). The platelet-activating effect of NbD2 tetramers was further investigated in a whole blood flow cytometry assay. NbD2 tetramers induced a dose-dependent increase in P-selectin expression and fibrinogen binding with a

mean (95% CI) half-maximal effective concentration of 2.1 (1.2-6.7) nM and 1.8 (1.0-3.8) nM, respectively (**Fig. 2d, e**). Combined, these data indicate that NbD2 tetramers act as platelet agonists in LTA and flow cytometry.

In order to investigate why NbD2 dimers do not induce platelet activation, and tetramers do, signaling events were investigated after stimulation with CRP-XL, NbD2 dimers, or NbD2 tetramers with Western blotting (**Fig. 2f**). NbD2 tetramers induced tyrosine phosphorylation events, as well as substantial SYK phosphorylation, similar to CRP-XL, whereas NbD2 dimers did not. Src inhibitor dasatinib and SYK inhibitor PRT-060318 inhibited tyrosine phosphorylation after stimulation with NbD2 tetramers and CRP-XL. These results demonstrate that NbD2 tetramers stimulate potent platelet activation through GPVI, similar to CRP-XL, while NbD2 dimers fail to induce intracellular signaling events.

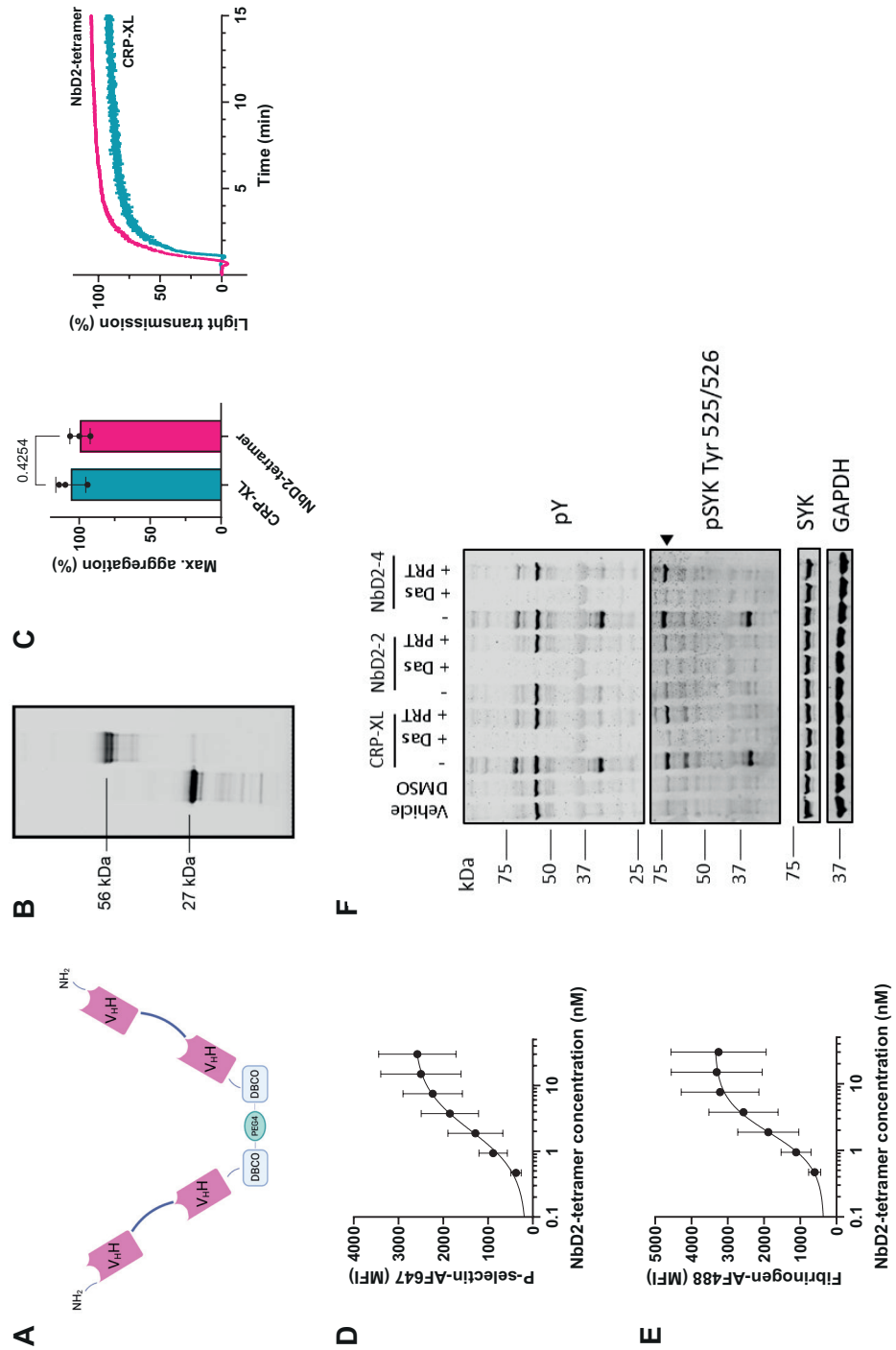

Fig. 2: Tetramers of anti-glycoprotein VI nanobody D2 (NbD2) induce platelet aggregation. a, A C-terminal azido group was introduced into NbD2 dimers with sortagging, followed by the formation of NbD2 tetramers with a DBCO-PEG4-DBCO (DBCO) linker with copper-free click chemistry. **b**, Coomassie blue staining of NbD2 dimers (27 kDa) before sortase A treatment and NbD2 tetramers (56 kDa) after sortase A treatment, DBCO-linking and size-exclusion chromatography. **c**, Platelet-rich plasma from healthy donors (n = 3) was stimulated with either 18 nM NbD2 tetramers or 1 µg/mL cross-linked collagen-related peptide (CRP-XL). Aggregation was monitored for 15 minutes at 37 °C. Bar graphs represent the maximum amplitude of aggregation. Representative traces of a single donor are shown. **d**,**e**, Whole blood from healthy donors (n = 3) was pre-incubated with NbD2 tetramers as indicated. (**d**) Platelet P-selectin expression and (**e**) fibrinogen binding were assessed in a flow cytometer, and median fluorescent intensities (MFI) were plotted as a function of NbD2 tetramer concentration. **f**, Signal transduction in platelet lysates was assessed using Western blotting. Platelets were stimulated with 1 µg/mL CRP-XL, 18 nM NbD2 dimers (NbD2-2), or 18 nM NbD2 tetramers (NbD2-4) for 10 minutes at 37 °C with or without 10 µM Src inhibitor dasatinib (Das) or 1 µM SYK inhibitor PRT-060318 (PRT). phosphoSYK (pSYK) and phosphotyrosine (pY) were detected. The arrow indicates SYK. SYK and GAPDH were used as lane loading controls. Statistical analysis was performed with a Student's t-test. Error bars represent mean ± SD. AF647/488, AlexaFluor 647/488; V_HH, heavy-chain variable domain antibodies. DMSO, dimethyl sulfoxide.

NbD2 tetramers can be used as GPVI agonists during the diagnostic follow-up of patients with a suspected platelet function disorder

Next, we investigated whether NbD2 tetramers can be used to detect platelet function disorders. Hereto, platelets were treated with $P2Y_{12}$ inhibitor cangrelor or cyclo-oxygenase 1 inhibitor indomethacin to mimic platelet disorders, followed by stimulation with either CRP-XL or NbD2 tetramers. P-selectin expression and fibrinogen binding were assessed using flow cytometry. Both P-selectin and fibrinogen binding were decreased in cangrelor-treated blood, but P-selectin expression was decreased, while fibrinogen binding was normal in indomethacin-treated blood compared with untreated blood. No differences in P-selectin expression or fibrinogen binding after stimulation with CRP-XL or NbD2 tetramers were observed in both untreated and inhibited samples; in untreated samples (**Fig. 3a, b**), the mean ± SD P-selectin expression was 1613 ± 934 with NbD2 tetramers compared with 1805 ± 801 for CRP-XL (P = .26). For fibrinogen binding, this was 2249 ± 812 and 2602 ± 698, respectively (P = .07). When platelets were inhibited with cangrelor (**Fig. 3a**), P-selectin expression was 1036 ± 561 with D2 tetramers and 1103 ± 466 with CRP-XL (P = .82). For fibrinogen binding, D2 tetramers resulted in an MFI of 1606 ± 527 compared with 1754 ± 590 with CRP-XL (P = .51). Lastly, indomethacin-treated blood (**Fig. 3b**) resulted in P-selectin expression of 961 ± 576 with NbD2 tetramers compared with 1010 ± 402 for CRP-XL (P = .85) and fibrinogen binding of 2177 ± 1050 and 2406 ± 935 (P = .41). The latter was not decreased compared with healthy controls for both agonists. These data suggest that NbD2 tetramers perform similarly to CRP-XL and might be suitable platelet agonists for diagnostic purposes.

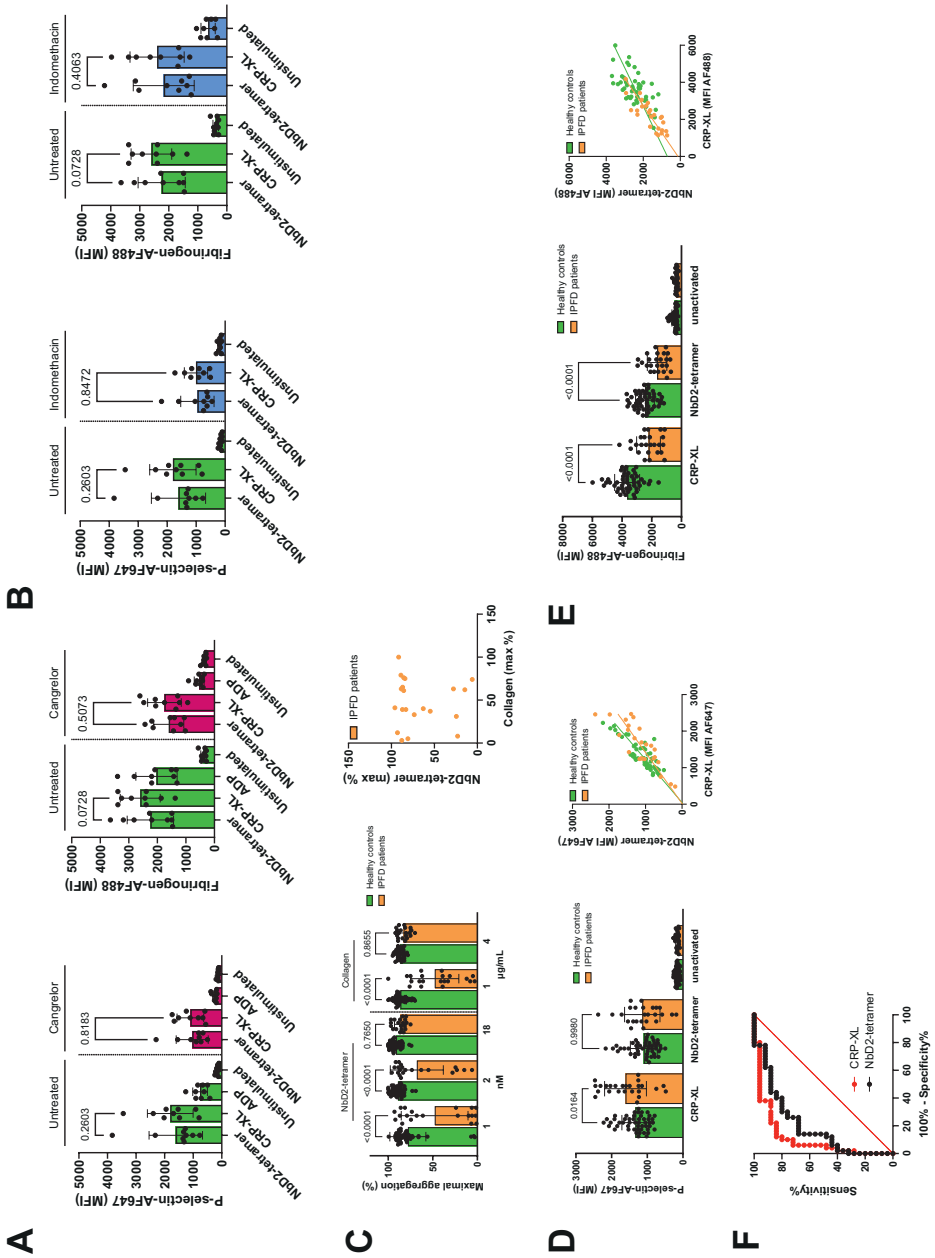

Fig. 3: Nanobody D2 (NbD2) tetramer can be used as a glycoprotein VI agonist during the diagnostic follow-up of patients with a suspected platelet function disorder. a,**b**, Human whole blood was incubated with 5 µM cangrelor or 200 µM indomethacin for 30 minutes at room temperature. Platelet activation was allowed for 10 minutes at 37 °C with either cross-linked collagen-related peptide (CRP-XL), NbD2 tetramers, or adenosine diphosphate (ADP), and P-selectin expression and fibrinogen binding was assessed with median fluorescent intensity (MFI) of fluorescently labeled nanobodies. Bar graphs represent mean P-selectin expression and fibrinogen binding in healthy donors (n = 9). **c**, Platelet-rich plasma from patients with an inherited platelet function disorder (IPFD; n = 21) and healthy controls (n = 50) were stimulated with either 1, 2, or 18 nM NbD2 tetramer or 1 or 4 µg/mL collagen. Aggregation was monitored for 15 minutes at 37 °C. Bar graphs represent the maximum amplitude of aggregation. A correlation plot is shown for maximum aggregation with 2 nM NbD2 tetramer and 1 µg/mL collagen. **d**,**e**, Whole blood from IPFD patients (n = 25) and healthy controls (n = 50) were stimulated with either 18 nM NbD2 tetramer or 1 µg/mL CRP-XL for 10 minutes at 37 °C. (**d**) P-selectin expression and (**e**) fibrinogen binding were assessed using flow cytometry. Data are expressed as MFI. Correlation plots for both agonists are shown for P-selectin expression and fibrinogen binding. **f**, Area under the receiver operating characteristic for CRP-XL vs NbD2 tetramer in flow cytometric fibrinogen binding in healthy controls and IPFD patients. Statistical analyses were performed with 1-way anova with Šidák correction. Error bars represent mean ± SD. AF647/488, AlexaFluor 647/488.

To further evaluate the diagnostic performance of platelet function testing with NbD2 tetramers, LTA and flow cytometry assays were performed in blood from 25 patients with a confirmed IPFD and in 50 healthy controls (**Table 1**). Five IPFD patients were excluded from the LTA analysis due to thrombocytopenia. Many IPFD patients showed decreased aggregation (mean maximum aggregation, 48 ± 27%) after stimulation with a low concentration of collagen (1 µg/mL) compared with healthy controls (86 ± 7%; P < .0001; **Fig. 3c**). Similar results were obtained with low concentrations of NbD2 tetramer (1 and 2 nM; 48 ± 37% and 68 ± 30% in IPFD patients and 78 ± 20% and 89 ± 6% in healthy controls; P < .0001). A high concentration of collagen (4 µg/mL) resulted in normal platelet aggregation in both IPFD patients (83 ± 6%) and healthy controls (87 ± 4%; P = .87). The same was seen for a high concentration of NbD2 tetramer (18 nM; 87 ± 7% in IPFD patients and 91 ± 6% in healthy controls; P = .77). However, the maximum aggregation response observed with 2 nM NbD2 tetramer correlated poorly with the response toward 1 µg/mL collagen (Pearson r = .03 in IPFD patients; **Fig. 3c**).

Platelet surface P-selectin expression after stimulation with CRP-XL was normal or increased in IPFD patients compared with healthy controls (**Fig. 3d**), whereas fibrinogen binding was decreased in IPFD patients (2225 ± 799 for CRP-XL and 1647 ± 659 for NbD2 tetramers) compared with healthy controls (3665 ± 840 and 2463 ± 635; P < .0001; **Fig. 3e**). P-selectin expression after CRP-XL stimulation correlated well with

P-selectin expression after stimulation with NbD2 tetramers in healthy controls and IPFD patients (Pearson r = .85 in both healthy controls and IPFD patients), as did fibrinogen binding (Pearson r = .64 and .83, respectively; **Fig. 3d, e**). The diagnostic performance of fibrinogen binding after stimulation with either agonist was similar, with an area under the receiver operating characteristic of 0.90 ± 0.04 for CRP-XL and 0.81 ± 0.05 for NbD2 tetramer (P = .21; **Fig. 3f**). For both agonists, sensitivity was 40% (95% CI, 23.40%-59.26%), and specificity was 98% (95% CI, 89.50%-99.90%), with a positive likelihood ratio (LR) of 20.0 and negative LR of 0.61. Corresponding cutoff values were 2100 MFI for CRP-XL and 1311 MFI for NbD2 tetramer. This indicates that NbD2 tetramers can be used to discriminate patients with IPFD from healthy controls with a flow cytometric diagnostic assay based on fibrinogen binding to platelets, with a similar sensitivity and specificity as CRP-XL.

Table 1: Baseline demographics and clinical characteristics of participants with inherited platelet function disorders.

Total patients (n)	**25**
Sex (n (%))	
Males	10 (40)
Females	15 (60)
Age (in years)	
Median	39
Range	21-75
Platelet count (x 10^9 / L)	
Median	237
Range	53-464
Thrombocytopenia (n)	
100-150 x 10^9 / L	3
50-100 x 10^9 / L	3
MPV (fL)	
Median	8.4
Range	6.8-10.7
IPFD (n)	25
SPD*	18
Hermanksy-Pudlak	1
RUNX1 familial platelet disorder	2
Platelet-type bleeding disorder-17	1
XLTT	1
Familial thrombopathic thrombocytopenia	1
Unspecified platelet aggregation defect	2

*Platelet ADP content <1.4 µmol / 10^{11} platelets

MPV; mean platelet volume, IPFD; inherited platelet function disorder, SPD; storage pool disease, XLTT; X-linked thrombocytopenia with thalassemia, LTA; light transmission aggregometry

DISCUSSION

This study shows that a tetrameric nanobody targeting platelet collagen receptor GPVI has the capability to activate platelets and can be utilized to study differences in platelet reactivity between IPFD patients and healthy controls. Based on our data, the nanobody recognizes an epitope that overlaps with the collagen-binding site on GPVI. While it effectively blocks GPVI-mediated activation by collagen when used as a dimer, it leads to full platelet activation in both LTA and flow cytometry-based platelet activation assays when used as a tetramer.

In previous studies using anti-GPVI nanobodies, it was shown that dimerization of GPVI is not sufficient for platelet activation, but tri- or tetramerization is[24,27]. Our data are in line with these observations, as our dimeric nanobody has an inhibiting effect on collagen or CRP-XL-induced platelet activation, and our tetrameric nanobody acts as an agonist.

Crystal structures of GPVI have shown that the primary binding site for collagen lies across the D1 domain β-sheet[28]. Our data suggest that the binding site of NbD2 on GPVI overlaps with the binding site on GPVI for collagen. Glenzocimab, an inhibitory antibody Fab-fragment against the D2 domain of GPVI that is currently under investigation in phase 2/3 clinical trials[29], was shown to prevent collagen binding to GPVI through steric hindrance[22]. Although NbD2 dimers (27 kDa) are smaller than glenzocimab (48 kDa), we cannot exclude steric hindrance, which plays a role in the effects of NbD2.

Fibrin is an additional ligand for GPVI, resulting in GPVI-mediated platelet activation[25]. Although the exact fibrin binding site on GPVI is not known, it is suggested that it is in close proximity to the collagen-binding site[30]. Our NbD2 dimers did not act as an inhibitor for fibrin-initiated platelet aggregation, suggesting that NbD2 binds remotely from the fibrin binding site. The relevance of fibrin binding to GPVI for diagnostics of platelet disorders remains to be determined.

Activation of platelets through GPVI is always included in diagnostic assays for platelet function disorders such as LTA and flow cytometry. The major ligand for GPVI, the matrix protein collagen, is insoluble and mostly used as poorly standardized suspensions of fibrillar collagen. Platelet disorders that show reduced platelet reactivity toward

collagen include GPVI deficiency, either congenital or acquired due to autoantibodies[8,9], GPVI-related signaling defects[6], and defects in reinforcing pathways of platelet activation, such as SPDs[12]. Patients with GPVI deficiency show strongly reduced platelet aggregation with collagen and decreased P-selectin expression and fibrinogen binding in flow cytometry diagnostic workup. The effects of SPD on collagen-induced platelet aggregation are less pronounced, with normal LTA responses in many patients with SPD[31]. None of the patients in our study had GPVI deficiency, and 72% of the patients in our study had SPD. In line with reported LTA outcomes in SPD, many patients displayed normal LTA responses to collagen and NbD2 tetramers.

LTA outcomes for collagen and NbD2 tetramers did not correlate. A possible explanation for the discrepancy between NbD2 tetramers and collagen in LTA could be that collagen binds to both GPVI and α2β1, whereas NbD2 only interacts with GPVI. A deficiency in integrin α2β1 results in reduced collagen-mediated aggregation[32], indicating that the α2β1 signaling pathway also plays a role in collagen-induced platelet aggregation. As NbD2 dimers fully block collagen-induced platelet activation, any α2β1-mediated responses toward collagen are likely to occur secondary to GPVI-mediated signaling.

In sharp contrast with LTA data, platelet fibrinogen binding after stimulation with NbD2 tetramers correlated well with fibrinogen binding after stimulation with CRP-XL in flow cytometry. Platelet responses to the NbD2 tetramer were similar to those with the GPVI-specific agonist CRP-XL in flow cytometry in both IPFD patients and healthy controls. The diagnostic performance of both agonists was similar, with very good discrimination between healthy controls and IPFD patients, supporting the potential application of NbD2 tetramers in the evaluation of platelet function during the diagnostic workup of primary hemostasis defects.

Limitations of this pilot study on diagnostic performance are that our cohort of 25 IPFD patients was relatively small, analysis was not performed blind to diagnosis, and SPD was overrepresented, which may have introduced an overestimation of diagnostic performance. Sensitivity and specificity should, therefore, be interpreted with caution. However, the LR, a measure insensitive to prevalence, suggests NbD2 tetramers are suitable for diagnostic use. Our findings need to be confirmed in a larger prospective study in a relevant patient population. Platelet function analysis is performed to confirm or exclude platelet disorders in patients with clinical symptoms

of a primary hemostasis defect characterized by a mucocutaneous bleeding tendency. Validation of NbD2 tetramers for diagnostic purposes will, therefore, require the evaluation of platelet function in a larger cohort of people with a mucocutaneous bleeding tendency. Such analyses are hampered by the lack of gold-standard tests for platelet function abnormalities.

Lastly, due to the stable and easily producible nature of nanobodies, this technique could be further developed for other receptors, as was already done by Martin *et al.*[24], who developed trivalent nanobody-based ligands for GPVI, C-type lectin-like receptor 2, and platelet endothelial aggregation receptor 1 and a tetravalent ligand for FcγRIIA. However, the diagnostic value of other platelet nanobody-based ligands would need to be determined.

In conclusion, we here show the development and functional characterization of a novel tetrameric GPVI-specific nanobody that may serve as a stable platelet agonist in diagnostic assays.

ADDENDUM

TiN study group: Erik Beckers, Maastricht, the Netherlands, Michiel Coppens, Amsterdam, the Netherlands, Jeroen Eikenboom, Leiden, the Netherlands, Louise Hooimeijer, Groningen, the Netherlands, Gerard Jansen, Rotterdam, the Netherlands, Roger Schutgens, Utrecht, the Netherlands, Rolf Urbanus, Utrecht, the Netherlands, and Minka Zivkovic, Utrecht, the Netherlands.

SYMPHONY consortium: Emile van den Akker, Amsterdam, the Netherlands, Wala Al Arashi, Rotterdam, the Netherlands, Ryanne Arisz, Rotterdam, the Netherlands, Lieke Baas, Utrecht, the Netherlands, Ruben Bierings, Rotterdam, the Netherlands, Maartje van den Biggelaar, Amsterdam, the Netherlands, Johan Boender, Amsterdam, the Netherlands, Anske van der Bom, Leiden, the Netherlands, Mettine Bos, Leiden, the Netherlands, Martijn Brands, Amsterdam, the Netherlands, Annelien Bredenoord, Utrecht, the Netherlands, Laura Bukkems, Amsterdam, the Netherlands, Lex Burdorf, Rotterdam, the Netherlands, Jessica Del Castillo Alferez, Amsterdam, the Netherlands, Michael Cloesmeijer, Amsterdam, the Netherlands, Marjon Cnossen, Rotterdam, the Netherlands, Mariëtte Driessens, Utrecht, the Netherlands, Jeroen Eikenboom, Leiden, the Netherlands, Karin Fijnvandraat, Amsterdam, the Netherlands, Kathelijn Fischer, Utrecht, the Netherlands, Geertje Goedhart, Leiden, the Netherlands, Tine Goedhart, Rotterdam, the Netherlands, Samantha Gouw, Amsterdam, the Netherlands, Rieke van der Graaf, Utrecht, the Netherlands, Masja de Haas, Amsterdam, the Netherlands, Lotte Haverman, Amsterdam, the Netherlands, Jan Hazelzet, Rotterdam, the Netherlands, Shannon van Hoorn, Rotterdam, the Netherlands, Elise Huisman, Rotterdam, the Netherlands, Nathalie Jansen, Utrecht, the Netherlands, Alexander Janssen, Amsterdam, the Netherlands, Sean de Jong, Hoofddorp, the Netherlands, Sjoerd Koopman, Amsterdam, the Netherlands, Marieke Kruip, Rotterdam, the Netherlands, Sebastiaan Laan, Leiden, the Netherlands, Frank Leebeek, Rotterdam, the Netherlands, Nikki van Leeuwen, Rotterdam, the Netherlands, Hester Lingsma, Rotterdam, the Netherlands, Moniek de Maat, Rotterdam, the Netherlands, Ron Mathôt, Amsterdam, the Netherlands, Felix van der Meer, Leiden, the Netherlands, Karina Meijer, Groningen, the Netherlands, Sander Meijer, Amsterdam, the Netherlands, Stephan Meijer, Den Haag, the Netherlands, Iris van Moort, Rotterdam, the Netherlands, Caroline Mussert, Rotterdam, the Netherlands, Hans Kristian Ploos van Amstel, Utrecht, the Netherlands, Suzanne Polinder, Rotterdam, the Netherlands, Diaz Prameyllawati, Rotterdam, the Netherlands, Simone Reitsma, Rotterdam, the Netherlands, Eliza Roest, Rotterdam, the Netherlands,

Lorenzo Romano, Rotterdam, the Netherlands, Saskia Schols, Nijmegen, the Netherlands, Roger Schutgens, Utrecht, the Netherlands, Rolf Urbanus, Utrecht, the Netherlands, Carin Uyl, Rotterdam, the Netherlands, Jan Voorberg, Amsterdam, the Netherlands, Huan Zhang, Amsterdam, the Netherlands, and Minka Zivkovic, Utrecht, the Netherlands.

Declaration of competing interest

M.Z.: no conflicts of interest. E.P.v.V.: no conflicts of interest. V.v.d.V.: no conflicts of interest. S.A.E.S.: no conflicts of interest. A.S.d.M.: no conflicts of interest. S.J.A.K.: no conflict of interest. R.E.G.S.: The institution of R.E.G.S. has received speaker's fees and/or research grants from Bayer, CSL Behring, Hemab, Novartis, Novo Nordisk, Octapharma, Roche, Sobi, and Takeda. R.T.U.: The institution of R.T.U. has received research grants from Hemab.

Acknowledgements

We gratefully acknowledge the patients and healthy donors who participated in this study.

Author contributions

M.Z.: conceptualization, methodology, validation, formal analysis, investigation, resources, data curation, writing (original draft), writing (review and editing), and visualization. E.P.v.V.: conceptualization, methodology, validation, formal analysis, investigation, resources, data curation, and visualization. V.v.d.V.: investigation, resources, and data curation. S.A.E.S.: methodology, investigation, resources, and data curation. A.S.d.M.: resources. S.J.A.K.: conceptualization and methodology. R.E.G.S.: writing (review and editing), supervision, project administration, and funding acquisition. R.T.U.: conceptualization, methodology, formal analysis, resources, writing (review and editing), supervision, and project administration.

Funding sources

This work was supported by the SYMPHONY consortium (Dutch Research Counsil – Dutch Research Agenda [I-NWA] grant number 1160.18.038).

REFERENCES

1. Mammadova-Bach E, Ollivier V, Loyau S, et al. Platelet glycoprotein VI binds to polymerized fibrin and promotes thrombin generation. *Blood*. 2015;126(5):683-691. Doi:10.1182/blood-2015-02-629717
2. Moroi M, Jung SM. Platelet glycoprotein VI: its structure and function. *Thromb Res*. 2004;114(4):221-233. Doi:10.1016/j.thromres.2004.06.046
3. Nieswandt B, Watson SP. Platelet-collagen interaction: is GPVI the central receptor? *Blood*. 2003;102(2):449-461. Doi:10.1182/blood-2002-12-3882
4. Damaskinaki F-N, Jooss NJ, Martin EM, et al. Characterizing the binding of glycoprotein VI with nanobody 35 reveals a novel monomeric structure of glycoprotein VI where the conformation of D1+D2 is independent of dimerization. *J Thromb Haemost*. 2023;21(2):317-328. Doi:10.1016/j.jtha.2022.11.002
5. Dumont B, Lasne D, Rothschild C, et al. Absence of collagen-induced platelet activation caused by compound heterozygous GPVI mutations. *Blood*. 2009;114(9):1900-1903. Doi:10.1182/blood-2009-03-213504
6. Arthur JF, Dunkley S, Andrews RK. Platelet glycoprotein VI-related clinical defects. *Br J Haematol*. 2007;139(3):363-372. Doi:10.1111/j.1365-2141.2007.06799.x
7. Hermans C, Wittevrongel C, Thys C, Smethurst PA, Van Geet C, Freson K. A compound heterozygous mutation in glycoprotein VI in a patient with a bleeding disorder. *J Thromb Haemost*. 2009;7(8):1356-1363. Doi:10.1111/j.1538-7836.2009.03520.x
8. Boylan B, Chen H, Rathore V, et al. Anti-GPVI-associated ITP: an acquired platelet disorder caused by autoantibody-mediated clearance of the GPVI/FcRgamma-chain complex from the human platelet surface. *Blood*. 2004;104(5):1350-1355. Doi:10.1182/blood-2004-03-0896
9. Nurden P, Jandrot-Perrus M, Combrié R, et al. Severe deficiency of glycoprotein VI in a patient with gray platelet syndrome. *Blood*. 2004;104(1):107-114. Doi:10.1182/blood-2003-11-3842
10. Bellucci S, Huisse MG, Boval B, et al. Defective collagen-induced platelet activation in two patients with malignant haemopathies is related to a defect in the GPVI-coupled signalling pathway. *Thromb Haemost*. 2005;93(1):130-138. Doi:10.1160/TH04-05-0312
11. Dunkley S, Arthur JF, Evans S, Gardiner EE, Shen Y, Andrews RK. A familial platelet function disorder associated with abnormal signalling through the glycoprotein VI pathway. *Br J Haematol*. 2007;137(6):569-577. Doi:10.1111/j.1365-2141.2007.06603.x
12. Weiss HJ. Inherited abnormalities of platelet granules and signal transduction. In: Colman R, Hirsh J, Marder VJ, Salzman JB, eds. *Hemostasis and Thrombosis: Basic Principles and Clinical Practice*. 3rd ed. ; 1994.
13. Dawood BB, Lowe GC, Lordkipanidzé M, et al. Evaluation of participants with suspected heritable platelet function disorders including recommendation and validation of a streamlined agonist panel. *Blood*. 2012;120(25):5041-5049. Doi:10.1182/blood-2012-07-444281

14. van Asten I, Blaauwgeers M, Granneman L, et al. Flow cytometric mepacrine fluorescence can be used for the exclusion of platelet dense granule deficiency. *J Thromb Haemost*. 2020;18(3):706-713. Doi:10.1111/jth.14698
15. Hagemeyer CE, von Zur Muhlen C, von Elverfeldt D, Peter K. Single-chain antibodies as diagnostic tools and therapeutic agents. *Thromb Haemost*. 2009;101(6):1012-1019. Doi:10.1160/TH08-12-0816
16. Cnossen MH, van Moort I, Reitsma SH, et al. SYMPHONY consortium: Orchestrating personalized treatment for patients with bleeding disorders. *J Thromb Haemost*. 2022;20(9):2001-2011. Doi:10.1111/jth.15778
17. Blaauwgeers MW, Kruip MJHA, Beckers EAM, et al. Bleeding phenotype and diagnostic characterization of patients with congenital platelet defects. *Am J Hematol*. 2020;95(10):1142-1147. Doi:10.1002/ajh.25910
18. Blaauwgeers MW, van Asten I, Kruip MJHA, et al. The limitation of genetic testing in diagnosing patients suspected for congenital platelet defects. *Am J Hematol*. 2020;95(1):E26-E28. Doi:10.1002/ajh.25667
19. de Haas CJC, Weeterings C, Vughs MM, de Groot PG, Van Strijp JA, Lisman T. Staphylococcal superantigen-like 5 activates platelets and supports platelet adhesion under flow conditions, which involves glycoprotein Ibalpha and alpha IIb beta 3. *J Thromb Haemost*. 2009;7(11):1867-1874. Doi:10.1111/j.1538-7836.2009.03564.x
20. de Maat S, van Dooremalen S, de Groot PG, Maas C. A nanobody-based method for tracking factor XII activation in plasma. Thromb Haemost. 2013;110(3):458-468. Doi:10.1160/TH12-11-0792
21. van Moorsel MVA, Urbanus RT, Verhoef S, et al. A head-to-head comparison of conjugation methods for VHHs: Random maleimide-thiol coupling versus controlled click chemistry. *International Journal of Pharmaceutics: X*. 2019;1:100020. Doi:10.1016/j.ijpx.2019.100020
22. Billiald P, Slater A, Welin M, et al. Targeting platelet GPVI with glenzocimab: a novel mechanism for inhibition. *Blood Adv*. 2023;7(7):1258-1268. Doi:10.1182/bloodadvances.2022007863
23. van Dijk WEM, Poolen GC, Huisman A, et al. Evaluation of the procoagulant state in chronic immune thrombocytopenia before and after eltrombopag treatment-a prospective cohort study. *J Thromb Haemost*. 2023;21(4):1020-1031. Doi:10.1016/j.jtha.2022.11.039
24. Martin EM, Clark JC, Montague SJ, et al. Trivalent nanobody-based ligands mediate powerful activation of GPVI, CLEC-2, and PEAR1 in human platelets whereas FcγRIIA requires a tetravalent ligand. *J Thromb Haemost*. 2024;22(1):271-285. Doi:10.1016/j.jtha.2023.09.026
25. Alshehri OM, Hughes CE, Montague S, et al. Fibrin activates GPVI in human and mouse platelets. *Blood*. 2015;126(13):1601-1608. Doi:10.1182/blood-2015-04-641654
26. Gandhi PS, Zivkovic M, Østergaard H, et al. A bispecific antibody approach for the potential prophylactic treatment of inherited bleeding disorders. *Nat Cardiovasc Res*. February 8, 2024. Doi:10.1038/s44161-023-00418-4

27. Maqsood Z, Clark JC, Martin EM, et al. Experimental validation of computerised models of clustering of platelet glycoprotein receptors that signal via tandem SH2 domain proteins. *PloS Comput Biol*. 2022;18(11):e1010708. Doi:10.1371/journal.pcbi.1010708

28. Feitsma LJ, Brondijk HC, Jarvis GE, et al. Structural insights into collagen binding by platelet receptor glycoprotein VI. *Blood*. 2022;139(20):3087-3098. Doi:10.1182/blood.2021013614

29. ACTISAVE: AcuTe Ischemic Stroke Study Evaluating Glenzocimab Used as Add-on Therapy Versus placEbo – Full Text View – ClinicalTrials.gov. Accessed May 27, 2024. https://classic.clinicaltrials.gov/ct2/show/NCT05070260

30. Induruwa I, Moroi M, Bonna A, et al. Platelet collagen receptor Glycoprotein VI-dimer recognizes fibrinogen and fibrin through their D-domains, contributing to platelet adhesion and activation during thrombus formation. *J Thromb Haemost*. 2018;16(2):389-404. Doi:10.1111/jth.13919

31. Nieuwenhuis HK, Akkerman JW, Sixma JJ. Patients with a prolonged bleeding time and normal aggregation tests may have storage pool deficiency: studies on one hundred six patients. *Blood*. 1987;70(3):620-623.

32. Nieuwenhuis HK, Akkerman JW, Houdijk WP, Sixma JJ. Human blood platelets showing no response to collagen fail to express surface glycoprotein Ia. *Nature*. 1985;318(6045):470-472. Doi:10.1038/318470a0

Chapter 3

A rapid whole-blood adenosine triphosphate secretion test can be used to exclude platelet-dense granule deficiency

Minka Zivkovic[1,2], Roger EG Schutgens[1], Vossa van der Vegte[1,2], Janoek A Lukasse[1,2], Mark Roest[3], Dana Huskens[3], Annick S de Moor[1], Idske CL Kremer Hovinga[1], Rolf T Urbanus[1,2]; for the TiN study group and SYMPHONY consortium

[1] Center for Benign Haematology, Thrombosis and Haemostasis, Van Creveldkliniek, University Medical Center Utrecht, Utrecht University, Utrecht, the Netherlands

[2] Circulatory Health Research Center, University Medical Center Utrecht, Utrecht, the Netherlands

[3] Synapse Research Institute, Maastricht, the Netherlands

J Thromb Haemost. 2025 Feb 10:S1538-7836(25)00056-X.

SUMMARY

Background: Delta storage pool disease (δ-SPD) is a rare platelet function disorder (PFD) characterized by a deficiency of dense granules or defective granule secretion, leading to bleeding diathesis. Diagnostics of δ-SPD are difficult and lack standardization, leading to underestimation of its prevalence. Current diagnostic methods are based on granule content assays or lumi-aggregometry, which have limited availability. Therefore, there is an unmet need for a rapid, accessible test for δ-SPD.

Objectives: To evaluate the diagnostic value of a rapid whole-blood adenosine triphosphate (ATP) secretion test for δ-SPD.

Methods: ATP secretion after PAR-1 activating peptide (PAR-1 AP; TRAP-6) stimulation was assessed in whole blood using luminescence in 50 healthy controls, 22 patients with a suspected PFD other than storage pool disease (non-SPD) and 25 patients with δ-SPD and corrected for platelet count. Diagnostic value of the test was determined with C-statistics, sensitivity, specificity, likelihood ratios (LLRs), and predictive values (PVs).

Results: PAR-1 AP mediated ATP secretion in the rapid test was lower in δ-SPD than in healthy controls and non-SPD patients ($P < .0001$). The rapid test was able to discriminate between δ-SPD and non-SPD patients (C-statistic 0.88; 95% CI, 0.78-0.98). At a cutoff value of the highest value of the δ-SPD group, the sensitivity was 100% and the specificity was 64%. This cutoff value corresponded with a positive LLR of 2.75, an optimal negative LLR of 0.00, positive PV of 76%, and negative PV of 100%.

Conclusion: A whole-blood ATP secretion test can be used to exclude δ-SPD in patients presenting with a primary hemostasis defect.

Keywords: Blood Platelet Disorder; Diagnostic Tests; Luminescent Assay; Platelet Function Tests; Platelet Storage Pool Deficiency

INTRODUCTION

Platelets play a critical role in hemostasis by forming a platelet plug at sites of vascular injury. Upon activation, platelets release the contents of their storage organelles, including alpha (α) and dense (δ) granules, which further promote platelet activation and coagulation[1-3]. Among the molecules secreted from dense granules are adenosine diphosphate (ADP) and adenosine triphosphate (ATP). ADP facilitates secondary platelet activation via the $P2Y_{12}$ receptor and is vital for thrombus stability[4].

Storage pool disease (SPD) arises from either a reduced number or complete absence of granules or a diminished granule content, leading to decreased granule release[5,6]. On the other hand, defects in the membrane fusion machinery, due to impaired signal transduction or granule trafficking, are linked to secretion failure upon platelet activation[7]. SPD can be classified into 3 types: α-SPD, lacking α-granules, δ-SPD lacking dense granules and αδ-SPD, lacking both α- and δ-granules[8-10].

Platelet δ-granules belong to a family of lysosome-related organelles, which also includes pigment-containing melanosomes and lytic granules in natural killer cells and T lymphocytes[11,12]. Quantitative or qualitative defects in platelet δ-granules are very heterogeneous in origin. Causative mutations have been identified for rare syndromic disorders such as Chediak-Higashi disease, Hermansky-Pudlak syndrome, and Griscelli syndrome in which patients present with δ-SPD and oculocutaneous albinism with or without immune deficiencies. Affected genes in these disorders encode proteins involved in biogenesis, trafficking, or membrane fusion of lysosome-related organelles, resulting in a variety of affected cell types[13-17]. δ-SPD is also observed in patients with rare mutations in transcription factors GATA1, RUNX1, or Fli1, involved in the regulation of hematopoiesis. Causative mutations for nonsyndromic forms of δ-SPD, in which only the megakaryocytic lineage is affected, are not known yet[11,12]. SPD is one of the most common platelet disorders, representing up to 28% of diagnosed platelet disorders in tertiary treatment centers in the United States[18].

Although dense granule deficiency is a common platelet disorder, diagnostics for this disorder lack standardization and are costly and difficult to implement routinely in hemostasis laboratories[12,19]. This was highlighted by a worldwide survey conducted by the International Society on Thrombosis and Haemostasis (ISTH)[20]. In this study, more than half of the 202 responding laboratories did not evaluate platelet granule

content or release during investigation of patients with suspected platelet defects. Among the laboratories where granule release was evaluated, the used diagnostic methods were diverse and poorly standardized[20-22]. In addition, there are no validated recommendations regarding the decision tree or the prioritization of tests necessary to achieve an accurate diagnosis of δ-SPD[12,22]. Consequently, SPD diagnostics are not performed in every patient with a mucocutaneous bleeding tendency, possibly leading to underestimation of the prevalence of SPD.

Currently, the most used method to diagnose δ-SPD is lumi-aggregometry. This test cannot distinguish between decreased granule content and a secretion defect[23]. Moreover, it is time and labor-intensive and requires large volumes of blood, which can be especially challenging in pediatric patients[24,25]. Another frequently used method is het measurement of nucleotides ADP and ATP in platelet lysates, where luciferase catalyzes the conversion of ATP and luciferin to light. Although this assay can accurately detect δ-granule deficiency, it is insensitive to secretion defects. Another diagnostic method involves counting the total number of δ-granules per platelet with whole-mount transmission electron microscopy, which is complex, requires specialized equipment, and is not widely accessible in diagnostic laboratories. A study performed by the Scientific and Standardization Committee of the ISTH among laboratory specialists indicated that measurement of the total content and secreted fraction of either ATP/ADP or serotonin by high-performance liquid chromatography (HPLC) are appropriate methods for the evaluation of dense granule content and secretion[21], but this is not widely available either.

Given that <50% of expert laboratories perform routine platelet SPD assessment, there is an unmet need for consensus for standardization and validation of platelet SPD diagnostics[22,26]. A possible way forward is by exploring other options for SPD diagnostics. Previous studies have already shown that the determination of platelet surface markers like P-selectin and CD63 with flow cytometry is useful in detecting granule deficiencies[27,28]. Additionally, super-resolution microscopy for the evaluation of CD63 was shown to be effective in predicting Hermansky-Pudlak syndrome[29]. However, these tests are not validated for diagnostic purposes[12]. We and others have shown that flow cytometric assessment of mepacrine fluorescence can be used as a screening tool to exclude δ-SPD in patients presenting with a suspected inherited platelet function disorder (IPFD)[27,28,30]. Here, we used a similar approach to evaluate

a more rapid screening assay based on ATP secretion in whole blood as a diagnostic tool for δ-granule deficiency.

MATERIALS AND METHODS

Subjects

Individuals with confirmed δ-SPD were included in the Thrombocytopathy in the Netherlands (TiN) study (study number NL53207.041.15), a nationwide cross-sectional study focused on disease phenotyping, diagnostics, and genetics, conducted at the University Medical Center Utrecht. As a reference group, patients with a suspected IPFD based on a mucocutaneous bleeding tendency (ISTH-BAT >5 for women or >3 for men) who were eligible for diagnostic workup of a platelet disorder were recruited at the Van Creveldkliniek of the University Medical Center Utrecht (Biobank number 24-059). Healthy control participants were recruited from the staff and students at the University Medical Center Utrecht by the MiniDonor biobank facility (Biobank number 18-774). Subjects were allocated to the δ-SPD or non-SPD group based on platelet ADP content. Approval from the medical ethics committee was obtained and all subjects provided written informed consent in accordance with the declaration of Helsinki.

Blood collection

For all participants, blood was collected from the antecubital vein using 3.2% trisodium citrate vacutainer tubes (BD) via phlebotomy. Patients attended a single hospital visit during which blood was collected for various analyses, including complete blood count, light transmission aggregometry (LTA) with 7 agonists, platelet surface receptor expression, nucleotide content, and the whole-blood ATP secretion test. The blood was processed within 1 to 4 hours after collection. All measurements were performed on the same sample in a nonblinded manner.

Nucleotide content in platelet lysate

Whole blood was centrifuged at 200 *g* for 10 minutes without brake, to obtain platelet-rich plasma (PRP). PRP was isolated and the remainder of the blood was centrifuged at 1500 *g* for 15 minutes to obtain platelet-poor plasma. Platelet counts were adjusted with platelet-poor plasma to a maximum of 250 × 10^9/L. Next, 500 µL PRP was diluted in ice-cold 1 mL EDTA-Ethanol (1:9 vol:vol 0.1 M sodium-EDTA in 96% ethanol) and stored at −80 °C until further use. After thawing on ice, samples

were vortexed and centrifuged at 1500 *g* for 10 minutes at 4 °C. Two fractions of phosphoenolpyruvate (PEP)/pyruvate kinase (PK) (95 µM PEP [Roche] and 25 µg/mL PK [Roche] in 0.2 M Tris-maleate, 10 mM KCl, 15 mM $MgSO_4$, pH 7.4) were made, of which, one was inactivated for 20 minutes at 80 °C and the other one remained active. Platelet lysates were added to either active or inactive PEP/PK, mixed well, and incubated for 15 minutes at 37 °C or room temperature (RT), respectively. The active PEP/PK converts all ADP to ATP (ATP+ADP fraction), whereas the inactive PEP/PK is used to only measure the ATP concentration (ATP fraction). Both reactions were stopped by heating for 10 minutes at 80 °C. ATP levels were determined in both fractions with the ATPlite 1step Luminescence Assay System kit (Perkin Elmer) according to the manufacturer's protocol. Luminescence was measured on a SpectraMax L luminometer (Molecular Devices) at all wavelengths, and ATP levels were determined from an ATP calibration curve. ADP levels were calculated by subtracting the concentration of the ATP fraction from the ATP+ADP fraction. ADP and ATP levels were expressed as µmol per 10^{11} platelets. Reference values were ≥1.4 µmol/10^{11} platelets ADP, ≥2.7 µmol/10^{11} platelets ATP, and 1.20 to 2.00 ATP/ADP ratio. Patients were considered to have δ-SPD when they had platelet ADP levels <1.4 µmol/10^{11} platelets.

Flow cytometry assays

Platelet surface expression of P-selectin (CD62P) and CD63 were assessed with flow cytometry as described[31]. In short, 5 µL whole blood from healthy donors or patients with a (suspected) IPFD was incubated with fluorescein-5-isothiocyanate-conjugated anti-CD42b (clone HIP1; 1:25; BD Pharmingen), R-Phycoerythrin (rPE)-conjugated anti-CD62P (clone AK-4; 1:25; BD Pharmingen) and AlexaFluor (AF)647-conjugated anti-CD63 (clone H5C6; 1:50; BD Pharmingen) with or without 25 µM or 2.5 µM protease-activated receptor-1 activating peptide (PAR-1 AP; TRAP-6; SFLLRN; Bachem) and incubated in the dark at 37 °C for 10 minutes. Reactions were stopped by fixation at RT for 20 minutes in the dark with 1.11% fixative solution (137 mM NaCl, 2.7 mM KCl, 1.12 mM NaH_2PO_4, 1.15 mM KH_2PO_4, 10.2 mM Na_2HPO_4, 4 mM EDTA, 1.11% formaldehyde, pH 6.8). After fixation, samples were diluted 1:1 (v/v) in FACS-HBS buffer (10 mM HEPES, 150 mM NaCl, 1 mM $MgSO_4$, 5 mM KCl, pH 7.4) and analyzed on a BD FACSCanto II Flow Cytometer. Platelets were gated based on forward and sideward scatter, as well as CD42b (GPIbα) expression. Data are expressed as median fluorescent intensity (MFI).

Whole-blood ATP secretion test

Secretion of ATP from stimulated platelets was assessed with a whole-blood luminescence-based assay. 25 µL of whole blood was carefully resuspended 8 times in 75 µL of a mixture, resulting in final concentrations of 2.5 µM PAR-1 AP, 8 µg/mL recombinant luciferase (Synapse B.V.), and 1 mM luciferin (Synchem UG & Co KG). Afterward, the luminescence signal was directly measured at all wavelengths for 10 minutes at 37 °C with 30-second intervals on a SpectraMax iD3 (Molecular Devices), and ATP secretion was determined as a maximal signal. The coefficient of variation was 14.8%. Data are expressed as relative light units (RLUs) per 10^9 platelets. The whole-blood ATP secretion test was performed on the same day as the granule nucleotide assay. Patients and healthy controls were not measured on the same day.

Statistical analysis

ATP secretion data were obtained using SoftMax Pro Software (Molecular Devices). Diagnostic performance was analyzed with receiver operating characteristic-curves and the concordance statistic (c-statistic), as well as calculation of positive (PPV) and negative predictive value (NPV) and positive and negative likelihood ratios (LLRs). Statistics were analyzed with GraphPad Prism version 10.0.3 and 2024 MedCalc Software Ltd. Flow cytometry data were analyzed using BD FACSDiva Software.

RESULTS

Patient population

Twenty-five patients with confirmed δ-SPD and 22 patients with a suspected IPFD other than δ-SPD (non-SPD) were included in this study (**Table 1**). Six patients with δ-SPD and 5 non-SPD patients had mild thrombocytopenia (50-150 × 10^9/L). All other patients had a normal platelet count (>150 × 10^9/L). LTA was performed in 24 of 25 patients with δ-SPD; LTA could not be performed in 1 due to low platelet count in PRP (<100 × 10^9/L). Seven patients (29%) had aberrant aggregation, of whom 4 were in response to collagen, 4 to arachidonic acid, and 1 to PAR-1 AP. Ten out of 22 (45%) non-SPD patients had aberrant LTA patterns, of whom 5 in response to ADP, 5 to collagen, 3 to arachidonic acid, 1 to PAR-1 AP, 2 to U-46619, and 3 to epinephrine.

Table 1: Demographic and baseline characteristics.

	δ-SPD	non-SPD
n	25	22
Sex (n (%))		
Males	9 (36)	6 (27)
Females	16 (64)	16 (73)
Age (in years)		
median (range)	41 (21-75)	36 (21-75)
Platelet count (*109 / L) (NR: 150-450)		
median (range)	262 (53-392)	231 (57-391)
MPV (fL) (NR: 7.0-9.5)		
median (range)	8.1 (6.8-9.6)	8.1 (6.8-10.5)
Platelet nucleotide content		
ADP (µmol/1011 platelets) (NR: 1.4-3.3)		
median (range)	0.8 (0.2-1.37)	2.0 (1.5-2.9)
ATP (µmol/1011 platelets) (NR: 2.7-4.8)		
median (range)	3.0 (2.2-4.6)	3.85 (2.8-5.8)
ADP/ATP ratio (NR: 1.20-2.00)		
median (range)	3.83 (2.21-15.65)	1.81 (1.41-2.85)
LTA (%)		
ADP (5 µM) (NR: 50-100)		
median (range)	80.5 (52-100)	73 (19-100)
Collagen (4 µg/ml) (NR: 75-100)		
median (range)	83 (56-92)	81 (29-93)
AA (1.5 mM) (NR: 60-100)		
median (range)	88 (19-100)	84 (9-95)
Epinephrine (5 µM) (NR: 5-100)		
median (range)	78 (11-100)	62 (2-91)
PAR-1 AP (10 µM) (NR: 75-100)		
median (range)	94 (60-100)	91 (50-100)
U-46619 (4 µM) (NR: 75-100)		
median (range)	91 (43-100)	94 (58-100)
Ristocetin (0.6 mg/ml) (NR: 0-25)		
median (range)	12 (6-71)	7 (2-57)
Ristocetin (1.2 mg/ml) (NR: 75-100)		
median (range)	94 (77-100)	92 (45-100

MPV; mean platelet volume, IPFD; inherited platelet function disorder, LTA; light transmission aggregometry, NR; normal range, AA; arachidonic acid

In order to distinguish between secretion defects and the absence of granule content in patients with δ-SPD, surface expression of dense granule marker CD63 was assessed in PAR-1 AP stimulated platelets with whole-blood flow cytometry. Mean±SD CD63 expression in patients with δ-SPD was 2107 ± 937 MFI and was decreased compared with non-SPD patients (3568 ± 716 MFI; $P < .0001$) (**Fig. 1a**). No CD63 expression was observed in unstimulated platelets (δ-SPD: 276.8 ± 149.8 MFI; non-SPD: 296.2 ± 56.4 MFI healthy controls: 245.5 ± 61.8 MFI). CD63 expression in non-SPD patients was within the normal reference range, based on CD63 expression in 50 healthy controls. Nine patients with δ-SPD had normal CD63 expression after platelet activation despite low platelet nucleotide content, suggesting dense granules were present but did not contain ADP. To confirm platelets responded normally to stimulation with PAR-1 AP, platelet P-selectin levels were determined.

P-selectin expression in patients with δ-SPD was similar to P-selectin expression in non-SPD patients with IFPD ($P = .25$) and both groups were mostly within the reference range of healthy controls (**Fig. 1b**). Three δ-SPD (12%) and 4 non-SPD patients (18%) were below the reference range, possibly indicating α-granule defects or reduced reactivity to PAR-1 AP in these patients. No P-selectin expression was observed in unstimulated platelets (δ-SPD: 227.6 ± 61.8 MFI; non-SPD: 213.9 ± 69.6 MFI healthy controls: 552.3 ± 371.3 MFI).

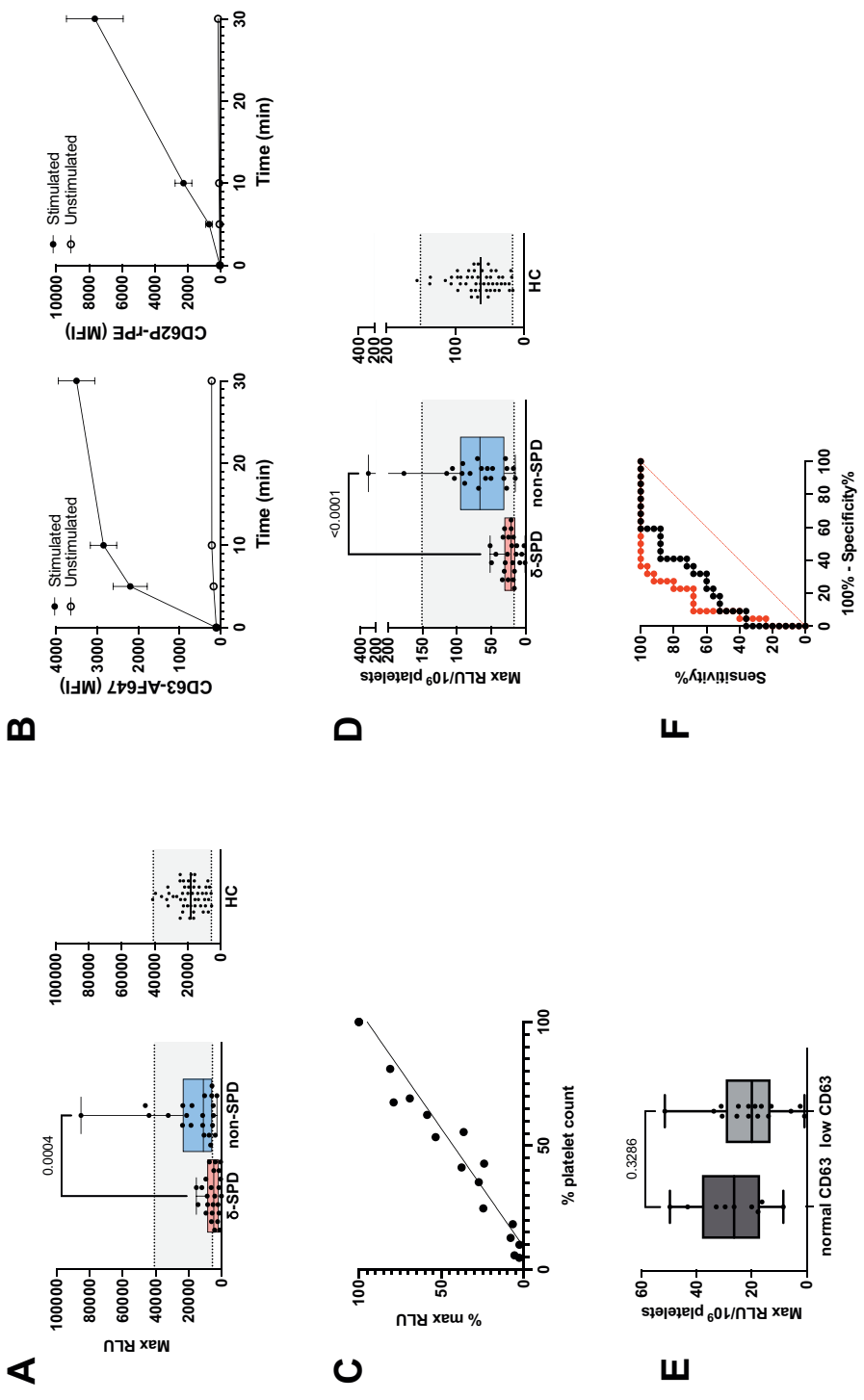

Fig. 1: Expression of markers of platelet granule release upon activation. a,**b**, Expression of (**a**) dense granule marker CD63 and (**b**) α-granule, and platelet activation marker P-selectin (CD62P) on the platelet surface was assessed in whole blood using flow cytometry in patients with δ-storage pool disease (n = 25) (red), non-storage pool disease patients (n = 22) (blue) and healthy controls (n = 50). Platelets were stimulated with 25 µM PAR-1 activating peptide for 10 minutes at 37 °C. The grey area between dotted lines represents the 2.5th to 97.5th percentile of receptor expression in healthy controls. Boxplots with whiskers from minimum to maximum and all individual data points. Statistical analyses were performed with Student's *t*-test.

ATP secretion in whole blood is decreased in δ-SPD

Platelet ATP secretion after stimulation with 2.5 µM PAR-1 AP was assessed in all patients (**Fig. 2a**). This PAR-1 AP concentration induced rapid and sustained CD63 expression in healthy controls, consistent with δ-granule release, as well as P-selectin expression (**Fig. 2b**). As ATP secretion strongly depends on platelet count (**Fig. 2c**), ATP secretion was corrected for platelet count in each participant. ATP secretion was lower in patients with δ-SPD (mean ± SD ATP secretion 22.94 ± 13.13 RLU/10^9 platelets) than in non-SPD patients (78.07 ± 62.08 RLU/10^9 platelets; $P < .0001$) and healthy controls (65.76 ± 31.85 RLU/10^9 platelets; $P < .0001$) (**Fig. 2d**). ATP secretion was normal (reference range, 16.73-150.80 RFU/10^9 platelets) in 21 of 22 non-SPD patients (95%) and 17 of 25 (68%) patients with δ-SPD. Seven of 9 (78%) patients with decreased ATP secretion had a normal P-selectin expression after platelet stimulation with PAR-1 AP. This suggests that decreased ATP secretion is not due to disturbed PAR-1-mediated signaling. Patients with δ-SPD with normal CD63 expression had similar ATP secretion compared with patients with δ-SPD with reduced CD63 expression ($P = .23$) (**Fig. 2e**).

ATP secretion in whole blood can be used for exclusion of δ-SPD

ATP secretion corrected for platelet count as a predictor for δ-SPD yielded a C-statistic of 0.88 (95% CI, 0.78-0.98) (**Fig. 2f**). When ATP secretion was not corrected for platelet count, the C-statistic was 0.79 (95% CI, 0.67-0.92; $P = .29$). Although not significantly different, the performance ATP secretion was better after platelet count correction (**Fig. 2f**). The performance parameters with their corresponding cutoff value are depicted in **Table 2**. Using the 2.5th percentile of the healthy control group as cutoff value (16.41 RLU/10^9 platelets) resulted in a specific (95%) test with low sensitivity (28%). Corresponding LLRs were 6.16 (LLR+) and 0.75 (LLR-) and PPV was 87% and NPV 54%. In the most optimal condition according to the receiver operating characteristic-curve (cutoff 31.45 RLU/10^9 platelets), the sensitivity of the ATP secretion test for

δ-SPD was 80% and specificity was 77%. The corresponding LLR+ was 3.52 and LLR- was 0.26 with a PPV of 80% and NPV of 77%. Using the highest value of the δ-SPD group as cutoff value (53.67 RLU/10^9 platelets) resulted in maximum sensitivity (100%), but moderate specificity (64%). This cutoff value corresponded with an LLR+ of 2.75 and an optimal LLR- of 0.00, PPV of 76%, and NPV of 100%, suggesting this cutoff value can be used for the exclusion of δ-SPD.

Table 2: C-statistics with cutoff values of corrected ATP secretion in relative light units and corresponding sensitivity, specificity, positive likelihood ratio (LLR+), and negative likelihood ratio (LLR-).

Cutoff value	Sensitivity (%)	Specificity (%)	PPV (%)	NPV (%)	LLR+	LLR-
< 16.41	28	95	87	54	6.16	0.75
< 31.45	80	77	80	77	3.52	0.26
< 53.67	100	64	76	100	2.75	0.00

The diseased group is confirmed δ-SPD patients (n = 25). The control group is non-SPD patients (n = 22). ATP, adenosine triphosphate; LLR, likelihood ratio; NPV, negative predictive value; PPV, positive predictive value.

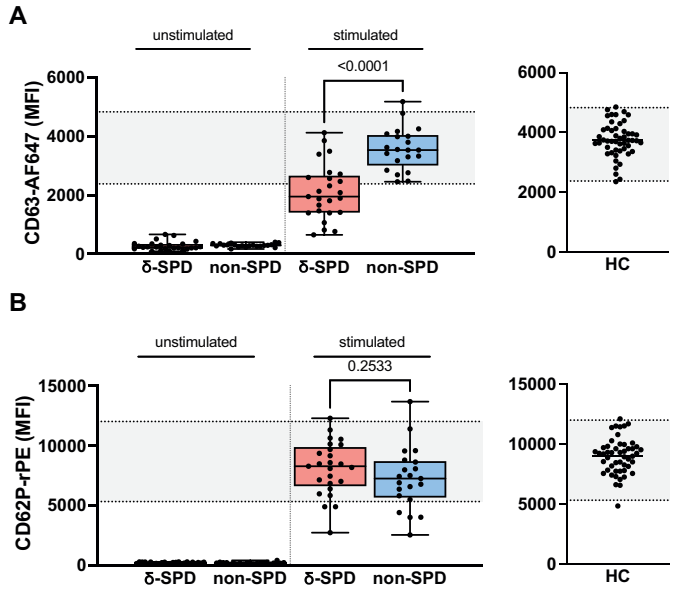

Fig. 2: Platelet adenosine triphosphate (ATP) secretion as determined with the whole-blood ATP secretion test. a, Whole blood was stimulated with 2.5 µM PAR-1 activating peptide at 37 °C and ATP secretion was detected with luminescence in patients with delta storage pool disease (δ-SPD) (n = 25) (red), non-storage pool disease (SPD) patients (n = 22) (blue), and healthy controls (n = 50). ATP secretion is defined as maximum relative light units (RLUs) within 10 minutes after platelet stimulation. **b**, Expression of dense granule marker CD63 and α-granule, and platelet activation marker P-selectin (CD62P) on the platelet surface was assessed in whole blood using flow cytometry in healthy controls (n = 3). Platelets were stimulated with 2.5 µM PAR-1 activating peptide for 0 to 30 minutes at 37 °C. **c**, ATP secretion was determined in reconstituted whole blood with varying platelet counts in healthy donors (n = 3). Both RLU and platelet count are depicted in percentages for each donor. **d**, ATP secretion was corrected for platelet count and expressed as maximum RLU per 10^9 platelets. Grey area between dotted lines represents the 2.5th to 97.5th percentile of ATP secretion in healthy controls. **e**, ATP secretion with the whole-blood ATP secretion test in δ-SPD patients with normal (n = 16) and decreased (n = 9) CD63 expression. **f**, Concordance statistics with receiver operating characteristic curve with non-SPD patients as a reference group and patients with δ-SPD as a diseased group. Black dots represent uncorrected ATP secretion. Red dots represent ATP secretion per 10^9 platelets. Boxplots with whiskers from minimum to maximum and all individual data points. Statistical analyses were performed with a Mann–Whitney U-test. δ-SPD; delta storage pool disease; ATP, adenosine triphosphate; RLU, relative light unit; SPD, storage pool disease.

DISCUSSION

In this study, we showed that ATP secretion in a whole–blood-based assay is decreased in patients with confirmed δ-SPD compared with patients with an IPFD other than SPD and healthy controls. We demonstrate the diagnostic value of this rapid test for the exclusion of dense granule deficiency in patients who present with a suspected primary hemostasis defect. The ISTH Scientific and Standardization Committee Subcommittee on Platelet Physiology highlighted the need for validation of platelet secretion assays for clinical practice, as it is a crucial step in the diagnosis of IPFDs[21]. This study introduces a one-stage whole-blood ATP secretion assay, aiming to provide a more accessible and rapid diagnostic tool for δ-SPD. Whereas current ATP secretion assays are known to be useful in IPFD diagnostics, our test measures ATP release directly in whole blood using luminescence, thereby decreasing the extensive sample preparation and large blood volumes, which is particularly beneficial for pediatric patients.

Our finding that ATP secretion upon platelet activation in whole blood is severely decreased in patients with δ-SPD compared to non-SPD patients and healthy controls indicates the diagnostic potential of our test. However, our performance data indicate that the whole-blood ATP secretion test cannot be used for the identification of δ-SPD: high sensitivity is related to low specificity and vice versa. The most balanced combination with a sensitivity of 80% and specificity of 77% still misses a substantial part of the positive cases. However, using the test with a high cutoff value results in a maximal sensitivity and NPV, meaning it can identify all true positive cases. In this way, the whole-blood ATP secretion test can be used as an exclusion test for δ-SPD in the first line of platelet diagnostics. In those patients in whom δ-SPD cannot be excluded with the rapid ATP secretion test, advanced tests with better specificity, such as luminometric measurement of ATP and ADP content in platelet lysate, measurement of platelet serotonin content in serum or platelet lysate with HPLC, whole-mount electron microscopy, or radiolabeled-serotonin based assays or other secretion assays will still be required[21,32,33]. It is currently unclear which of these advanced testing options has the highest specificity for δ-SPD. The specificity and sensitivity of ATP, ADP, or serotonin measurement with HPLC are reported to be high[33,34], although this needs to be confirmed in larger studies. Additionally, genetic testing can be used for syndromic variants of SPD[12,35]. However, this will not be available in the near future for nonsyndromic variants.

The most used assay for δ-SPD diagnosis, lumi-aggregometry, suffers from several disadvantages: it lacks sensitivity and reproducibility in detecting δ-SPD, it measures ATP rather than ADP, and it cannot distinguish between granule content deficiency and secretion defects[12,36]. The same applies to the rapid whole-blood ATP secretion test. However, the laborious protocol and large amounts of blood that are required for lumi-aggregometry are overcome with the rapid whole-blood ATP secretion test. Additionally, lumi-aggregometry is unreliable at low platelet counts. As the whole-blood ATP secretion test showed a linear relationship with platelet count, this assay might be more reliable for thrombocytopenic samples.

A limitation of this study is the use of a selected patient population, which led to an overestimation of the prevalence of δ-SPD. However, our data indicate that the rapid whole-blood ATP secretion test can be used for the exclusion of δ-SPD based on the low negative LLR, which is independent of prevalence. A second limitation is the absence of a gold standard for diagnosing SPD. In this study, δ-SPD was diagnosed using granule nucleotide content, an accepted and validated test for diagnosis of δ-SPD[21]. A strength of this study is the comparison of the test in patients with a similar bleeding pattern and a referral to a tertiary care center.

The findings of this study support the potential implementation of the whole-blood ATP secretion test as an accessible, first-line diagnostic exclusion tool for δ-SPD, especially in settings where rapid turn-around is essential or where traditional diagnostics are unavailable. Future research should focus on standardizing this assay, improving its accessibility, and integrating it into routine diagnostics. Additionally, further validation in a larger multicenter cohort would enhance its diagnostic accuracy and reliability.

In conclusion, the rapid whole-blood ATP secretion test may have additional value during platelet function testing, with the potential to exclude δ-SPD early in the diagnostic process.

ADDENDUM

TiN study group: Erik Beckers, Maastricht, the Netherlands, Michiel Coppens, Amsterdam, the Netherlands, Jeroen Eikenboom, Leiden, the Netherlands, Louise Hooimeijer, Groningen, the Netherlands, Gerard Jansen, Rotterdam, the Netherlands, Roger Schutgens, Utrecht, the Netherlands, Rolf Urbanus, Utrecht, the Netherlands, and Minka Zivkovic, Utrecht, the Netherlands.

SYMPHONY consortium: Emile van den Akker, Amsterdam, the Netherlands, Wala Al Arashi, Rotterdam, the Netherlands, Ryanne Arisz, Rotterdam, the Netherlands, Lieke Baas, Utrecht, the Netherlands, Ruben Bierings, Rotterdam, the Netherlands, Maartje van den Biggelaar, Amsterdam, the Netherlands, Johan Boender, Amsterdam, the Netherlands, Anske van der Bom, Leiden, the Netherlands, Mettine Bos, Leiden, the Netherlands, Martijn Brands, Amsterdam, the Netherlands, Annelien Bredenoord, Utrecht, the Netherlands, Laura Bukkems, Amsterdam, the Netherlands, Lex Burdorf, Rotterdam, the Netherlands, Jessica Del Castillo Alferez, Amsterdam, the Netherlands, Michael Cloesmeijer, Amsterdam, the Netherlands, Marjon Cnossen, Rotterdam, the Netherlands, Mariëtte Driessens, Utrecht, the Netherlands, Jeroen Eikenboom, Leiden, the Netherlands, Karin Fijnvandraat, Amsterdam, the Netherlands, Kathelijn Fischer, Utrecht, the Netherlands, Geertje Goedhart, Leiden, the Netherlands, Tine Goedhart, Rotterdam, the Netherlands, Samantha Gouw, Amsterdam, the Netherlands, Rieke van der Graaf, Utrecht, the Netherlands, Masja de Haas, Amsterdam, the Netherlands, Lotte Haverman, Amsterdam, the Netherlands, Jan Hazelzet, Rotterdam, the Netherlands, Shannon van Hoorn, Rotterdam, the Netherlands, Elise Huisman, Rotterdam, the Netherlands, Nathalie Jansen, Utrecht, the Netherlands, Alexander Janssen, Amsterdam, the Netherlands, Sean de Jong, Hoofddorp, the Netherlands, Sjoerd Koopman, Amsterdam, the Netherlands, Marieke Kruip, Rotterdam, the Netherlands, Sebastiaan Laan, Leiden, the Netherlands, Frank Leebeek, Rotterdam, the Netherlands, Nikki van Leeuwen, Rotterdam, the Netherlands, Hester Lingsma, Rotterdam, the Netherlands, Moniek de Maat, Rotterdam, the Netherlands, Ron Mathôt, Amsterdam, the Netherlands, Felix van der Meer, Leiden, the Netherlands, Karina Meijer, Groningen, the Netherlands, Sander Meijer, Amsterdam, the Netherlands, Stephan Meijer, Den Haag, the Netherlands, Iris van Moort, Rotterdam, the Netherlands, Caroline Mussert, Rotterdam, the Netherlands, Hans Kristian Ploos van Amstel, Utrecht, the Netherlands, Suzanne Polinder, Rotterdam, the Netherlands, Diaz Prameyllawati, Rotterdam, the Netherlands, Simone Reitsma, Rotterdam, the Netherlands, Eliza Roest, Rotterdam, the Netherlands,

Lorenzo Romano, Rotterdam, the Netherlands, Saskia Schols, Nijmegen, the Netherlands, Roger Schutgens, Utrecht, the Netherlands, Rolf Urbanus, Utrecht, the Netherlands, Carin Uyl, Rotterdam, the Netherlands, Jan Voorberg, Amsterdam, the Netherlands, Huan Zhang, Amsterdam, the Netherlands, and Minka Zivkovic, Utrecht, the Netherlands.

Declaration of competing interest

M.Z.: no conflicts of interest. R.E.G.S.: The institution of REG Schutgens has received speaker's fees and/or research grants from Bayer, CSL Behring, Hemab, Novartis, NovoNordisk, Octapharma, Roche, Sobi and Takeda. V.v.d.V.: no conflicts of interest. J.A.L.: no conflicts of interest. M.R.: employee of Synapse Research Institute. D.H.: employee of Synapse Research Institute. A.S.d.M.: no conflicts of interest. I.C.L.K.H.: no conflicts of interest. R.T.U.: The institution of RT Urbanus has received research grants from Hemab.

Acknowledgements

We gratefully acknowledge the patients and healthy donors who participated in this study.

Author contributions

M.Z.: conceptualization, methodology, validation, formal analysis, investigation, resources, data curation, writing (original draft), writing (review and editing), visualization. R.E.G.S.: writing (review and editing), supervision, project administration, funding acquisition. V.v.d.V.: investigation, resources, data curation. J.A.L.: investigation, resources, data curation. M.R.: conceptualization, methodology, writing (review and editing). D.H.: conceptualization, methodology, investigation, resources, writing (review and editing). A.S.d.M.: resources. I.C.L.K.H.: resources. R.T.U.: conceptualization, methodology, formal analysis, resources, writing (review and editing), supervision, project administration.

Funding sources

This work was supported by the SYMPHONY consortium (Dutch Research Counsil - Dutch Research Agenda [NWO-NWA] grant number 1160.18.038).

REFERENCES

1. Holmsen H, Weiss HJ. Secretable storage pools in platelets. *Annu Rev Med*. 1979;30:119-134. doi:10.1146/annurev.me.30.020179.001003
2. King SM, Reed GL. Development of platelet secretory granules. *Semin Cell Dev Biol*. 2002;13(4):293-302. doi:10.1016/s1084952102000599
3. Fukami MH, Salganicoff L. Human platelet storage organelles. A review. *Thromb Haemost*. 1977;38(4):963-970.
4. McNicol A, Israels SJ. Platelet dense granules: structure, function and implications for haemostasis. *Thromb Res*. 1999;95(1):1-18. doi:10.1016/s0049-3848(99)00015-8
5. McNicol A, Israels SJ, Robertson C, Gerrard JM. The empty sack syndrome: a platelet storage pool deficiency associated with empty dense granules. *Br J Haematol*. 1994;86(3):574-582. doi:10.1111/j.1365-2141.1994.tb04789.x
6. Heijnen H, van der Sluijs P. Platelet secretory behaviour: as diverse as the granules … or not? *J Thromb Haemost*. 2015;13(12):2141-2151. doi:10.1111/jth.13147
7. Zieger B. Defects of platelet granules and secretion. In: Gresele P, Kleiman NS, Lopez JA, Page CP, eds. *Platelets in Thrombotic and Non-Thrombotic Disorders*. Springer International Publishing; 2017:917-922. doi:10.1007/978-3-319-47462-5_61
8. Weiss HJ, Witte LD, Kaplan KL, et al. Heterogeneity in storage pool deficiency: studies on granule-bound substances in 18 patients including variants deficient in alpha-granules, platelet factor 4, beta-thromboglobulin, and platelet-derived growth factor. *Blood*. 1979;54(6):1296-1319.
9. Ingerman CM, Smith JB, Shapiro S, Sedar A, Silver MJ. Hereditary abnormality of platelet aggregation attributable to nucleotide storage pool deficiency. *Blood*. 1978;52(2):332-344.
10. Ferreira CR, Chen D, Abraham SM, et al. Combined alpha-delta platelet storage pool deficiency is associated with mutations in GFI1B. *Mol Genet Metab*. 2017;120(3):288-294. doi:10.1016/j.ymgme.2016.12.006
11. Beirat AF, Menakuru SR, Kalra M. Platelet Delta (δ)-Storage Pool Deficiency: A Case Series and Review of the Literature. *Hematol Rep*. 2023;15(3):405-410. doi:10.3390/hematolrep15030041
12. Dupuis A, Bordet J-C, Eckly A, Gachet C. Platelet δ-Storage Pool Disease: An Update. *J Clin Med*. 2020;9(8). doi:10.3390/jcm9082508
13. Barbosa MD, Nguyen QA, Tchernev VT, et al. Identification of the homologous beige and Chediak-Higashi syndrome genes. *Nature*. 1996;382(6588):262-265. doi:10.1038/382262a0
14. Ajitkumar A, Yarrarapu SNS, Ramphul K. Chediak-Higashi Syndrome. In: *StatPearls*. StatPearls Publishing; 2025.
15. Gahl WA, Huizing M. Hermansky-Pudlak Syndrome. In: Pagon RA, Adam MP, Ardinger HH, et al., eds. *GeneReviews(®)*. University of Washington, Seattle; 1993.

16. Griscelli C, Durandy A, Guy-Grand D, Daguillard F, Herzog C, Prunieras M. A syndrome associating partial albinism and immunodeficiency. *Am J Med*. 1978;65(4):691-702. doi:10.1016/0002-9343(78)90858-6
17. Westbroek W, Tuchman M, Tinloy B, et al. A novel missense mutation (G43S) in the switch I region of Rab27A causing Griscelli syndrome. *Mol Genet Metab*. 2008;94(2):248-254. doi:10.1016/j.ymgme.2008.02.009
18. Miller CH, Soucie JM, Byams VR, et al. Occurrence rates of inherited bleeding disorders other than haemophilia and von Willebrand disease among people receiving care in specialized treatment centres in the United States. *Haemophilia*. 2022;28(3):e75-e78. doi:10.1111/hae.14529
19. Handin RI. Inherited platelet disorders. *Hematology Am Soc Hematol Educ Program*. 2005:396-402. doi:10.1182/asheducation-2005.1.396
20. Gresele P, Harrison P, Bury L, et al. Diagnosis of suspected inherited platelet function disorders: results of a worldwide survey. *J Thromb Haemost*. 2014;12(9):1562-1569. doi:10.1111/jth.12650
21. Mezzano D, Harrison P, Frelinger AL, et al. Expert opinion on the use of platelet secretion assay for the diagnosis of inherited platelet function disorders: Communication from the ISTH SSC Subcommittee on Platelet Physiology. *J Thromb Haemost*. 2022;20(9):2127-2135. doi:10.1111/jth.15781
22. Mumford AD, Frelinger AL, Gachet C, et al. A review of platelet secretion assays for the diagnosis of inherited platelet secretion disorders. *Thromb Haemost*. 2015;114(1):14-25. doi:10.1160/TH14-11-0999
23. Gresele P, Subcommittee on Platelet Physiology of the International Society on Thrombosis and Hemostasis. Diagnosis of inherited platelet function disorders: guidance from the SSC of the ISTH. *J Thromb Haemost*. 2015;13(2):314-322. doi:10.1111/jth.12792
24. Pai M, Wang G, Moffat KA, et al. Diagnostic usefulness of a lumi-aggregometer adenosine triphosphate release assay for the assessment of platelet function disorders. *Am J Clin Pathol*. 2011;136(3):350-358. doi:10.1309/AJCP9IPR1TFLUAGM
25. Dovlatova N, Lordkipanidzé M, Lowe GC, et al. Evaluation of a whole blood remote platelet function test for the diagnosis of mild bleeding disorders. *J Thromb Haemost*. 2014;12(5):660-665. doi:10.1111/jth.12555
26. Baker RI, Choi P, Curry N, et al. Standardization of definition and management for bleeding disorder of unknown cause: communication from the SSC of the ISTH. *J Thromb Haemost*. 2024;22(7):2059-2070. doi:10.1016/j.jtha.2024.03.005
27. Cai H, Mullier F, Frotscher B, et al. Usefulness of Flow Cytometric Mepacrine Uptake/Release Combined with CD63 Assay in Diagnosis of Patients with Suspected Platelet Dense Granule Disorder. *Semin Thromb Hemost*. 2016;42(3):282-291. doi:10.1055/s-0035-1564836

28. Ramström AS, Fagerberg IH, Lindahl TL. A flow cytometric assay for the study of dense granule storage and release in human platelets. *Platelets*. 1999;10(2-3):153-158. doi:10.1080/09537109976239

29. Westmoreland D, Shaw M, Grimes W, et al. Super-resolution microscopy as a potential approach to diagnosis of platelet granule disorders. *J Thromb Haemost*. 2016;14(4):839-849. doi:10.1111/jth.13269

30. van Asten I, Blaauwgeers M, Granneman L, et al. Flow cytometric mepacrine fluorescence can be used for the exclusion of platelet dense granule deficiency. *J Thromb Haemost*. 2020;18(3):706-713. doi:10.1111/jth.14698

31. van Dijk WEM, Poolen GC, Huisman A, et al. Evaluation of the procoagulant state in chronic immune thrombocytopenia before and after eltrombopag treatment-a prospective cohort study. *J Thromb Haemost*. 2023;21(4):1020-1031. doi:10.1016/j.jtha.2022.11.039

32. Holmsen H, Dangelmaier CA. [16] Measurement of secretion of adenine nucleotides. In: *Platelets: Receptors, Adhesion, Secretion Part A*. Vol 169. Methods in Enzymology. Elsevier; 1989:195-205. doi:10.1016/0076-6879(89)69060-X

33. Aranda E, Iha S, Solari S, et al. Serotonin secretion by blood platelets: accuracy of high-performance liquid chromatography-electrochemical technique compared with the isotopic test and use in a clinical laboratory. *Res Pract Thromb Haemost*. 2023;7(5):102156. doi:10.1016/j.rpth.2023.102156

34. von Papen M, Gambaryan S, Schütz C, Geiger J. Determination of ATP and ADP Secretion from Human and Mouse Platelets by an HPLC Assay. *Transfus Med Hemother*. 2013;40(2):109-116. doi:10.1159/000350294

35. Sandrock K, Zieger B. Current strategies in diagnosis of inherited storage pool defects. *Transfus Med Hemother*. 2010;37(5):248-258. doi:10.1159/000320279

36. Badin MS, Graf L, Iyer JK, Moffat KA, Seecharan JL, Hayward CPM. Variability in platelet dense granule adenosine triphosphate release findings amongst patients tested multiple times as part of an assessment for a bleeding disorder. *Int J Lab Hematol*. 2016;38(6):648-657. doi:10.1111/ijlh.12553

Chapter 4

Proteomic analysis indicates lower abundance of platelet alpha-granule proteins in Glanzmann thrombasthenia

Minka Zivkovic[1], Tatiana M Shamorkina[2], Maaike W Blaauwgeers[1], Harm Post[2], Albert JR Heck[2], Roger EG Schutgens[1], Rolf T Urbanus[1]; for the TiN study group and SYMPHONY consortium

[1] Center for Benign Haematology, Thrombosis and Haemostasis, Van Creveldkliniek, University Medical Center Utrecht, Utrecht University, Utrecht, the Netherlands

[2] Biomolecular Mass Spectrometry and Proteomics, Bijvoet Center for Biomolecular Research and Utrecht Institute for Pharmaceutical Sciences, Utrecht University, Utrecht, The Netherlands

J Thromb Haemost. 2025 Apr 14:S1538-7836(25)00253-3.

SUMMARY

Background: Glanzmann thrombasthenia (GT) is an inherited platelet function disorder caused by mutations in the fibrinogen receptor αIIbβ3. The deficiency can be quantitative (type I/II) or qualitative (type III). This causes lack of platelet aggregation and leads to a moderate to severe bleeding tendency. Besides the absence or functional alteration of the integrins αIIb and β3, little is known about the proteomic landscape of platelets from people with GT.
Objectives: To evaluate the platelet proteome in GT.
Methods: Label-free quantification of platelet proteins was performed in thirteen genetically confirmed GT patients (11 type I and 2 type III) and thirteen healthy controls with liquid chromatography coupled with tandem mass spectrometry (LC-MS/MS). αIIbβ3 expression was quantified with whole blood flow cytometry. Medical ethics committee approval was obtained and all participants provided informed consent.
Results: 2677/3664 identified proteins were considered quantified. Dynamic range spanned 5 orders of magnitude, and the mean CV was 1.2%, indicating data were robust. Flow cytometry-based αIIb expression correlated well with ITGA2B abundance according to LC-MS/MS. Twentynine proteins were less abundant, and 32 proteins were more abundant in GT than in controls. Downregulated proteins were enriched for alpha (α)-granule proteins, including SPARC, APLP2, TIMP1 and TLT-1 in addition to the subunits of integrin αIIbβ3, fibrinogen and plasminogen. Unregulated proteins were mostly plasma proteins annotated to blood microparticles.
Conclusion: Glanzmann thrombasthenia platelets show reduced abundance of specific platelet α-granule proteins compared with healthy controls.

Keywords: Blood Platelets; Blood Platelet Disorders; Proteomics; Thrombasthenia

INTRODUCTION

Glanzmann thrombasthenia (GT) is a rare inherited platelet defect caused by mutations in the genes encoding integrin subunit α2b (ITGA2B) or integrin subunit β3 (ITGB3), resulting in a quantitative or qualitative defect of the platelet fibrinogen receptor integrin αIIbβ3[1,2]. People with GT are mostly diagnosed at an early age and suffer from a moderate to severe mucocutaneous bleeding tendency. Characteristic laboratory features are a severely impaired or absent platelet aggregation in response to physiologic platelet agonists, such as adenosine diphosphate (ADP), arachidonic acid (AA) or collagen[3]. GT can be classified according to platelet αIIbβ3 expression: in type I platelets lack αIIbβ3 (<5% expression), in type II there is residual expression (5-20%) and in type III or variant GT the expression is low to normal, but qualitative defects are present[1].

Beyond its major function in platelet adhesion and aggregation, integrin αIIbβ3 has been implicated to be the primary receptor for endocytosis and trafficking of fibrinogen into platelet alpha (α)-granules[4,5]. After binding of fibrinogen to αIIbβ3, outside-in signaling is triggered, leading to a cascade of intracellular signaling events that mediate irreversible stable platelet adhesion and spreading[6]. Additionally, the direct communication of αIIbβ3 with cytoplasmic actin filaments is essential for platelet aggregation and clot retraction[7,8]. Another binding ligand for αIIbβ3 is von Willebrand Factor (VWF), which plays an essential role in firm adhesion to collagen[9,10].

As of now, besides the absence of integrins α2b and β3, little is known about the proteomic landscape of platelets of GT patients. Proteomics is a core technology in understanding the molecular mechanisms underlying healthy and disease phenotype. Besides identification of the proteins present in a sample, it can assess protein abundance, localization, posttranslational modifications, isoforms, and molecular interactions[11]. For platelets, proteomics can provide detailed insight into their (quantitative) protein composition, their subcompartments, or platelet-derived microparticles, examined at resting or activated conditions[12,13]. In this study, we evaluated the platelet proteome of a cohort of 13 unrelated patients with GT in the Netherlands.

MATERIALS AND METHODS

Study population

Healthy controls

Healthy control participants were recruited from the staff and students at the University Medical Center Utrecht by the MiniDonor biobank facility (Biobank number 18-774). Approval for the study was obtained from the local ethics review board, and all participants provided written informed consent.

Glanzmann thrombasthenia patients

We selected GT patients from the Thrombocytopathy in the Netherlands (TiN) study, a nationwide cross-sectional study on disease phenotyping, diagnostics, and genetics in people with a (suspected) inherited platelet defect in the Netherlands, at the University Medical Center Utrecht[14,15]. These patients were diagnosed with GT based on clinical and hematological features and diagnosis was genetically confirmed in all patients. Approval for the study was obtained from the NedMec medical ethics review board at UMC Utrecht (registration number NL5878 in the Dutch trial registry) and all participants gave written informed consent in accordance with the declaration of Helsinki. Clinical and hematological features were assessed using complete blood count, a flow cytometric platelet activation assay, light transmission aggregometry and platelet granule ATP and ADP content, as described previously[16].

Flow cytometry

Platelet surface expression of platelet activation marker P-selectin and fibrinogen binding were assessed with fluorescence activated cell sorting (FACS), as described previously[17]. Five µL of whole blood or PC was added to 50 µL antibody/agonist mixture, consisting of 15 µg/mL R-Phycoerythyrin (rPE)-conjugated GPIbα nanobody (clone 17; in-house produced), 7.5 µg/mL AlexaFluor™ (AF)647-conjugated P-selectin nanobody (clone B10.6; in-house produced) and 25 µg/mL AF488-conjugated fibrinogen nanobody (in-house produced). Platelet agonists were either 25 µM Protease-Activated Receptor 1 activating peptide (PAR-1 AP) SFLLRN (Bachem, 141923-40-2), 250 µM PAR-4 AP AYPGKV (produced at the peptide facility of the Netherlands Cancer Institute), 60 µM adenosine diphosphate (ADP) (Sigma), 1 µg/mL cross-linked collagen related peptide (CambCol Laboratories) or 5 µM U-46619 (Cayman Chemical). Additionally, platelet receptors were detected on unstimulated platelets using eFluor660-conjugated anti-GPVI (clone HY101; 1:100; eBioscience),

FITC-conjugated anti-α2β1 (CD49b) (clone AK7; 1:25; BD Pharmingen) and rPE-conjugated anti-αIIbβ3 (CD41a) (clone HIP8; 1:100; BD Pharmingen). Whole blood was incubated in the antibody/agonist mixture in the dark at 37°C for 10 minutes. Platelet activation was stopped by fixation at room temperature (RT) for 20 minutes in the dark with 500 µL of fixative solution (137 mM NaCl, 2.7 mM KCl, 1.12 mM NaH2PO4, 1.15 mM KH2PO4, 10.2 mM Na2HPO4, 4 mM EDTA, 1.11% Formaldehyde, pH 6.8). After fixation, samples were diluted 1:1 (v/v) in 10 mM HEPES, 150 mM NaCl, 1 mM MgSO4, 5 mM KCl, pH 7.4 and analyzed on a BD FACSCanto™ II Flow Cytometer with FACSDiva™ Software. Platelets were gated based on forward and sideward scatter, as well as CD42b (GPIbα) expression. Data are expressed as median fluorescent intensity (MFI).

Light transmission aggregometry

Aggregation of platelets was assessed using light transmission aggregometry in a Chrono-Log model 700 (Kordia)[17]. Citrated whole blood was centrifuged at 160g for 15 minutes at RT without brake to obtain platelet-rich plasma (PRP). The remainder of the blood was centrifuged at 2,000g for 10 minutes at RT to obtain platelet-poor plasma (PPP) to serve as a blank in the aggregometer. PRP was added to a glass cuvette containing a magnetic stirrer. Aggregation was initiated by either 5 µM ADP, 1.5 mM arachidonic acid, 4 µg/mL Collagen Reagens HORM® Suspension (Takeda Pharmaceuticals) or 1 mg/mL ristocetin. Aggregation was monitored for 15 minutes at 37°C at 900 rpm.

Platelet isolation and sample preparation for LC-MS/MS

The proteome of platelets of people with GT and healthy controls was assessed using liquid chromatography with tandem mass spectrometry (LC-MS/MS). Hereto, PRP was prepared from human citrated whole blood by centrifugation at 120g for 20 min. After addition of 10 mM EDTA, PRP was centrifuged at 400g for 20 min and supernatant was discarded. Platelet pellets contained <1 leukocyte per 10,000 platelets. The platelet pellet was resuspended in HEPES-buffered saline (HBS) (10 mM HEPES, 150 mM NaCl, 1 mM MgSO4*6 H2O, pH 7.4) with 10 mM EDTA, centrifuged at 400g for 20 minutes and supernatant was discarded. Platelet pellets were stored at -80ºC until further use. Platelet pellets were resuspended in lysis buffer (1% sodium deoxycholate, 10 mM TCEP, 100 mM Tris, 40 mM chloroacetamide, complete mini EDTA-free protease inhibitor cocktail (Roche), phosphoSTOP tablet (Roche), pH 8.5) and heated for 5 minutes at 95°C, followed by 30 minutes incubation on ice. Supernatant

was collected after 30 minutes centrifugation at 20,000g. Protein concentration was determined by Bradford protein assay (Bio-Rad) according to the manufacturer's protocol. Hundred µg of protein was digested with Lys-C (Sigma) for 1 hour (enzyme: protein ratio 1:75) followed by trypsin (Sigma) digestion overnight (1:100) at 37°C. Reaction was quenched with formic acid to 4% final concentration (v/v) and samples were desalted using standard Sep-pak 1cc columns (Waters) and vacuum-dried.

LC-MS/MS

One µg of peptides per sample was injected into an UHPLC 1290 system (Agilent) coupled to an Orbitrap Q Exactive HF mass spectrometer (Thermo Scientific). Peptides were first loaded onto in-house packed trap column (Dr Maisch Reprosil C18, 3 µm, 2 cm × 100 µm) and separated on an in-house packed analytical column (Agilent Poroshell EC-C18, 2.7 µm, 50 cm × 75 µm). Trapping was performed for 5 minutes in solvent A (0.1% formic acid in water), and the gradient was as follows: 0–10% buffer B (0.1% formic acid in 80% ACN) in 10 sec, 10–36% in 155 min, 36–100% in 3 min, and finally 100% for 1 min. Flow was passively split to 300 nL/min. The mass spectrometer was operated in data-dependent mode. Full-scan MS spectra in 375–1600 m/z mass range were acquired at a resolution of 60,000 after accumulation to a target value of 3 × 106. Up to 10 most intense precursor ions were selected for fragmentation. HCD fragmentation was performed at normalized collision energy of 27% after the accumulation to a target value of 1 × 105. MS/MS spectra were recorded at a resolution of 30,000.

Data analysis

Raw files were processed with MaxQuant (version 1.6.7.0). The database search was performed against the human Swissprot database (version March 29, 2019) using Andromeda as search engine. Cysteine carbamidomethylation was set as a fixed modification and methionine oxidation, protein N-term acetylation were set as a variable modification. Trypsin was specified as enzyme and up to two missed cleavages were allowed. Filtering was done at 1% false discovery rate (FDR) at the protein and peptide level. Label-free quantification (LFQ) was performed, and "match between runs" was enabled. The data were submitted to the PRIDE and can be accessed via Data Availability statement.

The data were further processed and analyzed using Perseus (version 2.0.7.0) to remove potential contaminants and reverse identifications and log2-transformed.

Missing values were imputed by normal distribution (width = 0.3, shift = 1.8). Proteins were used for the subsequent quantitative analyses when detected in at least 40% of samples in each group. Differences between GT patients and controls were assessed with t-tests, with correction for multiple testing (Benjamini Hochberg). Gene ontology (GO) term enrichment analysis was conducted for differentially expressed proteins, with the entire dataset as background and correction for multiple testing (Benjamini Hochberg). A Benjamin Hochberg adjusted p-value <.05 was considered statistically significant. Geometric coefficient of variation (CV) was calculated using log-transformed data with the following equation: $\sqrt{(e^{(\sigma^2)}-1)}$[18]. The data were plotted with RStudio (version 2023.12.1, ggplot2 package) and GraphPad Prism (version 20.2.2324).

RESULTS

A total of 13 unrelated adult GT patients were included in this study. The most common clinical features were mucocutaneous bleeds (epistaxis, oral cavity bleeding), bleeding from minor wounds and menorrhagia. Patients were aged 30-74 and 5 were men and 8 were women. The median platelet count was 193*109/L (IQR 141-235) and median mean platelet volume (MPV) was 9.3 fL (IQR 8.0-10.6) (**Table 1**). Four patients had mild thrombocytopenia (platelet count between 100*109/L and 150*109/L) and six patients had an increased MPV (>9.5 fL). All patients had normal VWF ristocetin cofactor activity. Platelet aggregation was severely reduced or absent in response to ADP, arachidonic acid and collagen and slightly reduced in response to ristocetin, in line with the diagnosis of GT (Table 1). Flow cytometry indicated reduced fibrinogen binding in response to all agonists compared with healthy controls and reduced surface expression of integrin αIIbβ3, varying from 0.6 to 28.7% (**Fig. 1a**). P-selectin expression was normal or increased in GT patients (**Fig. 1b**). Based on flow cytometric αIIbβ3 receptor expression, 11 patients were classified as type I GT (<5% expression) and 2 patients as type III GT (20.4% and 28.7% expression) (**Fig. 1c**). Expression of GPIbα, α2β1 and GPVI was normal or increased in GT patients based on flow cytometry analysis (**Fig. 1c**). Genetic mutations in ITGA2B or ITGB3 were identified in all 13 patients (**Table 2**), confirming GT genotype.

Table 1: Glanzmann thrombasthenia patient characteristics.

Sex (n)	Female (8), male (5)
Age; median (range)	59 (30-74)
ISTH-BAT; median (range)	20 (9-26)
Platelet count (*10^9/L); median (range) (NR: 150-450)	184 (106-307)
MPV (fL); median (range) (NR: 7.0-9.5)	9.2 (7.0-11.4)
Glanzmann type	
Type I (<5 % αIIbβ3 expression)	11
Type II (5-20 %)	0
Type III (>20 %)	2
LTA (% MA)*	
ADP; mean (IQR) (NR: 73-100)	3 (0-3)
Arachidonic acid; mean (IQR) (NR: 60-100)	2 (0-1)
Collagen; mean (IQR) (NR: 78-100)	13 (7-14)
Ristocetin; mean (IQR) (NR: 75-100)	42 (24-65)
Granule nucleotide content (μmol/10^{11} platelets)**	
ADP; mean (IQR) (NR: 1.4-3.3)	3.3 (2.2-4.0)
ATP; mean (IQR) (NR: 2.7-4.8)	5.5 (3.9-6.8)
Ratio; mean (IQR) (NR: 1.2-2.0)	1.7 (1.6-1.8)

*agonist concentrations; 5 μM ADP, 1.5 mM arachidonic acid, 4 μg/mL collagen, 1 mg/mL ristocetin

**missing in two patients

IQR, interquartile range; MPV, mean platelet volume; NR, normal range; LTA, light transmission aggregometry; MA, maximal aggregation

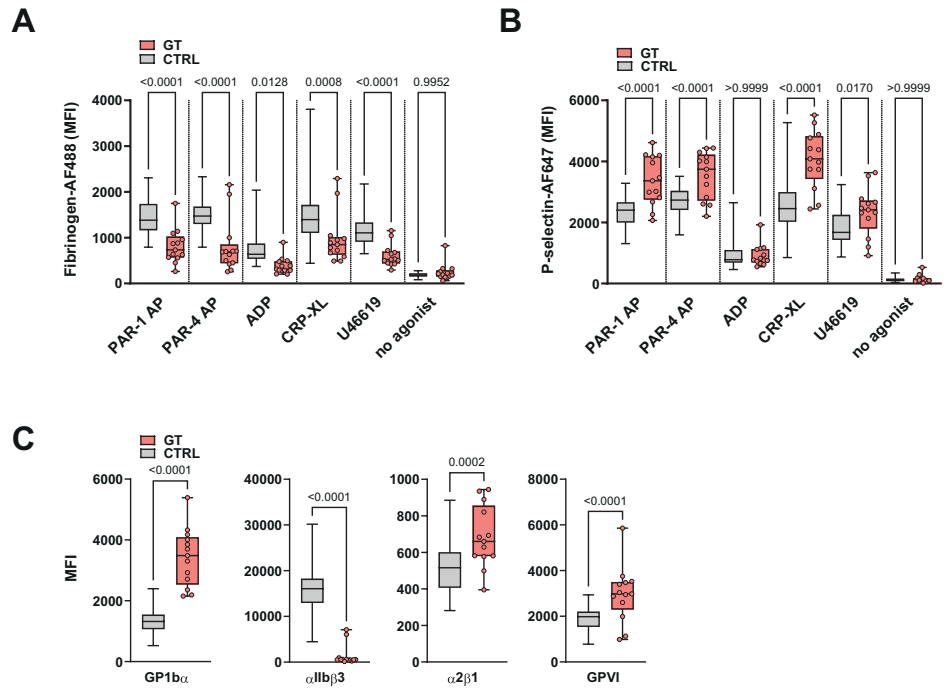

Fig. 1: Fibrinogen binding, P-selectin expression and glycoprotein presence on the platelet surface. a,**b**, Flow cytometric assessment of platelet activation markers (**a**) fibrinogen binding and (**b**) P-selectin expression after platelet stimulation with PAR-1 AP, PAR-4 AP, ADP, CRP-XL or U46619. **c**, Glycoprotein expression on resting platelets. Data are expressed as median fluorescent intensity (MFI). Boxplot with whiskers from min to max with line at median. Open circles represent individual values for Glanzmann thrombasthenia patients (GT; n=13). Grey boxes represent healthy controls (CTRL; n=49). Statistical analyses were performed with one-way analysis of variance with Šidák correction.

Table 2: Genetic findings in Glanzmann thrombasthenia patients.

Patient ID	**1**	**2**	**3**	**4**	**5**	**6**	**7**	**8**	**9**	**10**	**11**	**12**	**13**
Gene	ITGA2B	ITGA2B	ITGA2B	ITGA2B	ITGA2B	ITGB3	ITGA2B	ITGA2B	ITGA2B	ITGA2B	ITGA2B	ITGB3	ITGB3
Zygosity	Compound Het	Homo	Compound Het	Compound Het	Compound Het	Compound Het	Compound Het	Homo	Het	Compound Het	Compound Het	Compound Het	Compound Het
Variant	c.1787T>C c.2841+1G>T	c.3060+2T>C	c.3060+2T>C c.916C>T	c.3060+2T>C c.586C>T	c.526C>G c.2929C>T	c.262C>T c.450G>A	c.3060+2T>C c.2943+1G>A	c.3060+2T>C	c.3060+2T>C	c.3060+2T>C c.2348+1G>C	c.2348+1G>C c.800-1G>A	c.709_710del c.1637A>G	c.353T>A c.719G>A
Protein change	p.Ile596Thr p.?	p.Val982-Lys1020del	p.Gln306*. pVal982-Lys1020del	p.Val982-Lys1020del p.Arg196Cys	p.Pro176Ala p.Arg977*	p.Arg88* p.Met150Ile	p.Val982-Lys1020del p.?	p.Val982-Lys1020del	p.Val982-Lys1020del	p.Val982-Lys1020del p.?	p.?	p.Ser237fs p.Tyr546Cys	p.Leu118His p.Arg240Gln
Mutation type	Missense Splice site	Splice site	Splice site Nonsense	Splice site Missense	Missense Nonsense	Nonsense Missense	Splice site	Splice site	Splice site	Splice site	Splice site	Frameshift Missense	Missense Missense
Domain	Thigh Calf-1	Calf-2	Propeller Calf-2	Calf-2 Propeller	Propeller Calf-2	Hybrid β1	Calf-2	Calf-2	Calf-2	Calf-2 Calf-1	Calf-1 Propeller	β1 EGF-2	Hybrid β1

Het, heterozygous; Homo, homozygous

The platelet proteome of these 13 GT patients was analyzed using LC-MS/MS and compared with the platelet proteome of 13 healthy controls. MS analysis resulted in identification of 3664 unique proteins. After removal of reverse duplicates, contaminants such as keratin and trypsin, and immunoglobulins, 3596 proteins remained, of which 2677 were considered reliably quantified. Platelet count did not correlate with the number of quantified proteins in each sample (Spearman r = 0.09; 95% CI: -0.49 – 0.63). Ninety-one of the quantified proteins could be considered plasma proteins (based on Human Protein Atlas[19] and a benchmark study from Geyer *et al.*[20]). Comparison with an in-depth compilation of seven platelet proteome studies showed substantial overlap with the quantified proteins in our study (2640/2677) (**Fig. 2a**)[21]. LFQ intensities spanned over five orders of magnitude between the least and most abundant proteins, showing good dynamic range (**Fig. 2b**). Cytoskeletal proteins talin-1 (TLN1; Log2 LFQ 39.64±0.13) and filamin A (FLNA; Log2 LFQ 39.44±0.15), as well as platelet α-granule protein thrombospondin-1 (THBS1; Log2 LFQ 37.66±0.24) were amongst the most abundant proteins. In line with the platelet origin of our dataset, proteins annotated with platelet α-granules were more frequently quantified and measured amongst highly abundant proteins (GO-term 0031091; 71 out of 111 proteins were quantified), while proteins annotated with erythrocyte homeostasis (GO:0034101; 4/141 proteins were quantified), leukocyte degranulation (GO:0043299; 13/58 proteins were quantified) and nonsense-mediated mRNA decay (GO:0000184; 16/80 proteins were quantified) were less frequently quantified and measured in the mid-to-low range of detection (**Fig. 2c**). The median CV was 0.26% and, except for eight proteins, CVs were below 15%, indicating data were robust (**Fig. 2d**). Coefficient of variation for ITGA2B was 20.81%. Inspection of six proteins associated with platelets demonstrated high reproducibility across the range of measurement (**Fig. 2e**). Although flow cytometry indicated higher expression of GPIbα, α2β1 and GPVI per platelet in GT than in controls, LC-MS/MS indicated that the total amount of GP1BA, ITGA2, ITGB1 and GP6 protein was similar between GT and controls (**Fig. 2f**).

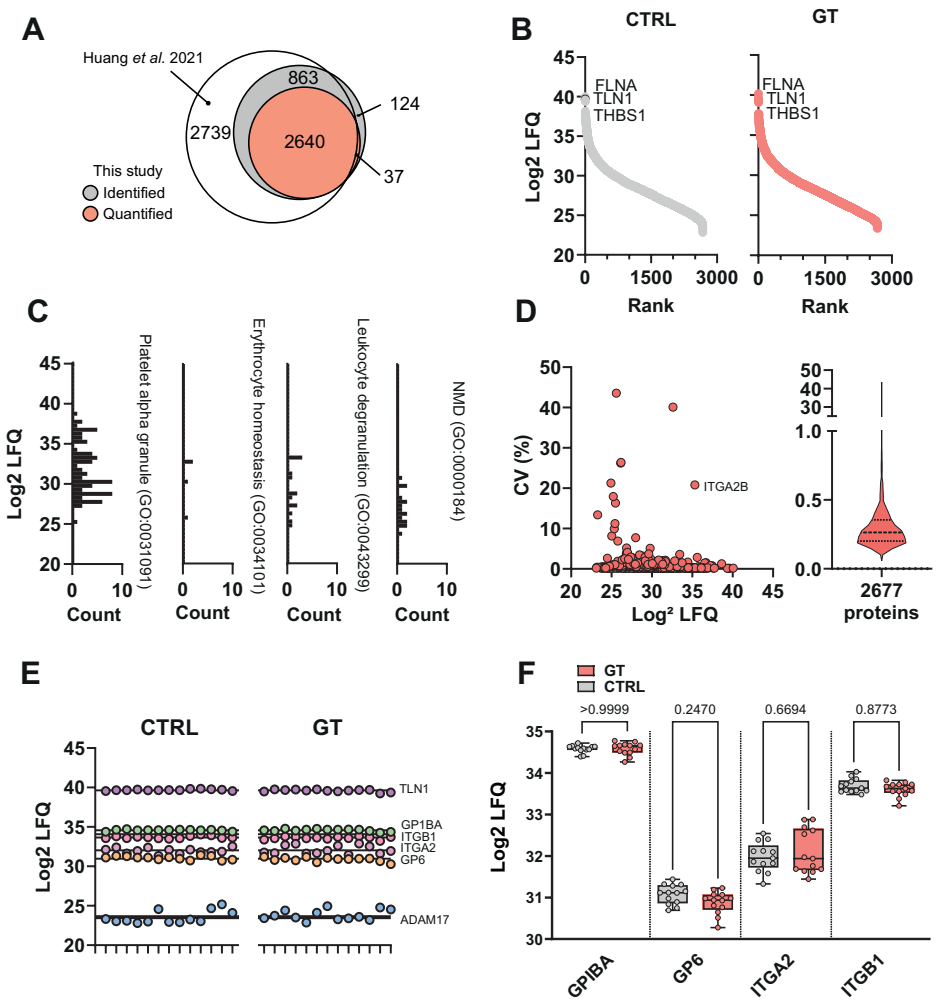

Fig. 2: Platelet proteomic depth and stability. **a**, Overlap of proteins identified by Huang *et al.*[20] and proteins identified (grey) and quantified (coral) in the present study. **b**, Dynamic range of quantified proteins in healthy controls (CTRL; grey) and Glanzmann thrombasthenia patients (GT; pink). Log2 of label free quantification (LFQ) values are shown, representing mean protein abundances. **c**, Intensity distribution of proteins annotated with platelet alpha-granules (GO:0031091), erythrocyte homeostasis (GO:0034101), leukocyte degranulation (GO:0043299) and nonsense-mediated mRNA decay (NMD; GO:0000184) gene ontology (GO) terms. **d**, Scatterplot and violin plot of coefficients of variation (CV), depicted in %. Horizontal dashed lines within violin plots represent median CV, dotted lines represent quartiles. **e**, LFQ intensities of platelet proteins covering the range of measurement (low abundant protein ADAM17, receptors GP6, ITGA2, ITGB1, GPIBA and high abundant protein TLN1). Solid lines represent mean LFQ intensities. Each circle represents a healthy control or GT patient. **f**, Levels of GPIBA, GP6, ITGA2 and ITGB1 as detected with LC-MS/MS. Data are represented as Log2 LFQ values. Statistical analysis was performed with one-way analysis of variance with Šidák correction.

Comparison of proteomes of GT patients and controls at an FDR of 1% indicated 29 proteins were less abundant and 32 were more abundant in GT patients compared with healthy controls (**Fig. 3a, b**). As expected, the abundance of ITGA2B (Log2 difference of 4.2 between the GT patients and controls; p-value = 2.56e-09) and ITGB3 (Log2 difference of 2.7 between GT patients and controls; p-value = 2.45e-10) was much lower in GT than in controls, as was the abundance of the plasma protein fibrinogen (FGB, FGG, FGA; Log2 differences of 3.4, 3.2 and 2.8 with p-values of 4.73e-06, 9.5e-06 and 3.94e-05 respectively). Canonical sequence information of ITGA2B and ITGB3 was used for quantification and peptide mapping. Similar abundance of ITGA2B and ITGB3 was found when individual genetic variations were included in the FASTA file used for database search and quantification analysis.

In general, expression of ITGA2B measured with flow cytometry correlated well with MS-based protein abundance (Spearman r = 0.84), with the two type III GT patients showing relatively high ITGA2B expression in both MS and flow cytometry (**Fig. 3c**). Additionally, ITGA2B expression correlated well with ITGB3 expression as measured with LC-MS/MS (Spearman r = 0.91) (**Fig. 3d**). ITGA2B abundance measured with LC-MS/MS was higher than ITGA2B expression measured with flow cytometry in five patients, suggesting the presence of residual non-functional or non-surface expressed ITGA2B (**Table 3**). The biggest difference in ITGA2B expression was observed in a compound heterozygous patient with both a nonsense and a missense mutation in ITGB3, who had ITGA2B levels consistent with type I GT based on flow cytometry, but levels consistent with type III GT based on LC-MS/MS.

All 29 downregulated proteins in GT were previously reported to be present in platelets[22]. GO-term analysis indicated enrichment of proteins annotated to platelet α-granules amongst downregulated proteins (10/29 downregulated proteins; FDR 1%, -log10(P-value)=7.43) (**Fig. 3e**): (fibrinogen alpha chain (FGA), beta chain (FGB) and gamma chain (FGG), osteonectin (SPARC), TREM-like transcript-1 (TREML1; TLT-1), syntaxin binding protein 1 (STXBP1), TIMP metallopeptidase inhibitor 1 (TIMP1), amyloid beta precursor-like protein 2 (APLP2) and integrin αIIbβ3 (ITGA2B, ITGB3)[23,24]. Twentynine out of 32 upregulated proteins were previously detected in platelet proteomes[21]. GO-term analysis indicated enrichment of proteins annotated to blood microparticles amongst upregulated proteins (20/32 upregulated proteins; FDR 1%, -log10(P-value)=20.80) (**Fig. 3f**). Of the 32 upregulated proteins in GT, 27 were genuine plasma proteins rather than platelet specific proteins[25]. Four of these plasma proteins

were also detected in platelet α-granules (alpha-2-macroglobulin (A2M), alpha-1-antitrypsin (SERPINA1), fibronectin 1 (FN1), kininogen 1 (KNG1))[24]. Platelet count did not correlate with any differentially expressed proteins, except for ITGA2B (Spearman r = -0.62; 95% CI: -0.88 - -0.09; P=0.026).

Table 3: Glanzmann thrombasthenia type classification based on flow cytometry vs mass spectrometry.

Patient ID	Flow cytometry based "classic" classification		MS based classification		
	ITGA2B (%)	Type	ITGA2B (%)	Type	Mutation
1	0,6	I	1,1	I	ITGA2B
2	1,8	I	5,3	II	ITGA2B
3	1,4	I	3,0	I	ITGA2B
4	1,4	I	8,7	II	ITGA2B
5	1,1	I	8,3	II	ITGA2B
6	2,7	I	23,7	III	ITGB3
7	1,8	I	2,9	I	ITGA2B
8	2,1	I	4,5	I	ITGA2B
9	2,3	I	3,0	I	ITGA2B
10	2,4	I	3,4	I	ITGA2B
11	0,9	I	0,5	I	ITGA2B
12	28,7	III	60,7	III	ITGB3
13	20,4	III	36,0	III	ITGB3

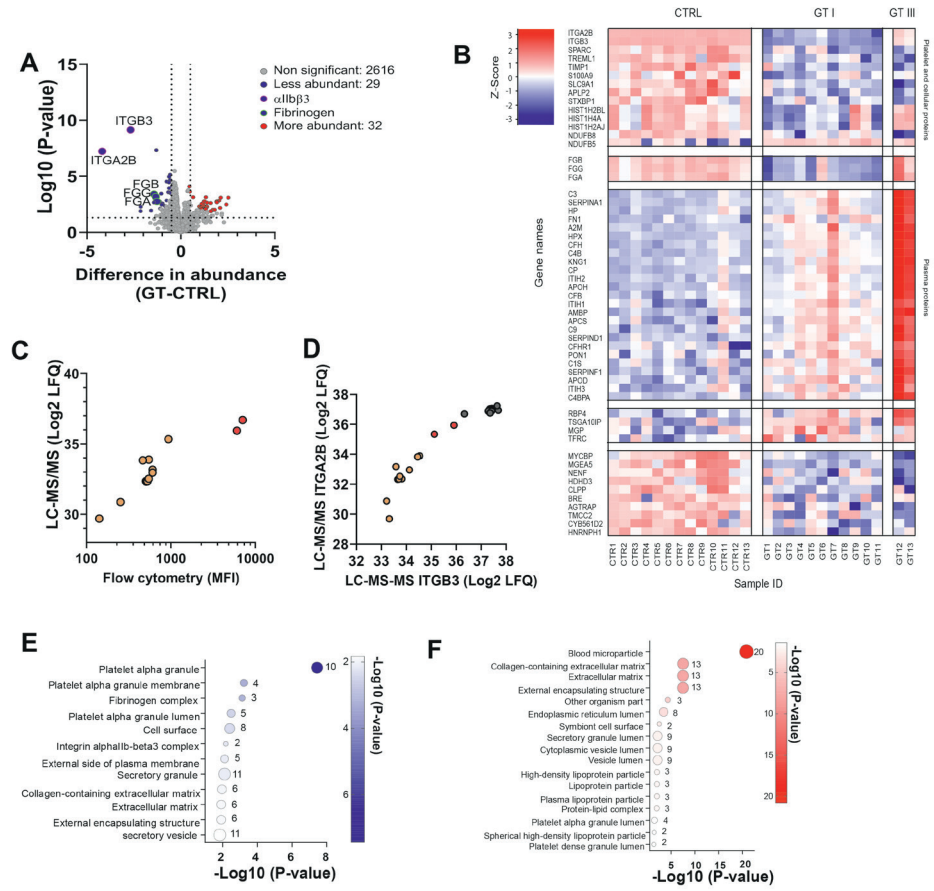

Fig. 3: Differentially expressed proteins in GT patients compared with healthy controls. **a**, Volcano plot with total proteins quantified (grey), downregulated proteins (blue) and upregulated proteins (red) in Glanzmann thrombasthenia patients (GT; n=13) compared with healthy controls (CTRL; n=13). Fibrinogen subunits and αIIbβ3 subunits are indicated separately. **b**, Heatmap of differentially expressed proteins in GT vs healthy controls. High Z-score (red) indicates upregulated proteins, lower Z-score (blue) indicates downregulated proteins. **c**, Correlation between ITGA2B expression as determined by flow cytometry and mass spectrometry for GT patients. Orange dots represent type I GT patients (n=11). Red dots indicate type III GT patients (n=2). **d**, Correlation between ITGA2B expression and ITGB3 expression as determined with mass spectrometry for GT type I patients (orange; n=11), GT type III patients (red; n=2) and healthy controls (grey; n=13). **e**, Gene ontology (GO)-term enrichment analysis amongst downregulated proteins in GT patients. Size of the shape corresponds to the number of proteins annotated to each GO-term. **f**, GO-term enrichment analysis amongst upregulated proteins in GT patients. Size of the shape corresponds to the number of proteins annotated to each GO-term.

The platelet proteome of the two type III patients followed a very different pattern, with plasma proteins being more abundant than in the 11 type I patients. To get a better overview of the platelet proteome of type I GT vs healthy controls, we excluded the two type III patients (**Fig. 4a, b**). This resulted in less differences between healthy and GT platelets: 21 less abundant proteins and 15 more abundant proteins in GT type I patients compared with healthy controls. Downregulated proteins remained enriched for α-granule proteins (10/21 downregulated proteins; FDR 1%; -log10(P-value) 9.86) (**Fig. 4c**). While downregulation of STXBP1 was no longer significant, two additional plasma proteins associated with platelet α-granules were downregulated in type I GT compared with healthy controls: plasminogen and vimentin. Upregulated proteins remained enriched for proteins annotated to blood microparticles (7/15 upregulated proteins; FDR 1%; -log10(P-value) 5.08) (**Fig. 4d**). Of the 15 upregulated proteins, 13 were plasma proteins.

Fibrinogen abundance (FGA, FGB and FGG) correlated well with abundance of plasminogen, and to a lesser extend with SPARC and vimentin levels (**Fig. 4e**). In addition, abundance of SPARC, APLP2, TIMP1 and TREML1 correlated well. Analysis of the relative abundance of downregulated annotated to α-granule proteins showed two different patterns (**Fig. 4f**). While fibrinogen (FGA, FGB, FGG) and plasminogen (PLG) levels were decreased in patients with type I GT compared with controls, they were much higher than controls in the two patients with type III GT. In contrast, the other α-granule proteins (TIMP1, SPARC, TREML1, APLP2, STXBP1 and VIM) were decreased or similar to controls in all GT patients.

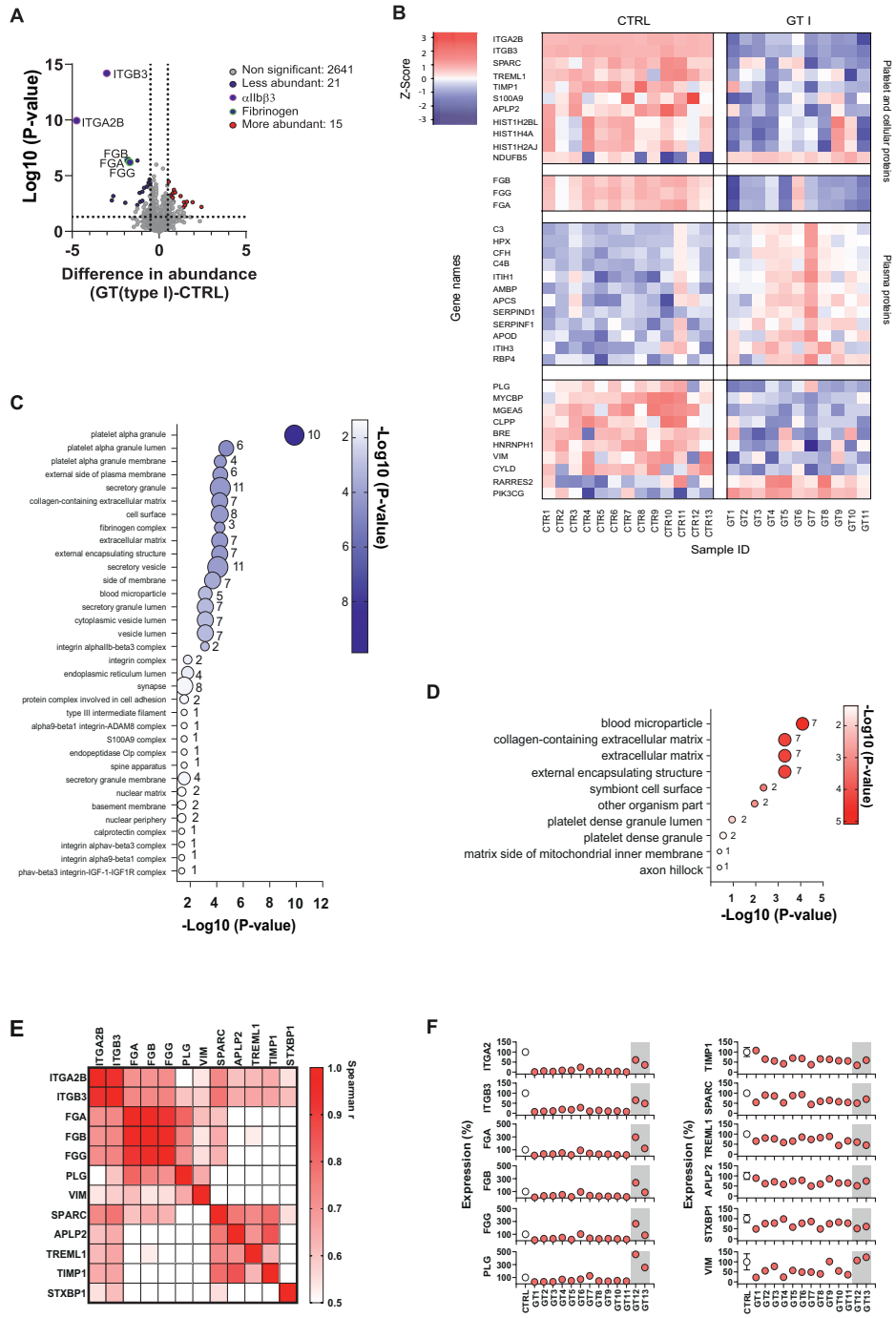

Fig. 4: Differentially expressed proteins in GT type I patients compared with healthy controls. a, Volcano plot with total proteins quantified (grey), downregulated proteins (blue) and upregulated proteins (red) in GT type I patients (n=11) compared with healthy controls (CTRL; n=13). Plasma protein fibrinogen is indicated separately. **b**, Heatmap of differentially expressed proteins in GT type I vs healthy controls. High Z-score (red) indicates upregulated proteins, lower Z-score (blue) indicates downregulated proteins. **c**, Gene ontology (GO)-term enrichment analysis amongst downregulated proteins in GT type I patients. Size of the shape corresponds to the number of proteins annotated to each GO-term. **d**, GO-term enrichment analysis amongst upregulated proteins in GT type I patients. Size of the shape corresponds to the number of proteins annotated to each GO-term. **e**, Spearman correlation matrix analysis for reduced α-granule proteins. **f**, Relative expression per patient of differentially expressed proteins, including the defective integrins (ITGA2, ITGB3), fibrinogen (FGA, FGB, FGG), plasminogen (PLG) and α-granule proteins (TIMP1, SPARC, TREML1, APLP2, STXBP1, VIM). Mean abundance in controls was set at 100%. Data for controls are expressed as mean±SD.

DISCUSSION

Here we reported the platelet proteome of 13 GT patients, of whom 11 were type I patients and two were type III patients. Aside from the strongly reduced expression of both subunits of αIIbβ3 and fibrinogen, our data indicate a reduction in specific α-granules proteins in platelets of GT patients.

Classification of GT is based on residual receptor expression on the platelet surface, usually measured with flow cytometry. Our data suggest good correlation for ITGA2B expression between flow cytometry and LC-MS/MS. However, assessment with LC-MS/MS showed higher levels of ITGA2B compared with flow cytometry in some patients. This may be due to detection of truncated or misfolded versions of the receptor with LC-MS/MS that are no longer recognized by the anti-CD41a antibody used for flow cytometric αIIb quantification. Both type III patients had a mutation in ITGB3, rather than an ITGA2B mutation. This is in line with previous reports of the association between ITGB3 mutations and qualitative αIIbβ3 defects[26]. One of the patients who was classified as type I GT with flow cytometry, but as type III with LC-MS/MS, had an ITGB3 mutation (Met150Ile) (**Table 3**). A Met150Val mutation in ITGB3 is associated with type III GT, with diminished surface expression and enhanced affinity for fibrinogen[27]. The Met150Ile found in this patient could present with the same phenotype, although flow cytometry-based surface expression of αIIbβ3 was very low. In line with enhanced fibrinogen binding capacity, platelet fibrinogen abundance in this patient was similar to levels observed in controls, while fibrinogen abundance was severely reduced in the other type I GT patients. Discrepancies between surface expression and receptor abundance determined with LC-MS/MS might provide leads for further insight in molecular mechanisms underlying GT.

Some variants in type III GT are known to be gain-of-function mutations, with enhanced ability of αIIbβ3 to interact with its ligands and therefore possibly increased receptor-mediate uptake of these proteins, which would explain the relatively high fibrinogen and plasminogen levels in these patients[28,29]. However, the ITGB3 Arg240Gln that is found in one of the type III GT patients is known to be a loss-of function-mutation[30]. Little is known about the other mutation found in this patient, Leu118His. The very high platelet fibrinogen and plasminogen levels we observed in this patient suggest this variant is a gain-of-function mutation. Additional research on the molecular characteristics combined with genotype in GT is necessary. Since there

were only two patients with type III GT in our dataset, we did not have sufficient statistical power to compare proteomes between type I and type III GT.

Overall, platelet proteomes in GT were quantitatively similar to proteomes in healthy controls, with a few notable exceptions. Of the proteins that were downregulated in GT besides ITGA2B and ITGB3, eight were associated with platelet α-granules, potentially indicating reduced abundance of α-granule proteins in GT platelets. Two other proteomics studies were performed in GT, one of which compared two unrelated patients with GT with three heterozygous family members and two healthy controls[31], the other compared one patient with GT with a cohort of 19 healthy controls as part of a larger analysis of platelet proteomes in bleeding disorders[13]. Both studies showed lower abundance of ITGA2B, ITGB3 and fibrinogen in GT, in line with what was already known. In addition, Loroch *et al*. reported reduced plasminogen levels. Although Kreft *et al*. also reported a lower abundance of the same α-granule proteins we identified, statistical significance was not reached, which might be due to the low sample size for GT in that study.

The question arises if GT platelets have less abundant platelet α-granules. Our data indicate that expression of α-granule membrane protein P-selectin is completely normal in GT platelets upon platelet activation, suggesting a normal number of α-granules per platelet and pointing in the direction of decreased α-granule content. Another option is that platelets are longer in circulation in their activated state, causing granule depletion. GT platelets fail to attach to sites of injury through incorporation into aggregates. Instead, they might tether to the damaged sub-endothelium, become activated and release part of their cargo, only to be released in the circulation again. Longer circulation of activated platelets would also lead to a reduction in dense (δ)-granule molecules. However, our data show that ADP and ATP content was normal in GT platelets. Moreover, downregulated proteins in GT were not enriched for proteins annotated to dense granules (**Table 1**). A third explanation of our findings could be that the proteins that were downregulated in our dataset are normally receptor-mediated endocytosed by αIIbβ3, either directly or together with fibrinogen. Of the downregulated α-granule proteins, four are known to interact with fibrinogen: plasminogen, vimentin, osteonectin and TLT-1[32-35]. As no direct associations of these proteins with αIIbβ3 are known, direct endocytosis of these proteins by the fibrinogen receptor is unlikely. However, the known association of these proteins with fibrinogen, which cannot be endocytosed in GT[5], points towards

lower uptake of these proteins that are bound to fibrinogen, in line with what has been reported previously for plasminogen[31]. Correlation analysis suggests this may indeed be the case for VIM and SPARC (**Fig. 4e**). However, neither APLP2, TIMP1 or TLT-1 abundance correlated with fibrinogen abundance, suggesting other mechanisms are responsible for decreased abundance of these proteins.

Although we observed an approximate 60% reduction in total TLT-1 abundance with proteomics, a previous study showed that the platelet surface expression of TLT-1 was similar in GT patients compared with controls[17]. TLT-1 exists in several variants, among which the transmembrane full-length variant and the soluble variant (sTLT-1). Full-length TLT-1 is stored in α-granules and is rapidly upregulated to the surface upon platelet activation[36,37]. The majority of sTLT-1 is present in plasma due to shedding from the activated platelet surface and the remainder is an alternative splicing isoform that is stored and released in α-granules[38]. We speculate that the decreased TLT-1 levels in platelets is caused by lack of αIIbβ3-mediated endocytosis of sTLT-1 that is bound to fibrinogen. However, the lack of correlation between fibrinogen and TLT-1 decreases the likelihood of this hypothesis. Additional research on the presence of TLT-1 variants in GT platelets will be required to shed light on the discrepancy between these observations.

Besides downregulation of specific α-granule proteins in GT, our data showed upregulation of several other proteins in GT compared with healthy controls. Almost all upregulated proteins were plasma proteins, several of which were annotated to blood microparticles according to GO-term enrichment analysis, suggesting they are commonly enriched in microparticle preparations. Although this might reflect contamination of the GT samples with plasma proteins, we cannot exclude their increased concentration is associated with GT. This is supported by the higher number of enriched plasma proteins in the two type III patients with a putative gain-of-function mutation. Whether their increased abundance is caused by increased association of microparticles with platelets in GT remains to be determined.

Strengths of this study were the relatively large and well characterized GT cohort, with extensive phenotyping and genetic data. Additionally, all mass spectrometry samples were processed on the same day, causing minimal experimental variation. A limitation of this study is the fact that healthy controls and GT patients were not sex- and age-matched, as both factors may influence the platelet proteome[39-41].

Another limitation is the possibility of contamination with proteins from erythrocytes or leukocytes. The platelet origin of our dataset is supported by the low number of quantified proteins annotated to erythrocyte homeostasis, leukocyte granule secretion or nonsense-mediated mRNA decay. As downregulated proteins in our dataset were enriched for proteins annotated to platelet α-granules, the impact of any contaminants was likely low. A third limitation is that we were not able confirm the reduced expression of α-granule proteins with a different biochemical technique such as Western blotting due to limited sample availability. Although the pattern we observed was consistent in all GT patients and in line with previous observations[13], additional studies are required to confirm downregulation of specific α-granule proteins in GT.

In conclusion, we found reduced abundance of a subset of α-granule proteins in GT. As GT platelets lack a functional fibrinogen receptor and platelet fibrinogen was shown to play a minor role in primary hemostasis[42], it is unlikely that decreased platelet fibrinogen content will impact primary hemostasis in GT patients. Whether the relatively mild reduction in other α-granule proteins we observed impacts primary hemostasis, fibrinolysis or wound healing remains to be determined.

The use of mass spectrometry in this analysis provided valuable insights into the proteomic landscape of GT and offers potential leads for further mechanistic research within the field of GT.

ADDENDUM

TiN study group: Erik Beckers, Maastricht, the Netherlands, Michiel Coppens, Amsterdam, the Netherlands, Jeroen Eikenboom, Leiden, the Netherlands, Louise Hooimeijer, Groningen, the Netherlands, Gerard Jansen, Rotterdam, the Netherlands, Roger Schutgens, Utrecht, the Netherlands, Rolf Urbanus, Utrecht, the Netherlands, and Minka Zivkovic, Utrecht, the Netherlands.

SYMPHONY consortium: Emile van den Akker, Amsterdam, the Netherlands, Wala Al Arashi, Rotterdam, the Netherlands, Ryanne Arisz, Rotterdam, the Netherlands, Lieke Baas, Utrecht, the Netherlands, Ruben Bierings, Rotterdam, the Netherlands, Maartje van den Biggelaar, Amsterdam, the Netherlands, Johan Boender, Amsterdam, the Netherlands, Anske van der Bom, Leiden, the Netherlands, Mettine Bos, Leiden, the Netherlands, Martijn Brands, Amsterdam, the Netherlands, Annelien Bredenoord, Utrecht, the Netherlands, Laura Bukkems, Amsterdam, the Netherlands, Lex Burdorf, Rotterdam, the Netherlands, Jessica Del Castillo Alferez, Amsterdam, the Netherlands, Michael Cloesmeijer, Amsterdam, the Netherlands, Marjon Cnossen, Rotterdam, the Netherlands, Mariëtte Driessens, Utrecht, the Netherlands, Jeroen Eikenboom, Leiden, the Netherlands, Karin Fijnvandraat, Amsterdam, the Netherlands, Kathelijn Fischer, Utrecht, the Netherlands, Geertje Goedhart, Leiden, the Netherlands, Tine Goedhart, Rotterdam, the Netherlands, Samantha Gouw, Amsterdam, the Netherlands, Rieke van der Graaf, Utrecht, the Netherlands, Masja de Haas, Amsterdam, the Netherlands, Lotte Haverman, Amsterdam, the Netherlands, Jan Hazelzet, Rotterdam, the Netherlands, Shannon van Hoorn, Rotterdam, the Netherlands, Elise Huisman, Rotterdam, the Netherlands, Nathalie Jansen, Utrecht, the Netherlands, Alexander Janssen, Amsterdam, the Netherlands, Sean de Jong, Hoofddorp, the Netherlands, Sjoerd Koopman, Amsterdam, the Netherlands, Marieke Kruip, Rotterdam, the Netherlands, Sebastiaan Laan, Leiden, the Netherlands, Frank Leebeek, Rotterdam, the Netherlands, Nikki van Leeuwen, Rotterdam, the Netherlands, Hester Lingsma, Rotterdam, the Netherlands, Moniek de Maat, Rotterdam, the Netherlands, Ron Mathôt, Amsterdam, the Netherlands, Felix van der Meer, Leiden, the Netherlands, Karina Meijer, Groningen, the Netherlands, Sander Meijer, Amsterdam, the Netherlands, Stephan Meijer, Den Haag, the Netherlands, Iris van Moort, Rotterdam, the Netherlands, Caroline Mussert, Rotterdam, the Netherlands, Hans Kristian Ploos van Amstel, Utrecht, the Netherlands, Suzanne Polinder, Rotterdam, the Netherlands, Diaz Prameyllawati, Rotterdam, the Netherlands, Simone Reitsma, Rotterdam, the Netherlands, Eliza Roest, Rotterdam, the Netherlands,

Lorenzo Romano, Rotterdam, the Netherlands, Saskia Schols, Nijmegen, the Netherlands, Roger Schutgens, Utrecht, the Netherlands, Rolf Urbanus, Utrecht, the Netherlands, Carin Uyl, Rotterdam, the Netherlands, Jan Voorberg, Amsterdam, the Netherlands, Huan Zhang, Amsterdam, the Netherlands, and Minka Zivkovic, Utrecht, the Netherlands.

Declaration of competing interest

M.Z.: no conflicts of interest. T.M.S.: no conflicts of interest. M.W.B.: no conflicts of interest. H.P.: no conflicts of interest. A.J.R.H.: no conflicts of interest. R.E.G.S.: The institution of REG Schutgens has received speaker's fees and/or research grants from Bayer, CSL Behring, Hemab, Novartis, NovoNordisk, Octapharma, Roche, Sobi and Takeda. R.T.U.: The institution of RT Urbanus has received research grants from Hemab.

Acknowledgements

We gratefully acknowledge the patients and healthy donors that were willing to participate in this study.

Author contributions

M.Z.: conceptualization, methodology, validation, formal analysis, investigation, resources, data curation, writing (original draft), writing (review and editing), visualization. T.M.S.: proteomics experiments, data analysis and curation, writing (review and editing). M.W.B.: data curation, investigation. H.P.: proteomics experiments and data analysis. A.J.R.H.: writing (review and editing), supervision proteomics analyses, funding acquisition. R.E.G.S.: writing (review and editing), supervision, project administration, funding acquisition. R.T.U.: conceptualization, methodology, formal analysis, resources, writing (review and editing), supervision, project administration.

Funding sources

This work was supported by the SYMPHONY consortium (NWO-NWA grant number 1160.18.038). Additional support for the proteomics analyses was offered by NWO through the X-omics Road Map program (project 184.034.019).

REFERENCES

1. George JN, Caen JP, Nurden AT. Glanzmann's thrombasthenia: the spectrum of clinical disease. *Blood*. 1990;75(7):1383-1395.
2. Newman PJ, Seligsohn U, Lyman S, Coller BS. The molecular genetic basis of Glanzmann thrombasthenia in the Iraqi-Jewish and Arab populations in Israel. *Proc Natl Acad Sci USA*. 1991;88(8):3160-3164. doi:10.1073/pnas.88.8.3160
3. Kannan M, Saxena R. Glanzmann's thrombasthenia: an overview. *Clin Appl Thromb Hemost*. 2009;15(2):152-165. doi:10.1177/1076029608326165
4. Handagama P, Scarborough RM, Shuman MA, Bainton DF. Endocytosis of fibrinogen into megakaryocyte and platelet alpha- granules is mediated by alpha IIb beta 3 (glycoprotein IIb-IIIa) [published erratum appears in Blood 1993 Nov 1;82(9):2936]. *Blood*. 1993;82(1):135-138. doi:10.1182/blood.V82.1.135.bloodjournal821135
5. Coller BS, Seligsohn U, West SM, Scudder LE, Norton KJ. Platelet fibrinogen and vitronectin in Glanzmann thrombasthenia: evidence consistent with specific roles for glycoprotein IIb/IIIA and alpha v beta 3 integrins in platelet protein trafficking [see comments]. *Blood*. 1991;78(10):2603-2610. doi:10.1182/blood.V78.10.2603.2603
6. Huang J, Li X, Shi X, et al. Platelet integrin αIIbβ3: signal transduction, regulation, and its therapeutic targeting. *J Hematol Oncol*. 2019;12(1):26. doi:10.1186/s13045-019-0709-6
7. Bennett JS. Structure and function of the platelet integrin alphaIIbbeta3. *J Clin Invest*. 2005;115(12):3363-3369. doi:10.1172/JCI26989
8. Liu J, Lu F, Ithychanda SS, et al. A mechanism of platelet integrin αIIbβ3 outside-in signaling through a novel integrin αIIb subunit-filamin-actin linkage. *Blood*. 2023;141(21):2629-2641. doi:10.1182/blood.2022018333
9. Bennett JS. Structural biology of glycoprotein IIb-IIIa. *Trends Cardiovasc Med*. 1996;6(1):31-36. doi:10.1016/1050-1738(95)00126-3
10. Aoki T, Tomiyama Y, Honda S, et al. Association of the antagonism of von Willebrand factor but not fibrinogen by platelet alphaIIbbeta3 antagonists with prolongation of bleeding time. *J Thromb Haemost*. 2005;3(10):2307-2314. doi:10.1111/j.1538-7836.2005.01534.x
11. Shoemaker LD, Geschwind DH. Genomics, proteomics, and neurology. In: *From Neuroscience to Neurology*. Elsevier; 2005:217-236. doi:10.1016/B978-012738903-5/50014-X
12. Burkhart JM, Gambaryan S, Watson SP, et al. What can proteomics tell us about platelets? *Circ Res*. 2014;114(7):1204-1219. doi:10.1161/CIRCRESAHA.114.301598
13. Kreft IC, Huisman EJ, Cnossen MH, et al. Proteomic landscapes of inherited platelet disorders with different etiologies. *J Thromb Haemost*. 2023;21(2):359-372.e3. doi:10.1016/j.jtha.2022.11.021

14. Blaauwgeers MW, Kruip MJHA, Beckers EAM, et al. Bleeding phenotype and diagnostic characterization of patients with congenital platelet defects. *Am J Hematol*. 2020;95(10):1142-1147. doi:10.1002/ajh.25910

15. Blaauwgeers MW, van Asten I, Kruip MJHA, et al. The limitation of genetic testing in diagnosing patients suspected for congenital platelet defects. *Am J Hematol*. 2020;95(1):E26-E28. doi:10.1002/ajh.25667

16. van Asten I, Blaauwgeers M, Granneman L, et al. Flow cytometric mepacrine fluorescence can be used for the exclusion of platelet dense granule deficiency. *J Thromb Haemost*. 2020;18(3):706-713. doi:10.1111/jth.14698

17. Gandhi PS, Zivkovic M, Østergaard H, et al. A bispecific antibody approach for the potential prophylactic treatment of inherited bleeding disorders. *Nat Cardiovasc Res*. February 8, 2024. doi:10.1038/s44161-023-00418-4

18. Brenes AJ. Calculating and Reporting Coefficients of Variation for DIA-Based Proteomics. *J Proteome Res*. 2024;23(12):5274-5278. doi:10.1021/acs.jproteome.4c00461

19. The Human Protein Atlas. Accessed February 10, 2025. https://www.proteinatlas.org/

20. Geyer PE, Voytik E, Treit PV, et al. Plasma Proteome Profiling to detect and avoid sample-related biases in biomarker studies. *EMBO Mol Med*. 2019;11(11):e10427. doi:10.15252/emmm.201910427

21. Huang J, Swieringa F, Solari FA, et al. Assessment of a complete and classified platelet proteome from genome-wide transcripts of human platelets and megakaryocytes covering platelet functions. *Sci Rep*. 2021;11(1):12358. doi:10.1038/s41598-021-91661-x

22. Burkhart JM, Vaudel M, Gambaryan S, et al. The first comprehensive and quantitative analysis of human platelet protein composition allows the comparative analysis of structural and functional pathways. *Blood*. 2012;120(15):e73-82. doi:10.1182/blood-2012-04-416594

23. Maynard DM, Heijnen HFG, Horne MK, White JG, Gahl WA. Proteomic analysis of platelet alpha-granules using mass spectrometry. *J Thromb Haemost*. 2007;5(9):1945-1955. doi:10.1111/j.1538-7836.2007.02690.x

24. Maynard DM, Heijnen HFG, Gahl WA, Gunay-Aygun M. The α-granule proteome: novel proteins in normal and ghost granules in gray platelet syndrome. *J Thromb Haemost*. 2010;8(8):1786-1796. doi:10.1111/j.1538-7836.2010.03932.x

25. Farrah T, Deutsch EW, Omenn GS, et al. A high-confidence human plasma proteome reference set with estimated concentrations in PeptideAtlas. *Mol Cell Proteomics*. 2011;10(9):M110.006353. doi:10.1074/mcp.M110.006353

26. Nurden AT, Fiore M, Nurden P, Pillois X. Glanzmann thrombasthenia: a review of ITGA2B and ITGB3 defects with emphasis on variants, phenotypic variability, and mouse models. *Blood*. 2011;118(23):5996-6005. doi:10.1182/blood-2011-07-365635

27. González-Manchón C, Butta N, Larrucea S, et al. A variant thrombasthenic phenotype associated with compound heterozygosity of integrin beta3-subunit: (Met124Val)beta3 alters the subunit dimerization rendering a decreased number of constitutive active alphaIIbbeta3 receptors. *Thromb Haemost*. 2004;92(6):1377-1386. doi:10.1160/TH04-06-0380

28. Ruiz C, Liu CY, Sun QH, et al. A point mutation in the cysteine-rich domain of glycoprotein (GP) IIIa results in the expression of a GPIIb-IIIa (alphaIIbbeta3) integrin receptor locked in a high-affinity state and a Glanzmann thrombasthenia-like phenotype. *Blood*. 2001;98(8):2432-2441. doi:10.1182/blood.v98.8.2432

29. Kashiwagi H, Kunishima S, Kiyomizu K, et al. Demonstration of novel gain-of-function mutations of αIIbβ3: association with macrothrombocytopenia and glanzmann thrombasthenia-like phenotype. *Mol Genet Genomic Med*. 2013;1(2):77-86. doi:10.1002/mgg3.9

30. Bajt ML, Ginsberg MH, Frelinger AL, Berndt MC, Loftus JC. A spontaneous mutation of integrin alpha IIb beta 3 (platelet glycoprotein IIb-IIIa) helps define a ligand binding site. *J Biol Chem*. 1992;267(6):3789-3794.

31. Loroch S, Trabold K, Gambaryan S, et al. Alterations of the platelet proteome in type I Glanzmann thrombasthenia caused by different homozygous delG frameshift mutations in ITGA2B. *Thromb Haemost*. 2017;117(3):556-569. doi:10.1160/TH16-07-0515

32. Adelman B, Quynn P. Plasminogen interactions with immobilized fibrinogen. *Thromb Haemost*. 1989;62(4):1078-1082. doi:10.1055/s-0038-1647121

33. Martinez-Vargas M, Cebula A, Brubaker LS, et al. A novel interaction between extracellular vimentin and fibrinogen in fibrin formation. *Thromb Res*. 2023;221:97-104. doi:10.1016/j.thromres.2022.11.028

34. Wang H, Workman G, Chen S, et al. Secreted protein acidic and rich in cysteine (SPARC/osteonectin/BM-40) binds to fibrinogen fragments D and E, but not to native fibrinogen. *Matrix Biol*. 2006;25(1):20-26. doi:10.1016/j.matbio.2005.09.004

35. Washington AV, Gibot S, Acevedo I, et al. TREM-like transcript-1 protects against inflammation-associated hemorrhage by facilitating platelet aggregation in mice and humans. *J Clin Invest*. 2009;119(6):1489-1501. doi:10.1172/JCI36175

36. Barrow AD, Astoul E, Floto A, et al. Cutting edge: TREM-like transcript-1, a platelet immunoreceptor tyrosine-based inhibition motif encoding costimulatory immunoreceptor that enhances, rather than inhibits, calcium signaling via SHP-2. *J Immunol*. 2004;172(10):5838-5842. doi:10.4049/jimmunol.172.10.5838

37. Smith CW, Raslan Z, Parfitt L, et al. TREM-like transcript 1: a more sensitive marker of platelet activation than P-selectin in humans and mice. *Blood Adv*. 2018;2(16):2072-2078. doi:10.1182/bloodadvances.2018017756

38. Senis YA. TLT-1: please release me, let me go. *Blood*. 2018;132(23):2427-2429. doi:10.1182/blood-2018-10-879676

39. Winkler W, Zellner M, Diestinger M, et al. Biological variation of the platelet proteome in the elderly population and its implication for biomarker research. *Mol Cell Proteomics*. 2008;7(1):193-203. doi:10.1074/mcp.M700137-MCP200

40. Chen H-L, Wang Q-Y, Qi R-M, Cai J-P. Identification of the changes in the platelet proteomic profile of elderly individuals. *Front Cardiovasc Med*. 2024;11:1384679. doi:10.3389/fcvm.2024.1384679

41. Sabetta A, Lombardi L, Stefanini L. Sex differences at the platelet-vascular interface. *Intern Emerg Med*. 2022;17(5):1267-1276. doi:10.1007/s11739-022-02994-y

42. Remijn JA, Wu YP, Ijsseldijk MJ, Zwaginga JJ, Sixma JJ, de Groot PG. Absence of fibrinogen in afibrinogenemia results in large but loosely packed thrombi under flow conditions. *Thromb Haemost*. 2001;85(4):736-742.

Part II

NOVEL THERAPEUTICS

Chapter 5

A bispecific antibody approach for the potential prophylactic treatment of inherited bleeding disorders

Minka Zivkovic[1*], Prafull S Gandhi[2*], Henrik Østergaard[2*], Amalie C Bonde[2], Torben Elm[3], Monika N Løvgreen[3], Gerd Schluckebier[3], Eva Johansson[3], Ole H Olsen[4], Eva HN Olsen[5], Ian-Arris de Bus[6], Karien Bloem[6], Oskar Alskär[7], Catherine J Rea[1], Søren E Bjørn[8], Roger EG Schutgens[1], Benny Sørensen[2], Rolf T Urbanus[1], Johan H Faber[2]

**These authors contributed equally.*

[1] Center for Benign Haematology, Thrombosis and Haemostasis, Van Creveldkliniek, University Medical Center Utrecht, Utrecht University, Utrecht, the Netherlands.
[2] Hemab Therapeutics, Copenhagen, Denmark.
[3] Novo Nordisk A/S, Måløv, Denmark.
[4] Novo Nordisk Foundation Center for Basic Metabolic Research, University of Copenhagen, Copenhagen, Denmark.
[5] EO Assay Consult, Ballerup, Denmark.
[6] Sanquin Diagnostic Services, Amsterdam, the Netherlands.
[7] qPharmetra, Stockholm, Sweden.
[8] Cymab Therapeutics, Copenhagen, Denmark.

Nat Cardiovasc Res. 2024 Feb;3(2):166-185

SUMMARY

Inherited bleeding disorders such as Glanzmann thrombasthenia (GT) lack prophylactic treatment options. As a result, serious bleeding episodes are treated acutely with blood product transfusions or frequent, repeated intravenous administration of recombinant activated coagulation factor VII (rFVIIa). Here we describe HMB-001, a bispecific antibody designed to bind and accumulate endogenous FVIIa and deliver it to sites of vascular injury by targeting it to the TREM (triggering receptor expressed on myeloid cells)-like transcript-1 (TLT-1) receptor that is selectively expressed on activated platelets. In healthy nonhuman primates, HMB-001 prolonged the half-life of endogenous FVIIa, resulting in its accumulation. Mouse bleeding studies confirmed antibody-mediated potentiation of FVIIa hemostatic activity by TLT-1 targeting. In *ex vivo* models of GT, HMB-001 localized FVIIa on activated platelets and potentiated fibrin-dependent platelet aggregation. Taken together, these results indicate that HMB-001 has the potential to offer subcutaneous prophylactic treatment to prevent bleeds in people with GT and other inherited bleeding disorders, with a low-frequency dosing regimen.

INTRODUCTION

During the past seven decades, the treatment options for hemophilia A (HA) and B (HB) have advanced from transfusion of blood products to long-acting recombinant concentrates, to nonfactor therapies such as antibodies and small interfering RNAs, and now to gene therapy[1,2,3]. Consequently, the current standard of care for hemophilia treatment is largely focused on prophylaxis or preventing bleeding episodes. In contrast, many other serious bleeding disorders, including Glanzmann thrombasthenia (GT), coagulation factor VII (FVII) deficiency and Bernard–Soulier syndrome, completely lack prophylactic treatment options. As a result, patients experience frequent bleeds, which are treated acutely with approaches such as blood product transfusions or administration of prothrombin complex concentrates or recombinant activated FVII (rFVIIa)[4,5,6].

GT is an autosomal recessive disorder associated with a severe bleeding phenotype[7,8,9]. Approximately 50% of patients report experiencing one bleed daily and the negative impact of bleeding on their quality of life[10]. Mucocutaneous bleeding and heavy menstrual bleeding are the most commonly reported events[11,12], and bleeds can be life-threatening. GT results from quantitative or qualitative mutations in the platelet membrane glycoprotein (GP) IIb/IIIa (αIIbβ3), which is essential for platelet aggregation and clot formation[9,13] (**Fig. 1a**). Bleed management in people with GT (PwGT) is confounded by a lack of treatment options and evidence-based guidelines. Recommendations for managing minor bleeds include compression, elevation of the injured area, systemic tranexamic acid and topical application of antifibrinolytic agents[8,9,14,15]. For major bleeds and surgical interventions, one option is platelet transfusions. However, transfusions are often not readily available, especially for patients with anti-αIIbβ3 antibodies, and are complicated by the risk of alloimmunization, resulting in the person becoming refractory to further transfusions[8,9,14,15]. rFVIIa is licensed for acute bleed management in PwGT who are refractory to platelet transfusions and when platelets are unavailable[16]. It is also frequently used off-label to prevent surgical bleeds[9,17]. However, although effective in controlling bleeds, rFVIIa needs frequent intravenous infusions (several times per week) due to its short half-life[15,18]. The only other option is allogeneic human stem cell transplantation, which, although potentially curative, is associated with high mortality and morbidity risks[8,9,15,17].

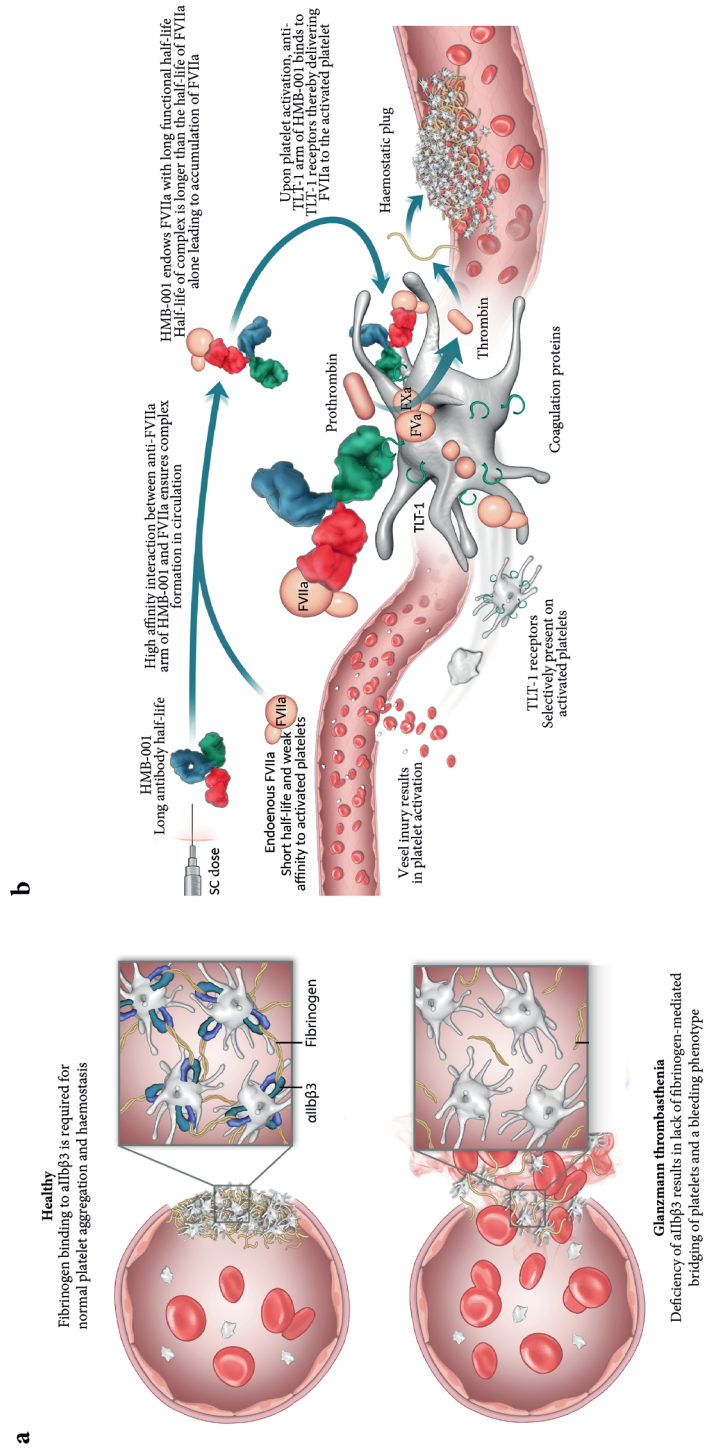

Fig. 1: Proposed MoA of HMB-001. a, αIIbβ3 is a receptor for fibrinogen on platelets. In the case of normal platelets, fibrinogen binding to αIIbβ3 bridges platelets and is a required step for normal platelet aggregation and subsequent formation of a hemostatic plug. In the case of GT, deficiency of αIIbβ3 results in a lack of fibrinogen-mediated bridging of platelets, leading to abnormal platelet function manifesting in a severe bleeding phenotype. Due to the autosomal pattern of inheritance, GT affects both sexes equally. **b**, HMB-001 is a biAb designed to restore hemostasis through a mechanism mimicking that of rFVIIa but relying exclusively on the proteolytic activity of endogenous FVIIa. One arm of HMB-001 binds to endogenous FVIIa with high affinity. The half-life of HMB-001 is much longer than that of endogenous FVIIa. Therefore, the binding of HMB-001 to circulating FVIIa confers endogenous FVIIa with an extended half-life, resulting in progressive accumulation of plasma FVIIa until a new steady-state level is reached. The second arm of HMB-001 binds to the TLT-1 receptor on activated platelets. In the case of vascular injury, the binding of the anti-TLT-1 arm of HMB-001 to the TLT-1 receptor mediates increased recruitment of FVIIa onto the surface of the activated platelet. Here, HMB-001-delivered FVIIa drives FX activation and consequently enhances local thrombin generation to support the formation of a hemostatic plug. HMB-001 has the potential to offer subcutaneous-based prophylactic treatment, with a low frequency of dosing ranging from once a week to once a month, to prevent bleeds in PwGT and those with other rare bleeding disorders for which rFVIIa has been historically effective.

Mechanism of action (MoA) studies suggest that rFVIIa may function through a combination of tissue factor (TF)-independent and TF-dependent pathways[19-24]. In GT, it is proposed that rFVIIa drives factor X (FX) activation on the activated platelet surface in a TF-independent manner, generating an augmented thrombin burst at sites of vascular injury. rFVIIa-mediated thrombin generation results in fibrin formation on activated platelets, leading to fibrin-dependent but αIIbβ3-independent platelet aggregation and the formation of a hemostatic plug[13,20,25].

rFVIIa has a very short systemic half-life (2–3 h), low subcutaneous bioavailability[26] and weak binding affinity to activated platelets[27]. These features combined indicate the need for a dosing regimen of rFVIIa with multiple doses in the range of 90–270 µg kg^{-1} to treat an ongoing bleed, leading to peak plasma concentrations of 25–75 nM[28]. Several rFVIIa analogues with varying degrees of backbone modifications were developed and investigated in preclinical and clinical studies to improve rFVIIa-based treatment[29-35]. These studies confirmed that the hemostatic properties of rFVIIa can be enhanced by improving its systemic half-life, activity or both. One strategy to improve FVIIa activity is by enhancing its affinity for activated platelets. This can be achieved by localizing FVIIa to a receptor on activated platelets[36]. Ideally, such a receptor should display high tissue specificity, be expressed selectively on activated platelets instead of resting platelets, be expressed abundantly on the surface and be amenable to therapeutic targeting without interfering with its intrinsic function.

TREM (triggering receptor expressed on myeloid cells)-like transcript-1 (TLT-1) fulfills each of these criteria. TLT-1 is a membrane-bound protein consisting of an extracellular N-terminal immunoglobulin variable (IgV) domain (amino acids 1–110) connected to a linker called the stalk peptide (amino acids 111–147), a transmembrane segment (amino acids 148–169) and a cytoplasmic domain (amino acids 170–296)[37]. TLT-1 is present exclusively in intracellular pools of resting platelets and megakaryocytes[38]. Upon platelet activation, TLT-1 is redistributed from α-granules to the platelet surface, exposing it to blood at the site of vascular injury[38,39]. Although TLT-1 has been demonstrated to bind fibrinogen, likely through its IgV domain, it appears to have a minor role in normal hemostasis, as TLT-1 knockout mice exhibit only a minor prolongation of bleeding time[40].

A recent study demonstrated that FVIIa conjugated to an anti-TLT-1 Fab (fragment antigen-binding) fragment increased the affinity of FVIIa for activated platelets, leading to substantial enhancement of *in vivo* potency relative to free rFVIIa[41]. Building on the potential of targeted therapy and, at the same time, allowing for infrequent subcutaneous administration, we have designed a bispecific antibody (biAb) designated HMB-001. Using the DuoBody technology[42] for biAb assembly, HMB-001 has been engineered to bind with high affinity to endogenous FVIIa with one arm and to TLT-1 on activated platelets with the second arm. Due to its long antibody half-life, HMB-001 confers endogenous FVIIa with a longer systemic half-life, resulting in the accumulation of HMB-001:FVIIa complexes in the circulation. Upon vascular injury, TLT-1 expression on activated platelets recruits HMB-001:FVIIa to the site of the lesion, resulting in enhanced FVIIa-driven hemostatic activity and potentiation of downstream thrombin generation and fibrin formation (**Fig. 1b**). Hence, HMB-001 builds upon the MoA of rFVIIa, except that it acts exclusively through endogenous FVIIa. In addition, HMB-001 serves as an example of antibody-mediated accumulation and targeting of an activated endogenous protein as a means of therapeutic intervention. Here, we describe the full characterization of HMB-001 and show that it results in improved hemostatic activity of FVIIa in *ex vivo* models of GT.

MATERIALS AND METHODS

Inclusion and ethics

The mouse *in vivo* study was conducted at Novo Nordisk, Denmark. The study was approved by the Danish Animal Experiments Council, the Danish Ministry of Environment

and Food, and the Novo Nordisk Welfare Body. The nonhuman primate PK/PD study was conducted at Labcorp, UK. Labcorp is licensed by the UK Home Office to undertake animal studies. The nonhuman primate PK/PD study (no. 8469444) was approved by the Labcorp Animal Welfare and Ethics Review Board. Human studies were approved by the NedMec medical ethics review board at University Medical Center Utrecht (registration no. NL5878 in the Dutch trial registry (ClinicalTrialregister.nl)), and all participants provided informed consent.

PwGT and healthy controls

Thirteen PwGT were included in the Thrombocytopathy in the Netherlands (TiN) study, a nationwide cross-sectional study on disease phenotyping, diagnostics and genetics in people with a (suspected) platelet disorder in the Netherlands, at the University Medical Center Utrecht. PwGT were aged 30–74 years, of whom five were men and eight were women. Stored plasma samples (n = 13) were used for the analysis of FVII activity and FVIIa levels, and fresh blood samples (n = 4) were used for platelet phenotyping and functional characterization of HMB-001. Full details of the TiN study have been described elsewhere[61,62].

Healthy controls were recruited among personnel and students at University Medical Center Utrecht by the Mini Donor biobank facility of the University Medical Center Utrecht (biobank no. 18-774). Controls were aged 24–65 years, of whom 40% were men and 60% were women. All participants provided written informed consent.

In all participants, blood was collected from the antecubital vein into trisodium citrate or sodium heparin Vacutainer tubes (BD) through phlebotomy. Blood was processed within 1–6 h of collection. Plasma was obtained within 4 h of collection by centrifugation of whole blood at 3,000g for 5 min. Plasma was stored at −80 °C until used.

Preparation of recombinant proteins

FVIIa or rFVIIa (NovoSeven) was from Novo Nordisk. Recombinant zymogen FVII was produced in Chinese hamster ovary (CHO) cells and purified as described elsewhere[63]. Following purification, FVII was dialyzed into 10 mM MES, 100 mM NaCl, 10 mM $CaCl_2$, pH 6.0 buffer. The level of FVIIa in the preparation was determined by measuring activity against a chromogenic substrate. By relating this to a standard curve prepared with known concentrations of rFVIIa, the measured activity could be converted to a molar concentration of FVIIa in the FVII preparation. A recombinant zymogen FVII

variant (FVII-S195A) with an alanine substitution of the active site serine (S195A) was produced in CHO cells (CHO-EBNALT85, Icosagen) and purified as described elsewhere64. Following purification, FVII-S195A was dialyzed into 20 mM HEPES, 150 mM NaCl, 5 mM $CaCl_2$, pH 7.5 buffer. The introduction of the S195A mutation was verified by the lack of activity against the chromogenic substrate. rFVIIa without the N-terminal Gla domain (FVIIa-desGLA) was produced in CHO cells (CHO-EBNA, Icosagen), purified by affinity chromatography (VIISelect, Cytiva) and desalted using a HiPrep column (Sephadex G-25, Cytiva). Active site-inhibited FVIIa (FVIIai) was prepared by incubating FVIIa-desGLA with an active site inhibitor (H-D-Phe-Phe-Arg-chloromethyl ketone (FFR-cmk), Bachem). The anti-FVIIa Fab fragment of HMB-001, used for x-ray crystallography studies, was expressed using transient transfection of HEK293 suspension cells (293Expi, Invitrogen) and purified by affinity chromatography (MabSelect SuRe, Cytiva). The anti-TLT-1 Fab fragment was produced in CHO cells (Gibco) and purified by affinity chromatography (KappaSelect, Cytiva). HMB-001 and biAb0097 were generated using the DuoBody technology[42] by assembling the two parental monospecific bivalent antibodies, that is, the anti-FVIIa antibody with DuoBody mutations F405L and R409K and the anti-TLT-1 (pTLT-1) antibody without DuoBody mutations. HMB-001 was purified from residual levels of parental monospecific bivalent antibodies using ion exchange chromatography. The parental affinity variants of the monospecific bivalent anti-FVIIa (with DuoBody mutations F405L and R409K) and anti-TLT-1 antibodies were produced using transient transfection of HEK293 suspension cells (293Expi, Invitrogen) and purified by protein A affinity followed by size-exclusion chromatography (SEC). The affinity matrix biAbs (approximate molecular weight 150 kDa) were assembled using the DuoBody technology, as described elsewhere[42]. The two monovalent cAbs (approximate molecular weight 100 kDa) were also generated using the DuoBody technology by combining parental antibodies with an empty Fc (E216–G446 in EU numbering). The two monovalent cAbs were purified using ion exchange chromatography, and their molecular weights were confirmed using SDS–PAGE. In addition, binding between the two cAbs and their respective antigens (FVIIa or sTLT-1) was confirmed using a surface plasmon resonance (SPR) binding assay. Fragments of TF corresponding to amino acids 1–219 (sTF) and 1–244 (TF) were produced in *Escherichia coli* (*E. coli*) as described elsewhere[65,66]. Preparations of 25:75 phosphatidylserine/phosphatidylcholine vesicles with and without incorporation of TF were prepared as described elsewhere[66]. sTLT-1, corresponding to amino acids 1–147 of mature TLT-1, was expressed with a C-terminal histidine (His) tag and a two amino acid (valine–aspartic acid) linker in between using transient transfection of

CHO cells (ExpiCHO, Gibco). It was then purified using the standard His-tag purification strategy (HisTrap column, Cytiva), followed by dialysis in 20 mM HEPES, 100 mM NaCl, pH 7.3. The 37-mer TLT-1 peptide, EEEEETHKIGSLAENAFSDPAGSANPLEPSQDEKSIP, corresponding to amino acids 111–147 of mature TLT-1, was prepared by standard peptide synthesis methods and is referred to as the sTLT-1 stalk peptide. Bivalent and specific heavy-chain variable domain (V_HH) antibodies against human FVIIa[67] and monovalent V_HH antibodies against P-selectin (clone B10.6), fibrinogen (clone C3), GPIbα (clone 17) and fibrin (clone B12), as well as isotype control V_HH antibody (clone R2) were produced with a tobacco etch virus (TEV) protease-cleavable N-terminal His tag in *E. coli*. V_HH antibodies were purified from bacterial lysate with immobilized metal affinity chromatography on TALON Sepharose. His tags were removed from clones B10.6, C3, 17, R2 and B12 with TEV protease. Incompletely cleaved V_HH, TEV protease and free His tags were removed with immobilized metal affinity chromatography. V_HH antibodies were separated from the remaining impurities with SEC. Reactive thiols were introduced in V_HH antibody clone 17 with Pierce N-succinimidyl S-acetylthioacetate (Thermo Fisher Scientific), followed by labeling with maleimide-activated phycoerythrin (PE) (AnaSpec) according to the manufacturer's instructions. The anti-FVIIa V_HH antibody and clones B10.6 and R2 were labeled with NHS-Alexa Fluor-647 (Thermo Fisher Scientific), and clones C3, R2 and B12 were labeled with NHS-AlexaFluor-488 (Thermo Fisher Scientific) according to the manufacturer's instructions. All reported replicate measurements were taken from distinct samples.

Effect of an HMB-001 analogue and FVIIa on bleeding in an HA mouse model

For this *in vivo* study, an analogue of HMB-001 was used such that the anti-TLT-1 arm is identical to the one in HMB-001. Meanwhile, the anti-FVIIa arm of the analogue is the murine version of the corresponding arm in HMB-001 before humanization. This biAb is referred to as biAb0097. The potency of FVIIa alone and FVIIa coformulated with biAb0097 in a 1:1 molar ratio was compared in a TVT model[68,69] in HA ($F8^{-/-}$) mice expressing the human TLT-1 receptor. The mouse model was generated by replacing the mouse *treml1* gene with the human variant and breeding them with $F8^{-/-}$ mice, which are exon 16-disrupted C57Bl/129S mice. Human TLT-1-positive $F8^{-/-}$ mice were identified by PCR; the generation of this model has been described in more detail elsewhere[41]. Mice were housed under standard conditions at Novo Nordisk, Måløv, Denmark (20–23 °C, 30–60% relative humidity, a 12-h light/dark cycle, and free access to food and water) in environmentally enriched cages. The sample size was determined based on earlier similar studies in $F8^{-/-}$ mice[69]. For the

experiment, mice of both sexes (approximately 50:50) and 12–16 weeks of age were anesthetized with isoflurane and placed on a heating pad set to maintain animal body temperature and with the tail submerged in saline (37 °C). For practical reasons, the *in vivo* study with FVIIa was performed just before the study wherein FVIIa was coformulated with biAb0097. Within each study, mice were randomized and blinded. Test compounds were administered intravenously (5 ml kg^{-1}) into the right lateral tail vein 5 min before the injury, as summarized in **Supplementary Table 1**. After transection of the left lateral vein where the tail diameter equals 2.5 mm, the bleeding time and total blood loss were recorded in a 40-min observation window as described previously[68]. If the bleeding stopped at 10, 20 or 30 min, the tail was removed from the saline and the wound was gently wiped with a saline-wetted gauze swab. Total blood loss was determined by quantifying the amount of hemoglobin (Hb) in the saline and is expressed as nmol Hb.

At the end of the observation window, a blood sample was collected from the orbital plexus into 3.8% trisodium citrate. The blood was centrifuged, plasma aliquoted and stored at −80 °C before measuring the plasma concentration of FVIIa using a luminescent oxygen channeling immunoassay. In this assay, acceptor beads were coated with an anti-FVIIa antibody (4F9, Novo Nordisk) and donor beads were coated with streptavidin; streptavidin donor beads were used in combination with a biotinylated anti-FVIIa antibody (4F7, Novo Nordisk). The FVIIa concentrations in plasma samples were determined by comparing the results to a calibration curve prepared with known amounts of human FVIIa.

Dose–response curves were generated from the measured blood loss as a function of dose or the measured plasma concentration of FVIIa at the end of the observation window. From the latter, EC_{50} values were estimated by nonlinear least-squares fitting using a three-parameter sigmoidal dose–response model (GraphPad Prism), with top and bottom values shared between the two datasets.

Affinity of FVIIa and sTLT-1 to HMB-001 and its variants

The binding of FVIIa or sTLT-1 to biAbs was determined by SPR technology (Biacore 8K) at 25 °C (n = 2). Anti-human IgG (25 µg ml^{-1}) was immobilized on flow cells (FC) 1 and 2 of a CM4 sensor chip (both supplied by Cytiva) using standard amine coupling chemistry. BiAbs (0.5–4 nM) were injected at a flow rate of 10 µl min^{-1} for 2 min in FC 2 alone. Subsequently, FVIIa (between 0 and 4 nM) was injected in FC 1 and 2 at a

flow rate of 30 µl min^{-1} for 400 s to allow for binding to biAbs. This was followed by a 540-s running buffer injection, allowing for dissociation from biAbs. Similarly, sTLT-1 (between 0 and 60 µM) was injected in FC 1 and 2 at a flow rate of 30 µl min^{-1} for 180 s to allow for binding to biAbs. This was followed by a 360-s running buffer injection, allowing for dissociation from biAbs. The running buffer was prepared by tenfold dilution of 10× HEPES-buffered saline (HBS) with surfactant P20 (HBS-P buffer, Cytiva) and supplemented with 1 mg ml^{-1} BSA and 5 mM $CaCl_2$ to give 10 mM HEPES, 150 mM NaCl, 0.05% v/v polysorbate 20, pH 7.4, 5 mM $CaCl_2$ and 1 mg ml^{-1} BSA. The running buffer was also used to dilute biAb, FVIIa and sTLT-1 samples. The chip was regenerated using the recommended regeneration buffer consisting of 3 M $MgCl_2$ (supplied by Cytiva) injected at a flow rate of 30 µl min^{-1} for 30 s in FC 1 and 2. Binding data were analyzed according to a Langmuir 1:1 binding kinetics model using Biacore Insight Evaluation software supplied by the manufacturer (Cytiva). For sTLT-1 binding to biAb0095 and biAb0090, binding data were analyzed according to a Langmuir 1:1 binding steady-state model using Biacore Insight Evaluation software supplied by the manufacturer (Cytiva). This SPR binding setup is preferred when comparing FVIIa or sTLT-1 binding affinities to HMB-001 and its variants, as any potential inaccuracy in biAb concentrations does not affect the affinity ranking of biAbs.

Affinity affects biAb-mediated stimulation of FVIIa activity

To determine the effect of affinity on biAb-mediated potentiation of FVIIa activity, several anti-FVIIa and anti-TLT-1 monoclonal antibodies (mAbs) with varying affinities for FVIIa and TLT-1, respectively, were tested in a bispecific format in an FX activation assay using lipidated TLT-1 (n = 3). FX activation was measured in the presence of 4 nM recombinant TLT-1 incorporated into 25:75 phosphatidylserine/phosphatidylcholine vesicles, 2.5 nM FVIIa, and biAb in a concentration series from 0 to 500 nM. Following 10-min preincubation in assay buffer (50 mM HEPES, 100 mM NaCl, 10 mM $CaCl_2$, pH 7.3, 1 mg ml^{-1} BSA and 0.1% polyethylene glycol (PEG) 8000) at room temperature (RT), 150 nM plasma-derived FX was added to give a total volume of 50 µl. Activation was allowed to proceed for 20 min. The activation was then terminated by adding 25 µl of quench buffer (50 mM HEPES, 100 mM NaCl, 80 mM ethylenediaminetetraacetic acid (EDTA), pH 7.3). The generated FXa was quantified by hydrolysis of 1 mM S-2765 chromogenic substrate (Chromogenix), which was observed at 405 nm for 10 min in a SpectraMax iD3 plate reader and analyzed with SoftMax Pro software (Molecular Devices). From the slope of linear absorbance increase, the specific activities of free FVIIa (A_{free}) and FVIIa in the presence of biAb (A_{biAb}) were determined. The stimulatory

activity of each biAb concentration was calculated as the A_{biAb}/A_{free} ratio and visualized with GraphPad Prism software.

Affinity of FVIIa and FVII to HMB-001

The binding of FVIIa and FVII to HMB-001 was determined by SPR technology (Biacore 8K) at 25 °C (n = 2). Anti-FVII IgG1 (50 µg ml^{-1}, FVII mAb CaFVII-22, MA5-17631, Invitrogen), targeting the N-terminal Gla domain of FVII, was immobilized on FC 1 and 2 of a CM4 sensor chip (Cytiva) using standard amine coupling chemistry. FVIIa (2.5 nM) or FVII (2.5 nM) was injected at a flow rate of 10 µl min^{-1} for 2 min in FC 2 alone. Subsequently, HMB-001 (between 0 and 4 nM) was injected in FC 1 and 2 at a flow rate of 30 µl min^{-1} for 300 s to allow for binding to FVIIa or FVII. This was followed by a 540-s running buffer injection, allowing for dissociation from FVIIa or FVII. The running buffer was prepared by tenfold dilution of 10× HBS-P buffer (supplied by Cytiva) and supplemented with 1 mg ml^{-1} BSA and 5 mM $CaCl_2$ to give 10 mM HEPES, 150 mM NaCl, 0.05% v/v polysorbate 20, pH 7.4, 5 mM $CaCl_2$ and 1 mg ml^{-1} BSA. The running buffer was also used to dilute FVIIa, FVII and HMB-001 samples. The chip was regenerated using a regeneration buffer consisting of 10 mM HEPES, 150 mM NaCl, 0.05% v/v polysorbate 20, pH 7.4 and 50 mM EDTA injected at a flow rate of 30 µl min^{-1} for 30 s in FC 1 and 2. Binding data were analyzed according to a Langmuir 1:1 binding kinetics model using Biacore Insight Evaluation software supplied by the manufacturer (Cytiva).

Effect of HMB-001 on FVII autoactivation

To determine the effect of HMB-001 on FVII autoactivation, activation of FVII was measured in the presence of lipidated TF, zymogen FVII, a limiting amount of FVIIa, and HMB-001 (n = 3). Activity measurements were performed at RT in assay buffer (50 mM HEPES, 100 mM NaCl, 10 mM $CaCl_2$, 0.1% PEG 8000, 1 mg ml^{-1} BSA, pH 7.3). FVII autoactivation was measured in a 50-µl reaction volume containing 2 nM FVIIa, 145 nM FVII, and 0 or 500 nM HMB-001. The reactions were initiated at different time points and incubated for 0–60 min at RT by adding 2 nM lipidated TF. Following incubation, the amount of generated FVIIa, as deduced by a calibration curve, was quantified by adding 200 nM sTF and 1 mM S-2288 chromogenic substrate (Chromogenix), which was observed at 405 nm for 10 min in a SpectraMax iD3 plate reader, analyzed with SoftMax Pro software (Molecular Devices) and visualized with GraphPad Prism software.

Effect of HMB-001 on TF-(in)dependent activation of FX by FVIIa

To determine the effect of HMB-001 on the TF-independent and TF-dependent proteolytic activity of FVIIa, activation of FX by FVIIa was evaluated in the absence or presence of lipidated TF (n = 3). Activity measurements were performed at RT in assay buffer (50 mM HEPES, 100 mM NaCl, 10 mM $CaCl_2$, pH 7.3, 1 mg ml^{-1} BSA and 0.1% PEG 8000). In the absence of TF, FX activation was measured in a 50-µl reaction volume containing 20 nM FVIIa, 0 or 500 nM HMB-001, and 25 µM 25:75 phosphatidylserine/phosphatidylcholine vesicles. In the presence of TF, FX activation was measured in a 50-µl reaction volume containing 100 pM FVIIa, 0 or 500 nM HMB-001, and 2 pM lipidated TF. Reactions were initiated by adding 0–250 nM (TF-independent) or 0–50 nM (TF-dependent) human plasma-derived FX and incubated for 20 min at RT. After the incubation, reactions were quenched by adding 25 µl quench buffer (50 mM HEPES, 100 mM NaCl, 80 mM EDTA, pH 7.3), followed by 1 mM S-2765 chromogenic substrate (Chromogenix). The reactions were observed at 405 nm for 10 min in a SpectraMax iD3 plate reader. The measured slope, analyzed with SoftMax Pro software (Molecular Devices), was converted to the generated FXa using a calibration curve. Enzyme kinetic parameters were estimated by nonlinear curve fitting of the data to the Michaelis–Menten equation with GraphPad Prism software.

Effect of HMB-001 on the inhibition of FVIIa by AT

The inhibition of FVIIa by human plasma-derived AT in the absence or presence of HMB-001 was performed under pseudo-first-order conditions using a discontinuous assay (n = 3). The assay was conducted at RT in 50 µl assay buffer (50 mM HEPES, 100 mM NaCl, 10 mM $CaCl_2$, pH 7.3, 1 mg ml^{-1} BSA and 0.1% PEG 8000) containing 200 nM FVIIa, 12 µM low-molecular-weight heparin, and 0 or 500 nM HMB-001. Following 10-min preincubation, the reaction was initiated by adding 5 µM AT at selected time points (0–2 h). The inhibition reaction was quenched by adding 0.5 mg ml^{-1} polybrene, immediately followed by adding 200 nM sTF and 1 mM S-2288 chromogenic substrate (Chromogenix). The residual FVIIa activity was measured as described above and determined as the slope of the linear progress curves. These were subsequently fitted to a first-order exponential decay function to derive the pseudo-first-order rate constant (k_{app}) for the reaction (GraphPad Prism). An apparent second-order rate constant (k_{inh}) was estimated as the k_{app} divided by the AT concentration.

Effect of HMB-001 on the inhibition of FVIIa by TFPI

TFPI inhibition of FX activation by the FVIIa:TF complex was conducted at RT in 50 µl assay buffer (50 mM HEPES, 100 mM NaCl, 10 mM $CaCl_2$, pH 7.3, 1 mg ml^{-1} BSA and 0.1% PEG 8000) containing 100 pM FVIIa, 2 pM lipidated TF, 0–20 nM recombinant TFPI, and 0 or 500 nM HMB-001 (n = 3). Following 10-min preincubation, the reaction was initiated by adding 50 nM plasma-derived FX and incubated for 30 min. The inhibition reaction was quenched by adding 25 µl quench buffer (50 mM HEPES, 100 mM NaCl, 80 mM EDTA, pH 7.3), immediately followed by the addition of 1 mM S-2765 chromogenic substrate (Chromogenix). The residual FXa activity was measured as described above and determined as the slope of the linear progress curves. These were subsequently fitted to a three-parameter sigmoidal dose–response model to derive the half-maximal inhibitory concentration (IC_{50}) for the inhibition reaction (GraphPad Prism).

Influence of HMB-001 on triggering TLT-1 shedding

The shedding of TLT-1 from the surface of activated platelets was assessed using citrated whole blood from healthy donors. PRP was isolated by centrifugation at 160g for 15 min, and 1:10 v/v acid citrate dextrose (85 mM trisodium citrate, 71 mM citric acid, 111 mM D-glucose) was added. PRP was centrifuged at 400g for 15 min; the plasma was discarded; and the platelet pellet was resuspended in the same volume of HEPES Tyrode (HT) buffer (145 mM NaCl, 5 mM KCl, 0.5 mM Na_2HPO_4, 1 mM $MgSO_4$, 10 mM HEPES, 5.55 mM D-glucose, pH 6.5) with 10 ng ml^{-1} prostacyclin. The platelet suspension was centrifuged again at 400g for 15 min; the supernatant was discarded; and the platelet pellet was resuspended in HT buffer (pH 7.3) to a platelet count of 200 × 10^9 l^{-1}. Rested platelets (500 µl) were added to a glass cuvette (Chrono-Log) and recalcified with 3 mM $CaCl_2$. Collagen Reagens HORM suspension (4 µg ml^{-1}) was added to initiate aggregation, which was monitored for 1 h at 37 °C at 900 r.p.m. in a Chrono-Log model 700 aggregometer (Kordia) with AGGRO/LINK software, in the absence or presence of 100 nM HMB-001. Samples were drawn at 0, 5 and 60 min. Further shedding after these time points was inhibited by adding 25 mM EDTA. Thereafter, samples were centrifuged for 10 min at 20,000g. Samples were drawn from the supernatant and the resuspended aggregate pellet and were diluted 3:1 in 3× sample buffer (15.5% glycerol, 96.8 mM Tris–HCl, pH 6.8, 0.6% SDS, 0.003% bromophenol blue), reduced with 25 mM dithiothreitol, heated at 95 °C for 10 min and loaded on a 4–12% Bis–Tris precast gel. Western blot analysis was performed with 1 µg ml^{-1} polyclonal goat anti-human sTLT-1 antibody (R&D Systems)

and IRDye 800CW-labeled donkey anti-goat IgG secondary antibody (LI-COR) at a 1:10,000 dilution. Data were analyzed with Empiria Studio software (LI-COR).

Influence of HMB-001 on fibrinogen binding to sTLT-1

The influence of HMB-001 and parental monospecific bivalent anti-TLT-1 (pTLT-1) antibody on fibrinogen binding to sTLT-1 was probed by SPR technology (Biacore 8K) at 25 °C (n = 2) using the ABA injection strategy. Anti-His antibody (50 µg ml^{-1}; His capture kit, Cytiva) was immobilized on FC 1 and 2 of a CM5 sensor chip (Cytiva) using standard amine coupling chemistry. His-tagged sTLT-1 (400 nM) was injected at a flow rate of 10 µl min^{-1} for 2 min in FC 2 alone. For the ABA strategy, solution A consisted of running buffer or 1 µM HMB-001 or 1 µM pTLT-1 antibody. Corresponding to solution A, solution B consisted of a fibrinogen concentration series (0, 62.5, 125, 250, 500 and 1,000 nM) in the presence of either running buffer or 1 µM HMB-001 or 1 µM pTLT-1 antibody (**Fig. 7d**). As indicated by the black horizontal lines in **Fig. 7a**, the preanalyte contact time was 120 s (solution A), the analyte contact time was 90 s (solution B) and the postanalyte contact time was 90 s (solution A). The flow rate was set to 30 µl min^{-1}, and the ABA strategy was implemented on both FC 1 and 2. The running buffer consisted of 10 mM HEPES, 150 mM NaCl, 0.05% v/v polysorbate 20, pH 7.4, 5 mM $CaCl_2$ and 1 mg ml^{-1} BSA. The running buffer was also used to dilute sTLT-1, fibrinogen and antibody samples. The chip was regenerated with a 30-s pulse of 10 mM glycine (pH 1.5) in FC 1 and 2. In addition to reference subtraction (FC 2 – FC 1), the sensorgram corresponding to 0 nM fibrinogen concentration was used as a control sensorgram and subtracted from the rest of the sensorgrams. Final binding sensorgrams were visualized using Biacore Insight Evaluation software supplied by the manufacturer (Cytiva). Fibrinogen is a homodimeric molecule and is expected to have two distinct binding sites for sTLT-1. Considering the assay setup, the binding of sTLT-1 at the first site of fibrinogen will potentially influence the binding at the second site. Therefore, data were not fit to a Langmuir 1:1 binding kinetics model.

X-ray crystallography of HMB-001 in complex with FVIIa and TLT-1

The anti-FVIIa Fab fragment of HMB-001 was crystallized in complex with FVIIai and sTF using the hanging-drop method as described elsewhere[70]. Crystals of an SEC-purified Fab:FVIIai:sTF complex were grown using the sitting-drop vapor-diffusion technique at 18 °C. A protein solution of 360 nl protein complex (4.5 mg ml^{-1}) in 20 mM HEPES, 150 mM NaCl and 0.1 mM $CaCl_2$ (pH 7.4) was mixed with 360 nl of a

precipitant solution containing 0.15 M CsCl and 15% w/v PEG 3350 and 360 nl water and equilibrated against 80 µl precipitant solution. Crystals grew within 6 weeks. The crystals were cryoprotected in a solution of 0.15 M CsCl, 15% w/v PEG 3350 and 20% v/v glycerol before flash cooling in liquid nitrogen. Diffraction data were collected at 100K on a Rigaku FR-X rotating anode generator equipped with a Dectris Pilatus 1M detector. Data reduction was performed with programs from the XDS package[71]. All crystallographic calculations were performed using the PHENIX (Python-based Hierarchical ENvironment for Integrated Xtallography)[72] suite of crystallographic programs. The structure was determined by molecular replacement using the Phaser program[73], with the coordinates of the complex structure obtained as a search model. The search model consisted of a previously crystallized similar complex wherein the Fab was the murine version of the corresponding anti-FVIIa Fab fragment of HMB-001 before humanization (unpublished work by G. Schluckebier). The asymmetric unit contains four Fab:FVIIai:sTF complexes. Iterative cycles of manual rebuilding using Coot (Crystallographic Object-Oriented Toolkit)[74] and PHENIX refinement[72] yielded the final model.

The anti-TLT-1 Fab and the sTLT-1 stalk peptide were mixed at a 1:2 molar ratio in HEPES buffer consisting of 20 mM HEPES (pH 7.3) and 150 mM NaCl. The 1:1 Fab–sTLT-1 stalk peptide complex was isolated using gel filtration on a Superdex 200 column eluted with HEPES buffer. It was subsequently concentrated to approximately 11 mg ml^{-1} and used for crystallization. Crystals of the gel-filtrated 1:1 molar Fab–sTLT-1 stalk peptide complex were grown using the sitting-drop vapor-diffusion technique at 18 °C. A 150-nl protein solution of 10.8 mg ml^{-1} Fab–sTLT-1 stalk peptide complex in HEPES buffer was mixed with 50 nl of 1 M LiCl, 0.1 M Na citrate–citric acid (pH 4.0) and 20% w/v PEG 6000 as precipitant and incubated over 60 µl precipitant. The crystal was cryoprotected by adding 1 µl of precipitant (20% ethylene glycol in the precipitant solution) to the crystallization drop before flash cooling in liquid nitrogen. Diffraction data were collected at 100K on the BioMAX beamline at the MAX IV synchrotron facility (Lund, Sweden) using an Eiger 16M hybrid-pixel detector from Dectris. Autoindexing, integration and scaling of the data were performed with programs from the XDS package[71]. The asymmetric unit contains two Fab–peptide complexes, as judged by Matthews coefficient analysis. The structure was determined by molecular replacement. Phaser[73], as implemented in the program suite PHENIX[72], was used with the chains H and L of PDB entry 5KMV as a search model localizing two Fabs. These were model-built with the correct amino acid sequence using the

software Coot[74] and thereafter refined using PHENIX refinement[75]. Amino acids 7–21 from the peptide were clearly seen in the difference electron density maps and could be model-built manually using Coot. The model was further refined using the steps of PHENIX refinement and manual rebuilding in Coot.

Molecular model of the ternary complex on the membrane

To obtain a structure template for model building of HMB-001, we used its sequence to search the Research Collaboratory for Structural Bioinformatics PDB database for structures with homologous sequences. A structure with highly homologous sequences (PDB 5DK3)[76] was identified. Its C-terminal 338 amino acids (out of 448) of the heavy chains and its C-terminal 110 amino acids (out of 218) of the light chains are identical to those of HMB-001. Essentially, the sequences differ only in the heavy- and light-chain hypervariable regions. The two x-ray crystallographic structures of FVIIai:sTF (PDB 8CN9) and the TLT-1 fragment (131–146) (PDB 8CHE) in complex with the two Fabs of HMB-001 described above were then applied in the following manner. The Fabs binding to FVIIai:sTF and sTLT-1 (131–146), denoted anti-FVIIa Fab and anti-TLT-1 Fab, respectively, were structurally aligned using PyMOL (PyMOL molecular graphics system version 2.0, Schödinger) to those of 5DK3. Hence, in the resulting HMB-001 model, the heavy chain binding to FVIIa consists of anti-FVIIa Fab (HC(1–115)) in combination with 5DK3 (HC(113–444)), whereas the heavy chain of the other arm binding to TLT-1 consists of anti-TLT-1 Fab (HC(1–206)) combined with 5DK3 (HC(213–444)). The light chain binding to FVIIa consists of anti-FVIIa Fab (LC(1–106)) and 5DK3 (LC(111–218)) and that to TLT-1 consists of anti-TLT-1 Fab(LC). Note that the resulting HMB-001 model preserves binding to the antigens FVIIa and TLT-1 fragment (131–146). The sequence numbering was updated according to the HMB-001 sequence. As only a fraction of TLT-1 is cocrystalized with the Fab domain, its structured N-terminal domain (PDB 2FRG (TLT-1(20–125))) was combined with TLT-1 (131–146) from the anti-TLT-1 Fab structure (part of the HMB-001 model), followed by an unstructured C-terminal region (residues 147–220) that harbors the transmembrane helix (residues 165–190). This was obtained using DaReUS-Loop[77,78]. Finally, models of FVIIa (in complex with TF) embedded in the membrane were obtained from Y.Z. Ohkubo[79]. Hence, aligning the FVIIa structure bound to HMB-001 with membrane-bound FVIIa results in an initial model of HMB-001 in complex with FVIIa and TLT-1 (20–220) on the membrane surface.

HMB-001 PK and PD evaluation in cynomolgus monkeys

Cynomolgus monkey PK study

To assess the PK properties of HMB-001 and probe its ability to accumulate endogenous FVIIa, a measure of HMB-001 PD activity, we carried out a study in cynomolgus monkeys at Labcorp (Labcorp Early Development Laboratories, Harrogate, UK). The monkeys were exposed to 12-h light/dark cycles. The ambient temperature was maintained at 19–23 °C, and the relative humidity was set at 36–77%. Three groups were administered HMB-001 subcutaneously once weekly with clinically relevant loading and maintenance doses of 1 and 0.15, 1 and 0.45, and 3 and 1.35 mg kg^{-1}, respectively. A fourth group was administered an intravenous bolus injection of 3 mg kg^{-1} HMB-001. The sample size was sufficient to provide meaningful results; four naive cynomolgus monkeys (two females and two males) were included in each group. At the start of the study, the age of all animals ranged from 99 to 143 weeks, and their weight was between 2.21 and 4.46 kg.

Bioanalysis assays

Bioanalysis assays were used to determine the concentrations of HMB-001, total FVII(a) and FVIIa in plasma samples from cynomolgus monkeys. Values reported in **Fig. 6a** represents plasma concentrations for individual animals that were negative for antidrug antibody (ADA). The presence of ADAs toward the anti-FVIIa arm or the anti-TLT-1 arm was established with two separate ADA assays (not described below).

HMB-001 assay

For quantification of total HMB-001 in 3.2% citrated plasma from cynomolgus monkeys, an ELISA was developed and validated. To capture HMB-001, we coated an anti-idiotypic mAb against the anti-TLT-1 arm of HMB-001 (Sanquin, clone 7D11) on a microtiter plate. Samples, calibrators and quality controls (QCs) were added to the wells and incubated. After washing off unbound drug, bound HMB-001 was detected using a biotinylated anti-idiotypic mAb against the anti-FVII arm of HMB-001 (Sanquin, clone 1A9), followed by adding horseradish peroxidase (HRP)-labeled streptavidin (Sigma) and the chromogenic substrate 3,3′-5,5′-tetramethyl-benzidine (TMB) (Thermo Fisher Scientific). Substrate conversion was stopped after adding 0.2 M HCl (Sulpeco), after which the ELISA plate was analyzed on a microtiter plate reader (Epoch 2 Biotek) at 450/540 nm. During the detection step, the plate was incubated for 2 h at 37 °C, enhancing the FVII(a) target tolerance and the detection of both free and FVII(a)-bound HMB-001.

Quantification of HMB-001 was achieved by back-calculating the sample response from the HMB-001 calibration curve fitted using a logistic regression model. The assay has been validated using QC samples representing the lower limit of quantification (LLOQ, 2.70 nM), low (6.92 nM), middle (20.7 nM), high (138 nM), upper limit of quantification (ULOQ, 173 nM) and very high (8.65 µM) HMB-001 concentrations. The assay validation study showed dilution linearity up to an HMB-001 concentration of at least 8.65 µM.

Total FVII(a) assay

For quantification of total FVII(a) in 3.2% citrated plasma from cynomolgus monkeys, a human anti-FVII/FVIIa Asserachrom VII:Ag ELISA kit (Stago) was established, optimized to overcome drug interference and validated. The ELISA kit uses assay strips precoated with rabbit anti-human FVII/FVIIa F(ab')2 fragment polyclonal antibody (pAb) to capture total FVII(a). Calibrators, samples (1:168) and QCs (1:168) were prepared as described below and incubated for 1 h at RT. After washing off unbound FVII(a), bound FVII(a) was detected using a rabbit anti-human FVII(a) antibody coupled to peroxidase and the chromogenic substrate TMB. Substrate conversion was stopped after adding 50 µl of 2.0 M H_2SO_4, after which the ELISA plate was analyzed for 15–60 min on a Biotek Epoch 2 microtiter plate reader at 450/540 nm.

Because HMB-001 binds to FVIIa and zymogen FVII, drug interference was observed in the assay setup. As such, the assay methodology was adjusted by first saturating the calibrator, samples and QCs with HMB-001 before analysis on the ELISA plate. The calibrator consisted of lyophilized human plasma with a known quantity of human FVII. Samples and QCs were prepared by mixing 3.2% citrated cynomolgus monkey plasma, a normal human plasma pool with a known quantity of total FVII(a) (internal reference pool of Sanquin), and reconstituted human plasma control with a known quantity of FVII from the assay kit with assay buffer to a 168-fold dilution. The total FVII(a) concentration was back-calculated from the calibration curve using logit regression. A run was accepted if the goodness of fit of the calibrator was ≥0.99 and if both control samples were within the reference range and deviated ≤20% when compared to the average. Samples were accepted when the deviation from the average was ≤20%. The LLOQ was 46.6% for samples in a 168-fold dilution. The ULOQ was set as the highest point of the calibrator, which equals a theoretical value of 1,616% when using a 168-fold dilution.

In the current setup, cynomolgus total FVII(a) was measured (in percentage units) using a kit for measuring human total FVII(a). Thus, the data represent human-equivalent total FVII(a) levels in cynomolgus plasma. In addition, as the calibration curve is composed of human FVII(a) in plasma instead of cynomolgus FVII(a), the obtained results are semiquantitative. The results from this assay could be used for PK modeling by converting the semiquantitative total FVII(a) levels obtained in percentages (%) to nM values. To do so, we analyzed samples containing either native human FVII or human rFVIIa against the calibration curve. This resulted in an approximate conversion factor of 16% total FVII(a) per 1 nM of total FVII(a), which was used throughout this study for reference purposes.

FVIIa activity assay

FVIIa activity in 3.2% citrated plasma from cynomolgus monkeys was quantified using a Staclot VIIa–rTF kit (Stago). For quantification of FVIIa activity in 3.2% citrated plasma from cynomolgus monkeys, the assay procedure was modified and fit-for-purpose qualified. The activity assay was performed on a Sysmex CS-5100 turbidimeter (Siemens Healthineers). The Sysmex turbidimeter measures transmitted light, which was converted to clotting time. The calibrator (reagent 4) containing a known quantity of human rFVIIa was dissolved in water (Fresenius Kabi). At the same time, recombinant sTF (rsTF)–phospholipids (reagent 3) and FVII-deficient plasma (reagent 2) were dissolved in water (Fresenius Kabi). First, a calibration curve was measured by placing the reagents in the Sysmex CS-5100 and the calibrator solution. A six-point calibrator was determined by measuring 1:10, 1:20, 1:40, 1:80, 1:160 and 1:320 dilutions in the Sysmex CS-5100. Before adding FVII-deficient human plasma, a prerinse with Clean 1 (1.0% sodium hypochlorite solution, Honeywell Fluka) was performed, followed by a postrinse with Clean 1. Then, the rsTF–phospholipid solution was added 20 s after the addition of FVII-deficient plasma. At 220 s after adding rsTF–phospholipids, 0.025 M $CaCl_2$ (Stago) was added to induce clot formation after a prerinse with Clean 1.

After successful calibration, 3.2% citrated cynomolgus monkey plasma samples from HMB-001-treated animals were measured in a 20-fold predilution in reagent buffer. Pretreatment samples were measured undiluted. To prevent FVIIa potentiation by HMB-001, we mixed the samples with sTLT-1 peptide (Schafer-N). Before sample analysis, control samples (reagents 5a and 5b) with known concentrations of human rFVIIa were dissolved in water (Fresenius Kabi) and mixed. Samples and controls were

then analyzed in three dilutions of 1:10, 1:20 and 1:40 using the same mixing sequence in the Sysmex CS-5100 as the calibrator.

Samples and controls were compared to the calibration curve using parallel-line assay analysis. For the run to be accepted, the controls had to fall within the documented reference range of the kit manufacturer, and the parallelism ratio of the controls had to fall within 0.8–1.2. In addition, samples were accepted if their parallelism ratio was within 0.8–1.2 and if at least one of the sample points was within the calibrated assay range. The LLOQ was determined at 40.5 mIU ml^{-1}, and the ULOQ was theoretically set at 7,026 mIU ml^{-1}.

In the current setup, cynomolgus FVIIa was measured (in mIU) using a kit for measuring human FVIIa. Thus, the data represent human-equivalent FVIIa levels in cynomolgus plasma. The equivalence between the mIU and ng units has been established, verified experimentally and found to be approximately 30 mIU ng^{-1} [80]. This allows for further conversion of the FVIIa signals to nM, resulting in an assay range of 0.027–18.8 nM.

PK/PD model

PK/PD analysis of the HMB-001, FVIIa and total FVII(a) concentrations obtained in the study was carried out using a validated installation of NONMEM (version 7.4.3, ICON Development Solutions) under Windows 10 Professional and the GNU gfortran compiler version 4.5.0. Postprocessing of NONMEM analysis results was carried out in R version 4.0.5 (Comprehensive R Network (R Development Core Team, 2008)[81]). NONMEM run execution and visual predictive check were carried out using PsN (Perl-speaks-NONMEM, version 4.8.1)[82]. Parameter estimation was carried out using first-order conditional estimation with interaction.

During model development, a single additional parameter in the structural model was included if the difference in the objective function value between two models was >6.635, significant at the $P < 0.01$ level. The final model was determined based on maximized likelihood (lowest stable objective function value, physiological plausibility of parameter values, successful numerical convergence, parameter precision and acceptable visual predictive check).

The PK properties of HMB-001 were described by a two-compartment model with first-order subcutaneous absorption. FVIIa and total FVII(a) concentrations over time

were modeled using turnover models in which increases in FVIIa and total FVII(a) after HMB-001 administration were described by two separate Emax functions stimulating the endogenous production of FVIIa and total FVII(a), respectively.

The developed PK/PD model was scaled to humans using established allometric scaling approaches, assuming a human body weight of 70 kg and a cynomolgus monkey weight of 2.76 kg. All clearances were allometrically scaled with a power of 0.85; volumes were scaled with a power of 1; and the absorption rate constant was scaled with a power of −0.25[83]. E_{max} was allometrically scaled with a power of 0.75[84]. Human baseline values of 0.067 nM[56] and 10 nM[85] were used for FVIIa and total FVII(a), respectively. The remaining parameters (Hill coefficient, EC_{50}) were assumed to be similar to those of monkeys.

Simulations of HMB-001 dosing regimens in humans

A human body weight of 70 kg, an FVIIa baseline of 0.067 nM[56] and an FVII baseline of 10 nM[85] were used for the simulations. To illustrate the impact of interindividual variability, we simulated 1,000 participants assuming the same interindividual variability as estimated for the cynomolgus monkey data. For doses of 0.34, 0.4, 0.5 and 0.6 mg kg^{-1}, the 66th, 56th, 42nd and 33rd percentiles give a twofold increase above the FVIIa baseline, respectively.

FVII activity and FVIIa plasma levels in GT plasma

FVII activity was measured using a prothrombin time (PT)-based factor assay. Standard clotting times were determined using 25 µl normal pooled plasma from healthy donors at 10-, 20-, 40- and 80-fold dilutions in 0.9% NaCl, mixed with 25 µl FVII-depleted plasma at 37 °C for 2 min. Plasma samples from 13 PwGT were diluted 20-fold in 0.9% NaCl, and 25 µl diluted patient plasma was mixed with 25 µl FVII-depleted plasma at 37 °C for 2 min. To initiate coagulation, we added 50 µl Dade Innovin PT reagent to the plasma samples and monitored the time to clotting.

Evaluation of HMB-001 efficacy in Glanzmann Thrombasthenia models

To further quantify FVIIa plasma levels, we performed an ELISA using a V_HH against FVIIa[67]. A 2 µg ml^{-1} concentration of the bivalent monoclonal anti-FVIIa-specific V_HH in coating buffer (5 mM Na_2CO_3, 35 mM $NaHCO_3$, 3 mM NaN_3) was coated on a 96-well plate for 30 min at RT at 600 r.p.m. and then overnight at 4 °C. The wells were emptied and blocked for 1 h at RT with blocking buffer (blocking reagent for ELISA

(Roche) + 0.05% Tween 20) at 600 r.p.m. Plasma samples from 50 healthy donors and 13 PwGT were diluted eightfold in blocking buffer, added to the wells and incubated for 1 h at RT at 600 r.p.m. The wells were washed three times, added with 50 µl of the 1:4,000 diluted primary antibody (sheep anti-FVII IgG affinity-purified, Cedarlane) in blocking buffer and incubated for 1 h at RT at 600 r.p.m. Next, the wells were washed three times with washing buffer (0.05% Tween-20 in PBS) and added with 50 µl of the 1:4,000 diluted secondary antibody (rabbit anti-sheep IgG HRP-conjugated) in blocking buffer. After incubation for 1 h at RT at 600 r.p.m., the wells were washed three times and stained with 50 µl TMB for 6 min. Substrate conversion was stopped using 25 µl of 0.3 M sulfuric acid in each well. Absorbance was measured at 450 nm, and FVIIa plasma levels were determined using a calibration curve of rFVIIa.

Localization of FVIIa on activated platelets

Localization of FVIIa on activated platelets was evaluated by fluorescence-activated cell sorting (FACS) with whole blood collected from healthy donors into sodium heparin Vacutainer tubes (BD). Blood was supplemented with 25 nM FVIIa with 0 or 25 nM HMB-001 in combination with 0 or 400 nM sTLT-1. Five microliters of whole blood was added to 50 µl HBS FACS buffer (10 mM HEPES, 150 mM NaCl, 1 mM $MgSO_4$, 5 mM KCl, pH 7.4) with 25 µM PAR-1 AP (SFLLRN, Bachem, 141923-40-2), 1 µg ml^{-1} CRP-XL (CambCol Laboratories), AlexaFluor-647-labeled anti-FVIIa V_HH antibody (10 µg ml^{-1}), fluorescein isothiocyanate (FITC)-labeled mouse anti-P-selectin antibody (clone VI-PL44, BD Biosciences) and R-PE-labeled anti-GPIbα V_HH antibody (15 µg ml^{-1}) and incubated at 37 °C in the dark for 10 min. Samples were fixed with 500 µl fixative buffer (137 mM NaCl, 2.7 mM KCl, 1.12 mM NaH_2PO_4, 1.15 mM KH_2PO_4, 10.2 mM Na_2HPO_4, 4 mM EDTA, 1.11% formaldehyde, pH 6.8) and incubated in the dark at RT for 20 min. Samples were diluted 1:1 v/v with HBS buffer and analyzed on a BD FACSCanto II flow cytometer with FACSDiva software. Platelets were gated based on forward and side scatter and GPIbα expression (**Supplementary Fig. 1**). FVIIa binding was expressed as median fluorescence intensity (MFI).

HMB-001 copy number on activated platelets

HMB-001 was conjugated to AlexaFluor-647 by incubating 17 µM HMB-001 in sodium bicarbonate buffer (100 mM in HBS) with 1:40 vol AlexaFluor-647 succinimidyl ester for 1 h at RT, protected from light and under continuous agitation. Free fluorophore was removed by centrifugation in a Zeba Spin desalting column (7K molecular weight

cutoff). Concentration and labeling degree were determined by the absorption at 280 and 650 nm.

HMB-001 copy number on activated platelets was determined using flow cytometry. Citrated whole blood from healthy human donors (n = 3) was incubated with AF647-conjugated HMB-001 (31.25 nM–2 µM) for 10 min at 37 °C in HBS FACS buffer containing 25 µM PAR-1 AP or buffer, R-PE-conjugated GPIbα nanobody (in-house produced) at 15 µg ml^{-1} as a platelet marker, FITC-conjugated mouse anti-human CD62P (clone VI-PL44, BD Biosciences 555523) at a 1:25 dilution as a platelet activation marker. Then, samples were fixed using fixative buffer for 20 min at RT with protection from light. The fixed samples were diluted 1:1 in FACS buffer, and MFI was measured in a BD FACSCanto II flow cytometer. Additionally, the MFIs of Quantum AlexaFluor-647 molecules of equivalent soluble fluorochrome (MESF) beads (Bangs Laboratories) and Rainbow calibration particles (eight peaks, 3.0–3.4 µm, BioLegend) were measured according to the manufacturer's instructions. MFI data were converted to MESF arbitrary units based on calibration with MESF beads and corrected for the number of fluorophores per HMB-001. Maximum binding was calculated with nonlinear regression assuming a 1:1 interaction (GraphPad Prism version 10.1).

TLT-1 and P-selectin expression and fibrinogen binding

Fresh citrated human whole blood was warmed at 37 °C for 10 min, and 5 µl was added to 50 µl HBS with fluorescent antibodies and a platelet agonist. For quantification of TLT-1 expression, the antibodies used were AlexaFluor-647-labeled anti-P-selectin V_HH antibody (7.5 µg ml^{-1}), R-PE-labeled anti-GPIb V_HH antibody (15 µg ml^{-1}), and AlexaFluor-488-coupled pTLT-1 antibody (30 µg ml^{-1}) or AlexaFluor-488-labeled IgG4 isotype control (ACROBiosystems, DNP-M3-1mg, 30 µg ml^{-1}). For quantification of P-selectin expression and fibrinogen binding, the antibodies used were R-PE-labeled anti-GPIb V_HH antibody (15 µg ml^{-1}) and either AlexaFluor-647-labeled anti-P-selectin V_HH antibody (7.5 µg ml^{-1}) and AlexaFluor-488-labeled anti-fibrinogen V_HH antibody (25 µg ml^{-1}) or AlexaFluor-488- and AlexaFluor-647-labeled isotype control V_HH antibody R2. The platelet agonists used were 25 µM PAR-1 AP, 250 µM PAR-4 AP AYPGKV (produced at the peptide facility of the Netherlands Cancer Institute), 60 µM adenosine diphosphate (ADP) (Sigma, 01897), 1 µg ml^{-1} CRP-XL and 5 µM U-46619 (Cayman Chemical, 16450). This was incubated for 10 min at 37 °C in the dark to allow platelet activation. Platelet activation was stopped as described for FVIIa binding to activated platelets. Samples were subjected to FACS analysis on a BD FACSCanto II

flow cytometer with FACSDiva software, and platelets were gated based on forward and side scatter and GPIbα expression. Results are expressed as MFI.

Influence of HMB-001 on platelet aggregation

Citrated whole blood from healthy human donors was centrifuged at 160g for 15 min at RT without brake to obtain PRP. The remainder of the blood was centrifuged at 2,000g for 10 min at RT to obtain platelet-poor plasma (PPP) to serve as a blank in the aggregometer. PRP (300 µl) was added to a glass cuvette containing a magnetic stirrer in the absence and presence of 100 nM HMB-001. Aggregation was initiated by either 5 µM ADP, 5 µM epinephrine, 4 µg ml^{-1} Collagen Reagens HORM Suspension or 10 µM PAR-1 AP. Aggregation was monitored for 15 min at 37 °C at 900 r.p.m. by light transmission aggregometry.

HMB-001 aggregates GT and GT-like platelets through FVIIa

Aggregation of GT and GT-like (αIIbβ3-inhibited) platelets was assessed using light transmission aggregometry in a Chrono-Log model 700 (Kordia)[13,25]. To isolate platelets, we centrifuged citrated whole blood from healthy donors at 160g for 15 min without brake at RT. PRP was isolated, and 1:10 v/v acid citrate dextrose (85 mM trisodium citrate, 71 mM citric acid, 111 mM D-glucose) was added. PRP was centrifuged at 400g for 15 min without brake at RT; plasma was discarded; and the platelet pellet was resuspended in the same volume of HT buffer (145 mM NaCl, 5 mM KCl, 0.5 mM Na_2HPO_4, 1 mM $MgSO_4$, 10 mM HEPES, 5.55 mM D-glucose, pH 6.5) with 10 ng ml^{-1} prostacyclin. The platelet suspension was centrifuged again at 400g for 15 min at RT. The supernatant was then discarded, and the platelet pellet was resuspended in HT buffer (pH 7.3). The platelet count was adjusted to 200 ×10^9 l^{-1}, and platelets were rested for 30 min at RT before aggregation. To obtain GT-like platelets, we added 500 µM H-D-Arg-Gly-Asp-Trp (D-RGDW) (Bachem, 4026559) to the isolated platelets; this occupies the αIIbβ3 receptor on platelets and thereby inhibits platelet aggregation. Five hundred microliters of isolated GT-like platelets was added to a cuvette containing a magnetic stirrer. A coagulation mixture containing varying concentrations of FVIIa, 10 µg ml^{-1} human plasma-derived FX (Enzyme Research Laboratories, HFX 1010), 20 ng ml^{-1} human plasma-derived prothrombin (Enzyme Research Laboratories, HP 5530AL), 0.5 mg ml^{-1} human plasma-derived fibrinogen (Enzyme Research Laboratories, FIB3 5404L) and 3 mM $CaCl_2$ was added to the platelets, and aggregation was initiated with 4 µg ml^{-1} Collagen Reagens HORM Suspension. Aggregation was monitored at 37 °C at 900 r.p.m. for 1 h.

To establish the potentiation of platelet aggregation by HMB-001, we isolated platelets from PwGT and added the coagulation mixture containing 10 nM FVIIa with or without 10 nM HMB-001 to 500 µl GT platelets. Aggregation was initiated after stimulation with 4 µg ml^{-1} Collagen Reagens HORM Suspension and monitored at 37 °C at 900 r.p.m. To establish the concentration–response profile of FVIIa and FVIIa in the presence of HMB-001, we prepared the coagulation mixture consisting of different concentrations of FVIIa (0.125–10 nM) alone and in the presence of equimolar concentrations of HMB-001. With each coagulation mixture, aggregation of GT-like platelets was initiated and monitored as described herein. For each platelet aggregation experiment, the lag time (defined as the time until half-maximal aggregation was reached) was measured and plotted against the FVIIa concentration. Data were fit to a four-parameter agonist versus response (variable slope) model using nonlinear regression to derive the EC_{50} values (GraphPad Prism). To characterize TLT-1 dependency, we performed platelet aggregation experiments using GT-like platelets in the presence of 400 nM sTLT-1 to study its effect on platelet aggregation mediated by 1 nM FVIIa with and without 1 nM HMB-001. In addition, we mimicked a clinically relevant scenario (scenario 3, **Supplementary Table 8**) using GT-like washed platelets (n = 3). The predicted accumulated levels of total FVII(a) and FVIIa for clinical scenario 3 (**Supplementary Table 8**) were reconstituted by adding FVII-S195A and FVIIa. HMB-001 was added as indicated. Aggregation was induced with 4 µg ml^{-1} collagen in buffer with 3 mM $CaCl_2$, 10 µg ml^{-1} FX, 20 ng ml^{-1} prothrombin and 0.5 mg ml^{-1} fibrinogen. Light transmission was monitored for 1 h (**Fig. 7**).

HMB-001 affects thrombin generation in GT-like platelets

The effect of HMB-001 on FVIIa in the presence of FVII was evaluated by a calibrated automated thrombin generation assay in human PRP under GT-like conditions and compared to the effect of rFVIIa alone. The PRP thrombin generation assay was made sensitive to FVIIa by introducing HA-like conditions and antagonizing any residual TF in plasma. In this context, the predicted plasma levels of HMB-001, FVIIa and total FVII(a) were reconstituted, and the effect on thrombin generation was evaluated following the initiation of platelet activation. The background plasma concentrations of FVIIa and total FVII(a) were assumed to be 67 pM[56] and 10 nM, respectively. The predicted accumulated levels of total FVII(a) and FVIIa for the five different clinical scenarios (**Supplementary Table 8**) were reconstituted by adding FVII-S195A and FVIIa after accounting for the background plasma concentration of total FVII(a) and FVIIa, respectively. Citrated human whole blood was centrifuged for 15 min at 160g

without brake to obtain PRP. The remainder of the blood was centrifuged for 10 min at 2,000g to obtain PPP, which was used to adjust the platelet count to 250 × 10^9 l^{-1}. PRP was incubated for 60 min at 37 °C with 500 µM D-RGDW to mimic GT conditions, 25 µg ml^{-1} neutralizing sheep anti-FVIII pAb and 10 nM neutralizing mouse anti-TF mAb. Next, the predicted plasma levels of HMB-001, FVIIa and total FVII(a) from the five different clinical scenarios in HBS/0.2% BSA buffer were added to the PRP (as indicated in **Supplementary Table 8**), and platelets were activated with a trigger mixture consisting of 30 µM PAR-1 AP and 1 µg ml^{-1} CRP-XL for 10 min at 37 °C. Finally, thrombin generation was initiated by adding 16.7 mM $CaCl_2$ and monitored by measuring fluorogenic thrombin substrate (Z-Gly-Gly-Arg-7-amino-4-methylcoumarin·HCl (I-1140)) conversion at 400/500 nm for 3 h at 37 °C in a SpectraMax iD3 microtiter plate reader (Molecular Devices) with SoftMax Pro software. Thrombin generation was deduced from fluorescence data as previously described[86].

HMB-001 affects fibrin formation in GT and GT-like platelets

Coverslips were functionalized by incubating in 1:1 v/v 12.1 N hydroxychloride and methanol for 30 min at RT, followed by incubating with a 1:100 dilution of 95% aminopropyltriethoxysilane in ethanol for 30 s at RT. Finally, coverslips were incubated in a 1:20 dilution of 25% glutaraldehyde in HBS for 1 h at RT. Washing steps in between were performed with water or ethanol. Coverslips were dried and stored in HBS at 4 °C until use. Before use, coverslips were washed[87], dried and coated with 0.3 mg ml^{-1} collagen type I solution from bovine skin (Sigma) in HBS for 1 h, then blocked with HBS/1% BSA buffer at 4 °C overnight. Polydimethylsiloxane parallel-plate microfluidic devices were washed three times with hydrochloric acid, acetone and 96% ethanol for 15 min. Next, devices were rinsed and blocked with HBS/1% BSA buffer at 4 °C overnight. Washed and dried coverslips were attached to the polydimethylsiloxane device using vacuum and mounted on a Zeiss Axiovert Observer Z1 widefield fluorescence microscope with Colibri LEDs. Platelets were labeled with MitoTracker Orange CMTMRos (Thermo Fisher Scientific) for 30 min. Citrated human whole blood was subsequently supplemented with 8.3 µg ml^{-1} AlexaFluor-488-conjugated V_HH anti-fibrin and 20 µg ml^{-1} corn trypsin inhibitor (Enzyme Research Laboratories) with or without 0–25 nM FVIIa or 0–100 nM HMB-001 and was recalcified with 20 mM $CaCl_2$. In healthy controls, αIIbβ3 was blocked with 500 µM D-RGDW, and blood was aspirated through the flow chamber with a syringe pump at a shear rate of 300 s^{-1}. Platelet adhesion and fibrin deposition were monitored at 200× magnification at a frame rate of three per minute for 20 min.

RESULTS

To identify anti-FVIIa and anti-TLT-1 antibodies for subsequent assembly into biAbs (**Fig. 2a**), we applied immunization and functional screening strategies to maintain the functionality of the two targets upon binding while allowing for productive assembly of the ternary FVIIa:biAb:TLT-1 complex on a procoagulant membrane surface. The anti-FVIIa arm of HMB-001 was selected based on the absence of effects on FVIIa-dependent thrombin generation and normal inhibition of FVIIa by antithrombin (AT). The anti-TLT-1 arm of HMB-001 was derived from the anti-TLT-1 Fab fragment already used for targeting FVIIa to activated platelets; this arm binds to the membrane-proximal stalk region of TLT-1[41] and is anticipated not to affect the intrinsic properties of TLT-1. First, to determine whether targeting of FVIIa to TLT-1 on activated platelets with a biAb can potentiate FVIIa activity, we assembled an anti-FVIIa candidate and the lead anti-TLT-1 arm into a biAb and tested it in a tail vein transection (TVT) injury model in transgenic HA mice ($F8^{-/-}$) expressing human TLT-1. FVIIa administration reduced blood loss after TVT in a concentration-dependent (**Fig. 2b**; half-maximal effective concentration (EC_{50}) 5.4 nM, 95% confidence interval (95% CI) 1.7–14.3 nM) and dose-dependent manner (**Extended Data Fig. 1**). When FVIIa was coformulated with an equimolar amount of the biAb (to overcome the lack of cross-reactivity with murine FVIIa), the efficacy of FVIIa was enhanced by 15-fold (EC_{50} 0.36 nM, 95% CI 0.005–1.3 nM). The shorter half-life and, consequently, faster *in vivo* elimination of free FVIIa compared to the FVIIa:biAb complex were accounted for by estimating the EC_{50} values (**Fig. 2b**) based on the FVIIa concentrations measured in plasma at the end of the bleeding window. The improved efficacy of FVIIa in the presence of the biAb suggests that biAb-mediated targeting of FVIIa to platelet TLT-1 *in vivo* (**Supplementary Table 1**) is feasible. Next, several variants of the biAb with different target affinities were engineered to select optimal affinities for binding to FVIIa and TLT-1 (**Fig. 2c**, **Extended Data Fig. 2** and **Supplementary Table 2**). The ability of each biAb to enhance TLT-1-dependent FVIIa activity was assessed in an FX activation assay (**Fig. 2c**). From this, the biAb with the highest affinity for FVIIa and the soluble extracellular fragment of TLT-1 (sTLT-1) was found to be associated with the greatest stimulation of FVIIa activity. Consequently, this candidate was selected as HMB-001. Subsequent titration of HMB-001 from 0 to 500 nM revealed a close-to-maximum potentiation of FVIIa activity in a broad concentration range encompassing HMB-001's anticipated clinically relevant plasma concentration of 100 nM. In comparison, monovalent control antibodies (cAbs) comprising either the FVIIa- or TLT-1-binding

arm of HMB-001 had no effect on FX activation, indicating that the combined action of both arms is required for the enhancing effect of HMB-001. HMB-001 bound to FVIIa, zymogen FVII and sTLT-1 with equilibrium dissociation constant (K_D) values of 0.37, 0.4 and 2.3 nM, respectively (**Fig. 2d** and **Supplementary Table 3**). Consistent with the absence of TLT-1 on resting platelets, FVIIa localization was undetectable on resting platelets in the presence of HMB-001. In contrast, HMB-001 facilitated significant localization of FVIIa to platelets when these were preactivated with a cocktail of the protease-activated receptor-1 activating peptide (PAR-1 AP) SFLLRN and cross-linked collagen-related peptide (CRP-XL) (**Fig. 2e**). As expected, this was TLT-1 dependent, as demonstrated by a significantly impaired FVIIa localization when an excess (400 nM) of the competitor sTLT-1 was included in the assay. Neither the anti-FVIIa cAb nor the anti-TLT-1 cAb facilitated FVIIa binding (**Extended Data Fig. 3a**), demonstrating that FVIIa localization to activated platelets requires both arms of the HMB-001 biAb.

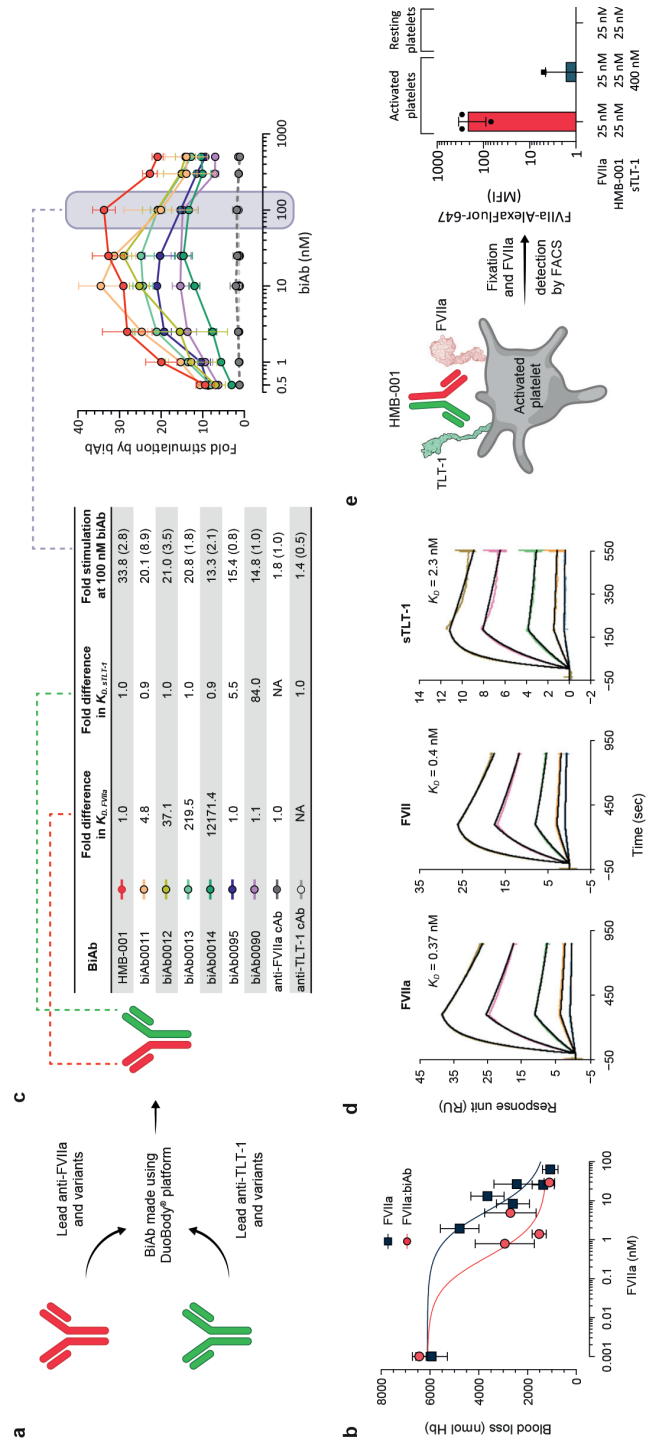

Fig. 2: Optimal affinity for FVIIa and TLT-1 binding by HMB-001 leads to efficient TLT-1-dependent FVIIa localization on the activated platelet. a, BiAbs were made using the DuoBody platform. **b**, The ability of the biAb to potentiate FVIIa activity *in vivo* was evaluated in transgenic HA mice expressing human TLT-1 and using the TVT injury model. Anesthetized mice were placed on a heating pad set to maintain animal body temperature and with the tail submerged in saline (37 °C). FVIIa alone (n = 3–10, dark squares) or coformulated with an equimolar concentration of the biAb (n = 6, red circles) was administered intravenously into the right lateral tail vein 5 min before the injury. Total blood loss was determined by quantifying the amount of hemoglobin (Hb) in the saline and is expressed as nmol Hb. FVIIa concentrations were measured at the end of the bleeding window. Data are expressed as mean blood loss ± s.d. **c**, BiAbs with different affinities, as measured using surface plasmon resonance (SPR) technology (n = 2), toward FVIIa and sTLT-1 were generated. FX (150 nM) was activated with FVIIa (2.5 nM) in the presence of lipidated TLT-1 and biAbs at the indicated concentrations for 20 min (n = 3). Reactions were quenched, and FXa formation was assessed with a chromogenic substrate. At the anticipated clinically relevant biAb plasma concentration of 100 nM, shown in the shaded gray region, data are expressed as mean fold-stimulation in FXa generation compared to the absence of the biAb. Error bars indicate s.d. NA, not applicable. **d**, Binding of HMB-001 to FVIIa, zymogen FVII and sTLT-1 was assessed with SPR technology at 25 °C and pH 7.4 (n = 2). Kinetic data were fitted to a Langmuir 1:1 binding model to obtain KD values. **e**, Whole blood from healthy donors (n = 3) was incubated with FVIIa, HMB-001 or sTLT-1, as indicated, in the presence of an AlexaFluor-647-labeled FVIIa-specific V_HH with or without a cocktail of 25 µM PAR-1 AP and 1 mg ml^{-1} CRP-XL for 10 min. FVIIa binding to platelets was assessed with FACS. Data are expressed as mean MFI ± s.d.

HMB-001 does not affect the normal function of FVIIa or TLT-1

As maintaining the normal physiological functions of FVIIa by HMB-001 is crucial, we investigated the effects of HMB-001 on known reactions involving FVIIa or FVII. First, we addressed the impact of HMB-001 on the activation of downstream effectors of FVIIa[43,44]. HMB-001 did not affect FVII autoactivation or FX activation by TF-bound FVIIa but slightly enhanced FX activation by FVIIa in the absence of TF (**Fig. 3a–c** and **Supplementary Table 4**). Next, we analyzed the effect of HMB-001 on FVIIa inhibition. We observed little to no effect of HMB-001 on FVIIa inhibition by AT, which is responsible for elimination of rFVIIa from the circulation[45], or tissue factor pathway inhibitor (TFPI), a key downregulator of TF-bound FVIIa during coagulation[46] (**Fig. 3d, e** and **Supplementary Table 4**).

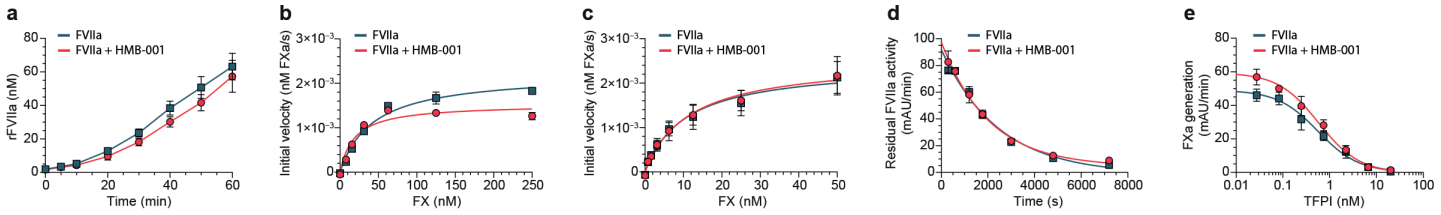

Fig. 3: HMB-001 does not interfere with the normal functioning of FVIIa. a, FVII autoactivation. FVII (145 nM) was activated with FVIIa (2 nM) in the presence of lipidated TF (2 nM) and 0 or 500 nM HMB-001 for 0–60 min (n = 3). FVIIa activity was assessed with a chromogenic substrate in the presence of 200 nM lipidated TF. Data are expressed as mean ± s.d. **b**, TF-independent FX activation. Human plasma-derived FX (0–250 nM) was activated with FVIIa (20 nM) in the presence of 0 or 500 nM HMB-001 for 20 min (n = 3). FXa was assessed with a chromogenic substrate. FXa generation rates (nM FXa per s) were plotted as a function of FX concentration. Data are expressed as mean ± s.d. **c**, TF-dependent FX activation. Human plasma-derived FX (0–50 nM) was activated with FVIIa (100 pM) in the presence of 0 or 50 nM HMB-001 and 2 pM lipidated TF for 20 min (n = 3). FXa was assessed with a chromogenic substrate. FXa generation rates (nM FXa per s) were plotted as a function of FX concentration. Data are expressed as mean ± s.d. **d**, FVIIa inactivation by AT. FVIIa (200 nM) was preincubated with 12 mM low-molecular-weight heparin and 0 or 500 nM HMB-001 for 10 min, followed by incubation with AT for 0–2 h (n = 3). Residual FVIIa activity (mAU min^{-1}) was assessed with a chromogenic substrate and plotted as a function of time. Data are expressed as mean ± s.d. **e**, FVIIa inactivation by TFPI. FVIIa (100 pM) was preincubated with 2 pM TF, 0–20 nM TFPI and 0 or 500 nM HMB-001 for 10 min, followed by incubation with 50 nM FX for 30 min (n = 3). FXa activity was assessed with a chromogenic substrate, and residual FXa activity (mAU min^{-1}) was plotted as a function of TFPI concentration. Data are expressed as mean ± s.d.

Furthermore, HMB-001 had no effect on platelet degranulation or activation, as evidenced by normal P-selectin secretion and fibrinogen binding after stimulation with agonists (**Fig. 4a, b**). In addition, HMB-001 did not influence the capacity of platelets to aggregate (**Fig. 4c**). Representative traces of platelet aggregation in a single donor with or without HMB-001 are shown in **Extended Data Fig. 4**. The biology of TLT-1 involves its partial downregulation through proteolytic cleavage and shedding on the activated platelet[47]. HMB-001 had no discernible effect on the shedding of TLT-1 (**Fig. 4d**) and allowed fibrinogen to engage with sTLT-1 (**Extended Data Fig. 5**). At saturating concentrations of HMB-001, its copy number per activated platelet ranged from 8,230 to 38,435, which is in line with previous reports of the number of TLT-1 copies per platelet[48,49]. Based on these data, HMB-001 was concluded to have little to no effect on normal FVIIa or platelet physiology.

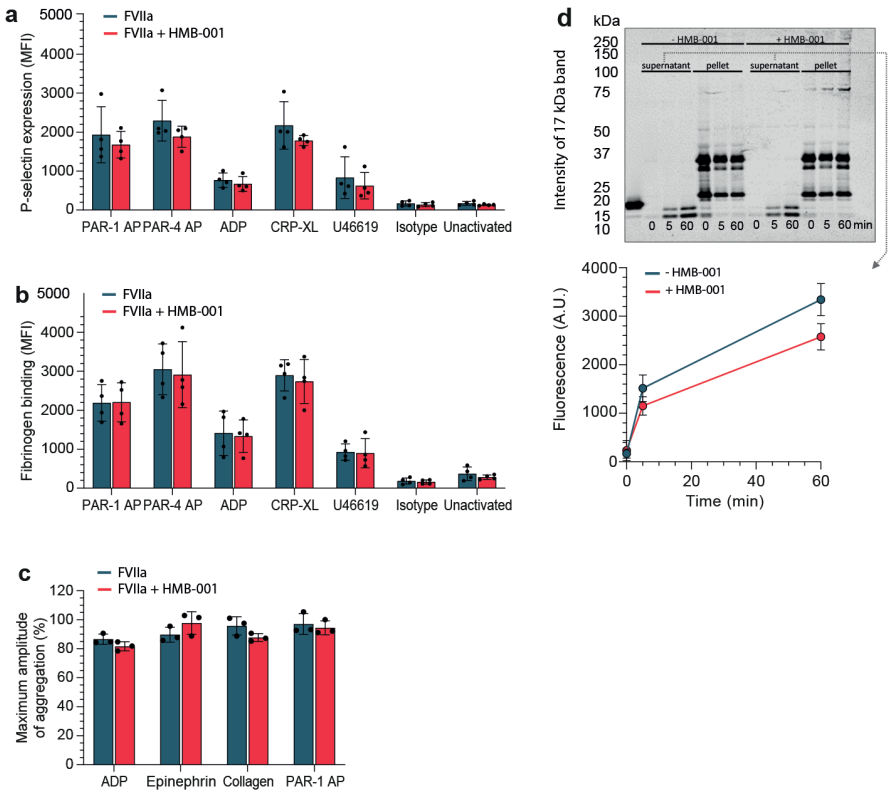

Fig. 4: HMB-001 does not influence key platelet properties. a,**b**, Whole blood from healthy donors (n = 3) was incubated with 0 or 100 nM HMB-001 and buffer or platelet agonists (PAR-1 AP, PAR-4 AP, ADP, CRP-XL or U-46619) for 10 min. Platelet P-selectin expression (**a**) and fibrinogen binding (**b**) were measured with FACS. Data are expressed as mean MFI ± s.d. **c**, PRP from healthy donors (n = 3) was incubated with 0 or 100 nM HMB-001 and activated with ADP, epinephrine, collagen or PAR-1 AP with stirring at 900 r.p.m. Platelet aggregation was monitored with light transmission for 15 min. Data are expressed as the maximal amplitude of the aggregation trace and represent mean ± s.d. **d**, TLT-1 shedding. Washed platelets from healthy human donors (n = 3) were stimulated with collagen in an aggregometer for 0–60 min. Platelet fractions and supernatant were separated with centrifugation and subjected to SDS–PAGE. TLT-1 was visualized with western blotting. The intensity of the 17-kDa band was analyzed with Empiria Studio 2.1 software. Data represent mean ± s.d.

To characterize the binding epitopes of HMB-001 on FVIIa and TLT-1, we solved the x-ray crystal structures of the anti-FVIIa Fab fragment in complex with the active site-inhibited FVIIa:soluble TF (sTF) complex (Protein Data Bank (PDB) 8CN9) and the anti-TLT-1 Fab fragment in complex with the synthetic stalk peptide of TLT-1 (PDB 8CHE). The data collection and refinement statistics are summarized in **Supplementary Table 5**. The crystal structure of the anti-FVIIa Fab in complex with the active site-

inhibited FVIIa:sTF complex (**Extended Data Fig. 6a**) showed that the anti-FVIIa arm of HMB-001 recognizes an epitope on FVIIa composed of residues from the epidermal growth factor-like 2 and protease domains of FVIIa. The binding epitope does not overlap with the active site of FVIIa, the binding interface with TF or the N-terminal γ-carboxyglutamic acid (Gla) domain of FVIIa that is involved in membrane binding. A comparison to the published molecular model of the FVIIa:sTF:activated FX (FXa) complex further suggests that the epitope is distinct from the predicted binding site of FX/FXa (**Extended Data Fig. 6b**), consistent with functional studies. The crystal structure of the anti-TLT-1 Fab in complex with the TLT-1 stalk peptide (**Extended Data Fig. 6c**) showed that this arm of HMB-001 recognizes a linear segment in the stalk region comprising amino acids from K118 to A131 (mature TLT-1 receptor numbering). Consequently, the binding epitope is distant from the N-terminal globular IgV domain and the transmembrane sequence of the TLT-1 receptor. By using the two crystal structures, a model of the ternary complex among HMB-001, FVIIa and TLT-1 receptor embedded in the phospholipid membrane was generated (**Fig. 5**). Consistent with the two crystal structures and available functional data, the generated model supports the lack of interference of HMB-001 with the known functional properties of FVIIa and TLT-1. In addition, the orientation of the HMB-001:FVIIa complex with respect to the HMB-001:TLT-1 receptor complex and the fragment crystallizable (Fc) domain of HMB-001 allows HMB-001 to simultaneously engage with FVIIa and TLT-1, while the FVIIa N-terminal Gla domain is free to dock in an apparent productive orientation on the phospholipid membrane surface[50].

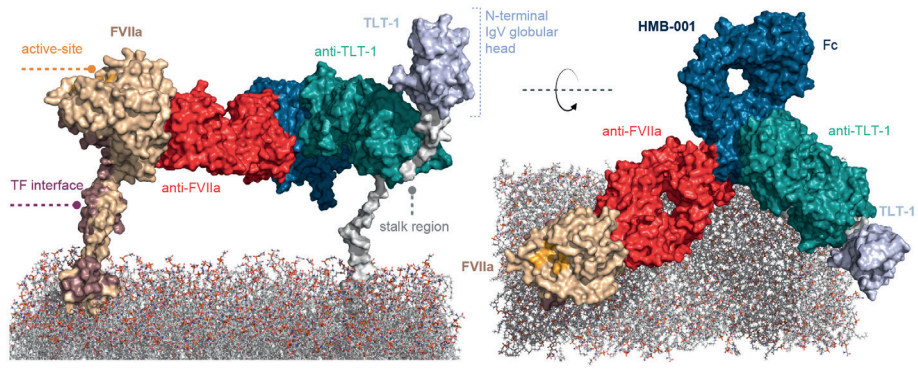

Fig. 5: Ternary complex among HMB-001, FVIIa and TLT-1 on the phospholipid membrane surface. The model was generated by aligning (using PyMOL) the two crystal structures from the current study (PDB 8CN9 and 8CHE) with an antibody structure template (PDB 5DK3) and subsequently performing short molecular dynamics simulations on the initial starting structure.

HMB-001 accumulates endogenous FVIIa in nonhuman primates

To assess the pharmacokinetic (PK) properties of HMB-001 and probe its ability to accumulate endogenous FVIIa, a measure of HMB-001 pharmacodynamic (PD) activity, we carried out a study in cynomolgus monkeys. In all animals, we observed a dose- and time-dependent accumulation of endogenous FVIIa and total FVII(a) (that is, total FVII including zymogen FVII, FVIIa and other forms of FVIIa (for example, inhibited forms of FVIIa)) (**Fig. 6a**). The predose and maximum plasma concentrations (C_{max}) of FVIIa and total FVII(a) for each group are summarized in **Supplementary Table 6**. In the group receiving the highest subcutaneous dose of HMB-001, FVIIa increased up to 20-fold and total FVII(a) increased up to 5.6-fold relative to the predose levels. At C_{max} on day 6 for this group, FVIIa and total FVII(a) reached mean levels of 1.6 and 23.3 nM, respectively, compared to the predose levels of 0.08 and 4.2 nM, respectively. All animals completed the study. In addition, no significant changes in platelet counts were observed (**Supplementary Table 7a**), and the change in body weight was as expected (**Supplementary Table 7b**). Based on the obtained PK results, a PK/PD model was built and scaled to the human situation using allometric principles (Methods). As shown in **Fig. 6b**, the PK/PD model predicts that endogenous FVIIa concentrations in the low-nM range can be reached in a dose-dependent fashion following subcutaneous administration of HMB-001 in humans, with a dosing frequency of once weekly to once monthly.

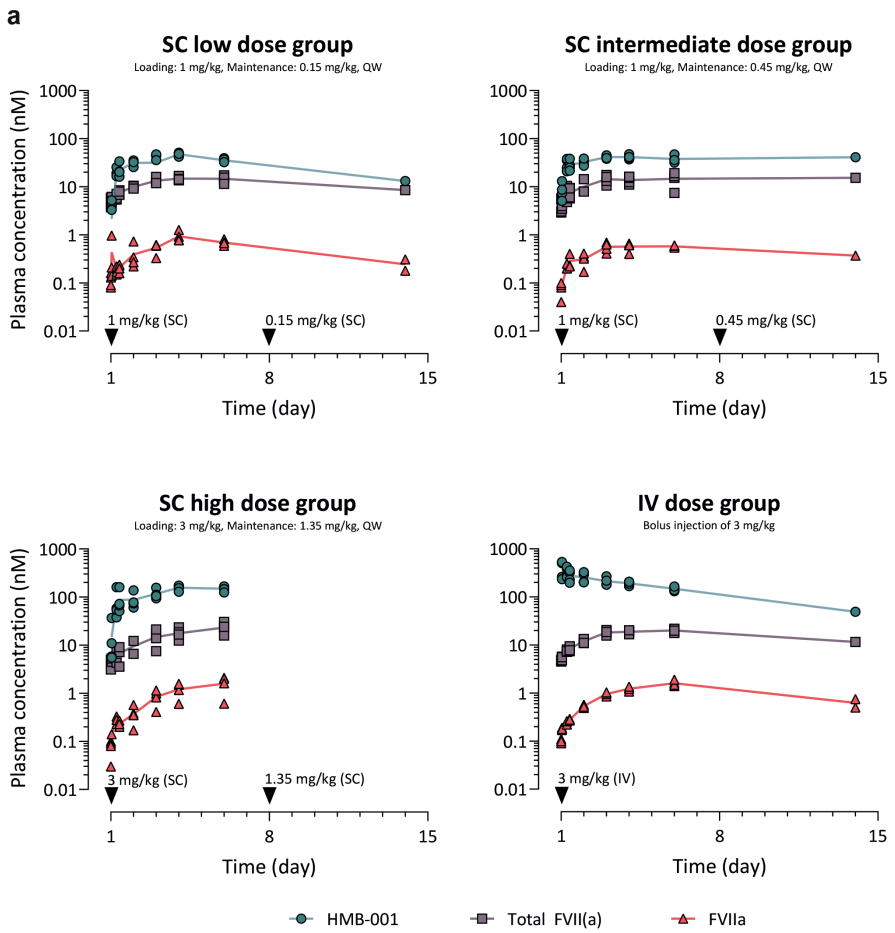

Fig. 6: HMB-001 leads to time- and dose-dependent accumulation of endogenous FVIIa and total FVII(a). a, PK results of HMB-001 and time course of FVIIa and total FVII(a) accumulation in cynomolgus monkeys following subcutaneous (SC) and intravenous (IV) administration of HMB-001. Three groups (n = 4) were administered HMB-001 subcutaneously once weekly (QW), with clinically relevant loading and maintenance doses of 1 and 0.15, 1 and 0.45, and 3 and 1.35 mg kg^{-1}, respectively. A fourth group (n = 4) was administered an intravenous bolus injection of 3 mg kg^{-1} HMB-001. Measured plasma concentrations of FVIIa (red triangles), total FVII(a) (gray squares) and HMB-001 (green circles) are shown for individual animals. For clarity purposes, only data points from ADA-negative plasma samples are shown. Solid lines connect the calculated means for each time point. Cynomolgus monkey FVIIa and total FVII(a) were measured using modified human FVIIa clot activity and human FVII ELISA kits (Stago) and, hence, are referred to as human-equivalent levels (Methods). **b**, Simulation of multiple-dose subcutaneous administration of HMB-001 in humans using a PK/PD model scaled to the human setting. For once-weekly simulations, five different clinical scenarios were simulated to identify the HMB-001 once-weekly dose to reach target accumulated endogenous FVIIa levels of 0.21, 0.52, 1, 1.38 and 1.78 nM (shown by horizontal dotted lines). Corresponding levels of total FVII(a) and HMB-001 are summarized in Supplementary Table 8. Every-2-week (Q2W) and every-4-week (Q4W) simulations were undertaken to show that endogenous FVIIa can be accumulated to target levels of 0.5 and 1 nM (horizontal dotted lines) with less frequent dosing regimens. HMB-001 doses predicted to be needed to reach each target FVIIa level are shown in blue and purple.

Potential of HMB-001 to treat GT

The presence of circulating FVIIa and the expression of TLT-1 upon platelet activation are essential for the MoA of HMB-001. To explore the potential of HMB-001 to treat GT, we quantified FVII activity, FVIIa levels and platelet TLT-1 expression in PwGT and healthy volunteers. FVII activity and FVIIa plasma levels were similar in healthy volunteers and PwGT (**Fig. 7a, b**). Similar to P-selectin, TLT-1 was not expressed on resting platelets but was induced to a similar degree on healthy and GT platelets after stimulation with a panel of agonists (**Fig. 7c**).

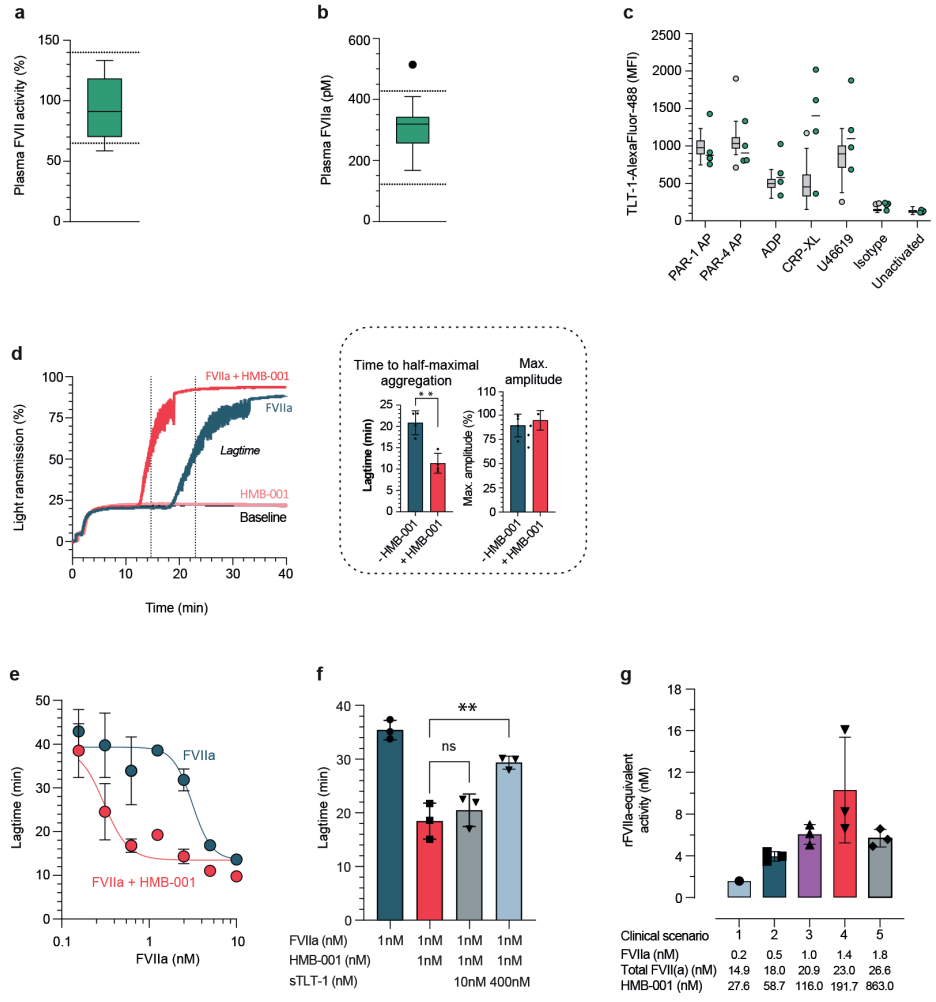

Fig. 7: HMB-001 enhances FVIIa-dependent thrombin generation and aggregation in GT platelets. a, Plasma FVII activity was assessed with a PT-based activity assay in 13 PwGT. Box plot represents the interquartile range. Horizontal line represents the median. Whiskers represent the upper and lower adjacent values. Dotted lines represent the local hospital reference range. **b**, Plasma FVIIa levels were measured with ELISA in 13 PwGT. Box plot represents the interquartile range. Horizontal line represents the median. Whiskers represent the upper and lower adjacent values. Outliers are indicated as filled black circles. Dotted lines represent the 2.5th and 97.5th percentiles of the FVIIa levels in 50 healthy controls. **c**, TLT-1 expression was measured with FACS in whole blood of four PwGT (green) and 51 healthy controls (gray) in resting platelets or after stimulation with agonists. A labeled IgG4 was used as an isotype control. Box plots represent the interquartile range. Horizontal lines represent the median. Whiskers represent the upper and lower adjacent values. Outliers are shown as filled grey circles. **d**, Fibrin-dependent platelet pseudoaggregation was measured in four PwGT. Light transmission was monitored for 40 min. Shown are representative traces of light transmission aggregometry in a PwGT (left) and the mean ± s.d. of

lag time and the maximum amplitude of the aggregation traces with and without HMB-001 (right, inside the dashed box). Lag time is defined as the time to half-maximal aggregation and is indicated by the vertical dotted lines. Data were analyzed with a two-sided unpaired t test (**P = 0.0019). **e**, Fibrin-dependent platelet pseudoaggregation was measured in washed platelets from healthy controls supplemented with D-RGDW to obtain GT-like platelets (n = 3 for each concentration). Aggregation lag time was determined in the presence of FVIIa with or without HMB-001. Data represent mean ± s.d. aggregation lag time at the indicated FVIIa concentration. **f**, Fibrin-dependent platelet pseudoaggregation was measured in GT-like washed platelets in the presence of 1 nM FVIIa; 0 or 1 nM HMB-001; and 0, 10 or 400 nM sTLT-1. Data are expressed as mean lag time ± s.d. (n = 3). Data were analyzed with a two-sided unpaired t test (**P = 0.0061). NS, not significant. **g**, rFVIIa-equivalent activity was measured in PRP from healthy controls (n = 3) supplemented with D-RGDW to obtain GT-like platelets and a blocking anti-TF antibody to ensure TF independence. FVIIa, FVII and HMB-001 were added at the concentrations obtained by simulating five clinical scenarios (Supplementary Table 8). Bars represent the mean rFVIIa-equivalent activity; error bars represent s.d.

Fibrinogen-dependent platelet aggregation is absent in GT, but platelet aggregation responses can occur when fibrin formation is allowed, for example, by rFVIIa[13]. This aggregation response reflects platelet capture in a fibrin mesh[15], which we will refer to as fibrin-dependent pseudoaggregation. To determine whether HMB-001 potentiates FVIIa activity on activated GT platelets, we stimulated washed GT platelets with collagen in the presence of FVIIa, FX, prothrombin and fibrinogen to allow fibrin formation. In the absence of FVIIa or the presence of HMB-001 alone, no fibrin-dependent pseudoaggregation occurred after collagen stimulation, demonstrating the complete absence of the fibrinogen receptor. Addition of 10 nM FVIIa resulted in complete fibrin-dependent pseudoaggregation after a mean (s.d.) lag time of 20.9 (2.8) min (**Fig. 7d**), consistent with the ability of rFVIIa to induce fibrin-dependent platelet pseudoaggregation in GT[13]. Fibrin-dependent pseudoaggregation was potentiated when FVIIa was supplemented with equimolar concentrations of HMB-001 (10 nM each), resulting in a mean (s.d.) lag time of 11.4 (2.3) min.

Next, the relationship between FVIIa concentration and lag time was investigated in the presence and absence of an equimolar concentration of HMB-001 under GT-like conditions. To mimic GT conditions, we incubated washed platelets from healthy donors with the D-RGDW[25] antagonist peptide to inhibit the fibrinogen receptor. While the mean (s.d.) EC_{50} value for FVIIa alone was 3.12 (0.75) nM, the mean (s.d.) EC_{50} value decreased to 0.31 (12) nM in the presence of HMB-001, representing a tenfold potentiation by HMB-001 (**Fig. 7e**). Monovalent cAbs did not potentiate fibrin-dependent pseudoaggregation (**Extended Data Fig. 3b**). To verify the TLT-1 dependency of the potentiating activity of HMB-001, we performed aggregation

experiments in the presence of the competitor sTLT-1, which indeed antagonized the effect of HMB-001, confirming the TLT-1-dependent MoA of HMB-001 (**Fig. 7f**).

Next, we determined whether HMB-001 has the potential to bring the activity of accumulated endogenous FVIIa and total FVII(a) to levels approaching the range of rFVIIa that is considered efficacious in treating acute bleeds in PwGT. PK/PD studies in cynomolgus monkeys indicated that HMB-001 accumulates both FVIIa and total FVII(a). To compare the efficacy of HMB-001-mediated accumulation of FVIIa and total FVII(a) to that of rFVIIa alone, we analyzed thrombin generation in platelet-rich plasma (PRP) under HA- and GT-like conditions using five different simulated clinical scenarios of HMB-001 administration (**Fig. 6b** and **Supplementary Table 8**). By comparing the endogenous thrombin potential observed in each modeled clinical scenario to the response obtained with rFVIIa alone, an rFVIIa-equivalent activity for each scenario was calculated (**Fig. 7g** and **Extended Data Fig. 7**). The rFVIIa-equivalent activity ranged from 1.6 to 10.3 nM and was dose dependent, except at the highest concentration of HMB-001 tested (863 nM, scenario 5), in which a decline in rFVIIa-equivalent activity from 10.3 to 5.7 nM was observed. This is likely due to the competition between the excess free HMB-001 and HMB-001:FVIIa for binding to TLT-1 receptors on the activated platelets. Monovalent cAbs did not enhance FVIIa activity (**Extended Data Fig. 3c**). At FVIIa and total FVII(a) levels predicted to be present during HMB-001 treatment, HMB-001 also potentiated the fibrin-dependent pseudoaggregation of GT-like platelets (**Extended Data Fig. 8**).

Having determined the ability of HMB-001 to potentiate FVIIa activity under static conditions, we next evaluated the efficacy of HMB-001 in a model of GT through a microfluidic assay, which allows for the evaluation of platelet adhesion and fibrin formation in flowing blood and has been used extensively to evaluate thrombus formation in bleeding disorders[51]. For example, in one such assay, FVIIa enhanced thrombin generation on GT platelets adhered to collagen in the absence of TF[25]. We perfused whole blood over a collagen-coated surface and monitored platelet adhesion and fibrin deposition. In blood from healthy controls, platelet aggregation on the collagen surface occurred rapidly with little fibrin deposition observed after 20 min (**Fig. 8a**). Under GT-like conditions, supplementation of FVIIa resulted in a dose-dependent increase in fibrin deposition (**Fig. 8b**). Substantial fibrin deposition on adhered GT-like platelets was seen with 25 nM rFVIIa (**Fig. 8a**), which corresponds to the peak FVIIa plasma concentration reached after a therapeutic dose of 90 µg kg^{-1}

rFVIIa[28]. The addition of 100 nM HMB-001 potentiated the effect of FVIIa at all concentrations tested in the range from 0 to 7.5 nM FVIIa (**Fig. 8b**). At 5 nM FVIIa, fibrin deposition in the presence of 100 nM HMB-001 was higher than that achieved with 25 nM rFVIIa alone. In contrast, fibrin deposition in the presence of 100 nM monovalent cAbs was similar to fibrin deposition with 5 nM FVIIa alone (**Extended Data Fig. 3d**). These results were confirmed in whole blood from three PwGT. Here, fibrin deposition at 2.5 nM FVIIa and 100 nM HMB-001 was similar to that achieved with 25 nM rFVIIa alone in GT-like conditions (**Fig. 8a, c, d**).

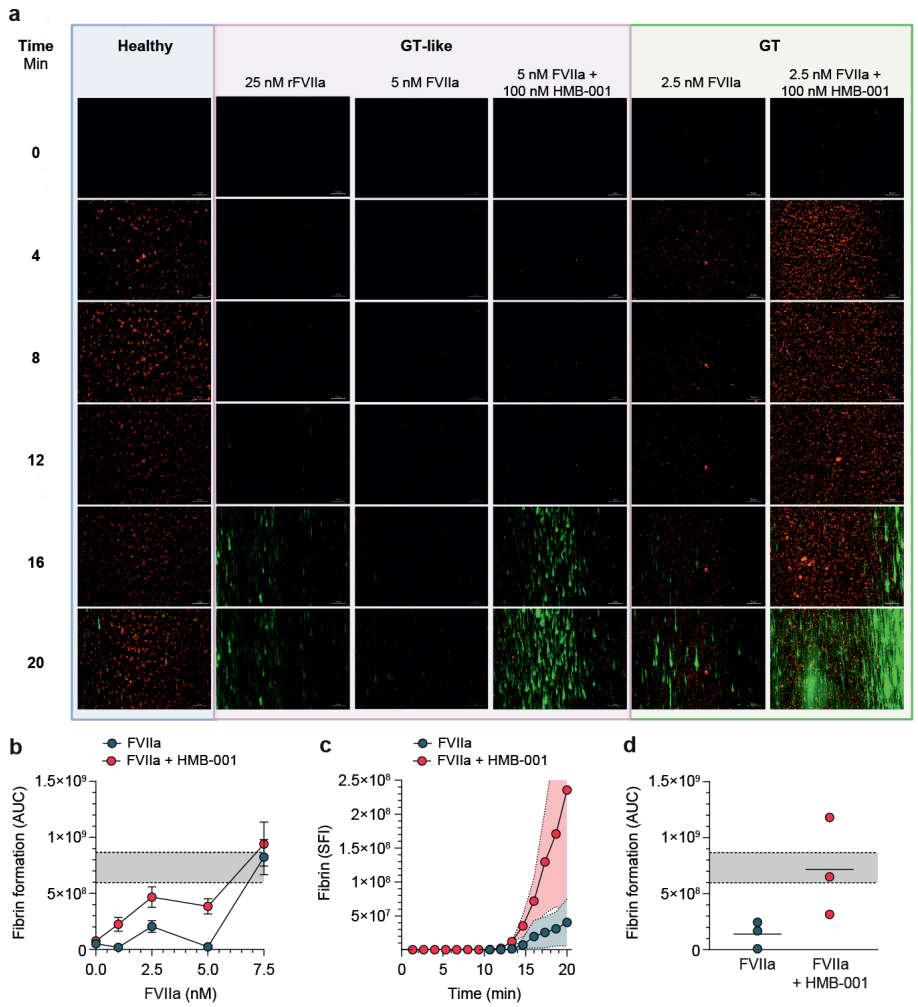

Fig. 8: HMB-001 enhances fibrin formation on adhered GT platelets in flowing blood. **a–d**, Recalcified whole blood was perfused over a collagen-coated surface in a microfluidic device at a shear rate of 300 s^{-1}. Platelets were labeled with MitoTracker Orange CMTMRos, and fibrin was detected with an AlexaFluor-488-conjugated V_HH antifibrin antibody. Platelet adhesion and fibrin deposition were monitored in whole blood from healthy controls, whole blood from healthy controls supplemented with D-RGDW (GT-like), and whole blood from PwGT. Platelet adhesion and fibrin deposition were monitored for 20 min at a frame rate of three per minute using a Zeiss Observer Z1 widefield fluorescence microscope with Colibri LEDs at 200-fold magnification. **a**, Representative time-lapse of platelet adhesion (orange) and fibrin deposition (green) in blood from healthy controls; GT-like whole blood with 25 nM rFVIIa, 5 nM FVIIa, and 0 or 100 nM HMB-001; and whole blood from a PwGT supplemented with 2.5 nM FVIIa and 0 or 100 nM HMB-001. **b**, Fibrin deposition was quantified using ZEN 2 (blue edition) software. Data are expressed as the area under the curve (AUC) of fibrin deposition on platelets adhered to collagen in GT-like whole blood supplemented with 0–7.5 nM FVIIa and 0 or 100 nM HMB-001 (n = 3–7 for each concentration). Gray

area between dotted lines represents the mean area under the curve ± s.d. of fibrin deposition in GT-like whole blood supplemented with 25 nM rFVIIa (n = 7). **c**, Fibrin deposition on platelets adhered to collagen after the perfusion of whole blood from PwGT (n = 3) supplemented with 2.5 nM FVIIa and 0 or 100 nM HMB-001. Data are expressed as the mean sum of fluorescence intensity on each frame (SFI) as a function of time. Shaded areas indicate s.d. **d**, Area under the curve of fibrin deposition in whole blood from PwGT (n = 3) supplemented with 0 or 100 nM HMB-001. Gray area between dotted lines represents the mean area under the curve ± s.d. of fibrin deposition in GT-like whole blood supplemented with 25 nM rFVIIa (n = 7).

DISCUSSION

HMB-001 is a biAb that binds FVIIa and TLT-1 and is designed to restore hemostasis through a mechanism mimicking that of rFVIIa but relying exclusively on the proteolytic activity of endogenous FVIIa. Here, we have shown that HMB-001 does not interfere with the normal functioning of FVIIa or influence key platelet properties while effectively targeting FVIIa to the activated platelet surface. Subcutaneous dosing of HMB-001 in cynomolgus monkeys resulted in a dose- and time-dependent accumulation of endogenous FVIIa to the low-nM range (0.6–1.6 nM). Experiments in *ex vivo* GT models showed that HMB-001 enhanced the effect of FVIIa on fibrin-dependent platelet pseudoaggregation by approximately tenfold (**Fig. 7e**) and substantially improved fibrin formation on adhered GT platelets in flowing blood. Using an analogue of HMB-001, *in vivo* studies in a mouse bleeding model showed a similar 15-fold potency enhancement of FVIIa activity (**Fig. 2b**).

Structural studies revealed that HMB-001 engages FVIIa at an epitope distant from known physiologically important surface patches, providing a rationale for the observed lack of effect in non-cell-based functional studies. In addition, the minor role of TLT-1 in hemostasis[40] combined with the location of the binding epitope in the stalk region of TLT-1 ensures that HMB-001 does not influence platelet properties and TLT-1 function. The lack of effect of HMB-001 on platelet physiology supports this notion. Taken together, these results support the intended mechanism involving high-affinity binding and dose-dependent accumulation of endogenous FVIIa and the delivery of FVIIa to the surface of activated platelets to restore hemostasis when platelets are activated following vessel wall injury (**Fig. 1b**). As the TLT-1 receptor is absent on the surface of resting platelets and is redistributed to the surface from α-granules upon platelet aggregation[38], HMB-001-mediated localization of FVIIa is strongly dependent on the activation status of platelets. Therefore, HMB-001, both free and FVIIa bound, will circulate latently in the blood and exert its hemostatic

effect only upon vascular injury with subsequent platelet activation and TLT-1 expression. It is worth noting that other receptors, such as platelet GPIbα and endothelial protein C receptor, have been shown to interact with FVIIa, potentially influencing the localization of FVIIa-related procoagulant reactions[52].

Platelet aggregation is compromised in PwGT due to the lack of functional αIIbβ3 on the platelet surface (**Fig. 1a**)[8,53]. In the absence of effective prophylaxis, multiple intravenous administration of rFVIIa is a preferred treatment option to control episodes of acute severe bleeding. The MoA of rFVIIa involves the rescue of platelet aggregation by TF-independent fibrin generation[13,25]. One way fibrin formation on platelets might contribute to hemostasis is through fibrin-dependent pseudoaggregation. However, the exact mechanism behind this process and its contribution to hemostasis in PwGT remain to be elucidated. While αIIbβ3 is reported to have a role in the interaction between fibrin and platelets[54], our data and others' reports indicate that fibrin-dependent pseudoaggregation readily occurs with GT platelets[13], suggesting that this process is independent of functional αIIbβ3. Our data show that HMB-001 potentiated FVIIa-dependent, fibrin-mediated pseudoaggregation of GT platelets (**Fig. 7d**) and enhanced FVIIa-dependent fibrin generation in flowing blood, achieving fibrin deposition on adhered platelets similar to that obtained with the recommended rFVIIa dose for treating ongoing bleeds. The mean (s.d.) normal plasma level of total FVII(a) is 9.1 (1.4) nM, of which FVIIa constitutes approximately 71.6 (28.8) pM (range 10–168 pM)[55,56]. As expected, our data indicate that FVII and FVIIa levels in PwGT are within the normal range. Based on clinical experiences with rFVIIa[57] and a novel rFVIIa variant[58], it can be estimated that a plasma FVIIa activity of >3 nM (corresponding to >6 IU ml^{-1}) is needed for effective rFVIIa-based prophylactic treatment. Our data demonstrated a >3 nM rFVIIa-equivalent activity in thrombin generation assays in relevant clinical scenarios for HMB-001 (scenarios 2–5; **Fig. 7g** and **Extended Data Fig. 7**). Others have reported biological variation in TLT-1 expression on activated platelets[48,49], and our data are in line with those observations. Differences in the copy number of TLT-1 and the strength of platelet activation[47] will affect the number of TLT-1 receptors on the surface of activated platelets, thereby modulating the HMB-001-mediated response. Nevertheless, our data indicate that while TLT-1 expression varies among PwGT (**Fig. 7c** and **Extended Data Fig. 9**), the effects of FVIIa and HMB-001 on fibrin formation in flowing blood are robust (**Fig. 8d**). Through the accumulation and localization of endogenous FVIIa, HMB-001 provides an rFVIIa-equivalent activity in the hemostatically active range comparable to that obtained

with therapeutic doses of exogenous rFVIIa. Combined with PK/PD modeling, these data suggest that HMB-001 could offer a subcutaneous-based prophylactic treatment with a low-frequency dosing regimen for PwGT.

HMB-001 binds equally well to FVII and FVIIa, providing a rationale for the accumulation of total FVII(a) observed in cynomolgus monkeys. Despite similar affinities, the fold accumulation of total FVII(a) was lower than that of FVIIa, likely explained by the continuous conversion of FVII to FVIIa by known physiological mechanisms involving FXa, FIXa and FVIIa itself. Upon platelet activation, it is expected that the HMB-001:FVII complex will also bind to expressed TLT-1 receptors on activated platelets. Our data confirm the potentiating effect of HMB-001 at predicted levels of FVII and FVIIa during HMB-001 treatment. Whether localized HMB-001:FVII is activated on the surface of activated platelets and thus contributes to the overall observed hemostatic activity of HMB-001 remains to be determined. In the presence of high concentrations of HMB-001, we observed a modest decline in the effect of HMB-001 in FX activation and thrombin generation assays, likely due to the competition between free HMB-001 and the HMB-001:FVIIa complex for binding to TLT-1 receptors and thus naturally dampening the effect of high-dose HMB-001 (**Figs. 2c and 7g**).

rFVIIa is licensed for the treatment of bleeds in people with congenital HA or HB with inhibitors. While GT and HA differ in the cause and nature of the hemostatic defect, restoration of hemostasis by pharmacological doses of rFVIIa relies on the same underlying mechanism[27]. The presented data from thrombin generation assays suggest that HMB-001 contributes sufficient hemostatic activity to support prophylaxis in HA. Further support for the utility of HMB-001 in HA comes from *in vivo* studies in HA mice, in which a 15-fold potency enhancement of FVIIa activity was observed when FVIIa was coformulated with an HMB-001 analogue (**Fig. 2b**). Thus, HMB-001 could provide an alternative prophylactic treatment option for people with HA. People with Bernard–Soulier syndrome represent another population without a prophylactic treatment option available that might benefit from HMB-001. With a defect in the platelet GPIb–V–IX receptor complex, people with Bernard–Soulier syndrome are expected to have normal FVIIa and TLT-1 levels, and treatment with rFVIIa has been shown effective[4,59]. Further investigations are needed to determine whether HMB-001 could benefit patients with FVII deficiency or HB who are known to have low levels of endogenous FVIIa[60].

In conclusion, the present data suggest that the long half-life of HMB-001, combined with its ability to accumulate and potentiate the activity of endogenous FVIIa selectively on activated platelets, provides a sustained and localized procoagulant activity that may support prophylactic treatment of GT or other bleeding disorders for which rFVIIa has been shown efficacious in treating acute bleeds. Whether and how prophylaxis with HMB-001 would affect the treatment of breakthrough bleeds remains to be determined. In addition, the MoA of HMB-001 provides a general strategy for developing future antibody-based therapeutics using the principle of accumulation of target endogenous protein to therapeutically effective levels. An additional layer of enhancement and control of therapeutic activity can be engineered by site-specific targeting, as done with TLT-1 in the present study.

EXTENDED DATA

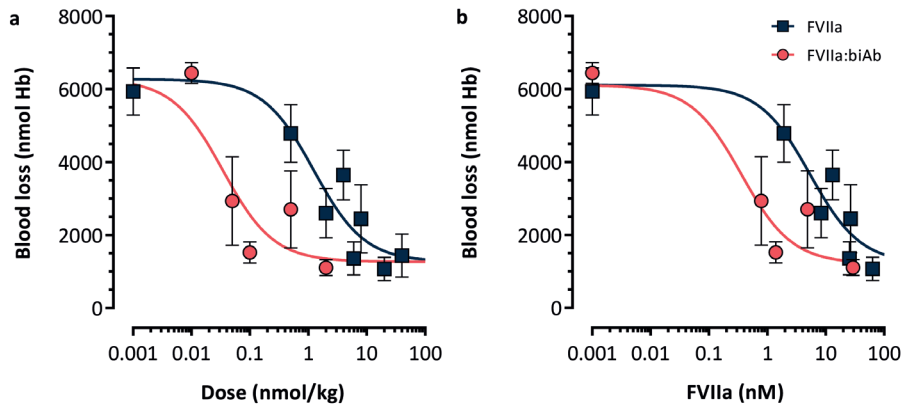

Extended Data Fig. 1: HMB-001 analogue biAb0097 reduces blood loss after tail vein transection in transgenic haemophilia A mice expressing human TLT-1. Mean blood loss as a function of (**a**) dose- and (**b**) plasma concentration of FVIIa following administration of FVIIa (n = 3–10, dark squares) or FVIIa coformulated with biAb0097 (1:1 mol/mol) (n = 6, red circles) in the tail vein transection model in HA mice carrying the human TLT-1 receptor. Data are mean blood loss ± s.d. FVIIa, activated factor VII; Hb, haemoglobin.

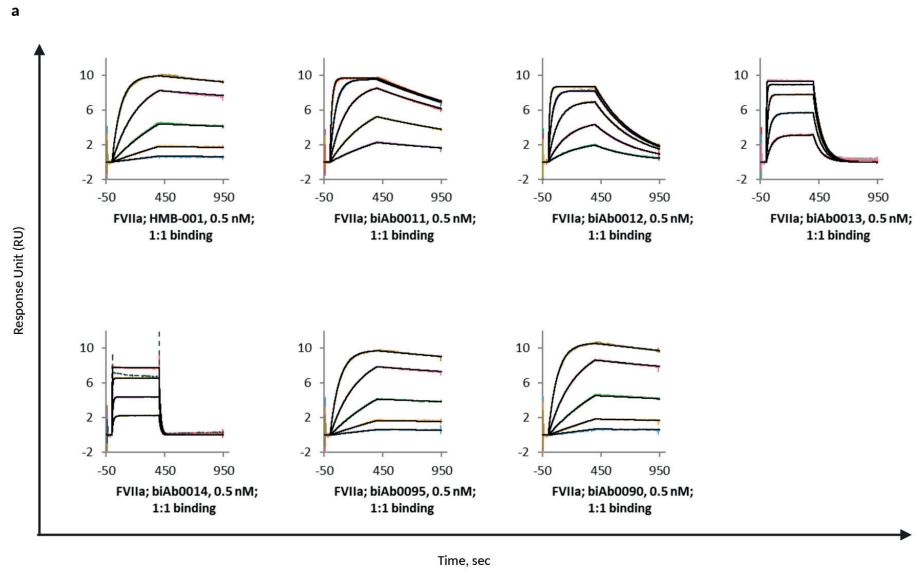

Extended Data Fig. 2: HMB-001 has the highest affinity for both FVIIa and sTLT-1. BiAbs (0.5–4 nM and as indicated on individual sensorgrams) were captured on immobilized anti-human IgG antibodies and binding of FVIIa (0–4 nM) (**a**) and sTLT-1 (0–60 mM) (**b**) was assessed with SPR at 25 °C and pH 7.4 (n = 2). Binding data were fitted to a Langmuir 1:1 binding model to determine association and dissociation rates as well as equilibrium dissociation constants (K_D). Coloured lines represent binding data and solid black lines represent the fit of the data. Representative sensorgrams from one run are shown below. BiAbs, bispecific antibodies; IgG, immunoglobulin G, FVIIa, recombinant factor VIIa; SPR, surface plasmon resonance; sTLT-1, soluble extracellular fragment of TREM-like transcript 1.

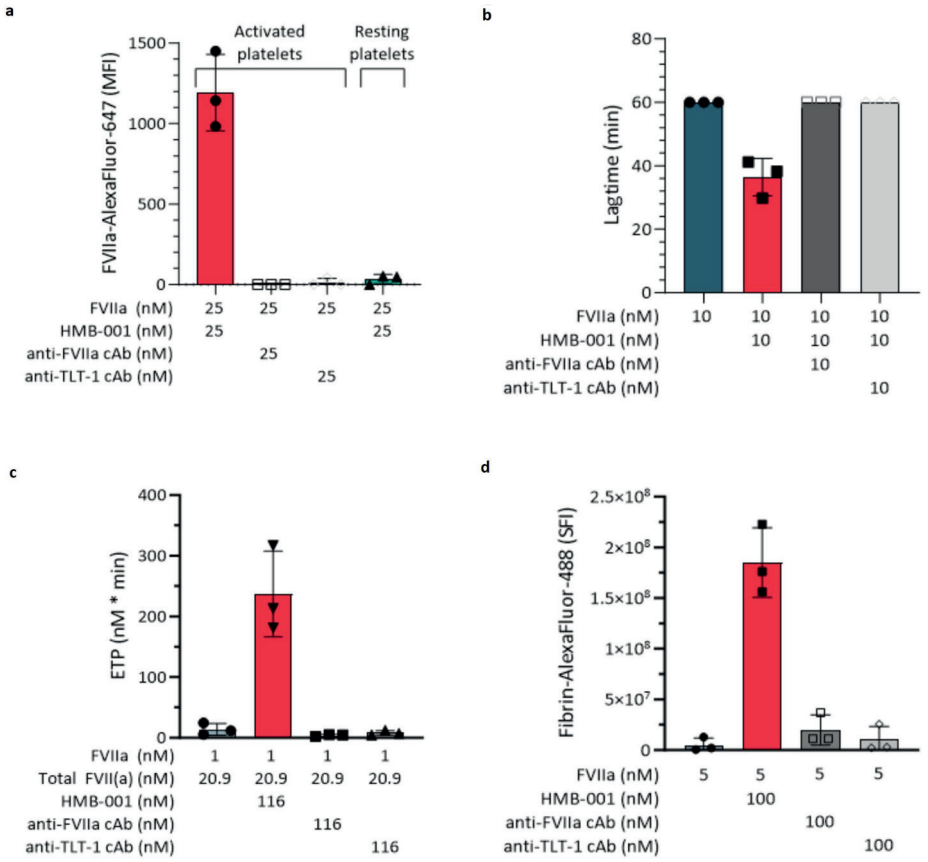

Extended Data Fig. 3: Effect of the two cAbs evaluated using different assays. a) Whole blood from healthy donors (n = 3) was incubated with FVIIa, HMB-001 or cAb as indicated in the presence of an AlexaFluor-647 labelled FVIIa-specific V_HH with or without 25 µM PAR-1 AP and 1 mg ml^{-1} CRP-XL for 10 min at 37 °C. FVIIa binding to platelets was assessed with FACS. Data are expressed as mean MFI ± s.d. **b**) Fibrin-dependent platelet pseudoaggregation was measured in GT-like washed platelets in presence of 10 nM FVIIa, 0 or 10 nM HMB-001 and 0 or 10 nM cAb. Data are expressed as mean lag time ± s.d. (n = 3). **c**) Platelets were stimulated with both CRP-XL and PAR-1 AP, and thrombin generation was measured for 240 min in conditions mimicking scenario 3 (Table S8) (n = 3). FVIIa, Total FVII(a), HMB-001 or cAb was added as indicated. Bars represent mean endogenous thrombin potentials (ETP), error bars represent s.d. **d**) Area under the curve (AUC) of fibrin deposition in GT-like whole blood from healthy donors (n = 3) with 5 nM FVIIa and 0 or 100 nM HMB-001 or 0 or 100 nM cAb. Bars represent mean total fibrin formation in 20 min (sum of fluorescent intensity; SFI), error bars represent s.d.

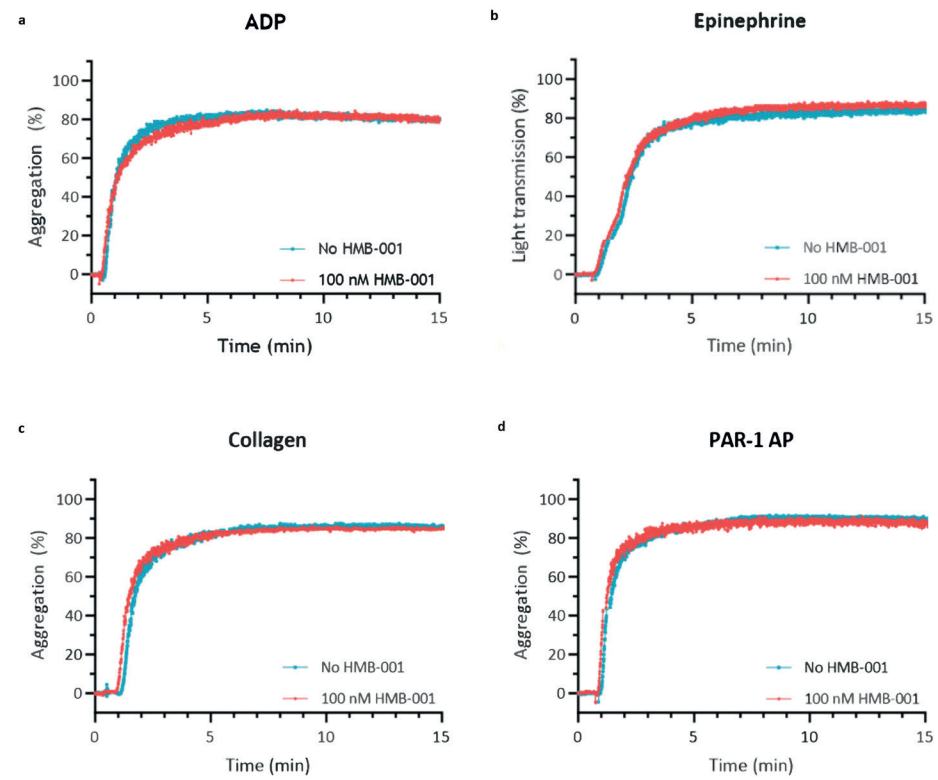

Extended Data Fig. 4: Effect of HMB-001 on normal platelet aggregation. Platelet rich plasma from healthy donors (n = 3) was incubated with 0 or 100 nM HMB-001 and activated with different activators while stirring at 900 rpm at 37 °C. Subsequent platelet aggregation was monitored with light transmission for 15 min. Shown are representative light transmission aggregometry traces in a single donor when activated with **a**) 5 µM ADP, **b**) 5 µM epinephrine, **c**) 4 µg ml^{-1} collagen, or **d**) 10 µM PAR-1 AP.

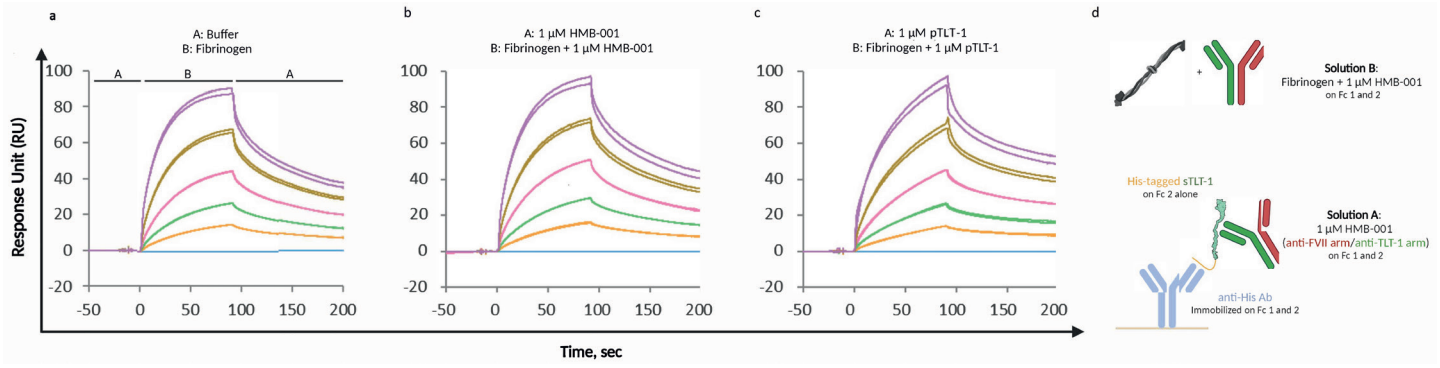

Extended Data Fig. 5: Fibrinogen binds to sTLT-1 in presence of HMB-001. Influence of **a**) Buffer, **b**) HMB-001, and **c**) parent TLT-1 Ab (pTLT-1) on the ability of fibrinogen to bind to sTLT-1 was probed using SPR at 25 °C and pH 7.4 (n = 2) using the ABA injection strategy. As shown in the SPR assay setup (**d**), sTLT-1 was captured using anti-His Ab. Solution A consisted of either running buffer or 1 µM HMB-001 or 1 µM pTLT-1 Ab. Solution B consisted of fibrinogen concentration series in presence of running buffer or 1 µM HMB-001 or 1 µM pTLT-1 Ab. Coloured lines represent different fibrinogen concentrations starting from the highest concentration of 1000 nM (purple), 500 nM (yellow), 250 nM (pink), 125 nM (green), 62.5 nM (orange), and 0 nM (blue). Sensorgram from both runs are overlaid and shown above.

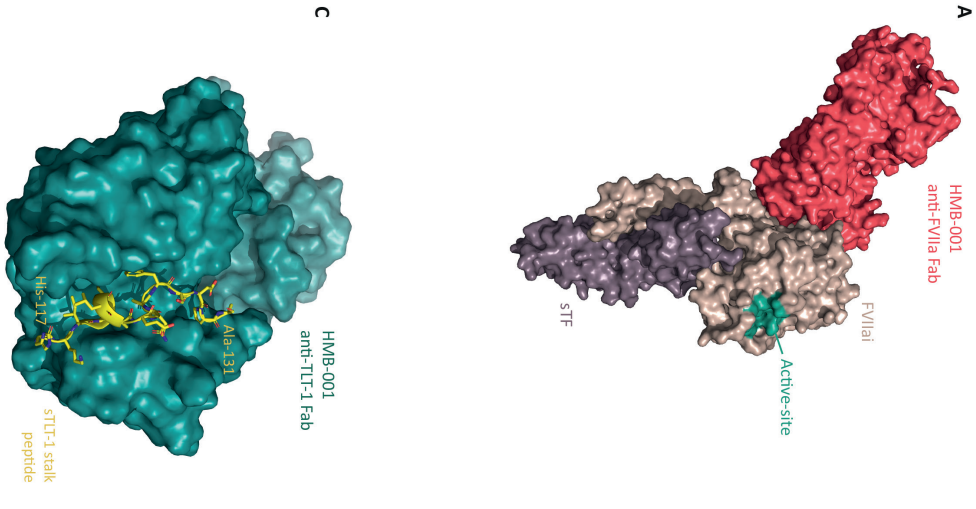

Extended Data Fig. 6: Structural overview. Crystal structures of **a**) anti-FVII Fab of HMB-001 bound to FVIIai:TF complex, **b**) Addition of the predicted structure of the Gla domain of FVIIai (yellow) and FX/FXa (gray) based on an overlay of the crystal structure of FVIIai:TF from:1DAN89 and a model of the FVIIai:TF:FXa complex90, respectively and **c**) anti-TLT-1 Fab of HMB-001 bound to sTLT-1 stalk peptide. FVIIai, active-site inhibited FVIIa-desGLA; sTF, soluble fragment of tissue factor; Gla domain, N-terminal γ-carboxyglutamic domain; FXa, coagulation activated factor X; sTLT-1, soluble fragment of TREM-like transcript 1.

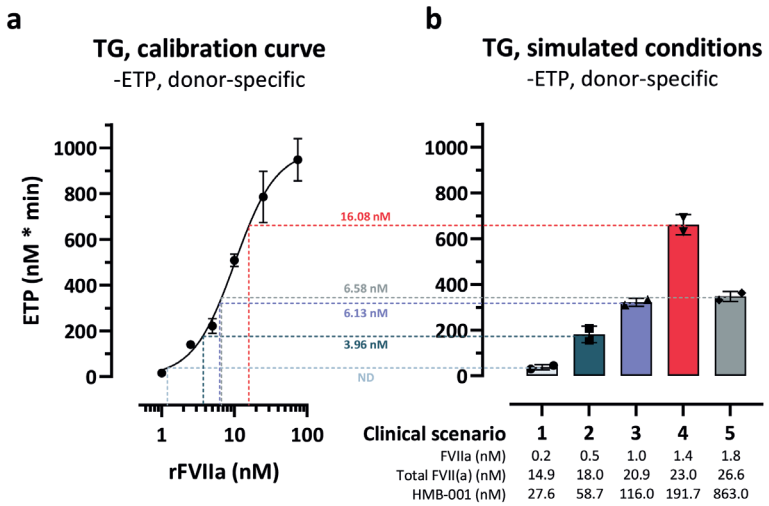

Extended Data Fig. 7: Representative data from a single donor showing enhanced FVIIa activity by HMB-001 at predicted plasma levels of FVIIa, total FVII(a) and HMB-001 following five different dosing regimens. rFVIIa-equivalent activity was measured in PRP from a healthy control (n = 3) supplemented with D-RGDW to obtain GT-like platelets and a blocking anti-TF antibody to ensure TF-independence. PRP was supplemented with rFVIIa (0–75 nM), platelets were stimulated with CRP-XL and PAR-1 AP, and thrombin generation was measured for 240 min. **a**) For each donor, Endogenous thrombin potential (ETP) was determined in duplicate as a function of rFVIIa concentration. Data represent mean ± s.d. **b**) ETP was determined in duplicate at 5 predicted clinical scenarios of FVIIa, total FVII(a) and HMB-001 in healthy controls (n = 3). The background plasma concentrations of FVIIa and total FVII(a) were assumed to be 67 pM and 10 nM, respectively. Predicted accumulated levels of total FVII(a) and FVIIa for 5 predicted clinical scenarios (Table S8) were reconstituted by adding FVII-S195A and FVIIa after accounting for the background plasma concentration of total FVII(a) and FVIIa respectively. HMB-001 was added as indicated. Data represent mean ± s.d. For each clinical scenario, the corresponding rFVIIa-equivalent activity (nM), as extrapolated from the X-axis of the calibration curve, is indicated next to the horizontal dotted line for the single donor. rFVIIa-equivalent activities for three donors are shown in Fig. 7g.

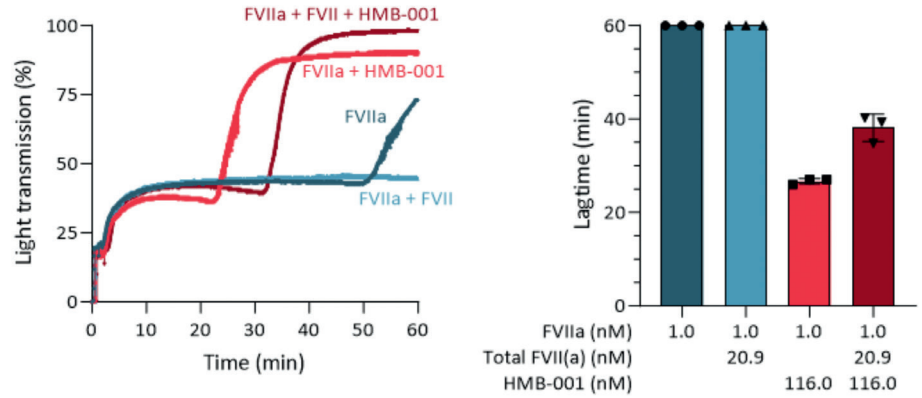

Extended Data Fig. 8: HMB-001 enhances fibrin dependent platelet aggregation at predicted plasma levels of FVIIa, total FVII(a) and HMB-001 following a once weekly HMB-001 dose of 0.67 mg kg^{-1}. Fibrin-dependent platelet pseudoaggregation was measured in washed platelets from healthy donors supplemented with D-RGDW (GT-like; n = 3). The data in the bar chart are expressed as mean ± s.d. Aggregation was induced with collagen in buffer with 3 mM $CaCl_2$, 10 mg ml^{-1} FX, 20 ng ml^{-1} prothrombin and 0.5 mg ml^{-1} fibrinogen. The background plasma concentrations of FVIIa and total FVII(a) were assumed to be 67 pM and 10 nM, respectively. Predicted accumulated levels of total FVII(a) and FVIIa for once weekly HMB-001 dose of 0.67 mg kg^{-1} (scenario 3, Table S8) were reconstituted by adding FVII-S195A and FVIIa after accounting for the background plasma concentration of total FVII(a) and FVIIa respectively. HMB-001 was added as indicated. Light transmission was monitored for 60 min. Shown are representative light transmission aggregometry traces in a single donor, as well as summary data on fibrin-dependent pseudoaggregation lag time in all donors.

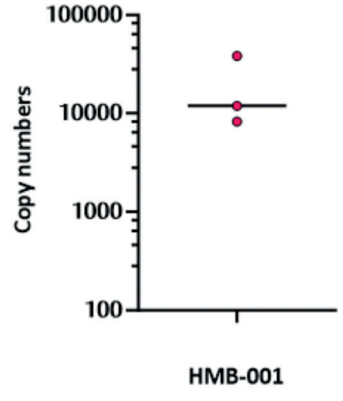

Extended Data Fig. 9: HMB-001 copy number on activated platelets. Whole blood from healthy donors (n = 3) was incubated with up to 2 µM AlexaFluor-647 labelled HMB-001 in the presence of 25 µM PAR-1 AP. HMB-001 copy number on activated platelets were calculated by conversion to arbitrary units using Quantum AlexaFluor-647 MESF and Rainbow beads.

SUPPLEMENT

HMB-001 analogue enhances the potency of FVIIa by about 15-fold in the tail vein transection mouse injury model. The ability of biAb to potentiate FVIIa activity *in vivo* was evaluated in transgenic haemophilia A (HA) mice expressing human TLT-1 and using the tail vein transection (TVT) injury model. Overview of treatment groups and test articles are provided in **Supplementary Table 1**. For the co-administration of FVIIa and biAb0097 (FVIIa:biAb0097), the two compounds were given in equimolar (1:1) amounts.

Table S1: Overview of treatment groups and test articles administered to transgenic haemophilia A mice expressing human TLT-1.

Test article	Dose in nmol kg^{-1} [number of animals per dose]
FVIIa	0.001 [n=10], 0.5 [n=9], 2 [n=10], 4 [n=10], 6 [n=9], 8 [n=10], 20 [n=10], 40 [n=3]
FVIIa:biAb0097	0.01:0.01 [n=6], 0.05:0.05 [n=6], 0.1:0.1 [n=6], 0.5:0.5 [n=6], 2:2 [n=6]

As shown in **Extended Data Fig. 1a** and **1b**, administration of FVIIa resulted in dose-dependent and FVIIa plasma concentration-dependent reductions of blood loss, respectively. Upon co-formulation of FVIIa with an equimolar amount of the HMB-001 sequence analogue (biAb0097), a left-shift of the dose- and concentration-response curves were observed corresponding to an apparent increased haemostatic effect of FVIIa. To account for a shorter half-life and consequently faster *in vivo* elimination of free FVIIa compared to the FVIIa:biAb0097 complex, the effect of biAb0097 was estimated from the EC_{50}-values derived from the concentration-response profiles where the concentrations of FVIIa were measured at the end of the bleeding window. With estimated EC_{50}-values (95% confidence intervals in square brackets) of 5.4 nM [1.7–14.3] and 0.36 nM [0.005–1.3] for FVIIa and the FVIIa:biAb0097 co-formulation, respectively, it could be concluded that biAb0097 reduces the EC_{50}-value of FVIIa by approximately 15-fold. This in turn corresponds to an apparent 15-fold potency enhancement of FVIIa by biAb0097.

Table S2: Binding characteristics of different biAb compositions to FVIIa and sTLT-1 determined with SPR at 25°C and pH 7.4.

BiAb	FVIIa binding characteristics				sTLT-1 binding characteristics			
	k_{on} (1/Ms)	k_{off} (1/s)	$K_{D, FVIIa}$ (nM)	Fold difference in K_D	k_{on} (1/Ms)	k_{off} (1/s)	$K_{D, sTLT-1}$ (nM)	Fold difference in K_D
HMB-001	2.90E+06	1.27E-04	0.04	1.0	2.74E+05	6.41E-04	2.34	1.0
biAb0011	2.72E+06	5.70E-04	0.21	4.8	3.08E+05	6.37E-04	2.07	0.9
biAb0012	1.74E+06	2.82E-03	1.63	37.1	2.96E+05	6.58E-04	2.22	1.0
biAb0013	1.88E+06	1.76E-02	9.61	219.5	2.97E+05	6.79E-04	2.29	1.0
biAb0014	1.34E+05	7.15E-02	532.5	12171.4	2.83E+05	5.82E-04	2.06	0.9
biAb0095	2.85E+06	1.21E-04	0.04	1.0	NA	NA	12.95	5.5
biAb0090	2.81E+06	1.35E-04	0.05	1.1	NA	NA	196.50	84.0

k_{on}, association rate; k_{off}, dissociation rate; K_D, equilibrium dissociation constant; NA, Not applicable.

Table S3: Binding characteristics of HMB-001 to FVIIa, FVII and sTLT-1 determined with SPR at 25°C and pH 7.4.

HMB-001	Run	k_{on} ± SE (1/Ms)	k_{off} ± SE (1/s)	K_D (nM)	R_{max} (RU)	Chi^2 (RU^2)	tc
FVIIa	Run 1	1.80E+06 ± 7.57E+02	6.66E-04 ± 5.45E-07	0.37	46.8	1.51E-01	3.58E+12
	Run 2	1.80E+06 ± 7.20E+02	6.64E-04 ± 5.18E-07	0.37	44.2	1.22E-01	1.55E+12
	Average	**1.80E+06**	**6.65E-04**	**0.37**			
FVII	Run 1	1.83E+06 ± 8.61E+02	7.25E-04 ± 6.15E-07	0.4	28.6	6.95E-02	8.66E+11
	Run 2	1.82E+06 ± 8.79E+02	7.25E-04 ± 6.13E-07	0.4	27.6	6.91E-02	1.95E+12
	Average	**1.83E+06**	**7.25E-04**	**0.4**			
sTLT-1	Run 1	2.62e+05 ± 1.93E+02	6.10e-04 ± 1.48E-06	2.33	11.7	2.73E-02	1.05E+12
	Run 2	2.86e+05 ± 1.87E+02	6.72e-04 ± 1.32E-06	2.35	10.9	1.97E-02	7.18E+09
	Average	**2.74e+05**	**6.41e-04**	**2.34**			

k_{on}, association rate; k_{off}, dissociation rate; K_D, equilibrium dissociation constant; R_{max}, maximum response when all ligand is occupied; Chi^2, closeness of the fit; tc, mass transfer coefficient.

Table S4: Effect of HMB-001 on catalytic activity of FVIIa and FVIIa inhibition.

FX activation	Without tissue factor		With tissue factor	
Mean (SD)	**Without HMB-001**	**With HMB-001**	**Without HMB-001**	**With HMB-001**
$k_{cat,}$ s^{-1}	1.11 (0.04) × 10^{-4}	0.77 (0.04) × 10^{-4}	1.21 (0.09)	1.27 (0.10)
$K_{m,}$ nM	43 (5)	19 (4)	10 (2)	11 (2)
$k_{cat}/K_{m,}$ nM^{-1} s^{-1}	2.6 (0.2) × 10^{-6}	4.1 (0.6) × 10^{-6}	0.12 (0.02)	0.11 (0.02)

k_{cat}: turnover number; K_m: Michaelis constant; k_{cat}/k_m: catalytic efficiency.

FVIIa inhibition		
Mean (SD)	**Without HMB-001**	**With HMB-001**
AT, $k_{i,}$ $M^{-1}s^{-1}$	82 (9)	98 (11)
TFPI, $IC_{50,}$ nM	0.56 (0.1)	0.58 (0.08)

AT: antithrombin; k_i: inhibitor constant; TFPI: tissue factor pathway inhibitor; IC_{50}: concentration at which 50% of the activity of 100 pM FVIIa is inhibited.

Table S5: Data collection refinement statistics from X-ray structure determination of the complex between **A**) FVIIai, sTF and anti-FVIIa Fab of HMB-001 and **B**) stalk region of TLT-1 receptor and anti-TLT-1 Fab of HMB-001.

A)		B)	
Parameter	**Result**	**Parameter**	**Result**
Wavelength (Å)	1.5418	**Wavelength**	0.9799
Resolution range (Å)	48.5 – 3.4 (3.52 – 3.4)	**Resolution range**	27.19 - 1.49 (1.543 - 1.49)
Space group	P 21 (No. 4)	**Space group**	P 1
Unit cell (Å)	144.78 100.79 181.74	**Unit cell (Å, deg)**	53.23 65.38 67.15 91.88 91.72 92.89
Unit cell (deg)	90 101.23 90	**Total reflections**	260182 (25651)
Total reflections	340557 (24056)	**Unique reflections**	140068 (9126)
Unique reflections	69058 (6423)	**Multiplicity**	1.9 (1.9)
Multiplicity	4.9 (3.7)	**Completeness (%)**	91.03 (62.10)
Completeness (%)	96.3 (91.4)	**Mean I/sigma(I)**	9.03 (1.37)
Mean I/sigma (I)	3.59 (0.86)	**Wilson B-factor (Å²)**	18.72
Wilson B-factor	63.86	**R-merge**	0.053 (0.59)
R-merge	0.31 (1.05)	**R-meas**	0.074 (0.84)
R-meas	0.347 (1.22)	**R-pim**	0.052 (0.59)
R-pim	0.151 (0.603)	**CC1/2**	0.994 (0.0678)

Table S5: Continued

A)		B)	
Parameter	**Result**	**Parameter**	**Result**
CC1/2	0.98 (0.697)	**CC***	0.999 (0.356)
CC*	0.995 (0.906)	**Reflections used in refinement**	134358 (9123)
Reflections used in refinement	684175 (6423)	**Reflections used for R-free**	1783 (123)
Reflections used for R-free	1957 (180)	**R-work**	0.1560 (0.2388)
R-work	0.3030 (0.4045)	**R-free**	0.1734 (0.2490)
R-free	0.3549 (0.4551)	**CC (work)**	0.964 (0.680)
CC (work)	0.881 (0.682)	**CC (free)**	0.961 (0.679)
CC (free)	0.853 (0.514)	**Number of non-hydrogen atoms**	8036
Number of non-hydrogen atoms	29520	**macromolecules**	7017
macromolecules	29476	**ligands**	0
ligands	44	**solvent**	1019
Protein residues	3818	**Protein residues**	896
RMS (bonds)	0.002	**RMS(bonds)**	0.009
RMS (angles)	0.50	**RMS(angles)**	0.96
Ramachandran favored (%)	95.48	**Ramachandran favored (%)**	97.29
Ramachandran allowed (%)	4.52	**Ramachandran allowed (%)**	2.60
Ramachandran outliers (%)	0.00	**Ramachandran outliers %)**	0.11
Rotamer outliers (%)	0.84	**Rotamer outliers (%)**	0.50
Clashscore	7.27	**Clashscore**	2.09
Average B-factor (Å2)	64.30	**Average B-factor (Å²)**	24.02
macromolecules	64.27	**macromolecules**	22.53
ligands	83.61	**solvent**	34.28
		Number of TLS groups	1
PDB accession code	8CN9	**PDB accession code**	8CHE

Statistics for the highest-resolution shell are shown in parentheses. Definitions of standard abbreviations included in the table are defined[91].

Table S6: Pre-dose and C_{max} plasma levels of endogenous FVIIa and total FVII(a) (measured as human equivalent), and HMB-001 in anti-drug antibody (ADA)-negative plasma samples in cynomolgus monkeys.

	FVIIa		Total FVII(a)		HMB-001
	Pre-dose (nM)	**C_{max} (nM)**	**Pre-dose (nM)**	**C_{max} (nM)**	**C_{max} (nM)**
Group 1	0.12 ± 0.03	0.9 ± 0.2	4.8 ± 0.9	14.8 ± 1.4	47 ± 4
Group 2	0.08 ± 0.03	0.6 ± 0.1	4.3 ± 1.5	14.6 ± 5.0	41 ± 4
Group 3	0.08 ± 0.03	1.6 ± 0.7	4.2 ± 0.8	23.3 ± 6.0	157 ± 20
Group 4	0.10 ± 0.01	1.6 ± 0.2	4.7 ± 0.2	20.0 ± 1.7	384 ± 158

Results are shown as the mean ± SD for the four animals in each group. C_{max} is the highest mean plasma level up to and including Day 6 where all animals are ADA negative. Cynomolgus monkey endogenous FVIIa and total FVII(a) were measured using modified human FVIIa clot activity and human FVII ELISA kits by Stago and hence are referred to as human equivalent (see Materials and Methods).

Table S7A: Mean platelet counts during the HMB-001 PK study in cynomolgus monkeys.

	Pre-dose		Day 1		Day 19	
	Male (n=2)	**Female (n=2)**	**Male (n=2)**	**Female (n=2)**	**Male (n=2)**	**Female (n=2)**
Group 1	420 ± 9.9	471 ± 60.1	396 ± 33.9	442 ± 64.3	453 ± 58.7	475 ± 98.3
Group 2	272 ± 50.2	389 (n=1)	289 ± 41.7	411 ± 44.5	314 ± 28.3	427 ± 99
Group 3	402 ± 116	339 ± 48.8	422 ± 149.9	384 ± 68.6	495 ± 139.3	343 ± 38.2
Group 4	530 ± 63.6	422 (n=1)	482 ± 18.4	415 ± 9.2	393 ± 55.2 (Day 14)	298 ± 141.4 (Day 14)

Results are shown as the mean ± SD for the 2 animals/sex/group in each group. Platelet counts are in $10E^9$/L. Pre-dose measurement was day 8 before dosing was initiated. For Group 4, platelet counts were measured on Day 14 instead of Day 19.

Table S7B: Mean change in body weight of cynomolgus monkeys in HMB-001 PK study.

	Day (1 - 8)		Day (8 - 15)		Day (15 - 22)	
	Male (n=2)	**Female (n=2)**	**Male (n=2)**	**Female (n=2)**	**Male (n=2)**	**Female (n=2)**
Group 1	0.12 ± 0.078	0.05 ± 0.014	0.07 ± 0.057	0.05 ± 0.014	0.04 ± 0.000	0.02 ± 0.021
Group 2	0.11 ± 0.049	0.02 ± 0.007	0.04 ± 0.021	0.06 ± 0.007	0.01 ± 0.071	0.00 ± 0.028
Group 3	0.09 ± 0.035	0.09 ± 0.021	-0.04 ± 0.042	0.10 ± 0.035	0.05 ± 0.014	0.02 ± 0.000
Group 4	0.06 ± 0.014	0.04 ± 0.000	0.01 ± 0.035	-0.03 ± 0.042	0.04 ± 0.007	0.01 ± 0.035

Results are shown as the mean ± SD for the 2 animals/sex/group in each group. Change in body weight is presented in units of kg.

Table S8: Predicted plasma levels of FVIIa, total FVII(a) and HMB-001 at 5 different clinical scenarios corresponding to 5 different dosing regimens.

	Target FVIIa (nM)	Predicted total FVII(a) (nM)	Predicted HMB-001 (nM)	HMB-001 QW dose (mg/kg)
1	0.21	14.9	27.6	0.16
2	0.52	17.95	58.7	0.34
3	1	20.9	116	0.67
4	1.38	23	191.7	1.1
5	1.78	26.6	863	5

QW, once weekly

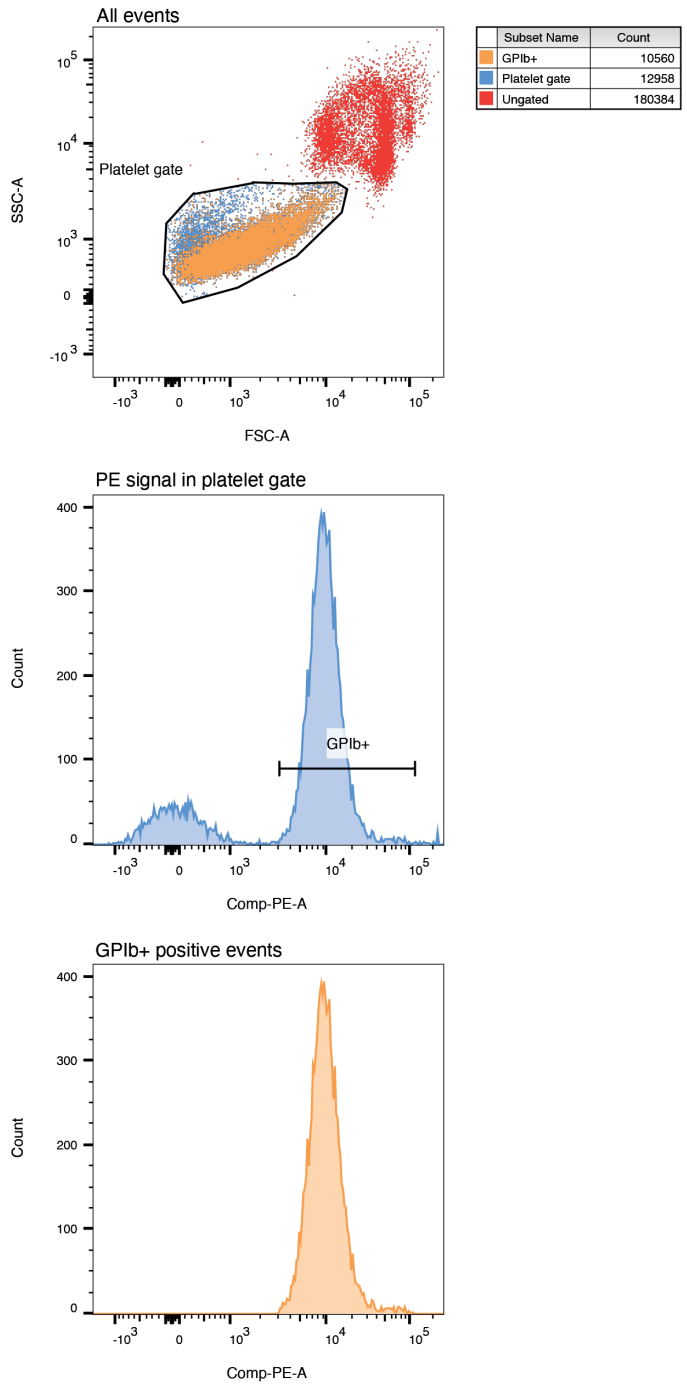

Supplementary Fig. 1: Flow cytometry gating strategy.

ADDENDUM

Declaration of competing interest

P.S.G.: employee and shareholder of Hemab Therapeutics. M.Z.: no conflicts of interest. H.Ø.: employee and shareholder of Hemab Therapeutics. A.C.B.: employee and shareholder of Hemab Therapeutics. T.E.: employee and shareholder of Novo Nordisk. M.N.L.: employee and shareholder of Novo Nordisk. G.S.: employee and shareholder of Novo Nordisk. E.J.: employee and shareholder of Novo Nordisk. O.H.O.: received consultation fees from Hemab Therapeutics. E.H.N.O.: no conflicts of interest. I.-A.d.B.: employee of Sanquin Diagnostic Services. K.B.: employee of Sanquin Diagnostic Services. O.A.: received consultation fees from Hemab Therapeutics. C.J.R.: employee and shareholder of Hemab Therapeutics. S.E.B.: shareholder of Hemab Therapeutics. R.E.S.: the institution of R.E.S. has received speaker's fees and/or research grants from Bayer, CSL Behring, Novartis, Novo Nordisk, Octapharma, Roche, Sobi and Takeda. B.S.: employee and shareholder of Hemab Therapeutics. R.T.U.: no conflicts of interest. J.H.F.: employee and shareholder of Hemab Therapeutics.

Acknowledgements

We acknowledge several current and previous employees of Novo Nordisk for an earlier investigation of HMB-001. We acknowledge expert assistance from H. Gluver and L. Kempf-Amkær (both employees of Hemab Therapeutics). Medical writing assistance was provided by D. Lester and C. Hoare from Bioscript Group, Macclesfield, UK, and funded by Hemab Therapeutics ApS, Copenhagen, Denmark. Financial support for this study was provided by Hemab Therapeutics ApS, Copenhagen, Denmark.

Author contributions

P.S.G.: conceptualization, methodology, formal analysis, investigation, resources, data curation, writing (original draft), writing (review and editing), visualization, supervision, project administration, funding acquisition. M.Z.: conceptualization, methodology, validation, formal analysis, investigation, resources, data curation, writing (original draft), writing (review and editing), visualization. H.Ø.: conceptualization, methodology, formal analysis, investigation, resources, data curation, writing (review and editing), supervision, project administration, funding acquisition. A.C.B.: methodology, formal analysis, investigation, resources, data curation, writing (review and editing), visualization. T.E.: methodology, formal analysis, investigation, data curation, writing

(review and editing), visualization. M.N.L.: investigation, resources, writing (review and editing). G.S.: investigation, writing (review and editing). E.J.: investigation, writing (review and editing). O.H.O.: visualization, writing (review and editing). E.H.N.O.: methodology, validation, investigation, supervision. I.-A.d.B.: methodology, validation, formal analysis, resources, writing (original draft), writing (review and editing). K.B.: methodology, validation, formal analysis, resources, writing (original draft), writing (review and editing). O.A.: methodology, formal analysis, writing (original draft). C.J.R.: writing (review and editing). S.E.B: conceptualization, methodology, writing (review and editing), supervision, project administration, funding acquisition. R.E.S.: resources, writing (review and editing), supervision. B.S.: design, interpretation, writing (review and editing). R.T.U.: conceptualization, methodology, formal analysis, resources, writing (original draft), writing (review and editing), supervision, project administration. J.H.F.: conceptualization, methodology, investigation, resources, writing (review and editing), interpretation, supervision, project administration, funding acquisition

REFERENCES

1. Franchini, M. & Mannucci, P.M. The More Recent History of Hemophilia Treatment. Semin Thromb Hemost 48, 904-910 (2022).
2. Croteau, S.E., Wang, M. & Wheeler, A.P. 2021 clinical trials update: Innovations in hemophilia therapy. Am J Hematol 96, 128-144 (2021).
3. Mannucci, P.M. Hemophilia treatment innovation: 50 years of progress and more to come. J Thromb Haemost 21, 403-412 (2023).
4. Almeida, A.M., Khair, K., Hann, I. & Liesner, R. The use of recombinant factor VIIa in children with inherited platelet function disorders. Br J Haematol 121, 477-481 (2003).
5. Chitlur, M.B., et al. An Update on rFVIIa Use in Females with Rare Bleeding Disorders. Blood 134, 1119 (2019).
6. Peyvandi, F. & Menegatti, M. Treatment of rare factor deficiencies in 2016. Hematology Am Soc Hematol Educ Program 2016, 663-669 (2016).
7. Glanzmann, W. Yearbook of Pediatrics (Hereditary haemorrhagic thrombasthenia. A contribution to the pathology of platelets), (1918).
8. Krause, K.A. & Graham, B. Glanzmann Thrombasthenia. in StatPearls. Treasure Island (FL) (2022).
9. Duncan, A., Kellum, A., Peltier, S., Cooper, D.L. & Saad, H. Disease Burden in Patients with Glanzmann's Thrombasthenia: Perspectives from the Glanzmann's Thrombasthenia Patient/Caregiver Questionnaire. J Blood Med 11, 289-295 (2020).
10. Zafarghandi Motlagh, F., et al. Molecular genetic diagnosis of Glanzmann syndrome in Iranian population; reporting novel and recurrent mutations. Orphanet J Rare Dis 14, 87 (2019).
11. Mathews, N., Rivard, G.E. & Bonnefoy, A. Glanzmann Thrombasthenia: Perspectives from Clinical Practice on Accurate Diagnosis and Optimal Treatment Strategies. J Blood Med 12, 449-463 (2021).
12. Khair, K. Glanzmann's 360 study. (Haemophilia, Wiley Online Library, 2023).
13. Toogeh, G., et al. Presentation and pattern of symptoms in 382 patients with Glanzmann thrombasthenia in Iran. Am J Hematol 77, 198-199 (2004).
14. Di Minno, G., et al. The international, prospective Glanzmann Thrombasthenia Registry: treatment modalities and outcomes of non-surgical bleeding episodes in patients with Glanzmann thrombasthenia. Haematologica 100, 1031-1037 (2015).
15. Lisman, T., Adelmeijer, J., Heijnen, H.F. & de Groot, P.G. Recombinant factor VIIa restores aggregation of alphaIIbbeta3-deficient platelets via tissue factor-independent fibrin generation. Blood 103, 1720-1727 (2004).

16. Bolton-Maggs, P.H., et al. A review of inherited platelet disorders with guidelines for their management on behalf of the UKHCDO. Br J Haematol 135, 603-633 (2006).

17. Tarawah, A., et al. Management of Glanzmann Thrombasthenia; Guidelines based on an expert panel consensus from gulf cooperation council countries. Journal of Applied Hematology 10, 1-9 (2019).

18. NovoSeven, R.T.N.N. Prescribing Information Coagulation Factor VIIa (recombinant). (2020).

19. NovoSeven, R.T.N.N. Summary of product characteristics Coagulation Factor VIIa (recombinant). (2020).

20. Poon, M.C., Di Minno, G., d'Oiron, R. & Zotz, R. New Insights Into the Treatment of Glanzmann Thrombasthenia. Transfus Med Rev 30, 92-99 (2016).

21. Andiç, N., Oğuz, N., Gündüz, E., Kiraz Bulduk, T. & Üsküdar Teke, H. Weekly low-dose recombinant factor VIIa prophylaxis in Glanzmann thrombasthenia. Blood Coagul Fibrinolysis 32, 349-351 (2021).

22. Feng, D., Whinna, H., Monroe, D. & Stafford, D.W. FVIIa as used pharmacologically is not TF dependent in hemophilia B mice. Blood 123, 1764-1766 (2014).

23. Lisman, T. & De Groot, P.G. Mechanism of action of recombinant factor VIIa. J Thromb Haemost 1, 1138-1139 (2003).

24. Giansily-Blaizot, M. & Schved, J.F. Recombinant human factor VIIa (rFVIIa) in hemophilia: mode of action and evidence to date. Ther Adv Hematol 8, 345-352 (2017).

25. Monroe, D.M., Hoffman, M., Oliver, J.A. & Roberts, H.R. A possible mechanism of action of activated factor VII independent of tissue factor. Blood Coagul Fibrinolysis 9 Suppl 1, S15-20 (1998).

26. Hoffman, M., Monroe, D.M. & Roberts, H.R. Platelet-dependent action of high-dose factor VIIa. Blood 100, 364-365; author reply 365 (2002).

27. van 't Veer, C., Golden, N.J. & Mann, K.G. Inhibition of thrombin generation by the zymogen factor VII: implications for the treatment of hemophilia A by factor VIIa. Blood 95, 1330-1335 (2000).

28. Butenas, S., Brummel, K.E., Branda, R.F., Paradis, S.G. & Mann, K.G. Mechanism of factor VIIa-dependent coagulation in hemophilia blood. Blood 99, 923-930 (2002).

29. Augustsson, C. & Persson, E. In vitro evidence of a tissue factor-independent mode of action of recombinant factor VIIa in hemophilia. Blood 124, 3172-3174 (2014).

30. Lisman, T., Moschatsis, S., Adelmeijer, J., Nieuwenhuis, H.K. & De Groot, P.G. Recombinant factor VIIa enhances deposition of platelets with congenital or acquired alpha IIb beta 3 deficiency to endothelial cell matrix and collagen under conditions of flow via tissue factor-independent thrombin generation. Blood 101, 1864-1870 (2003).

31. Tiede, A., et al. Safety and pharmacokinetics of subcutaneously administered recombinant activated factor VII (rFVIIa). J Thromb Haemost 9, 1191-1199 (2011).

32. Kjalke, M., Kjellev, S. & Rojkjaer, R. Preferential localization of recombinant factor VIIa to platelets activated with a combination of thrombin and a glycoprotein VI receptor agonist. J Thromb Haemost 5, 774-780 (2007).

33. Fernández-Bello, I., et al. The pharmacokinetics and pharmacodynamics of single-dose and multiple-dose recombinant activated factor VII in patients with haemophilia A or B. Haemophilia 23, 868-876 (2017).

34. Pittman, D., et al. A novel FVIIa variant with increased potency and duration of effect compared to wildtype FVIIa. A study in a dog model of hemophilia A. Blood 118, 2252 (2011).

35. Persson, E., Kjalke, M. & Olsen, O.H. Rational design of coagulation factor VIIa variants with substantially increased intrinsic activity. Proc Natl Acad Sci U S A 98, 13583-13588 (2001).

36. Mahlangu, J.N., et al. Phase I, randomized, double-blind, placebo-controlled, single-dose escalation study of the recombinant factor VIIa variant BAY 86-6150 in hemophilia. J Thromb Haemost 10, 773-780 (2012).

37. Stennicke, H.R., et al. Generation and biochemical characterization of glycoPEGylated factor VIIa derivatives. Thromb Haemost 100, 920-928 (2008).

38. Weimer, T., et al. Prolonged in-vivo half-life of factor VIIa by fusion to albumin. Thromb Haemost 99, 659-667 (2008).

39. Bar-Ilan, A., et al. In vitro characterization of MOD-5014, a novel long-acting carboxy-terminal peptide (CTP)-modified activated FVII. Haemophilia 24, 477-486 (2018).

40. Persson, E., Olsen, O.H., Bjorn, S.E. & Ezban, M. Vatreptacog alfa from conception to clinical proof of concept. Semin Thromb Hemost 38, 274-281 (2012).

41. Aleman, M.M., et al. Platelet-targeted rFVIIa-Xten improves thrombin generation and fibrin formation compared to recombinant FVIIa. Blood 126, 2269 (2015).

42. Gattis, J.L., et al. The structure of the extracellular domain of triggering receptor expressed on myeloid cells like transcript-1 and evidence for a naturally occurring soluble fragment. J Biol Chem 281, 13396-13403 (2006).

43. Washington, A.V., et al. A TREM family member, TLT-1, is found exclusively in the alpha-granules of megakaryocytes and platelets. Blood 104, 1042-1047 (2004).

44. Smith, C.W., et al. TREM-like transcript 1: a more sensitive marker of platelet activation than P-selectin in humans and mice. Blood Adv 2, 2072-2078 (2018).

45. Washington, A.V., et al. TREM-like transcript-1 protects against inflammation-associated hemorrhage by facilitating platelet aggregation in mice and humans. J Clin Invest 119, 1489-1501 (2009).

46. Enoksson, M., et al. Enhanced potency of recombinant factor VIIa with increased affinity to activated platelets. J Thromb Haemost 18, 104-113 (2020).

47. Labrijn, A.F., et al. Efficient generation of stable bispecific IgG1 by controlled Fab-arm exchange. Proc Natl Acad Sci U S A 110, 5145-5150 (2013).

48. Neuenschwander, P.F. & Morrissey, J.H. Deletion of the membrane anchoring region of tissue factor abolishes autoactivation of factor VII but not cofactor function. Analysis of a mutant with a selective deficiency in activity. J Biol Chem 267, 14477-14482 (1992).

49. Neuenschwander, P.F., Fiore, M.M. & Morrissey, J.H. Factor VII autoactivation proceeds via interaction of distinct protease-cofactor and zymogen-cofactor complexes. Implications of a two-dimensional enzyme kinetic mechanism. J Biol Chem 268, 21489-21492 (1993).

50. Agersø, H., et al. Recombinant human factor VIIa (rFVIIa) cleared principally by antithrombin following intravenous administration in hemophilia patients. J Thromb Haemost 9, 333-338 (2011).

51. Girard, T.J., et al. Functional significance of the Kunitz-type inhibitory domains of lipoprotein-associated coagulation inhibitor. Nature 338, 518-520 (1989).

52. Branfield, S. & Washington, A.V. The enigmatic nature of the triggering receptor expressed in myeloid cells -1 (TLT- 1). Platelets 32, 753-760 (2021).

53. McCallum, C.D., Hapak, R.C., Neuenschwander, P.F., Morrissey, J.H. & Johnson, A.E. The location of the active site of blood coagulation factor VIIa above the membrane surface and its reorientation upon association with tissue factor. A fluorescence energy transfer study. J Biol Chem 271, 28168-28175 (1996).

54. Schoeman, R.M., Lehmann, M. & Neeves, K.B. Flow chamber and microfluidic approaches for measuring thrombus formation in genetic bleeding disorders. Platelets 28, 463-471 (2017).

55. Margaritis, P. Does rFVIIa work solo in hemophilia? Blood 123, 1631-1633 (2014).

56. Botero, J.P., et al. Glanzmann thrombasthenia: genetic basis and clinical correlates. Haematologica 105, 888-894 (2020).

57. Buitrago, L., Lefkowitz, S., Bentur, O., Padovan, J. & Coller, B. Platelet binding to polymerizing fibrin is avidity driven and requires activated alphaIIbbeta3 but not fibrin cross-linking. Blood Adv 5, 3986-4002 (2021).

58. Peter, W., et al. Measurement of basal levels of factor vila in hemophilia A and B patients. Blood 80, 25-28 (1992).

59. Morrissey, J.H., Macik, B.G., Neuenschwander, P.F. & Comp, P.C. Quantitation of activated factor VII levels in plasma using a tissue factor mutant selectively deficient in promoting factor VII activation. Blood 81, 734-744 (1993).

60. Hedner, U. Dosing and monitoring NovoSeven treatment. Haemostasis 26 Suppl 1, 102-108 (1996).

61. Faraj, A., et al. Phase III dose selection of marzeptacog alfa (activated) informed by population pharmacokinetic modeling: A novel hemostatic drug. CPT Pharmacometrics Syst Pharmacol 11, 1628-1637 (2022).

62. Ozelo, M.C., Svirin, P. & Larina, L. Use of recombinant factor VIIa in the management of severe bleeding episodes in patients with Bernard-Soulier syndrome. Ann Hematol 84, 816-822 (2005).

63. Tjärnlund-Wolf, A. & Lassila, R. Phenotypic characterization of haemophilia B - Understanding the underlying biology of coagulation factor IX. Haemophilia 25, 567-574 (2019).

64. Blaauwgeers, M.W., et al. Bleeding phenotype and diagnostic characterization of patients with congenital platelet defects. Am J Hematol 95, 1142-1147 (2020).

65. Blaauwgeers, M.W., et al. The limitation of genetic testing in diagnosing patients suspected for congenital platelet defects. Am J Hematol 95, E26-E28 (2020).

66. Thim, L., et al. Amino acid sequence and posttranslational modifications of human factor VIIa from plasma and transfected baby hamster kidney cells. Biochemistry 27, 7785-7793 (1988).

67. Persson, E., Nielsen, L.S. & Olsen, O.H. Substitution of aspartic acid for methionine-306 in factor VIIa abolishes the allosteric linkage between the active site and the binding interface with tissue factor. Biochemistry 40, 3251-3256 (2001).

68. Freskgård, P.O., Olsen, O.H. & Persson, E. Structural changes in factor VIIa induced by Ca2+ and tissue factor studied using circular dichroism spectroscopy. Protein Sci 5, 1531-1540 (1996).

69. Smith, S.A. & Morrissey, J.H. Rapid and efficient incorporation of tissue factor into liposomes. J Thromb Haemost 2, 1155-1162 (2004).

70. Hyseni, A., et al. Increased mortality in systemic inflammatory response syndrome patients with high levels of coagulation factor VIIa. J Thromb Haemost 11, 2111-2117 (2013).

71. Carol Illa, A., et al. Tail Vein Transection Bleeding Model in Fully Anesthetized Hemophilia A Mice. J Vis Exp (2021).

72. Johansen, P.B., Tranholm, M., Haaning, J. & Knudsen, T. Development of a tail vein transection bleeding model in fully anaesthetized haemophilia A mice - characterization of two novel FVIII molecules. Haemophilia 22, 625-631 (2016).

73. Kirchhofer, D., et al. Activation of blood coagulation factor VIIa with cleaved tissue factor extracellular domain and crystallization of the active complex. Proteins 22, 419-425 (1995).

74. Kabsch, W. Xds. Acta Crystallogr D Biol Crystallogr 66, 125-132 (2010).

75. Liebschner, D., et al. Macromolecular structure determination using X-rays, neutrons and electrons: recent developments in Phenix. Acta Crystallogr D Struct Biol 75, 861-877 (2019).

76. McCoy, A.J., et al. Phaser crystallographic software. J Appl Crystallogr 40, 658-674 (2007).

77. Emsley, P., Lohkamp, B., Scott, W.G. & Cowtan, K. Features and development of Coot. Acta Crystallogr D Biol Crystallogr 66, 486-501 (2010).

78. Afonine, P.V., et al. Towards automated crystallographic structure refinement with phenix. refine. Acta Crystallogr D Biol Crystallogr 68, 352-367 (2012).

79. Scapin, G., et al. Structure of full-length human anti-PD1 therapeutic IgG4 antibody pembrolizumab. Nat Struct Mol Biol 22, 953-958 (2015).

80. Karami, Y., et al. DaReUS-Loop: a web server to model multiple loops in homology models. Nucleic Acids Research 47, W423-W428 (2019).

81. Karami, Y., Guyon, F., De Vries, S. & Tuffery, P. DaReUS-Loop: accurate loop modeling using fragments from remote or unrelated proteins. Sci Rep 8, 13673 (2018).

82. Ohkubo, Y.Z., Morrissey, J.H. & Tajkhorshid, E. Dynamical view of membrane binding and complex formation of human factor VIIa and tissue factor. J Thromb Haemost 8, 1044-1053 (2010).

83. Bourgeat, P., Jasmin, P., Migaud-Fressart, M. & Martinolli, J.L. Direct measurement of activated F. VII in plasma: development of an original assay. Thromb Haemostasis 73, 1204 (1995).

84. Team., R.D.C. R: A Language and Environment for Statistical Computing. (R Foundation for Statistical Computing, Vienna, Austria, 2008).

85. Lindbom, L., Pihlgren, P. & Jonsson, E.N. PsN-Toolkit--a collection of computer intensive statistical methods for non-linear mixed effect modeling using NONMEM. Comput Methods Programs Biomed 79, 241-257 (2005).

86. Deng, R., et al. Projecting human pharmacokinetics of therapeutic antibodies from nonclinical data: what have we learned? MAbs 3, 61-66 (2011).

87. Chen, X., DuBois, D.C., Almon, R.R. & Jusko, W.J. Characterization and Interspecies Scaling of rhTNF-alpha Pharmacokinetics with Minimal Physiologically Based Pharmacokinetic Models. Drug Metab Dispos 45, 798-806 (2017).

88. Fair, D.S. Quantitation of factor VII in the plasma of normal and warfarin-treated individuals by radioimmunoassay. Blood 62, 784-791 (1983).

89. Wagenvoord, R., Hemker, P.W. & Hemker, H.C. The limits of simulation of the clotting system. J Thromb Haemost 4, 1331-1338 (2006).

90. Neeves, K.B., et al. Microfluidic focal thrombosis model for measuring murine platelet deposition and stability: PAR4 signaling enhances shear-resistance of platelet aggregates. J Thromb Haemost 6, 2193-2201 (2008).

91. Karplus, P.A. & Diederichs, K. Linking crystallographic model and data quality. Science 336, 1030-1033 (2012).

92. Banner, D.W., et al. The crystal structure of the complex of blood coagulation factor VIIa with soluble tissue factor. Nature 380, 41-46 (1996).

93. Norledge, B.V., Petrovan, R.J., Ruf, W. & Olson, A.J. The tissue factor/factor VIIa/factor Xa complex: a model built by docking and site-directed mutagenesis. Proteins 53, 640-648 (2003).

Chapter 6

Summary and general discussion

SUMMARY

Platelet function plays a critical role in hemostasis, and dysfunction in this mechanism is implicated in a range of bleeding disorders. The most rare inherited platelet function disorders (IPFDs) are relatively easy to diagnose. However, the more prevalent IPFDs often show a high diagnostic difficulty, leading to underdiagnosis. In terms of treatment of IPFD patients, no prophylactic treatment is available, causing high patient burden and relatively low quality of life for patients suffering from a severe IPFD. This thesis describes novel diagnostic and therapeutic approaches for this group of disorders.

Advanced diagnostics ...

In **Chapter 2**, we described the characterization of a tetrameric nanobody-based glycoprotein VI (GPVI) platelet agonist and compared it to current agonists used in platelet diagnostics, that are hard to standardize and difficult to produce. We showed that our nanobody is able to discriminate between healthy controls and GPVI-related platelet disorders to a similar extent as collagen or cross-linked collagen-related peptide (CRP-XL). In this way, we provide a more stable, easier to produce alternative to current GPVI agonists, which is beneficial for standardization of platelet diagnostics.

In **Chapter 3**, we have validated a novel whole blood-based rapid test for delta storage pool disease (δ-SPD), based on platelet ATP secretion. The current standard for diagnosis of δ-SPD is laborious, has a long turn-around time and requires large volumes of blood. We aimed to introduce a microarray that decreases the labor intensiveness, turn-around time and required volume of blood. With its high sensitivity, this test is able to exclude δ-SPD, decreasing the need to send all patients for more advanced diagnostic techniques.

In **Chapter 4**, we have compared the platelet proteome of healthy controls and people with Glanzmann thrombasthenia (GT). We have shown that platelets from GT patients show downregulation of several platelet specific α-granule proteins.

... and novel therapeutics for inherited platelet function disorders

In **Chapter 5**, we introduced a potential novel prophylactic treatment for inherited bleeding disorders. HMB-001 is a bispecific antibody that recognizes (activated) coagulation factor VII (FVII(a)) and TREM-like transcript-1 (TLT-1) on the activated

platelet surface, thereby targeting FVIIa to the platelet surface and boosting fibrin formation to compensate for defects in primary hemostasis. Our preclinical data has shown that HMB-001 is effective in enhancing fibrin formation *ex vivo*, prolonging endogenous FVIIa half-life in nonhuman primates and potentiating FVIIa hemostatic activity in mouse bleeding studies. HMB-001 has therefore potential to offer subcutaneous prophylactic treatment to prevent bleeds in people with GT and other inherited bleeding disorders, with a low-frequency dosing regimen.

GENERAL DISCUSSION

Despite advances in the understanding of platelet biology and function, significant knowledge gaps remain in both the diagnosis and treatment of IPFDs. Conventional diagnostic methods often fall short in providing accurate and timely diagnoses. Current approaches, such as light transmission aggregometry (LTA) and flow cytometry are the mainstay assays, but are limited by their variability, complexity, and lack of standardization across laboratories. These challenges lead to inconsistent results, hindering both diagnosis and the ability to compare clinical data between institutions. Moreover, the limited availability of reagents, such as agonists for key platelet pathways like GPVI, further pose challenges in platelet diagnostics.

Another critical therapeutic gap is the lack of tailored treatments for IPFDs. Treatment strategies often rely on general on-demand approaches such as platelet transfusions or antifibrinolytics, which are not suitable for long-term prophylactic treatment. The emergence of prophylactic treatment would be life-changing for a significant group of IPFD patients, underlining the critical need for such a treatment.

In 2015, the Scientific Standardization Committee (SSC) of the ISTH published a guidance on the diagnosis of IPFDs[1]. As still substantial gaps remain in the diagnostics of IPFDs, we aimed within this thesis to contribute to evolving the landscape of platelet diagnostics and improve the current guidelines. Moreover, we aimed to broaden therapeutic strategies by utilizing emerging technologies and novel approaches to improve clinical outcomes for patients with IPFDs.

Challenges of light transmission aggregometry in platelet testing

Light transmission aggregometry is a widely used technique and is considered the gold standard for assessing platelet function. However, it has significant limitations, particularly in its sensitivity to various IPFDs. One of the primary issues is that LTA may not adequately detect all types of platelet dysfunctions, leading to misdiagnosis or underdiagnosis of certain conditions. This shortcoming specifically holds true for the mild IPFDs. Where the most rare conditions, like GT and Bernard-Soulier Syndrome (BSS) do show a specific LTA pattern, this is more variable for the mild ones, like SPD. There is no real consensus on when LTA results are aberrant from reference ranges and these ranges even vary from 5 to 100% for some agonists.

The challenges of LTA are mostly due to the lack of standardization in protocols and reagents, which can result in variable outcomes and reduced comparability between laboratories. A recent study from the SSC of the ISTH on Platelet Physiology revealed considerable inconsistencies and high inter-individual variability for the most commonly used platelet agonists[2]. These results demonstrate that the reagents used in diagnostic assays can dramatically affect the assay's sensitivity and specificity. Especially low concentrations of platelet agonists show high variation and should be avoided[2,3]. This variability contributes to the overall challenges in diagnosis of IPFDs. Although inter-individual variability cannot be avoided, intrinsic assay variability should be limited, for example by using only high agonist concentrations. The question remains if, even with standardized protocols and reagents, LTA would be sufficient in accurate detection of mild IPFDs, as the ISTH-SSC already stated that a standardized Dutch protocol for LTA does not result in smaller variability in healthy volunteers for all agonist concentrations[3].

The shortcomings of LTA in detecting specific IPFDs underscore the need for improved standardization and more sensitive diagnostic techniques, like flow cytometry. By addressing these issues, the field can move towards more accurate and reliable assessment of platelet function, ultimately leading to better patient management and outcomes.

Flow cytometry as upcoming diagnostic tool

Flow cytometry has emerged as a powerful tool in platelet diagnostics due to its ability to simultaneously assess multiple platelet surface markers, intracellular signaling pathways, and functional responses to different stimuli[4–9]. When using flow cytometry to measure glycoprotein expression, the focus is on quantifying the receptor levels, such as αIIbβ3 in GT, as we have done in **Chapter 4**, or GPIb in BSS. On the other hand, this technique can be used to monitor functional responses following the stimulation of platelets by various agonists. This approach evaluates how platelets respond to these agonists by measuring markers of platelet activation, such as P-selectin expression and fibrinogen binding and can for example be useful in defects of the GPVI-signaling pathway, as we have studied in **Chapter 2**.

Flow cytometry shows several advantages compared to LTA. It requires only small volumes of whole blood, decreasing the labor intensiveness for sample preparation, but also the patient burden in blood drawing, which can be especially beneficial for

pediatric patients. Additionally, flow cytometry is still suitable in samples with very low platelet counts, unlike LTA that requires a near normal platelet count to be reliable[10,11]. While flow cytometry has demonstrated promise in this field, its application as the new gold standard faces some challenges, particularly with regard to standardization across different laboratories and healthcare institutions. Variability can arise from differences in sample preparation, instrument calibration, and the specific protocols. The incorporation of beads for calibration and multi-center collaborations could address one of these issues. Calibration beads, like molecules of equivalent soluble fluorophores beads, can be used to ensure that fluorescence intensity measurements, which are critical for quantifying platelet surface marker expression, are consistent across various flow cytometry machines[12–14].

As discussed, the challenge of accurate diagnoses is especially evident in the more prevalent, mild IPFDs, like SPD. Current diagnostic assays for SPD, like lumi-aggregometry and nucleotide content assays, are all laborious and time-consuming, which leads to delays in setting the diagnosis. Flow cytometry could play an important role in improving the diagnosis of δ-SPD, for example using mepacrine, that specifically accumulates in platelet δ-granules[15]. Another marker that could be used in flow cytometry-based δ-SPD diagnostics is the dense granule specific marker CD63. Although it is recognized as a relevant biomarker for δ-SPD[16], it is not yet incorporated as a standard diagnostic marker in routine platelet diagnostics. Several studies[17–20], including our findings from **Chapter 3**, have demonstrated that CD63 is highly effective in distinguishing between δ-SPD, non-SPD IPFD, and healthy individuals. This further strengthens the argument for incorporating flow cytometry as standard tool in the diagnostic panels for platelet function.

Overall, it is clear that the current guidelines for diagnosis of IPFDs can use an update, where flow cytometry plays a pivotal role and LTA migrates to the background, or in the end can even be eliminated from platelet diagnostics. Although the ISTH-SSC guidance from 2015 already suggested flow cytometry to include in the first screening of platelet diagnostics, this was limited to the analysis of the major platelet surface glycoproteins, to detect GT and BSS, which are already relatively easy to diagnose and also have clear LTA patterns. We suggest to include the analysis of platelet reactivity to various agonists in flow cytometry in this first line of platelet diagnostics. In this way, we will have a more reliable evaluation of platelets, even in thrombocytopenic conditions. In **Fig. 1**, we show suggested adaptations on the 2015 ISTH-SSC guidance.

Although the common thread of this diagnostic algorithm can be maintained, we suggest the incorporation of standardized flow cytometry in first line platelet diagnostics. We believe this will have a significant impact on how we can move forward in helping patients that present with a primary hemostasis defect. Additionally, implementation of exclusion tests in the first line, like our rapid δ-SPD test from **Chapter 3**, are beneficial in decreasing the need to send all patients for advanced diagnostic tests in the second line.

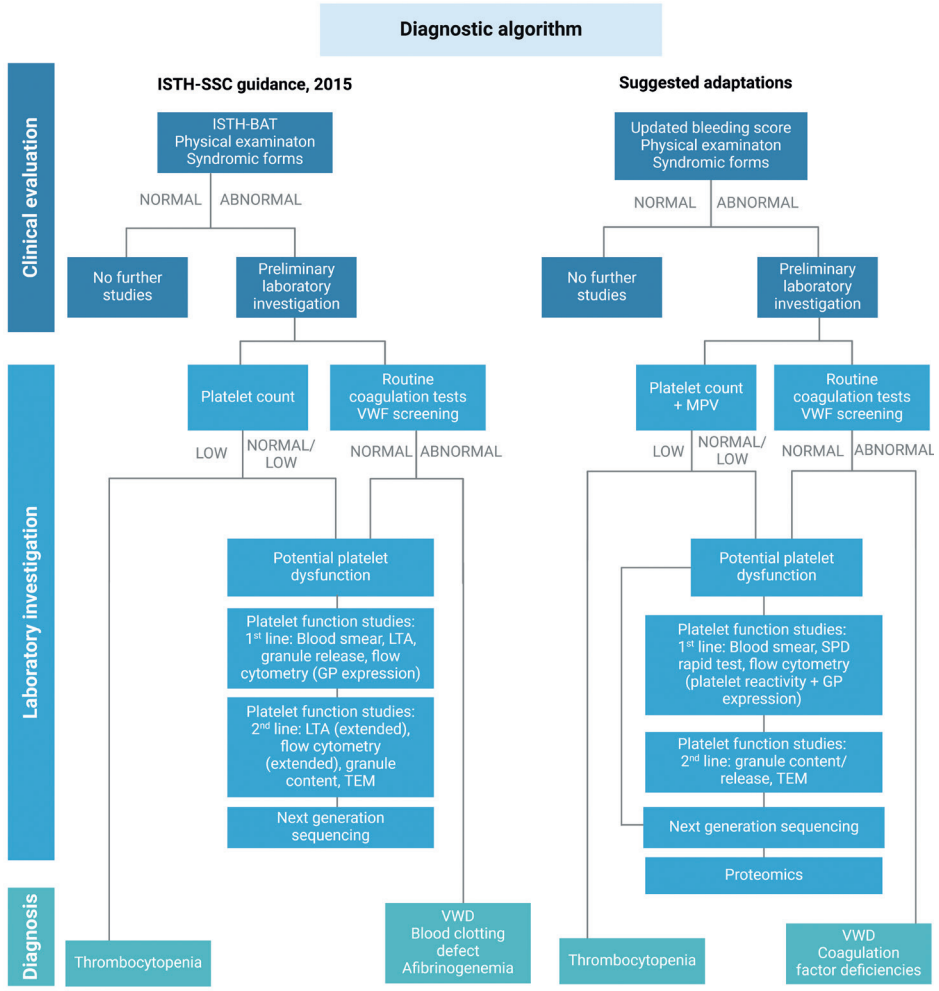

Fig. 1: Diagnostic algorithm flowchart. Suggested adaptations to the ISTH-SSC platelet diagnostics guidance for improved diagnosis of IPFDs. *Created in https://BioRender.com.*

What can proteomics tell us about platelets?

Besides our suggested adaptations in the first line platelet function studies, we suggest to add an extra step after DNA sequencing in the third line of diagnostics, namely the study of platelet proteomics (**Fig. 1**). Platelet proteome analyses can yield various types of information and can provide detailed insights into the (quantitative) protein composition of platelets. Additionally, proteomics can provide quantitative data on changes in protein levels, for example when comparing platelets from different donors, whether due to genetic differences or health versus disease status, as we have done for GT versus healthy platelets in **Chapter 4**. Unravelling the platelet proteome in a certain disease can identify novel signaling pathways or secreted proteins that may represent the disease, which contributes to greater knowledge of platelet function and biology, but is also beneficial for the diagnostic field. For example, proteomic techniques led to a diagnosis of Quebec Platelet Disorder in a family with severe bleeding of unknown cause[21]. Although the clinical features were not strongly indicative of this disorder, proteome analysis revealed a reduction in alpha (α)-granule proteins, leading to the correct diagnosis. This discovery built on the earlier proteomic characterization of platelet α-granules by Maynard *et al.*[22]. However, significant questions remain about how to best implement proteomics in clinical practice.

To explore the use of IPFD proteomics more effectively, we need large clinical studies to validate potential biomarkers. A small-scale national study in the Netherlands may provide initial insights, as done by Kreft *et al.*[23], but the rarity and diversity of IPFDs call for a broader, international approach. Although challenging, large international collaborative studies could pool data from diverse populations, increasing the likelihood of identifying proteomic abnormalities that contribute to platelet dysfunction. As for diagnostic strategies, proteomics shows potential to identify the proteins and pathways involved in platelet disorders. However, integrating proteomics into routine diagnostics for all patients may not be practical due to its complexity and labor-intensive nature. Additionally, its appliance in diagnostics is complicated due to the heterogenicity of platelets. Platelets are complex and dynamic and their proteome could vary due to external factors like age and use of medication. This would complicate its standardization and incorporation in diagnostics. Even with validated biomarkers, it remains challenging to incorporate those in a validated test that is affordable and easy to perform. Instead, proteomics could be used to discover new genetic abnormalities, especially for the mild IPFDs, which can then guide the development of more

streamlined genetic testing protocols. These genetic tests would be much less variable in outcome and far less resource-intensive, offering a more efficient diagnostic pathway.

Enhancing secondary hemostasis to compensate for defects in primary hemostasis

An interesting novel concept in the management of bleeding disorders is the potential to strengthen secondary hemostasis to compensate for deficits in primary hemostasis. The first evidence supporting this approach comes from the use of recombinant FVIIa (rFVIIa) (NovoSeven®)[24,25]. Initially developed for hemophilia patients with inhibitors, rFVIIa has been shown to improve hemostasis in patients with platelet function disorders, like GT and BSS, by promoting thrombin generation, thus enhancing secondary hemostasis[26–30]. Data collected from the Glanzmann Thrombasthenia Registry and the Novo Nordisk Safety Surveillance Database showed a consistent efficacy and safety profile in patients with GT, presenting a good alternative to platelet transfusions in GT patients with severe bleeding episodes[27]. However, a large pitfall in the use of rFVIIa is its short half-life, underlining the need for novel therapeutic options for this patient group.

Two novel antibody-based agents that show potential in enhancing secondary hemostasis and build upon the mechanism of rFVIIa are HMB-001, as we have studied in **Chapter 5**, and concizumab[31], by respectively accumulating FVIIa or preventing its inhibition (**Fig. 2**). Whereas we have primarily focused on GT, HMB-001 could possibly be extended to a great variety of bleeding disorders, like BSS or SPD or even outside the IPFD category, for example for FVII deficiency. Further research into its indication expansion would be of great value in broadening treatment options for patients with bleeding disorders. After its initial focus on hemophilia, concizumab now also shows promise for platelet defects, like GT[32].

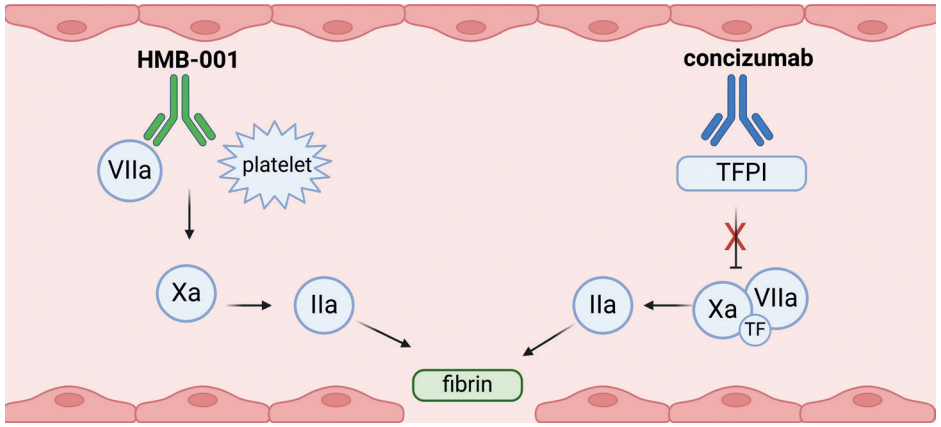

Fig. 2: Mechanism of action of HMB-001 vs concizumab. Primary hemostasis defects can be treated with agents that enhance secondary hemostasis. HMB-001 accumulates FVIIa and targets it to the activated platelet surface, enhancing fibrin formation. Concizumab targets TFPI, thereby abolishing its anticoagulant effect on the FXa/FVIIa/TF complex. TFPI; tissue factor pathway inhibitor. TF; tissue factor. *Created in https://BioRender.com.*

Both therapy options hold promise in treating platelet disorders and are of great relevance for the IPFD patient group. Where HMB-001 could be used as preventive prophylaxis therapy for IPFD patients, concizumab could be an alternative or additional option in cases of severe acute bleeds or in cases of TLT-1 deficiency or extreme low platelet counts.

Our preclinical studies of HMB-001 have demonstrated promising results in improving hemostasis. However, its long-term efficacy and safety, particularly in diverse patient populations with varying underlying platelet dysfunctions, remains to be determined. Currently, HMB-001 is in Phase 1/2 clinical trial to investigate safety, tolerability, pharmacokinetics, pharmacodynamics, and efficacy in GT patients, with promising first results[33]. Concizumab is approved for hemophilia patients with inhibitors, but remains to be clinically investigated for IPFD patients.

Collaborative research efforts

To make substantial progress in the diagnosis of mild IPFDs, international collaborations and achieving consensus are essential. As platelets are very sensitive to sample preparation, we need to find national, or even more broad, consensus about operating procedures. Currently, practices vary widely across different regions, probably due to lack of communication between institutions, leading to inconsistencies in diagnosis

and treatment. Collaborative research efforts within the SSC of the ISTH should lead to consensus on standard protocols that have to be universally implemented. Collaborations like this would also support large-scale validation studies with unselected patient populations across multiple institutions, which are necessary to confirm the clinical utility of emerging diagnostic tools, such as the rapid test for δ-SPD, that we have described in **Chapter 3**, or our nanobody-based GPVI agonist, that we have characterized in **Chapter 2**.

Besides collaborations within the ISTH-SSC to improve standardization of diagnostic protocols, Public-Private Partnerships are also critical in making progress in our field. A large part of the preclinical studies on HMB-001 from **Chapter 5** was a collaboration between Hemab Therapeutics and the University Medical Center Utrecht. The successful outcome is an example of the benefits and importance of combining forces between private sectors, like innovative bio-tech companies, and public sectors, like academia, and sharing expertise and resources. One of the primary benefits of such collaborations is the ability to leverage private sector efficiency, innovation, and funding capacity, which can accelerate project timelines and improve overall outcomes. By pooling resources, these partnerships allow for greater investment in critical areas such as drug development, but also medical technologies and diagnostic tools. Furthermore, collaborations like this enhance the ability to translate research into real-world applications, ensuring that innovations are rapidly brought to the market and made accessible to broader populations.

Finally, national and international academic consortia are indispensable in research. Our studies from **Chapter 2**, **3** and **4** were all made possible by the SYMPHONY consortium[34]. Within this consortium, we have worked together in a large interdisciplinary team from 7 clinical centers in the Netherlands to reach for our aims: 1. Treatment optimization by personalization with high quality of care at acceptable costs; 2. Guidance of complex clinical shared decision making for novel therapeutic options; and 3. Patient-orchestrated implementation of health care innovations using e-health modules. Collaborations within multi-center consortia are crucial for advancing academic research, particularly in fields that require large-scale, diverse datasets and interdisciplinary approaches. By pooling resources, expertise, and data across institutions, consortia can overcome limitations inherent in single-center studies, such as sample size constraints and localized biases. Furthermore, multi-center consortia promote innovation by bringing together researchers from different

disciplines, who contribute diverse perspectives and methodologies. These partnerships also promote the efficient use of funding and resources, while increasing the visibility and impact of the research on a global scale. Ultimately, multi-center consortia accelerate scientific discoveries and improve the translation of research findings into the clinic, making them a vital component of modern academic research.

CONCLUSION

In summary, within this thesis we gained more insight into platelet biology and contributed to advanced diagnostics and novel therapeutics for IPFDs. In the coming years, we hope to bring our findings into the clinic, improving and standardizing platelet diagnostics and providing a life-changing treatment option for IPFD patients.

REFERENCES

1. Gresele P, Subcommittee on Platelet Physiology of the International Society on Thrombosis and Hemostasis. Diagnosis of inherited platelet function disorders: guidance from the SSC of the ISTH. *J Thromb Haemost*. 2015;13(2):314-322. doi:10.1111/jth.12792
2. Alessi M-C, Coxon C, Ibrahim-Kosta M, et al. Multicenter evaluation of light transmission platelet aggregation reagents: communication from the ISTH SSC Subcommittee on Platelet Physiology. *J Thromb Haemost*. 2023;21(9):2596-2610. doi:10.1016/j.jtha.2023.05.027
3. Munnix ICA, Van Oerle R, Verhezen P, et al. Harmonizing light transmission aggregometry in the Netherlands by implementation of the SSC-ISTH guideline. *Platelets*. 2021;32(4):516-523. doi:10.1080/09537104.2020.1771549
4. van Asten I, Blaauwgeers M, Granneman L, et al. Flow cytometric mepacrine fluorescence can be used for the exclusion of platelet dense granule deficiency. *J Thromb Haemost*. 2020;18(3):706-713. doi:10.1111/jth.14698
5. Jourdi G, Ramström S, Sharma R, Bakchoul T, Lordkipanidzé M, FC-PFT in TP study group. Consensus report on flow cytometry for platelet function testing in thrombocytopenic patients: communication from the SSC of the ISTH. *J Thromb Haemost*. 2023;21(10):2941-2952. doi:10.1016/j.jtha.2023.07.006
6. Huskens D, Li L, Florin L, et al. Flow cytometric analysis of platelet function to improve the recognition of thrombocytopathy. *Thromb Res*. 2020;194:183-189. doi:10.1016/j.thromres.2020.06.037
7. De Cuyper IM, Meinders M, van de Vijver E, et al. A novel flow cytometry-based platelet aggregation assay. *Blood*. 2013;121(10):e70-80. doi:10.1182/blood-2012-06-437723
8. Keller Cecconello D, Spagnol F, Alegretti AP, Pilger DA, Farias MG. Flow cytometry immunophenotyping of healthy platelets and hospitalized patients with suspected platelet dysfunction: Challenges for establishing a cutoff value. *Hematology, Transfusion and Cell Therapy*. August 28, 2023. doi:10.1016/j.htct.2023.07.002
9. Yoon I, Han JH, Jeon H-J. Advances in Platelet-Dysfunction Diagnostic Technologies. *Biomolecules*. 2024;14(6). doi:10.3390/biom14060714
10. van Asten I, Schutgens REG, Urbanus RT. Toward flow cytometry based platelet function diagnostics. *Semin Thromb Hemost*. 2018;44(3):197-205. doi:10.1055/s-0038-1636901
11. van Asten I, Schutgens REG, Baaij M, et al. Validation of flow cytometric analysis of platelet function in patients with a suspected platelet function defect. *J Thromb Haemost*. 2018;16(4):689-698. doi:10.1111/jth.13952
12. Welsh JA, Arkesteijn GJA, Bremer M, et al. A compendium of single extracellular vesicle flow cytometry. *J Extracell Vesicles*. 2023;12(2):e12299. doi:10.1002/jev2.12299
13. Lozano-Andrés E, Van Den Broeck T, Wang L, et al. Intrinsic variability of fluorescence calibrators impacts the assignment of MESF or ERF values to nanoparticles and extracellular vesicles by flow cytometry. *Nanomedicine*. 2024;56:102720. doi:10.1016/j.nano.2023.102720

14. Wang L, Gaigalas AK, Abbasi F, Marti GE, Vogt RF, Schwartz A. Quantitating fluorescence intensity from fluorophores: practical use of MESF values. *J Res Natl Inst Stand Technol*. 2002;107(4):339-353. doi:10.6028/jres.107.027

15. Khourssaji M, Bareille M, Alberio L, et al. Mepacrine flow cytometry assay for the diagnosis of platelet δ-granule defects : literature review on methods - towards a shared detailed protocol. *Thromb Haemost*. September 11, 2024. doi:10.1055/a-2413-2870

16. Dupuis A, Bordet J-C, Eckly A, Gachet C. Platelet δ-Storage Pool Disease: An Update. *J Clin Med*. 2020;9(8). doi:10.3390/jcm9082508

17. Sandrock K, Zieger B. Current strategies in diagnosis of inherited storage pool defects. *Transfus Med Hemother*. 2010;37(5):248-258. doi:10.1159/000320279

18. Cai H, Mullier F, Frotscher B, et al. Usefulness of Flow Cytometric Mepacrine Uptake/Release Combined with CD63 Assay in Diagnosis of Patients with Suspected Platelet Dense Granule Disorder. *Semin Thromb Hemost*. 2016;42(3):282-291. doi:10.1055/s-0035-1564836

19. Dave RG, Geevar T, Chellaiya GK, et al. Stability and utility of flow cytometric platelet activation tests: A modality to bridge the gap between diagnostic demand and supply. *Platelets*. 2022;33(7):1043-1051. doi:10.1080/09537104.2022.2042232

20. Selle F, James C, Tuffigo M, et al. Clinical and Laboratory Findings in Patients with δ-Storage Pool Disease: A Case Series. *Semin Thromb Hemost*. 2017;43(1):48-58. doi:10.1055/s-0036-1584568

21. Maurer-Spurej E, Kahr WH, Carter CJ, Pittendreigh C, Cameron M, Cyr TD. The value of proteomics for the diagnosis of a platelet-related bleeding disorder. *Platelets*. 2008;19(5):342-351. doi:10.1080/09537100802010547

22. Maynard DM, Heijnen HFG, Horne MK, White JG, Gahl WA. Proteomic analysis of platelet alpha-granules using mass spectrometry. *J Thromb Haemost*. 2007;5(9):1945-1955. doi:10.1111/j.1538-7836.2007.02690.x

23. Kreft IC, Huisman EJ, Cnossen MH, et al. Proteomic landscapes of inherited platelet disorders with different etiologies. *J Thromb Haemost*. 2023;21(2):359-372.e3. doi:10.1016/j.jtha.2022.11.021

24. Hedner U. Recombinant activated factor VII as a universal haemostatic agent. *Blood Coagul Fibrinolysis*. 1998;9 Suppl 1:S147-52.

25. Hedner U. NovoSeven as a universal haemostatic agent. *Blood Coagul Fibrinolysis*. 2000;11 Suppl 1:S107-11. doi:10.1097/00001721-200004001-00020

26. Key NS, Aledort LM, Beardsley D, et al. Home treatment of mild to moderate bleeding episodes using recombinant factor VIIa (Novoseven) in haemophiliacs with inhibitors. *Thromb Haemost*. 1998;80(6):912-918.

27. Poon M-C. The Use of Recombinant Activated Factor VII in Patients with Glanzmann's Thrombasthenia. *Thromb Haemost*. 2021;121(3):332-340. doi:10.1055/s-0040-1718373

28. Erduran E, Aksoy A, Zaman D. The use of recombinant FVIIa in a patient with Glanzmann thrombasthenia with uncontrolled bleeding after tonsillectomy. *Blood Coagul Fibrinolysis*. 2009;20(3):215-217. doi:10.1097/MBC.0b013e32831d0f69

29. Ozelo MC, Svirin P, Larina L. Use of recombinant factor VIIa in the management of severe bleeding episodes in patients with Bernard-Soulier syndrome. *Ann Hematol*. 2005;84(12):816-822. doi:10.1007/s00277-005-1080-y

30. Tefre KL, Ingerslev J, Sørensen B. Clinical benefit of recombinant factor VIIa in management of bleeds and surgery in two brothers suffering from the Bernard-Soulier syndrome. *Haemophilia*. 2009;15(1):281-284. doi:10.1111/j.1365-2516.2008.01902.x

31. Hilden I, Lauritzen B, Sørensen BB, et al. Hemostatic effect of a monoclonal antibody mAb 2021 blocking the interaction between FXa and TFPI in a rabbit hemophilia model. *Blood*. 2012;119(24):5871-5878. doi:10.1182/blood-2012-01-401620

32. Dubut J, Goin V, Derray C, Huguenin Y, Fiore M. Targeting tissue factor pathway inhibitor with concizumab to improve hemostasis in patients with Glanzmann thrombasthenia: an in vitro study. *J Thromb Haemost*. 2024;22(9):2589-2600. doi:10.1016/j.jtha.2024.05.033

33. Sivapalaratnam S, Austin S, Lorch U, et al. A Phase 1/2, First-in-Human, Study to Investigate the Safety, Tolerability, Pharmacokinetics, Pharmacodynamics, and Efficacy of HMB-001 in Participants with Glanzmann Thrombasthenia. *Blood*. 2023;142(Supplement 1):1225-1225. doi:10.1182/blood-2023-187279

34. Cnossen MH, van Moort I, Reitsma SH, et al. SYMPHONY consortium: Orchestrating personalized treatment for patients with bleeding disorders. *J Thromb Haemost*. 2022;20(9):2001-2011. doi:10.1111/jth.15778

Appendices

Nederlandse samenvatting
List of publications
Dankwoord
About the author

NEDERLANDSE SAMENVATTING

Bloedplaatjes spelen een cruciale rol in de hemostase, en verstoring van dit mechanisme is geassocieerd met verschillende bloedingsstoornissen. De zeldzaamste erfelijke bloedplaatjesfunctiestoornissen (IPFDs) zijn relatief eenvoudig te diagnosticeren. Echter, de meer voorkomende IPFDs vertonen vaak een hoge diagnostische complexiteit, wat leidt tot onderdiagnose. Bovendien is er voor de behandeling van IPFD patiënten momenteel geen profylactische therapie beschikbaar, wat resulteert in een aanzienlijke patiëntenlast en een relatief lage levenskwaliteit voor patiënten met een ernstige IPFD. Dit proefschrift beschrijft nieuwe diagnostische en therapeutische benaderingen voor deze groep aandoeningen.

Geavanceerde diagnostiek ...

In **Hoofdstuk 2** beschrijven wij de karakterisering van een tetramerische nanobody-gebaseerde glycoproteïne VI (GPVI) bloedplaatjesagonist en vergelijken deze met de huidige agonisten die worden gebruikt in bloedplaatjesdiagnostiek, welke moeilijk te standaardiseren en te produceren zijn. Wij tonen aan dat onze nanobody in staat is om onderscheid te maken tussen gezonde controles en GPVI-gerelateerde bloedplaatjesstoornissen in een vergelijkbare mate als collageen of cross-linked collagen-related peptide (CRP-XL). Hiermee bieden wij een stabielere en eenvoudiger te produceren alternatieve GPVI-agonist, wat bijdraagt aan de standaardisatie van bloedplaatjesdiagnostiek.

In **Hoofdstuk 3** hebben wij een nieuwe snelle, op volbloed gebaseerde test voor delta-storage pool disease (δ-SPD) gevalideerd, gebaseerd op ATP secretie door bloedplaatjes. De huidige standaarddiagnose voor δ-SPD is arbeidsintensief, heeft een lange doorlooptijd en vereist grote hoeveelheden bloed. Wij hebben een microarray geïntroduceerd die de arbeidsintensiteit, doorlooptijd en benodigde bloedvolumes vermindert. Dankzij de hoge sensitiviteit kan deze test δ-SPD uitsluiten, waardoor minder patiënten hoeven te worden doorverwezen voor geavanceerde diagnostische technieken.

In **Hoofdstuk 4** hebben wij het bloedplaatjesproteoom van gezonde controles en patiënten met Glanzmann trombasthenie (GT) geanalyseerd. Wij hebben aangetoond dat bloedplaatjes van GT patiënten een verminderde expressie van specifieke α-granule-eiwitten vertonen.

... en nieuwe therapeutische benaderingen voor bloedplaatjesfunctiestoornissen

In **Hoofdstuk 5** introduceren wij een potentiële nieuwe profylactische behandeling voor erfelijke bloedingsstoornissen. HMB-001 is een bispecifiek antilichaam dat (geactiveerde) stollingsfactor VII (FVII(a)) en TREM-like transcript-1 (TLT-1) op het geactiveerde bloedplaatjesoppervlak herkent. Hierdoor wordt FVIIa gericht naar het bloedplaatjesoppervlak en wordt fibrinevorming bevorderd ter compensatie van defecten in de primaire hemostase. Onze preklinische data tonen aan dat HMB-001 effectief is in het verbeteren van fibrinevorming *ex vivo*, het verlengen van de endogene FVIIa-halfwaardetijd in non-humane primaten en het versterken van de hemostatische activiteit van FVIIa in muismodellen voor bloedingen. HMB-001 heeft daarom potentieel als subcutane profylactische therapie om bloedingen bij patiënten met GT en andere erfelijke bloedingsstoornissen te voorkomen, met een laagfrequent doseerschema.

CONCLUSIE

Samenvattend hebben wij in dit proefschrift meer inzicht verkregen in de biologie van bloedplaatjes en bijgedragen aan geavanceerde diagnostiek en nieuwe therapeutische benaderingen voor IPFDs. In de komende jaren hopen wij onze bevindingen naar de kliniek te brengen, waarbij wij de bloedplaatjesdiagnostiek verder willen verbeteren en standaardiseren en een levensveranderende behandelingsoptie voor IPFD patiënten willen bieden.

LIST OF PUBLICATIONS

Publications in this thesis

Zivkovic M, Shamorkina TM, Blaauwgeers MW, Post H, Heck AJR, Schutgens REG, Urbanus RT; Urbanus RT; TiN study group; SYMPHONY consortium. Proteomic analysis indicates lower abundance of platelet alpha-granule proteins in Glanzmann thrombasthenia. J Thromb Haemost. 2025 Apr 14:S1538-7836(25)00253-3.

Zivkovic M, Schutgens REG, van der Vegte V, Lukasse JA, Roest M, Huskens D, de Moor AS, Kremer Hovinga ICL, Urbanus RT; TiN study group; SYMPHONY consortium. A rapid whole-blood adenosine triphosphate secretion test can be used to exclude platelet-dense granule deficiency. J Thromb Haemost. 2025 Feb 10:S1538-7836(25)00056-X.

Zivkovic M, Pols-van Veen E, van der Vegte V, Sebastian SAE, de Moor AS, Korporaal SJA, Schutgens REG, Urbanus RT; Thrombocytopathy in the Netherlands (TiN) study group; SYMPHONY consortium. Functional characterization of a nanobody-based glycoprotein VI-specific platelet agonist. Res Pract Thromb Haemost. 2024 Oct 3;8(7):102582.

Zivkovic M, Gandhi PS, Østergaard H, Bonde AC, Elm T, Løvgreen MN, Schluckebier G, Johansson E, Olsen OH, Olsen EHN, de Bus IA, Bloem K, Alskär O, Rea CJ, Bjørn SE, Schutgens RE, Sørensen B, Urbanus RT, Faber JH. A bispecific antibody approach for the potential prophylactic treatment of inherited bleeding disorders. Nat Cardiovasc Res. 2024 Feb;3(2):166-185.

Other publications

Noordermeer T, Urbanus RT, Wong CY, Jansma JJ, Wiersma NM, **Zivkovic M**, Huisman A, Limper M. Interference in point-of-care international normalized ratio monitoring in patients with lupus anticoagulant is correlated with anti-β2-glycoprotein I antibody titers. Res Pract Thromb Haemost. 2022 Dec 12;7(1):100011.

Sanrattana W, Smits S, Barendrecht AD, van Kleef ND, El Otmani H, **Zivkovic M**, Roest M, Renné T, Clark CC, de Maat S, Maas C. Targeted SERPIN (TaSER): A dual-action antithrombotic agent that targets platelets for SERPIN delivery. J Thromb Haemost. 2022 Feb;20(2):353-365.

Silvis MJM, Fiolet ATL, Opstal TSJ, Dekker M, Suquilanda D, **Zivkovic M**, Duyvendak M, The SHK, Timmers L, Bax WA, Mosterd A, Cornel JH, de Kleijn DPV. Colchicine reduces extracellular vesicle NLRP3 inflammasome protein levels in chronic coronary disease: A LoDoCo2 biomarker substudy. Atherosclerosis. 2021 Oct;334:93-100.

Hofman ZLM, Clark CC, Sanrattana W, Nosairi A, Parr NMJ, **Živkovic M**, Krause K, Mahnke NA, Scheffel J, Hack CE, Maurer M, de Maat S, Maas C. A mutation in the kringle domain of human factor XII that causes autoinflammation, disturbs zymogen quiescence, and accelerates activation. J Biol Chem. 2020 Jan 10;295(2):363-374.

Oral & Poster presentations

2025 Oral presentation, 33rd Congress of the International Society on Thrombosis and Haemostasis, Washington, D.C., USA.
Title: Proteomic analysis indicates lower abundance of alpha granule proteins in Glanzmann thrombasthenia

2025 Oral presentation, 33rd Congress of the International Society on Thrombosis and Haemostasis, Washington, D.C., USA.
Title: A rapid whole blood ATP secretion test can be used to exclude platelet dense granule deficiency

2025 Poster presentation, 33rd Congress of the International Society on Thrombosis and Haemostasis, Washington, D.C., USA.
Title: HMB-001 in Glanzmann thrombasthenia: breakthrough bleed control with reduced platelet and rFVIIa use

2025 Poster presentation, 18th Annual Congress of the European Association for Haemophilia and Allied Disorders, Milan, Italy.
Title: A rapid whole blood ATP secretion test can be used to exclude platelet dense granule deficiency

2025 Poster presentation, 18th Annual Congress of the European Association for Haemophilia and Allied Disorders, Milan, Italy.
Title: The proteomic landscape of platelets in Glanzmann thrombasthenia

2025 Poster presentation, Dutch society for Thrombosis and Haemostasis / British Society for Haemostasis and Thrombosis Joint Annual Scientific meeting, Newcastle, United Kingdom.
Title: A rapid whole blood ATP secretion test can be used to exclude platelet dense granule deficiency

2024 Oral presentation, 16th Dutch Hematology Congress, Papendal, the Netherlands.
Title: HMB-001 – a novel bispecific antibody accumulating and targeting endogenous FVIIa to activated platelets supports enhanced haemostatic responses in models of Glanzmann thrombasthenia

2023 Oral presentation, 31st Congress of the International Society on Thrombosis and Haemostasis, Montréal, Canada.
Title: Functional characterization of a nanobody based GPVI specific platelet agonist

2023 Oral presentation, Symposium of Dutch society for Thrombosis and Haemostasis, Koudekerke, the Netherlands.
Title: HMB-001 – a novel bispecific antibody accumulating and targeting endogenous FVIIa to activated platelets supports enhanced haemostatic responses in models of Glanzmann thrombasthenia

2023 Poster presentation, Symposium of Dutch Society for Thrombosis and Haemostasis, Koudekerke, the Netherlands.
Title: Functional characterization of a nanobody based GPVI specific platelet agonist

2023 Poster presentation, 16th Annual Congress of the European Association for Haemophilia and Allied Disorders, Manchester, United Kingdom.
Title: HMB-001 – a novel bispecific antibody accumulating and targeting endogenous FVIIa to activated platelets supports enhanced haemostatic responses in models of Glanzmann thrombasthenia

2023 Oral presentation, British Society for Haemostasis and Thrombosis Annual Scientific meeting, Birmingham, United Kingdom.
Title: HMB-001 – a novel bispecific antibody accumulating and targeting endogenous FVIIa to activated platelets supports enhanced haemostatic responses in models of Glanzmann thrombasthenia

2022 Poster presentation, 30th Congress of the International Society on Thrombosis and Haemostasis, London, United Kingdom.
Title: The novel bispecific antibody HMB-001 enhances the haemostatic response in models of Glanzmann Thrombasthenia by targeting FVIIa to activated platelets

Awards

2025 Early Career Award by the 33rd Congress of the International Society on Thrombosis and Haemostasis.

2023 Award for Scientific Excellence for outstanding scientific achievements in biochemical research in the field of thrombosis and haemostasis by the Dutch Society for Thrombosis and Haemostasis. Made possible by the Nationaal Fonds Trombose en Hemostase (NFTH).

DANKWOORD

Dit proefschrift was niet tot stand gekomen zonder een heleboel mensen. Vrienden, familie en collega's, jullie waren onmisbaar. Dankzij jullie was het een feestje op en buiten het lab.

Op de eerste plek natuurlijk **Rolf**. Wat fijn dat je het al 5 jaar en counting met me uithoudt! Je inhoudelijke bijdrage aan dit proefschrift en je eindeloze kennis over allerlei moleculaire details spreken voor zich, maar ik wil je graag in het bijzonder bedanken voor de fijne werksfeer en de gezelligheid. Het feit dat onze werkbesprekingen tegenwoordig af en toe plaatsmaken voor iets minder wetenschappelijke onderwerpen bewijst dat je een zelfstandige onderzoeker van me hebt gemaakt, dank daarvoor! Ik kijk uit naar de rest van mijn tijd bij jou in de groep.

Roger, allereerst natuurlijk bedankt voor het bieden van de mogelijkheid te promoveren bij de Van Creveldkliniek. Je scherpe inzichten en enthousiasme zijn enorm waardevol! Bedankt dat ik mijn academische carrière bij jou mag voortzetten, ik kijk ernaar uit!

Geachte leden van de **beoordelingscommissie en oppositie**, hartelijk dank dat u mijn proefschrift heeft willen beoordelen en ik kijk uit naar het geleerd debat dat ik met u mag voeren.

Alle **patiënten** en **MiniDonoren** die bloed hebben gegeven voor mijn experimenten. Zonder jullie was dit proefschrift er niet geweest, bedankt voor jullie waardevolle bijdrage aan de wetenschap!

Mijn lieve paranimfen, **Danielle** en **Sarah**, wat ben ik blij en trots dat jullie twee naast mij staan op deze dag!
Lieve Daan, ik kan het me bijna niet meer voorstellen, maar ruim 4 jaar geleden begon jij bij mij als mijn eerste student, toen ik zelf ook nog maar net begonnen was. Hierdoor was het vaak niet helemaal duidelijk wie nou wie begeleidde wanneer je me weer moest helpen herinneren aan een van mijn vele vergeten meetings. Gelukkig bleven je zelfstandigheid en onderzoeksskills niet onopgemerkt (dus eigenlijk heb ik je gewoon een gunst verleend! 😉) en ben je bij ons komen werken. Inmiddels uitgegroeid tot super close vriendinnen en wat ben ik daar blij mee. Van de kaasbar tot de potlooien party, we maken er een feestje van samen. Ik kan niet wachten tot onze PhD/paranimf-moon naar Kaapverdië!

Lieve Saar, wij hebben niet veel nodig om aan het eind van de dag met buikpijn van het lachen weer naar huis te gaan. Of het nou in Maastricht, Eindhoven, Dommelen of Groot-Ammers is, bij jou (en die lieve Thijs, Femke, Marco en José) voel ik me altijd thuis. Samen met onze **Fleur** in de collegebanken begonnen en alle drie een andere weg ingeslagen, maar elkaar gelukkig nooit uit het oog verloren. Weekendjes Maastricht -toen onze Saar besloot de pipet in te ruilen voor de stethoscoop- en tripjes naar Italië of door België in de Oude Bessie zijn onvergetelijk met jullie. Dokter Saar je wordt een geweldige huisarts en Fleurie zo gaaf dat je de stap hebt gewaagd om naar Barcelona te verhuizen. Wel terugkomen hè!!! Ik ben zo blij met zulke lieve vriendinnen als jullie!

Op de volgende plek mag niet ontbreken ons fantastische team; RB! **Vossa**, wat ben ik blij dat we jou aan ons team hebben mogen toevoegen tijdens mijn PhD! Je was onmisbaar en hebt me zoveel geholpen met alle patiënten inclusies en andere zaken. Super bedankt! **Geke**, altijd in voor een goed gesprek of een luisterend oor en altijd even positief! Bedankt voor je gezelligheid en wat jammer dat je ons binnenkort gaat verlaten. Ik ben benieuwd naar je volgende stap! **Jente**, onze nieuwste aanwinst! Samen met Geke gingen we op boepa (bedankt voor het toevoegen van deze afko aan mijn vocabulaire) in Edinburgh. Wat hebben we gelachen! Heel veel succes de komende jaren! **Tessa**, niet ver voor mij begonnen met je PhD en de eerste stappen hebben we samen gezet! Fijn dat er eindelijk iemand anders ook K3 wilde aanvragen bij de DJ, je wordt gemist op de congres feestjes! Super knap hoe je je PhD en het gezinsleven kon combineren, bij jou lijkt alles vanzelf te gaan! Veel geluk bij je (niet meer zo) nieuwe baan en je mooie gezinnetje! **Silvie**, zelden ben ik iemand tegengekomen met zoveel structuur als jij. Als ik iets op het lab moet doen en blijkt dat jij het al eens gedaan hebt, ben ik altijd opgelucht, want dan weet ik dat alles exact is terug te vinden. Bedankt voor het op weg helpen in de eerste maanden van mijn PhD en ik wens je alle goeds voor wat er verder op je pad gaat komen! **Omayra**, naar jouw verhalen kon ik uren luisteren als je weer eens een nacht met het transplantatieteam had gewerkt en de volgende ochtend weer even vrolijk als altijd op het lab stond. Je passie voor je vak is zo bijzonder en ik gun je zo dat je je hart (😉) achterna kan gaan.

De deelnemers van het SYMPHONY consortium, **Marjon**, een inspiratiebron voor velen. Super knap hoe je het SYMPHONY consortium in het leven hebt geroepen. Van harte met je hoogleraarschap, enorm verdiend! **Simone**, bedankt voor je eindeloze inzet voor dit consortium en het aanbrengen van structuur, wanneer dat bij de PhDers weer eens ver te zoeken was. Alle mede PhD studenten van het SYMPHONY consortium, **Alexander**, **Bas**, **Caroline**, **Diaz**, **Huan**, **Jessica**, **Laura**, **Lieke**, **Lorenzo**, **Martijn**, **Michael**, **Rafael**, **Ryanne**, **Shannon**, **Sjoerd**, **Tine** en **Wala**. We zagen elkaar niet vaak maar we wisten elkaar altijd wel te vinden op de congressen en natuurlijk het jaarlijkse PhD uitje. Bedankt voor alle leuke momenten en veel succes allemaal met de volgende stap na de PhD.

Coen, **Pieter**, **Ray**, **Richard**, ondanks een VCK-gast te zijn op het CDL-research lab, heb ik me niet minder welkom gevoeld. Dank daarvoor!

Mijn stiefzusters, **Annet**, **Jerney** en **Noortje**. Met jullie is het nooit saai! Lieve Annet, altijd op de hoogte van alles en iedereen. We kunnen lachen en (bijna) huilen als we samen niet de piste af durven. Super leuk dat Daan en ik bij je mochten komen eten en de F1 komen kijken. Ik heb de solitaire nog steeds niet opgelost helaas! Lieve Jør, we kunnen altijd ons ei kwijt bij elkaar en begrijpen elkaar altijd meteen! Wat hebben we genoten bij jou in Ermelo, beh beh. Hopelijk nog veel meer van zulke weekendjes, sushi etentjes en andere uitjes! Lieve Noortje, samen met Daan in de Rummiclub, al komt het niet zo vaak van Rummikubben want we hebben altijd genoeg te kletsen en te lachen! En nu ook nog een kersverse mama, ik ben super trots op jou! **Arjan**, mijn mede lab 3 west-side OG! Ondanks dat ik soms een beetje schrik als je weer tegen jezelf praat en niet zelden mijn pipetten bij jou terugvind, had ik me geen betere bench-buurman kunnen wensen! Bedankt voor alles wat je me hebt geleerd over de FACS, de microscoop en het leven. Ik hoop dat onze gezamenlijke interesse voor bloedplaatjes en microscopie ons nog lang verbindt! **Arnold**, ongekend hoe jij nooit je geduld verliest bij alle non-stop vragen de hele dag door. Respect! Dank voor alles en wat zijn we een goed borrel-boodschappen team! **Simone**, samen als student begonnen al heel wat jaren geleden en wat hebben wij veel meegemaakt samen! De bruiloft van Wariya in Praag, het weekendje naar Barcelona met Rowan en Olaf, heel wat middagjes op het terras of het strand na onze ochtendshift tijdens Covid, onze influencermiddag op Pink Beach en ook een heleboel feestjes en festivals. Allemaal super waardevolle herinneringen!

Brigitte, **Cor**, **Jennifer**, **Sandra**, **Yanjuan**, of het nou een antilichaam uit de back-up, bestelling, of bezoekje aan de spoedeisende hulp is (bedankt Git!), jullie regel(d)en het altijd meteen! Dank voor jullie eindeloze inzet voor ons lab!

De oude garde! Wat ben ik blij dat we zo'n leuke groep PhDers hadden. **Diego** pinche pendejo! I have never seen such a Dutch Mexican. Thank you for the amazing cooking that you often did for us (luckily that part didn't become Dutch) and for all the laughing when you pull out an emergency fuet on the middle of the ski slope. **Jonathan**, onze beroepsbeoefenaar. Was je je beroep maar blijven beoefenen, dan hadden we je niet hoeven uitzwaaien. Ondanks onze niet altijd even vriendelijke verstandshouding kon ik je aanwezigheid ergens wel een beetje waarderen en ga ik je misschien zelfs wel een heel klein beetje missen. Tot in New York en ik zie je boeking bij de Librije wel verschijnen als je terug bent! **Luukie**, onze superster. Pipet doordeweeks, microfoon in het weekend. Super leuk om jou te zien shinen als je een optreden hebt. En dan ook nog het zonnetje in huis op het lab. Heel veel succes met je postdoc! **Marionaaaa**, I'm so glad we got to share the postdoc room together! Even though I don't understand what can be SO funny in all your scientific meetings, you are truly a ray of sunshine and you make even late nights in the office enjoyable! **Mariski**, altijd even lief en vrolijk! Met je aanstekelijke giechel weet je altijd dat jij in de buurt bent. Of het nou een marathon rennen is of een marathon pipetteren, jij kan het allemaal, ongekend! Heel veel succes weer in de kliniek! **Pollito**, hand in hand from day 1! Although you have scooped me multiple times (in both offices and with your defense date), I am so happy we have been together all this time. We have been joking we will stick together until our retirement home, I hope we do! **Rowan**, onze labrador! Ook al ben je soms een kip zonder kop, ik ben super trots op je hoe je je PhD hebt gecheft. Je bent een van de liefste personen die ik ken en ik baal ervan dat je ons binnenkort gaat verlaten (of misschien toch postdoc??). We gaan er nog wat moois van maken in Washington! **Willemijntje**, heerlijk hoe nuchter jij bent. Een beast achter de ONI en op de fiets, en na een avondje in de Flater altijd als eerste fris en fruitig weer aanwezig. Heel veel succes en plezier in Zürich, ik ga je missen!

Caro, **Clara**, **Hinde**, **Linglei**, **Naomie**, **Omnia**, **Qiangbing**, **Xin Jin**, thank you for all the gezellige moments in the lab, at TTT or at the PhD weekend. Wish you all the best! Also the new generation of PhD's, **Bart**, **Federica**, **Gaspard**, **Ludovica**, **Maryse**, **Nadine**, **Tanja**, **Titine**, super nice to see that you have found each other and so nice

that we got to share one ‘old vs new generation’ PhD weekend! Best of luck in the coming years!

Anil, **Dan**, **Demian**, **Maria Laura**, **Marcel**, **Martijn**, **Olivier**, **Sander**, **Tom**, thank you for showing me how it’s done. You are all super talented researchers!

Leida en **Martijn**, door jullie is het lab altijd weer spik en span (voor de 5 minuten die wij dat vol kunnen houden). Bedankt daarvoor en voor het kletsen op de gang! **Joukje**, iedereens externe geheugen! Bedankt voor alles wat je voor het lab regelt!

Ook onze vrienden van een verdieping lager, **Jort**, **Mark**, **Simon**, **Tim** en de rest van de **Experimentele Cardiologie**, bedankt voor alle gezelligheid op de gezamenlijke borrels en voor de potjes tafelvoetbal!

Al mijn kamergenoten door de jaren heen, **Alejandra**, **Caren**, **Elisa**, **Ernest**, **Marc**, **Myrthe**, Geke, Jonathan, Pol, Tessa, bedankt voor alle gezelligheid! Alejandra, thank you for showing me the cute pictures of your dog. It was a pleasure sharing an office with you! Caren, je was niet altijd op het CDL te vinden, maar als je er was, was het altijd gezellig! Bedankt voor alle leuke momenten, met name op de wintersport! Elisa and Ernest, thank you for adopting me in the postdoc office! Marc, sorry dat ik je onvrijwillig heb opgegeven voor het organiseren van het lab uitje met mij, maar wat was het een succes! Veel succes verder bij TargED! Myrthe, super knap hoe jij in een korte tijd zo’n dik boekje voor elkaar hebt gekregen! Bedankt voor de gezellige momenten op kantoor en daarbuiten, veel succes weer in de kliniek!

Ewaaa **Wariyaaa**, although it already feels like ages ago, I truly enjoyed the time that we were bench-neighbors. I hope by now you have recovered from some of the Dutch student habitats that I taught you and I really hope we meet again, either in Thailand, the Netherlands, or Coconut beach. **Zonne** en **Chantal**, mijn eerste babystapjes in de wetenschap waren toch wel een beetje onder jullie vleugels. Bedankt voor het goede voorbeeld en heel veel succes in jullie verdere carrière!

Idske, we waren een geoliede machine voor de inclusies van de TiNkids. Het was een fijne samenwerking met je. Dank daarvoor en voor al je inzet voor onze kleinste patiënten! Ook alle andere **artsen**, **verpleging**, **secretariaat en het research-team van de Van Creveldkliniek**, bedankt voor jullie waardevolle bijdrage aan mijn studie inclusies en de gezellige VCK-uitjes!

De PhD studenten van de Van Creveldkliniek, **Amber**, **Anne**, **Annick**, **Floor**, **Geoff**, **Gijs**, **Johan**, **Karlijn**, **Konrad**, **Sigrid**, **Thomas**, het veranderen van de maandelijkse dinsdag PhD meeting naar een ‘lekker informeel met bier’ meeting was toch wel een van onze betere ideeën. Super leuk om op de hoogte te zijn van elkaar en ook de kloof tussen lab en kliniek kleiner te maken. Naast gezelligheid was hier ook altijd ruimte voor inhoudelijke gesprekken en het delen van gezamenlijke struggles van het PhD leven. Veel succes het met afronden van jullie PhD en de vervolgstappen!

De studenten die ik heb mogen begeleiden tijdens hun stage. **Joline**, wat bracht jij veel vrolijkheid met je mee! Een dappere poging hebben we gedaan met de super-resolutie microscoop en ook al was het lab niet helemaal jouw ding, jij bracht iedereen samen en jullie kregen een super hecht groepje studenten, wat natuurlijk ook heel waardevol is! Alle goeds in je verdere carrière! **Lisa**, wat ben jij super gedreven! Er hoefde maar een half plan te liggen en de volgende dag had je het uitgewerkt en wel alweer klaarliggen. Dat werd beloond met een hele mooie tweede auteursplek! Heel veel succes bij je nieuwe baan! **Janoek**, je was maar 4 maanden bij ons, maar wat heb jij veel gedaan! Bedankt voor je belangrijke bijdrage aan mijn projecten en heel veel succes in je master! **Caya**, momenteel nog bezig met je stage en wat een gezelligheid dat jij erbij bent! Daarnaast ook nog lekker zelfstandig je project aan het draaien. Succes nog in de laatste maanden bij ons en in de rest van je master!

Dat er op het lab naast hard werken ook vriendschappen ontstaan heb ik ook bij jullie mogen meemaken. Ondanks dat jullie het lab leven hebben verlaten, zien we elkaar gelukkig nog. **Olaf**, altijd in voor gezelligheid, maar ook altijd even oprecht geïnteresseerd in hoe het gaat. We hebben een super leuke trip naar Barcelona gemaakt (toch Simone?) en je hebt zo vaak ontzettend lekker voor ons gekookt wanneer wij nog steeds niet verder kwamen dan pasta pesto, bedankt! **Ellis**, ik ben super blij dat we elkaar nog regelmatig zien, voor een sportlesje of voor een borreltje. Je bent een lieve vriendin en ik hoop dat we nog lang samen sporten en/of borrelen! Ook de andere meiden van de ‘moka mokkels’, **Chela** en **Nilda**, we zijn maar kort samen op het lab geweest maar we zien elkaar nog steeds. Jullie zijn super lieve meiden en ik kijk er altijd naar uit om weer gezellig met jullie bij te kletsen!

Richard, altijd in voor een goede wijn, lekker etentje of een spontane vakantie als de winterdip begint in te kicken. Wat hebben we een mooie reis door Marokko gemaakt! Je staat altijd voor me klaar, super bedankt daarvoor!

Lieve meiden van de Nobelstraat, **Maud**, **Daantje** en **Jiska**, wat was het een feestje om met jullie te wonen. Ook al was het niet zo lang, we zien elkaar nog steeds regelmatig voor een paasbrunch, kerstdiner of gewoon zomaar. Samen met **Lotte**, **Charlotte** en **Meike** is het altijd gezellig!

Femke, mijn partner in crime tijdens onze studententijd. Wat hebben we leuke jaren gehad samen bij onze roeiploeg en bij VIN. Inmiddels ben je helaas weer uitgevlogen naar het zuiden en hebben we de studentenactiviteiten ingeruild voor burgerlijke middagjes in de spa. Heel veel succes met het afronden van de AKO, ik ben benieuwd wat voor dokter je gaat worden!

De meiden van **damesdispuut VIN**, jullie hebben mijn studententijd onvergetelijk gemaakt. Bedankt voor alle leuke weekendjes, vakanties en andere uitjes!

Tot slot de belangrijkste mensen, mijn lieve familie, **Dennis**, **Maxime**, **Papa**, **Nana** en mijn beste vriendin **Mama**, jullie onvoorwaardelijke steun en liefde zijn de basis van dit proefschrift. Bedankt voor alles wat jullie voor mij doen. Volim vas!

ABOUT THE AUTHOR

Minka Zivkovic was born on the 11th of March 1997 in Ede, where she also grew up. After obtaining her gymnasium diploma at the Marnix College in Ede in 2014, she started the bachelor Biomedical Sciences at the Utrecht University. After completion in 2017, she enrolled the Master's program Biology of Disease, with a track in Cardiovascular Diseases at the same university. During her Master's, she completed her major research internship studying the interaction between contact activation and the fibrinolytic system in hereditary angioedema at the laboratory of clinical chemistry and hematology at the University Medical Center Utrecht. After, she went to the Amsterdam University Medical Center to join the pathology group for her extended minor research project. Here, she studied the effect of hypertension on the cerebral microvasculature, the crucial role of calprotectin in liver ischaemia/reperfusion injury and the immunometabolic fingerprint of the aged kidney. After obtaining her Master's degree in 2019, she went back to Utrecht to start her PhD project in February 2020 at the Van Creveldkliniek. Under supervision of Dr. Rolf Urbanus and Prof. Dr. Roger Schutgens, she worked on advanced diagnostics and novel therapeutics for inherited platelet function disorders, as part of the nationwide SYMPHONY consortium and in collaboration with Hemab Therapeutics. After obtaining the doctorate, she continues her academic career as postdoctoral researcher at the Van Creveldkliniek, to further explore potential novel prophylactic treatments for patients with inherited bleeding disorders.